QUANTUM LIQUIDS AND QUANTUM CRYSTALS

Study of the stabilization and recombination of nitrogen atoms in impurity–helium condensates

R. E. Boltnev,* I. N. Krushinskaya, and A. A. Pelmenev

Branch of the Institute of Energy Problems of Chemical Physics, Russian Academy of Sciences, pr. Akad. Semenova 1, str. 10, Chernogolovka, Moscow Region, 142432, Russia

E. A. Popov

Branch of the Institute of Energy Problems of Chemical Physics, Russian Academy of Sciences, pr. Akad. Semenova 1, str. 10, Chernogolovka, Moscow Region, 142432, Russia; University of Jyvaskyla, Survontie 9, FIN-40351, Jyvaskyla, Finland

D. Yu. Stolyarov

University of Southern California, Los Angeles, California 90089, USA

V. V. Khmelenko

Laboratory of Atomic and Solid State Physics, Cornell University, Ithaca, New York 14853, USA
(Submitted November 26, 2004; revised January 27, 2005)
Fiz. Nizk. Temp. **31**, 723–734 (July 2005)

The stabilization and recombination of nitrogen atoms N(^4S) in nitrogen-helium and nitrogen–neon-helium condensates obtained by the injection of impurity particles from a gas discharge into bulk superfluid helium are investigated by the EPR method. It is established that the stabilized nitrogen atoms reside inside and on the surface of impurity clusters forming a porous structure in the bulk superfluid helium. The possibility of increasing the specific energy of impurity–helium condensates by increasing their density through mechanical pressing is investigated. For nitrogen-helium condensates an eightfold increase in the specific energy is achieved. The recombination loss of N(^4S) upon heating of impurity–helium condensates in the temperature range 1.7–7 K is detected. This permits verification of the mechanism of thermoluminescence of impurity–helium condensates. © *2005 American Institute of Physics.* [DOI: 10.1063/1.2001631]

1. INTRODUCTION

Impurity-helium condensates (IHCs) have been attracting increasing interest in recent years as new porous nanomaterials whose unique properties can be used for various purposes. It has been proposed to use IHCs prepared on the basis of D_2 and D_2O as moderators for obtaining ultracold neutrons.[1] The most promising practical application of condensates is for polarization of ^{3}He, D_2, and ^{129}Xe nuclei in a strong magnetic field ~ 10 T at a temperature of ~ 1 mK.[2,3] Another application of IHCs, which has been the most attractive from the start, is the creation of new cryogenic materials with a high specific energy,[4] since record high concentrations of stabilized deuterium and nitrogen atoms have been achieved in IHCs.[5,6] Other possible applications of IHCs include investigation of the unique properties of superfluid ^{3}He and ^{4}He in disordered porous materials, determination of the rate constants of certain tunneling reactions, measurement of atomic diffusion in disordered structures, research on quantum phenomena in condensates with high densities of stabilized hydrogen atoms, study of model systems containing free radicals, investigation of the magnetic and electronic properties of nanoclusters, and research on nanoparticles of ice and their role in atmospheric processes and in astrophysics.

The technique of IHC preparation developed in 1974 by Gordon, Mezhov-Deglin, and Pugachev[7] is based on the injection of impurities into bulk superfluid helium (He II) by a jet of gaseous helium. A variant of this technique in which the gas jet passes through a radio-frequency (rf) discharge zone permits the accumulation of free radicals in the impurity–helium samples. The van der Waals interaction between helium atoms and the impurity particle in some cases is sufficient for the formation of a bound helium sheath around the particle. IHC samples can now be made from a number of different atomic and molecular impurities: Ne, Ar, Kr, D_2, N_2, H_2O, C_2H_5OH, Ba, and Na. IHCs are porous gel-like structures formed by impurity clusters with different sizes 3–10 nm and a low average concentration of the impurity substance $\sim 10^{20}$ cm^{-3} (Refs. 5, 8, and 9). The skeleton of impurity material is formed in superfluid helium, and the sample usually remains stable outside the liquid helium as well (in this case we regard it as a dry sample) at higher temperatures. It is assumed that the impurity skeleton is coated by a layer of adsorbed helium, preventing the coales-

cence of the impurity substance in the dry sample. Studies of the relative (elemental) composition of helium and the various impurities in dry impurity–helium samples have shown that there are of the order of 20 helium atoms for every Ne atom and N_2 molecule and 30–60 helium atoms for each Ar and Kr atom,[10–12] i.e., the samples consist mainly of solidified helium. Thus IHCs are highly porous materials with a wide distribution of pore sizes (from 10 to 1000 nm)[13] and an extremely large specific surface area.

An important advantage of IHCs over other porous substances used in experiments at helium temperatures is the possibility of varying the density of the IHC sample directly during the course of an experiment by compression (pressing) of the sample. Thus in a single experiment one can obtain data measured on an IHC sample with a controlled variation of the density of the impurities; this can be very useful for studying the dependence of the sound conversion efficiency in He II on the impurity density.[14] Pressing of an IHC sample also alters the distribution of pore sizes (this can be used to study the properties of superfluid helium in a restricted geometry) and the average density of radicals stabilized in the sample.

Mechanical pressing of IHCs to increase the concentration of stabilized nitrogen atoms was proposed in Ref. 15, but there have not yet been systematic measurements of the influence of pressing of samples on the concentration of atoms stabilized in them. Systems containing high concentrations of nitrogen atoms are particularly attractive for such investigations. The available results on the study of IHC samples have indicated the possibility of achieving values of the energy content of nitrogen-helium condensates comparable to the energy density stored in ordinary explosive materials. The results of our research have first demonstrated the possibility of mechanical pressing of IHC samples to increase the average concentration of stabilized nitrogen atoms during the time of an experiment. We have established the amount by which it is possible to increase the average concentration of nitrogen atoms by a simple pressing of the samples and the fraction of the atoms that remains in the sample after pressing.

In this paper we also present the results of studies of the recombination of nitrogen atoms stabilized in impurity-helium samples in the temperature range 1.7–7 K. These studies were done for the purpose of verifying the mechanism of thermoluminescence of nitrogen-helium condensates. In Ref. 16 we proposed the following mechanism for explanation the thermoluminescence in the blue region of the spectrum from nitrogen-, neon-, and argon-helium samples containing nitrogen atoms: recombination of the nitrogen atoms leads to the formation of an excited molecule and its subsequent luminescence:

$$N(^4S)+N(^4S)\rightarrow N_2(A^3\Sigma_u^+),$$

$$N_2(A^3\Sigma_u^+)\rightarrow N_2(X^1\Sigma_g^+)+h\nu.$$

In addition, it is known that in solid nitrogen the energy of a metastable molecule $N_2(A^3\Sigma_u^+)$ is efficiently transferred to a neighboring nitrogen atom in the ground state, with a transition of the latter to an excited state:

$$N_2(A^3\Sigma_u^+)+N(^4S)\rightarrow N_2(X^1\Sigma_g^+)+N(^2D).$$

This mechanism was proposed by Edwards to explain the thermoluminescence in the green region of the spectrum (α group) in a nitrogen matrix,[17] and it requires three $N(^4S)$ atoms for every $N(^2D)$ atom obtained; this should be manifested in a decrease of the concentration of stabilized $N(^4S)$ atoms in the samples upon thermoluminescence. An attempt to obtain a decrease in the number of $N(^4S)$ atoms in nitrogen-helium samples on heating from 1.5 to 2 K was unsuccessful.[18] Only at the λ-point transition in helium was a decrease ($<10\%$) observed in the number of $N(^4S)$ atoms in a nitrogen-helium sample. In view of this result and the complexity of the Edwards mechanism (a three-particle process in the solid phase at $T\approx 1.5$ K), another explanation for the thermoluminescence of impurity–helium samples in the green region of the spectrum was given preference—a version that suggests the long-term ($>5\times10^3$ s) existence of metastable $N(^2D)$ atoms after their trapping from the gas phase into the condensate as the sample is accumulated, and their subsequent luminescence.

In the present study the recombination of nitrogen atoms was observed during the pressing of impurity–helium samples in He II and also during their heating in the temperature range 1.7–7 K. The number of nitrogen atoms stabilized in the samples was determined by the EPR method, from which, together with the visually determined volumes of the impurity-helium samples, we determined the average concentration of atoms. From the linewidths of the recorded EPR spectra we could determine the local concentration of nitrogen atoms in the nanoclusters forming the IHCs. It is known from previous papers[5,6] that the observed values of the local concentration are 1–2 orders of magnitude higher than the average concentration of atoms stabilized in impurity-helium samples; this is explained by the high porosity of the samples. The loss of nitrogen atoms in the ground state registered by the EPR method indicates that the Edwards mechanism is applicable for explaining the thermoluminescence in the green region of the spectrum of IHCs.

We investigated samples in which the initial atomic concentrations differed by more than two orders of magnitude. To obtain the samples with the low initial density of nitrogen atoms, neon was added to the nitrogen–helium mixture, and neon-helium gas mixtures with an impurity nitrogen content of $\sim10^{-3}\%$ were also used.

2. EXPERIMENTAL TECHNIQUE

The samples were obtained by injecting atomic-molecular beams into bulk He II.[12] We investigated three types of samples, obtained by condensation of gaseous mixtures of different compositions: nitrogen-helium $[N_2]/[He]=1/20-1/500$, neon-helium $[Ne]/[He]=1/20$, and nitrogen-neon-helium $[N_2]/[Ne]/[He]=1/100/10000$. The conditions for obtaining the different samples are listed in Table I.

Immediately prior to condensation in He II the gaseous mixture was subjected to an rf discharge (frequency 40 MHz, power 40 W) for dissociation of impurity nitrogen molecules. Impurity–helium samples containing stabilized nitrogen atoms in the ^4S ground state were formed in the bulk He II, and the number of these atoms was determined by the EPR method. Since a molecular nitrogen impurity ($\sim10^{-3}\%$) is normally found to be present in our a neon–

TABLE I. Experimental conditions for formation of impurity–helium samples.

Sample No.	Composition of gas mixture	Gas flow rate dN/dt, x10^{19} 1/s	Sample accumulation time,s
1	$[N_2]$:[He] = 1:25	6.0	600
2	$[N_2]$:[He] = 1:100	5.9	900
3	$[N_2]$:[He] = 1:500	6.2	1800
4	$[N_2]$:[Ne]:[He] = 1:100:10000	13.0	660
5	$[N_2]$:[Ne]:[He] = 1:100:10000	10.0	960
6	[Ne]:[He] = 1:20	5.0	600
7	[Ne]:[He] = 1:20	6.0	600

helium gas mixture, the passage of such a mixture through an rf discharge region also results in the formation of nitrogen atoms in it, which are stabilized in the neon-helium condensate. The initiation of recombination processes was done both by mechanical action on the samples (pressing them) and by increasing their temperature from 1.7 to 7 K.

The low-temperature part of the apparatus is described in detail in Refs. 11 and 12. The samples were accumulated in a quartz cup filled with superfluid helium. The collection of the sample to the bottom of the cup was done mechanically.[11] After the sample accumulation was completed, the cup (inner diameter 0.7 cm) was filled to a height of 1.5–2 cm. The cup could be moved vertically downward along the axis so that the lower part of the cup, containing the sample, lay at the center of the microwave cavity of the EPR apparatus.[19] Figure 1 shows the location of the cavity with the sample in it. The characteristics of the cavity with respect to height are shown in Fig. 2a,b. The nonuniformity of the magnetic field is produced by the superconducting magnet is $\Delta H(h) = H(h) - H_0$, where H_0 is the value of the magnetic field at the center of the cavity, and the dependence of the value of the EPR signal of a DPPH reference standard (containing $N = 6.25 \times 10^{16}$ spins) on its displacement from the center along the axis of the cavity is given by $\gamma(h)$. The Q of the cavity at $T = 1.7$ K was 2000, and the resonance frequency was 8907 MHz. The EPR spectra were recorded using modulation of the magnetic field (modulation frequency 2.11 kHz, modulation amplitude $H_M = 1$ G). The magnetic field was monitored by recording the voltage across a standard resistance (10^{-3} Ω) connected to the supply circuit of the superconducting Helmholtz coils. The Helmholtz coils were supplied from a P-138 stabilized dc source controlled by a computer through a digital voltage generator. For modulation of the magnetic field we used a G3-117 oscillator, and the signal from the microwave detector was fed to a computer via a UPI-1 lock-in amplifier and an ATsP-16/60 analog-to-digital converter. The scan of the magnetic field in the 160 G range was done over a time of 5 min.

After recording the EPR signal from the sample we always recorded the signal from a ruby reference crystal placed in the lower part of the cavity (see Fig. 1). The absolute number of atoms in the sample was determined by comparing the signals obtained from the sample and from the

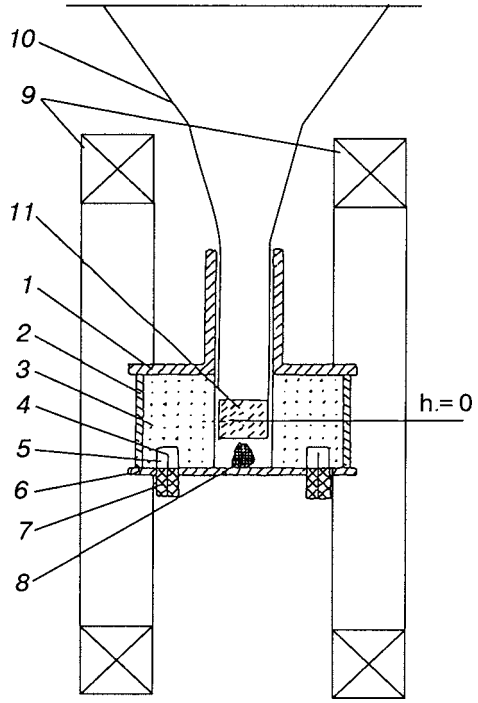

FIG. 1. Disposition of the microwave cavity: *1,6*—end caps of the cavity; *2*—glued-on thin copper rings; *3*—quartz cylinder; *4*—coupling loops; *5*—coupling aperture; *7*—microwave cable; *8*—ruby reference standard; *9*—Helmholtz coils; *10*—quartz cup, *11*—sample.

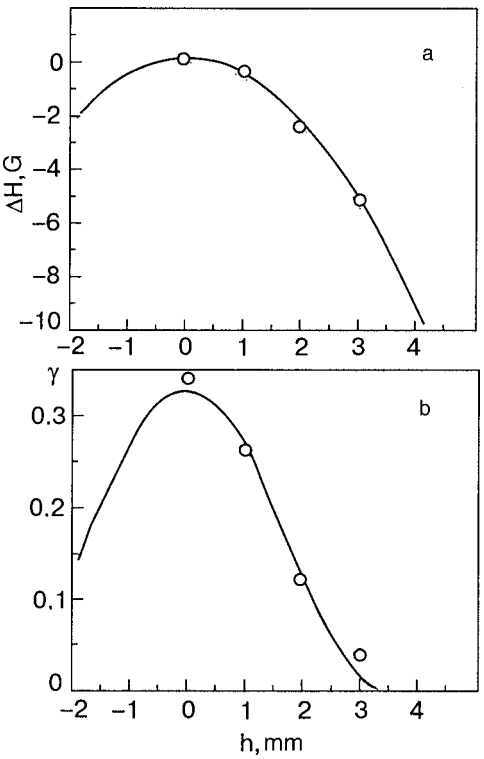

FIG. 2. Nonuniformity $\Delta H(h)$ of the magnetic field produced by the superconducting magnet along the axis of the cavity (a); dependence of the value of the EPR signal $\gamma(h)$ of a standard DPPH sample (number of spins $N = 6.25 \times 10^{16}$) on its displacement from the center along the axis of the cavity (b).

ruby standard under the same experimental conditions. The error in determination of the absolute numbers of atoms did not exceed 20%.

A change in temperature of the IHC samples from 1.7 to 4.2 K was brought about by changing the pressure of the saturated helium vapor in the Dewar. The temperature was measured by a TPK 1.5/20-22 semiconductor thermometer,[20] placed in the conical part of the cup above the sample. For heating above 4.2 K we raised the cup with the sample toward the source of the atoms and waited for the liquid helium to evaporate from the cup and for the temperature of the sample to reach the required value. After that, the sample was repositioned in the cavity and the EPR spectrum of the atoms was recorded at $T=4.2$ K.

The compression (pressing) of the samples was done in a cup filled with He II. The pressing was done using a Teflon cylinder 0.68 cm in diameter and with a mass of 1.2 g, suspended by a thread from a rod. The sample was compressed by the weight of the cylinder and remained in that state after the load was removed.

3. EXPERIMENTAL RESULTS

3.1. Determination of the average concentration of nitrogen atoms stabilized in impurity–helium samples

For determination of the average concentrations of atoms it is necessary to know the volume of the sample and the number of atoms in it. All of the samples studied had a cylindrical shape. After determining the visible diameter and height of the sample, we could calculate its volume. The number of atoms in the samples was determined by the EPR method. It is seen in Figs. 1 and 2 that the height of the registration zone is 0.5 cm. If the height of the sample $h_s < 0.5$ cm, then the number of atoms was determined directly from the measurement with allowance for the intensity distribution of the microwave magnetic field over the height of the sample, while if the sample height $h_s > 0.5$ cm then the number of atoms was calculated after the measurement on the assumption of a uniform distribution of atoms in the sample, i.e., the measured value was multiplied by a coefficient proportional to the ratio of the sample volume to the volume of the registration zone.

Table II gives the absolute numbers of stabilized atoms in the samples, their visible volumes, and the calculated average concentration of atoms for samples obtained by condensation of different gas mixtures. It is seen from Table II that the highest initial concentration of atoms, $n_0=1.2\times^{18}$ cm^{-3}, was achieved by the condensation of a nitrogen-helium gas mixture $[N_2]/[He]=1/100$, and the lowest, equal to 4.5×10^{15} cm^{-3}, as expected, by the condensation of a neon-helium gas mixture containing a minimal ($\sim10^{-3}$%) impurity of molecular nitrogen.

Figure 3 shows the EPR spectra of nitrogen atoms stabilized in samples obtained by the condensation of various gas mixtures.

3.2. Investigation of mechanical action on impurity–helium samples

For each of the samples studied the compression was carried out several times. After each compression the volume of the sample and the number of atoms in it were determined. The results of these studies are presented in Fig. 4. It is seen that in all cases, even for very low initial concentrations, the decrease of the sample volume due to the compression is accompanied by a recombination loss of nitrogen atoms. During the compression the samples were immersed in superfluid helium, and green luminescence in the region $\lambda \sim 520$ nm, propagating downward from the base of the Teflon plunger, was observed visually. The values of the sample volumes and the number and concentration of nitro-

TABLE II. Determination of the average concentration of N(^4S) atoms in impurity–helium samples.

Sample No.	Before pressing (after pressing)			Concentration increase
	Number of atoms in sample, $N_0(N_k)$, x10^6	Visible volume of sample, $V_0(V_k)$, cm^3	Concentration of atoms in sample, $n_0(n_k)$, x10^{17}, cm^{-3}	n_k/n_0
1	62.5 (21.0)	0.96 (0.04)	6.5 (52.5)	8.1
2	72.0 (29.0)	0.6 (0.08)	12.0 (36.0)	3.0
3	17.0 (10.2)	0.2 (0.08)	8.5 (12.1)	1.4
4	27.1 (12.4)	1.15 (0.2)	2.35 (6.2)	2.6
5	8.3 (6.3)	0.96 (0.2)	0.86 (3.0)	3.5
6	1.5 (0.45)	0.6 (0.04)	0.25 (1.1)	4.4
7	0.27 (0.084)	0.6 (0.08)	0.045 (0.105)	2.3

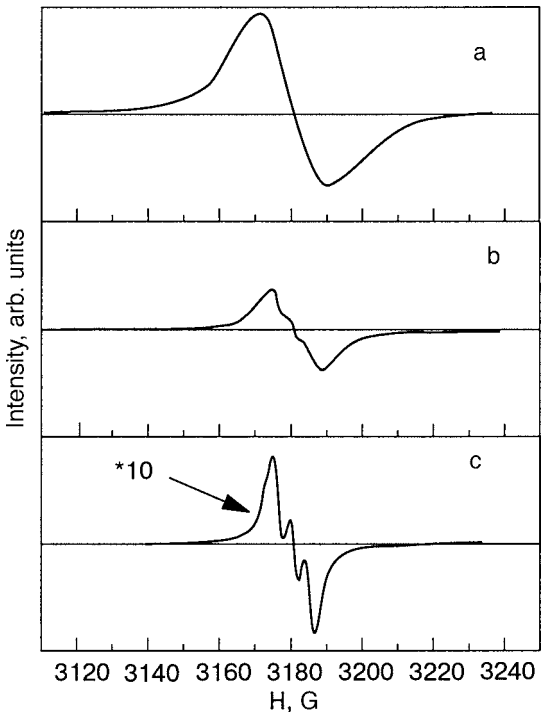

FIG. 3. EPR spectra of nitrogen atoms stabilized at $T=1.7$ K in samples obtained by condensation of various gas mixtures: $[N_2]:[He]=1:100$ (a), $[N_2]:[Ne]:[He]=1:100:10000$ (b), $[Ne]:[He]=1:20$ (c).

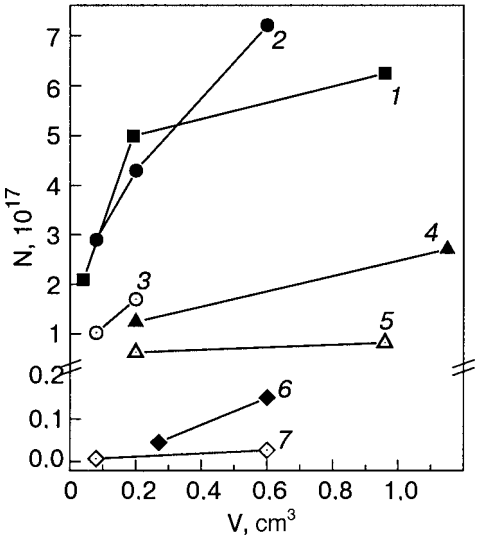

FIG. 4. Variation of the number of nitrogen atoms in IHC samples during their pressing. The curves are labeled by the sample No. in Tables I–III.

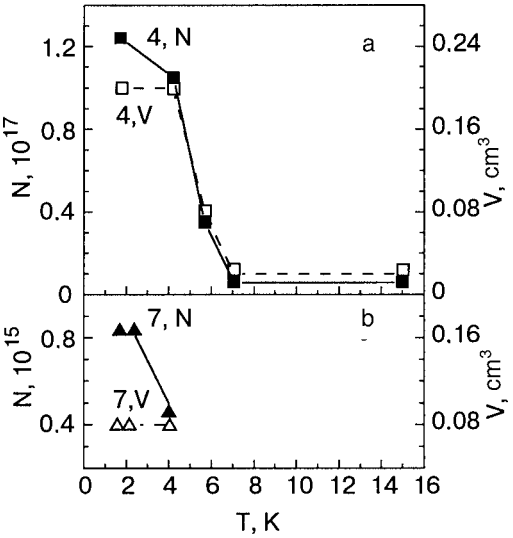

FIG. 5. Temperature dependence of the number of nitrogen atoms (solid curves, left-hand axis) and the visible volume (dashed curves, right-hand axis) for sample No. 4, with $[N_2]:[Ne]:[He]=1:100:10000$ (a) and sample No. 7, with $[Ne]:[He]=1:20$ (b).

gen atoms in the samples immediately after preparation and after pressing are given in Table II. It is seen that, despite the partial recombination, pressing of the samples leads to an increase in the average concentrations of nitrogen atoms in the samples (by a factor of 1.4–8.1). The maximum effect, an eightfold increase in the nitrogen atom concentration, is observed for the nitrogen-helium sample (No. 1): a decrease of the sample volume by a factor of 24 was accompanied by the recombination of 2/3 of the initial number of nitrogen atoms. It should be noted that the relative decrease of the total number of impurity atoms in the samples due to pressing depends weakly on the initial concentration of atoms. For nitrogen-helium and nitrogen-neon-helium samples, in which the initial concentrations of nitrogen atoms differ by more than 2 orders of magnitude (4.5×10^{15}–1.2×10^{18} cm^{-3}), the decrease of the total number of nitrogen atoms on pressing is by a factor of 1.33–3.4.

3.3. Initiation of recombination of nitrogen atoms by heating of IHC samples

In view of the fact that nitrogen-helium samples containing high concentrations of stabilized nitrogen atoms spontaneously explode[21] when removed from the liquid helium, the recombination of nitrogen impurity atoms in IHCs on heating was studied only in neon-helium samples containing low impurities of nitrogen atoms. To determine the influence of the initial concentration of nitrogen atoms on the recombination process we investigated samples condensed from neon-helium mixtures both with the natural impurity level of molecular nitrogen ($\sim$0.001%) and with a 0.01% nitrogen admixture. The temperature dependence of the number of nitrogen atoms in sample No. 4 and the temperature dependence of its visible volume are shown in Fig. 5a. The concentration of nitrogen atoms in the sample at the start of the heating was 6.2×10^{17} cm^{-3}. During heating from 1.7 to 4.2 K the sample was immersed in liquid helium, while the heating to higher temperatures was done for a dry sample. The recombination of nitrogen atoms occurs both in the sample immersed in liquid helium at $T>2.2$ K and in the sample removed from the helium, in the temperature range 4.2–7 K. The fact that heating above 8 K does not lead to recombination of atoms implies that a rigid lattice of impurity particles has already formed by that temperature. Significant structural changes in the sample in the temperature range 4.2–8 K are confirmed by the temperature dependence of the visible volume of the sample presented in Fig. 5a.

Figure 5b shows the number of nitrogen atoms in a neon–helium sample (No. 7) of volume 0.08 cm^3 on heating from 1.7 to 4.2 K. The concentration of nitrogen atoms n_0 in this sample after pressing was 1.05×10^{16} cm^{-3}. The volume of the sample did not change during heating. It is seen that on heating from 1.7 to 2.25 K one does not observe recombination of nitrogen impurity atoms, and only on further heating to 4.2 K does recombination of nitrogen atoms occur in the neon-helium sample. Holding this sample in liquid helium at a temperature of 4.2 K for over 1 hour did not lead to changes in its volume nor in the number of nitrogen atoms stabilized in it.

It is seen in Fig. 5 that the decrease in the number of atoms in a neon-helium sample with a low initial concentration $n_0\approx1.05\times10^{16}$ cm^{-3} occurs only after it is heated above the λ point in helium. We investigated this fact more carefully on the nitrogen-helium samples. For this we measured the number of atoms in the sample near the λ point several times for $T_1<T_\lambda$ first, and then the sample was heated to $T_2>T_\lambda$ and the measurement of the number of atoms in it was repeated. The results of such measurements for three different samples are presented in Fig. 6. It is seen that the λ-point transition in helium initiates recombination of a fraction (up to 40%) of the nitrogen atoms in the nitrogen-helium samples with $n_0\sim10^{18}$ cm^{-3}.

3.4. Processing of the EPR spectra of nitrogen atoms stabilized in impurity–helium samples

Analysis of the shape and width of the EPR line yields a vast amount of information about the interaction of paramagnetic centers in the system. As is seen in Fig. 3, for all the IHC samples the recorded EPR spectra of the nitrogen atoms

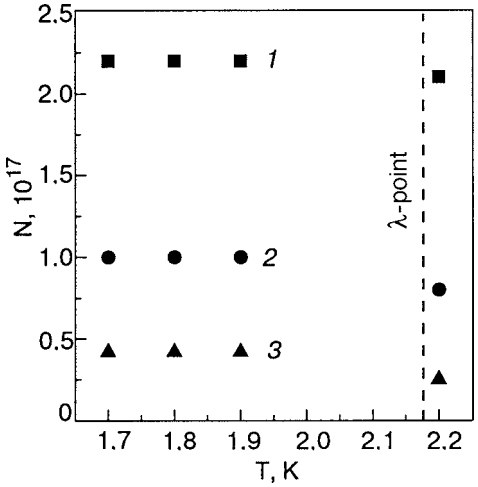

FIG. 6. Temperature dependence of the number of nitrogen atoms in IHC samples immersed in He II upon transition through the λ point: $[N_2]:[He]=1:25$, $n_0=5.5\times10^{18}$ cm^{-3}, $V=0.04$ cm^3 (*1*); $[N_2]:[He]=1:500$, $n_0=1.2\times10^{18}$ cm^{-3}, $V=0.08$ cm^3 (*2*); $[N_2]:[He]=1:500$, $n_0=0.7\times10^{18}$ cm^{-3}, $V=0.06$ cm^3 (*3*).

in the ^4S ground state are strongly broadened. Having determined the width of an individual component of the spectrum, one can obtain estimates of the local concentration of nitrogen atoms in the samples.[22] Determination of the width of individual components in the present study is complicated by the use of a nonuniform superconducting magnet and a quartz cavity of small size, while the macroscopic samples under study were comparatively large, ~0.1–0.5 cm. Thus in the processing of the spectra it was necessary to take into account the nonuniformity of the main magnetic field and the variation of the square of the amplitude of the microwave magnetic field H_1^2 over the height of the cavity.

For determination of the width of the individual components we used a method utilizing the experimentally measured nonuniformity of the magnetic field $\Delta H(h)$ and the measured variation of H_1^2 along the height of the sample. We recorded the EPR signals from a miniature (0.5 mm^3) sample of DPPH placed at different points on the axis of the cavity in the region where the sample was located. The values of the resonance magnetic field were determined from the position of the line center, and the values of H_1^2, from the amplitude of the recorded spectrum. The experimental curves, which are shown in Fig. 2, are well described by the formulas

$$\gamma(h)=A_\gamma\cos^2\left(\frac{\pi h}{d_\gamma}\right), \tag{1}$$

$$H(H_0,h)=H_0-\alpha h^2, \tag{2}$$

where $A_\gamma=0.328$, $d_\gamma=7.04$ mm, and $\alpha=0.590$ G/mm^2.

If the "natural" absorption contour of the sample is denoted by $g(H)$, the contour obtained with the nonuniformity taken into account will be described by the expression

$$\tilde{g}(H)=\frac{1}{h_s}\int_{h_b}^{h_t}\gamma(h)g[H(H_0,h)]dh, \tag{3}$$

where h_t and h_b are, respectively, the coordinates of the top and bottom surfaces of the sample along the axis of the cavity, and $h_s=h_t-h_b$ is the height of the sample.

Since the spectrum was recorded using the method of modulation of the magnetic field (the modulation frequency $\omega=6.3$ kHz and the modulation amplitude $H_M=1$ G), the recorded signal is proportional to the first coefficient of the Fourier series expansion of $\tilde{g}(H)$ (Ref. 23) and is described by the expression

$$f(H)=\frac{1}{\pi}\int_{-\pi}^{\pi}\cos(\omega t)\tilde{g}[H+H_M\cos(\omega t)]d(\omega t). \tag{4}$$

Substituting (3) into (4) and taking (1) and (2) into account, we obtain

$$f(H)=\frac{A_\gamma}{h_s\pi}\int_{-\pi}^{\pi}d(\omega t)\int_{h_b}^{h_t}dh\cos(\omega t)\cos^2\left(\frac{\pi h}{d_\gamma}\right)\times g[H-\alpha h^2+H_M\cos(\omega t)]. \tag{5}$$

As the initial contour for a nitrogen atom we chose a triplet of Lorentzian lines, since under the experimental conditions a chaotic distribution of spins was most likely realized, and the expected relative concentration of atoms was considerably less than 10%:

$$g(H)=A\left\{\frac{1}{1+\left(\frac{H-H_0}{\Delta H_L}\right)^2}+\frac{1}{1+\left(\frac{H-H_0+a}{\Delta H_L}\right)^2}+\frac{1}{1+\left(\frac{H-H_0-a}{\Delta H_L}\right)^2}\right\}, \tag{6}$$

where A is the amplitude, H_0 is the resonance field, a is the hyperfine interaction constant, and ΔH_L is the half width at half maximum of an individual component.

Substituting (6) into (5), we obtain a final expression describing the recorded EPR spectra of nitrogen atoms in IHC samples:

$$f(H)=\frac{AA_\gamma}{h_s\pi}\int_{-\pi}^{\pi}d(\omega t)\int_{h_b}^{h_t}dh\cos(\omega t)\cos^2\left(\frac{\pi h}{d_\gamma}\right)\times\left\{\frac{1}{1+\left(\frac{H-\alpha h^2+H_M\cos(\omega t)-H_0}{\Delta H_L}\right)^2}+\frac{1}{1+\left(\frac{H-\alpha h^2+H_M\cos(\omega t)-H_0+a}{\Delta H_L}\right)^2}+\frac{1}{1+\left(\frac{H-\alpha h^2+H_M\cos(\omega t)-H_0-a}{\Delta H_L}\right)^2}\right\}. \tag{7}$$

In the calculations the integration was done by the method of rectangles.

Some of the parameters were determined experimentally: in particular, $H_M=1$ G, $H_0=3181$ G. The other parameters a, ΔH_L, and A were chosen so as to minimize the mean square deviation of the experimental spectra from the spectra calculated according to formula (7). The mean square deviation was calculated from the formula

TABLE III. Local concentration of N(^4S) atoms in impurity–helium samples.

Sample No.	Half width at half maximum of individual component, ΔH_L, G	Local concentration, $n_L, \times 10^{19}$, cm^{-3}	Average concentration, $n, \times 10^{17}$, cm^{-3}
1	11.0	15.6	6.5
2	12.5	17.7	12
3	13.8	19.6	8.5
4	5.7	8.09	2.25
5	6.0	8.51	0.86
6	3.0	4.25	0.25
7	3.0	4.25	0.045

$$\sigma^2=\sum_i (y_i-f(H_i,a,\Delta H_L,A))^2, \tag{8}$$

where y_i is the intensity of the EPR signal for the field H_i measured experimentally, and $f(H_i)$ is the value calculated according to formula (7).

After a number of attempts we chose the parameter $a=4.2$ G, corresponding to the hyperfine splitting for a nitrogen atom found in a solid nitrogen matrix,[17] which was approximately equal to the splitting found for the nitrogen-helium samples studied.

Then the remaining parameters ΔH_L and A were varied to achieve good agreement of the calculated with the experimental spectrum. The spectra calculated according to formula (7) describe the experimental spectra well. Table III gives the parameters of the calculated spectra for which a good match was achieved to the experimental spectra of nitrogen atoms stabilized in the different impurity-helium samples.

Assuming that the line broadening is due to the dipole-dipole interaction of paramagnetic centers distributed randomly in a rigid lattice, one can obtain a relation between the half width ΔH_L of an individual component of the spectrum and the local atomic concentration n_L:[22]

$$\Delta H_L=\frac{4\pi^2}{9\sqrt{3}}\xi\beta_B n_L, \tag{9}$$

where β_B is the Bohr magneton, and $\xi=3/2$ for equivalent spins.

In that case (the case of equivalent spins) we obtain

$$\Delta H_L[\mathrm{G}]=7.05\cdot 10^{-20} n_L[\mathrm{cm}^{-3}] \quad \text{or} \quad n_L=1.43\cdot 10^{19}\Delta H_L. \tag{10}$$

The values of the local concentrations of nitrogen atoms calculated according to this relation for the different impurity–helium samples are also given in Table III. It is seen that the local concentrations of nitrogen atoms are substantially (about two orders of magnitude) higher than the average concentrations of atoms in the nitrogen-helium samples, while the nitrogen content in the neon-helium samples is much less; as a result, the concentrations differ by 3–4 orders of magnitude.

4. DISCUSSION OF THE RESULTS

For analysis of the processes occurring in IHCs it is necessary to take their structure into account. The concept of IHCs as amorphous solids forming as a result of the freezing of impurity–helium clusters centered around the impurity particles can explain a number of experimental results: the high relative concentrations of nitrogen atoms: $[N]/[N_2]\sim 0.1-0.5$,[6,11] and the elemental composition of the IHCs: $[He]/[Im]\sim 20-60$.[11,16] The spectral studies of N-Rg-helium samples[24] have shown that it is possible for small impurity clusters to be stabilized in solidified helium, and x-ray diffraction studies on samples obtained by injecting impurity particles from a gas jet into bulk superfluid helium in a narrow channel of the x-ray cryostat have shown that it is possible for clusters of impurity particles with a characteristic size of 3–10 nm to be stabilized in solidified helium.[5,8,9] It was concluded on the basis of the data obtained that impurity particles injected from the gas phase into superfluid helium are found mainly in nanoclusters (in the case of molecular nitrogen the number of impurity particles in the clusters reaches 5000). From a comparison of the intensities of the diffraction signals from the impurity atoms and the He atoms in these studies it was possible to estimate the average density of impurity particles found in the helium: $\sim 10^{20}$ cm^{-3} for nitrogen and neon, and $\sim 10^{21}$ cm^{-3} for deuterium. In studying the structure of the deuterium-helium condensates, thanks to the commensurate x-ray scattering intensities on the helium and deuterium atoms, it proved possible to detect the presence of $\sim 10^{21}$ atoms/cm^3 of helium bound to the impurity skeleton.[5]

The EPR method can determine not only the average concentration of atoms in a sample of known volume, from measurements of the absolute number of atoms in it, but also their local concentration—from analysis of the line shapes of the signal. This information also permits analysis of the structure of the sample.

The average concentration of nitrogen atoms in nitrogen-helium samples immediately after their preparation is $\sim 10^{18}$ cm^{-3} (see Table II). If the nitrogen atoms are uniformly distributed in the IHC, then the individual linewidths with the dipole-dipole interaction taken into account should be ~ 70 mG (0.5 G if it is assumed that the trapping sites are orbitally equivalent, mainly on account of the contact interaction of the unpaired electrons with the nuclear magnetic moments of the molecules). The experimentally observed widths, 22–27.6 G (see Table III), exceed this value by more than two orders of magnitude. Such a strong difference of the local and average concentrations of nitrogen atoms in IHC samples is explained by a nonuniform distribution of nitrogen atoms over the sample volume, i.e., the presence of regions with high local concentration—nitrogen nanoclusters. That the nitrogen atoms are located in molecular clusters of nitrogen is confirmed by the value of the hyperfine interaction constant, equal to 4.2 G.

The relative concentration $[N]/[N_2]$ in the nitrogen–helium samples is easily determined from the values ob-

TABLE IV. Specific energy in nitrogen–helium samples containing stabilized N(^4S) atoms.

Composition of condensed mixture $[N_2]/[He]$	Relative concentration of atomic nitrogen		Specific energy	
	$[N]/[N_2]\cdot 100\%$	$[N]/[He]\cdot 100\%$	J/cm^3	J/g
1/25	50	3.6	800	4650
1/40	29.4	2.1	470	2730
1/82	14	1.0	240	1400
1/100	54	3.9	860	5000
1/500	>13	> 0.9	> 210	> 1220

tained for the average and local concentrations. The ratio of the average atomic concentration $\sim 10^{18}$ cm^{-3} to the value of the nitrogen density in the nitrogen-helium samples obtained in x-ray diffraction experiments, $\sim 10^{20}$ cm^{-3}, equals 10^{-2}. A similar value of $[N]/[N_2]$ is obtained from the ratio of the local density of atoms $\approx 2\times 10^{20}$ cm^{-3} (see Table III) to the density of crystalline nitrogen 2.22×10^{22} cm^{-3} (Ref. 25) (assuming that the nanoclusters of molecular nitrogen have a density only a slightly lower than that).

Thus an analysis of the results of EPR studies of nitrogen atoms in nitrogen–helium samples leads to the conclusion that the nitrogen atoms are stabilized mainly in clusters of molecular nitrogen where the ratio of the average concentration to the local concentration is 10^{-2}. In neon-helium samples containing nitrogen as an impurity, the local concentration of the nitrogen impurity atoms exceeds the average concentration over the sample to an even greater degree. This indicates the formation of regions with a high local concentration of nitrogen in the neon-helium samples also.

For the case of the formation of samples of IHCs from clusters of minimum size (containing from one to several nitrogen molecules) it may be possible to achieve a higher relative concentration of nitrogen atoms. From a comparison of previously obtained experimental data on the determination of the elemental composition of IHC samples[10,12] and the EPR spectroscopy of nitrogen atoms in nitrogen-helium samples,[15] one can determine the energy content of the nitrogen-helium condensates.

The values of the relative concentrations of nitrogen atoms and the specific energy for samples obtained by condensation of nitrogen-helium mixtures of different composition which have passed through an rf discharge are presented in Table IV, where the values of the energy content shown are the maximum achieved.

In the calculations we used the value of the stoichiometric coefficient $[He]/[N]=14$ obtained in an experiment with a nitrogen-helium sample prepared with the use of an rf discharge. It is seen that because of the porosity of the samples their specific energy is not large (from 210 to 860 J/cm^3), but due to their low density (slightly larger than the density of liquid helium) the energy content per gram of the sample reaches appreciable values (up to 5 kJ/g), comparable to that of the better explosives.

In addition to such experimental facts as the achievement of a relative concentration $[N]/[N_2]\sim 0.1-0.5$ and the influence of the neon (krypton) content in the condensing gas jet on the shape of the α group,[24] evidence that the samples are formed of ultrafine clusters also comes from the fact that in the preparation of samples at $T\leqslant 1.4$ K we repeatedly observed the spontaneous destruction of nitrogen-helium samples directly in bulk superfluid helium, accompanied by bright flashes and the splashing of a significant amount (several cm^3) of liquid helium from the cup. The flashes occurred in a volume of ~ 1 cm^3, and, as a rule, nothing but liquid helium was observed in that part of the cup prior to the flash. This phenomenon can be explained by the fact that together with a high energy content, those samples have a somewhat different structure: such small clusters are hardly capable of forming an impurity skeleton with large pores (up to 800 nm in size, in which case the total pore volume in the sample can comprise up to 80% of its visible volume),[11] and in the absence of a rigid skeleton a much larger part of the volume is filled with the impurity substance and helium bound to it. In such a case, despite the fact that the sample is immersed in He II, heat transfer should be impeded at the sites of the highest concentration of the impurity substance, and as a result of recombination of the nitrogen atoms, local hot spots can appear which initiate further recombination of the nitrogen atoms. Thus the region with the highest concentration of nitrogen atoms burns itself out, while the helium in the overheating zone evaporates rapidly, forming a bubble that forces liquid helium out of the cup. The small size of the clusters and of the pores between them also explains why they cannot be seen.

It is clear that the energy content of these samples is in principle higher than that which can be reached at higher temperatures by simple mechanical pressing. This follows already from the fact that even at equal densities of the impurity substance, the number of nitrogen atoms in the samples obtained at $T<1.4$ K is an order of magnitude larger. In addition, pressing of the sample leads to initiation of recombination of the atoms: the clusters approach until their surfaces touch, since the helium adsorbed on the surfaces is not so tightly bound as to prevent this approach. The interaction of nitrogen atoms can initiate local heating and further recombination of the atoms in the immediate environment, leading to a decrease in the number of stabilized atoms.

It should be noted that at the high values of the local concentrations of nitrogen atoms (8×10^{20} cm^{-3}) stabilized in the nitrogen-helium samples[6] one expects to see exchange narrowing of the lines in the EPR spectra of the atoms.[22] Also of significant interest are processes occurring in the stage of destruction of nitrogen-helium samples containing high concentrations of stabilized nitrogen atoms. The compaction of the samples at the start of the their destruction causes an increase in the concentration of atoms and apparently causes the concentration of radicals to reach the limiting values for such systems. Further compaction of the samples is accompanied by recombination of a large fraction of the atoms stabilized in the sample. Knowledge of the lim-

iting concentrations of nitrogen atoms in impurity–helium condensates would permit determination of the energy content attainable in such systems. For studying such transient process it is necessary to use methods with higher time resolution for determining the number of spins in the samples. The use of pulsed EPR would make it possible to study unstable samples of nitrogen-helium condensates prepared at $T \leqslant 1.4$ K. From the parameters of the EPR spectra of the nitrogen atoms stabilized in clusters, one can determine whether or not the samples are formed by clusters of several nitrogen molecules. Recently a pulsed EPR spectrometer was built at Cornell University (USA) for studying fast processes in IHC samples.

The data obtained in the present study also confirm that both mechanical pressing and heating of impurity–helium samples are accompanied by a decrease of the number of nitrogen atoms in the ground state. This is evidence of recombination of nitrogen atoms in the samples, which gives rise to the metastable molecules and atoms of nitrogen responsible for the luminescence. Thus we have obtained direct experimental proof of the occurrence of thermoluminescence of impurity–helium samples containing stabilized nitrogen atoms by the mechanism proposed by Edwards for explaining the thermoluminescence of nitrogen atoms in a molecular nitrogen matrix.[17]

These studies have demonstrated the possibility of making measurements on IHC samples of progressively increasing density. The possibility of varying the geometry of IHCs (varying the pore size distribution) and density of an impurity substance (stabilized radicals) in the course of an experiment offers new prospects for doing low-temperature experiments, in particular, on the properties of superfluid helium in a restricted geometry with variation of the porosity of the sample during the experiment and for studying the dependence on the impurity density of the sound conversion efficiency in He II.[14]

CONCLUSION

The results obtained in this study permit the following conclusions.

(1) We have registered the recombination loss of nitrogen atoms in impurity–helium condensates (IHCs) during mechanical pressing of the samples in He II and during their heating in the temperature range 1.7–7 K. This proves that the cause of the thermoluminescence of IHC samples containing nitrogen atoms in the ground state is their recombination, which leads to the formation of excited atoms and nitrogen molecules. In the case of stabilization of high concentrations of nitrogen atoms in nitrogen-helium samples the explosive destruction of such samples can occur even in bulk superfluid helium.

(2) The results of EPR studies of IHC samples containing stabilized nitrogen atoms have shown that the nitrogen atoms reside mainly at the surface and in the interior of impurity clusters that form a porous structure of the samples.

(3) We have shown that it is possible in principle to increase effectively (by up to 8 times) the specific energy of nitrogen-helium condensates containing nitrogen atoms by mechanical pressing of IHC samples in superfluid helium.

(4) Experiments at helium temperatures were carried out on samples whose properties (volume, density of the impurity substance, and the concentration of stabilized radicals, pore size distribution) can be varied in a deliberate manner during the course of an experiment. This unique feature of IHCs opens up new prospects for low-temperature research.

*E-mail: boltnev@binep.ac.ru

[1] V. V. Nesvizhevsky, Yad. Fiz. **65**, 426 (2002) [Phys. At. Nucl. **65**, 400 (2002)].
[2] G. Frossati, J. Low Temp. Phys. **111**, 521 (1998).
[3] R. E. Boltnev, G. Frossati, E. B. Gordon, I. N. Krushinskaya, E. A. Popov, and A. Usenko, J. Low Temp. Phys. **127**, 245 (2002).
[4] B. Palaszewski, L. S. Ianovski, and P. Carrick, J. of Prop. and Power **14**, 641 (1998).
[5] E. P. Bernard, R. E. Boltnev, V. V. Khmelenko, V. Kiryukhin, S. I. Kiselev, and D. M. Lee, Phys. Rev. B **69**, 104201 (2004).
[6] E. P. Bernard, R. E. Boltnev, V. V. Khmelenko, and D. M. Lee, J. Low Temp. Phys. **134**, 199 (2004).
[7] E. B. Gordon, L. P. Mezhov-Deglin, and O. F. Pugachev, JETP Lett. **19**, 103 (1974).
[8] V. Kiryukhin, B. Keimer, R. E. Boltnev, V. V. Khmelenko, and E. B. Gordon, Phys. Rev. Lett. **79**, 1774 (1997).
[9] S. I. Kiselev, V. V. Khmelenko, D. M. Lee, V. Kiryukhin, R. E. Boltnev, E. B. Gordon, and B. Keimer, Phys. Rev. B **65**, 024517 (2001).
[10] R. E. Boltnev, E. B. Gordon, I. N. Krushinskaya, A. A. Pel'menev, E. A. Popov, O. F. Pugachev, and V. V. Khmelenko, Fiz. Nizk. Temp. **18**, 819 (1992) [Low Temp. Phys. **18**, 576 (1992)].
[11] E. B. Gordon, V. V. Khmelenko, A. A. Pelmenev, E. A. Popov, O. F. Pugachev, and A. F. Shestakov, Chem. Phys. **170**, 411 (1993).
[12] R. E. Boltnev, E. B. Gordon, I. N. Krushinskaya, M. V. Martynenko, A. A. Pel'menev, E. A. Popov, V. V. Khmelenko, and A. F. Shestakov, Fiz. Nizk. Temp. **23**, 753 (1997) [Low Temp. Phys. **23**, 567 (1997)].
[13] S. I. Kiselev, V. V. Khmelenko, and D. M. Lee, J. Low Temp. Phys. **121**, 671 (2000).
[14] Peter Brusov, J. M. Parpia, Paul Brusov, and G. Lawes, Phys. Rev. B **36**, 140507 (2001).
[15] E. B. Gordon, A. A. Pel'menev, E. A. Popov, O. F. Pugachev, and V. V. Khmelenko, Fiz. Nizk. Temp. **15**, 86 (1989) [Sov. J. Low Temp. Phys. **15**, 48 (1989)].
[16] R. E. Boltnev, E. B. Gordon, V. V. Khmelenko, I. N. Krushinskaya, M. V. Martynenko, A. A. Pelmenev, E. A. Popov, and A. F. Shestakov, Chem. Phys. **189**, 367 (1994).
[17] J. W. Edwards, "Chemical and physical studies of trapped radicals," in *Formation and Trapping of Free Radicals*, A. M. Bass and H. P. Broida (eds.), Academic Press, New York (1960).
[18] E. B. Gordon, V. V. Khmelenko, A. A. Pelmenev, E. A. Popov, and O. F. Pugachev, Chem. Phys. Lett. **155**, 301 (1989).
[19] E. B. Gordon, A. A. Pel'menev, O. F. Pugachev, and V. V. Khmelenko, Fiz. Nizk. Temp. **8**, 601 (1982) [Sov. J. Low Temp. Phys. **8**, 299 (1982)].
[20] L. I. Zarubin and I. Yu. Nemish, Poluprovodn. Tekh. Mikroelektron. **16**, 3 (1974).
[21] R. E. Boltnev, I. N. Krushinskaya, A. A. Pelmenev, D. Yu. Stolyarov, and V. V. Khmelenko, Chem. Phys. Lett. **305**, 217 (1999).
[22] Ya. S. Lebedev and V. I. Muromtsev, *EPR and Relaxation of Free Radicals* [in Russian], Khimiya, Moscow (1972).
[23] C. P. Poole, *Experimental Techniques in Electron Spin Resonance*, Wiley, New York (1966), Mir, Moscow (1970).
[24] R. E. Boltnev, E. B. Gordon, V. V. Khmelenko, M. V. Martynenko, A. A. Pelmenev, E. A. Popov, and A. F. Shestakov, J. Chim. Phys. **92**, 362 (1995).
[25] B. I. Verkin and A. F. Prikhod'ko (eds.), *Cryocrystals* [in Russian], Naukova Dumka, Kiev (1992).

Translated by Steve Torstveit

Superfluidity and charged vortices in systems with spontaneous interlayer coherence in the low-density limit

S. I. Shevchenko*

B. Verkin Institute for Low Temperature Physics and Engineering, National Academy of Sciences of Ukraine, pr. Lenina 47, Kharkov 61103, Ukraine

K. A. Nasedkin

National Technical University "Kharkov Polytechnical Institute," ul. Frunze 21, Kharkov 61002, Ukraine

(Submitted December 20, 2004)
Fiz. Nizk. Temp. **31**, 735–744 (July 2005)

The conditions for formation of a bound state between two-dimensional spatially separated electron and hole in a magnetic field normal to the plane of motion of the carriers are investigated. The binding energy, effective mass, and electric polarizability of the electron-hole pair are found as functions of the distance d between conducting layers. The features of the superfluidity of a Bose gas of electron-hole pairs in the case of low density are analyzed. It is established that quantized vortices in the superfluid phase have real electric charge, the value of which depends on the density of pairs and the distance between layers. In the case of small d and high magnetic fields the vortex charge $q=\nu e$, where ν is the filling factor of the lowest Landau level by carriers. The stability of the Bose gas of pairs against transition to the crystalline state is investigated, and it is shown that at small d the pair crystallization temperature T_m is substantially below the superfluid transition temperature T_c. With increasing d the temperature T_m grows more rapidly than T_c, and there exists a critical value d at which the superfluid phase vanishes. © *2005 American Institute of Physics.* [DOI: 10.1063/1.2001628]

1. INTRODUCTION

Experimental evidence of superfluidity of electron-hole pairs in two-layer electron systems has been presented in a number of recent papers.[1–3] We are talking about two-layer systems with electronic conductivity in a strong electric field normal to the layers in the case when the total filling factor of the layers $\nu_T \equiv \nu_1 + \nu_2 = 1$. In this case the number of unfilled sites, i.e., holes in the Landau band of one layer, is equal to the number of electrons in this same Landau band in another layer, and, owing to the Coulomb interaction, the electrons can form bound pairs with the holes. The current states of such pairs are accompanied by equal and oppositely directed electric currents, which are nondissipative below the temperature of the transition of the pairs to the superfluid state. The idea that superfluidity can exist in systems with pairing of spatially separated electrons and holes was first stated in Refs. 4 and 5. For the case of two-layer electron systems in a strong magnetic field these ideas were developed in Refs. 6–13.

As in other superfluid systems, quantized vortices can arise in systems with pairing of spatially separated electrons and holes. Rather unexpectedly it has turned out that although the electron-hole system is electronically neutral, in a strong magnetic field all the vortices carry real electric charge, localized at the center of the vortex. The presence of charge in the vortices was first noted in Ref. 9 for systems with filling factors $\nu_1 = \nu_2 = 1/2$, and it was predicted that the vortex charge should have a universal value $q=(1/2)e$. It was shown in a paper by one of the authors[14] that the appearance of electric charge on a vortex occurs in all superfluid systems in magnetic field and not just in electron-hole ones. This charge is quantized owing to the topological properties of the phase of the order parameter, but in the general case it is fractional. However, only in electron-hole superfluid systems does the vortex charge have a universal value $q=\nu e$, where $\nu = \nu_e = \nu_h$ (ν_e and ν_h are the filling factors of the Landau level for electrons in one layer and for holes in the other). In the other superfluid systems, because of the small electric polarizability and large mass of the atoms, the vortex charge is too small to be observed.

In Ref. 14 the properties of a two-layer structure in a strong magnetic field were investigated in the limit when the thickness d of the insulator layer separating the conducting layers is smaller than all lengths of the problem (in particular, d is less than the magnetic length $l_B=(c\hbar/eB)^{1/2}$ and the distance between carriers $n^{-1/2}$). But the case when d is not small *is* of interest, since systems with large d are easier to implement experimentally. However, with increase of d there is the danger of destroying the interlayer coherence because of different dependence on d of the potential and kinetic energies of the pairs. In this paper we study the properties of systems with pairing of spatially separated electrons and holes as the distance between conducting layers is increased. We consider the low density limit, when the mean distance between electron-hole pairs is much greater than the size of a pair. We obtain the dependence on d of the vortex charge and effective mass of an electron-hole pair, and we investigate the stability of the system of pairs against transition to the crystalline state.

2. ELECTRON-HOLE PAIR IN CROSSED ELECTRIC AND MAGNETIC FIELDS

Let us consider a two-layer system in a strong magnetic field normal to the layers. We shall assume that in one layer the charge carriers are electrons, and in the other, holes. We emphasize that in the absence of magnetic field both layers can have electronic conductivity. As was shown in Ref. 15, the particle-hole transformation carried out in the presence of a magnetic field in one of the layers causes the filling factor of the layer undergoing transformation to change from ν to $1-\nu$ and the sign of the current carrier to change from negative to positive. Therefore for a two-layer electron system the filling factors of which satisfy the equation $\nu_1+\nu_2=1$, after particle-hole transformation in one of the layers we arrive at an electron-hole system in which $\nu_e=\nu_h=\nu$. For generality we shall assume that the hole mass m_h is unequal to the electron mass m_e. In semiconductor heterostructures with layers which in the absence of magnetic field have electronic and hole-type conduction, usually $m_e=0.067m_0$ and $m_h=0.4m_0$, where m_0 is the free electron mass. In the low density limit under consideration here the electrons and holes are paired in coordinate space, and the pairing problem reduces to solution of the Schrödinger equation for a single electron-hole pair:

$$\left[\frac{1}{2m_e}\left(-ih\nabla_e+\frac{e}{c}\mathbf{A}_e\right)^2+\frac{1}{2m_h}\left(-ih\nabla_h-\frac{e}{c}\mathbf{A}_h\right)^2+e\mathbf{E}\cdot(\mathbf{r}_e-\mathbf{r}_h)-\frac{e^2}{\varepsilon_0\sqrt{|\mathbf{r}_e-\mathbf{r}_h|^2+d^2}}\right]\Psi(\mathbf{r}_e,\mathbf{r}_h)=\varepsilon\Psi(\mathbf{r}_e,\mathbf{r}_h). \tag{1}$$

Here $\mathbf{r}_e$ and $\mathbf{r}_h$ are two-dimensional radius vectors describing the positions of the electron and hole in their respective conducting layers (the conducting layers are assumed two-dimensional), d is the distance between conducting layers, and ε_0 is the dielectric constant of the system (the same for both layers). In writing this equation we have assumed that, in addition to the magnetic field $\mathbf{B}=\mathrm{curl}\,\mathbf{A}$, an electric field $\mathbf{E}$ of equal strength in both layers is applied parallel to the layers. We take the electron charge as $-e$.

A decisive circumstance for solution of Eq. (1) is the existence of a pair momentum operator

$$\hat{\boldsymbol{\pi}}=\left(-i\hbar\nabla_e+\frac{e}{c}\mathbf{A}_e\right)+\left(-ih\nabla_h-\frac{e}{c}\mathbf{A}_h\right)-\frac{e}{c}\mathbf{B}\times(\mathbf{r}_e-\mathbf{r}_h), \tag{2}$$

which, as was shown by Gor'kov and Dzyaloshinskii,[16] commutes with the Hamiltonian (1), and all the components of which commute with each other. The eigenfunctions of Eq. (2) are therefore simultaneously eigenfunctions of the operator $\hat{\boldsymbol{\pi}}$, and the energy ε is a function of the eigenvalues $\boldsymbol{\pi}$ of that operator.

For solution of Eq. (1) it is convenient, as in Ref. 14, to transform to a new representation in which the wave function $\tilde{\psi}=U\psi$, where

$$\hat{U}=\exp\left(i\frac{e}{c}\frac{\mathbf{A}(\mathbf{R})\cdot\mathbf{r}}{\hbar}\right). \tag{3}$$

Here $\mathbf{R}=(m_e\mathbf{r}_e+m_h\mathbf{r}_h/m_e+m_h)$ is the coordinate of the center of mass, and $\mathbf{r}=\mathbf{r}_e-\mathbf{r}_h$ is the relative coordinate. The advantage of this representation is that irrespective of the gauge of the vector potential $\mathbf{A}$, the momentum operator of a pair has the very simple form

$$\hat{\boldsymbol{\pi}}=U\hat{\pi}U^{-1}=-ih\frac{\partial}{\partial\mathbf{R}}. \tag{4}$$

Since the eigenfunction of this operator is $\exp(i\boldsymbol{\pi}\cdot\mathbf{R}/\hbar)$, we readily find that in the new representation the wave function of a pair with momentum $\boldsymbol{\pi}$ is equal to

$$\tilde{\Psi}(\mathbf{R},\mathbf{r})=\exp(i\boldsymbol{\pi}\cdot\mathbf{R}/\hbar)\Phi_\pi(\mathbf{r}). \tag{5}$$

The equation for the function $\Phi_\pi(\mathbf{r})$ can be obtained by substitution of Eq. (5) into the equation $\tilde{H}\tilde{\Psi}=E\tilde{\Psi}$, where $\tilde{H}=U\hat{H}U^{-1}$, and $\hat{H}$ is the operator on the left-hand side of Eq. (1). As a result, we arrive at the equation

$$\left[-\frac{\hbar^2}{2m}\frac{\partial^2}{\partial\mathbf{r}^2}-\frac{ie\hbar}{2mc}\gamma(\mathbf{B}\times\mathbf{r})\cdot\frac{\partial}{\partial\mathbf{r}}+\frac{e^2}{8mc^2}B^2r^2+\frac{e}{Mc}(\mathbf{B}\times\mathbf{r})\cdot\boldsymbol{\pi}+e\mathbf{E}\cdot\mathbf{r}-\frac{e^2}{\varepsilon_0\sqrt{r^2+d^2}}+\frac{|\pi|^2}{2M}\right]\Phi_\pi(\mathbf{r})=\varepsilon\Phi_\pi(\mathbf{r}). \tag{6}$$

Here $M=m_e+m_h$ is the total mass of a pair, $m=(m_em_h/m_e+m_h)$ is the reduced mass, and $\gamma=(m_h-m_e/m_h+m_e)$. The solution of Eq. (6) was found in Ref. 14 under the conditions

$$a_B^e\gg a_B^h,\quad l_B\gg d, \tag{7}$$

where $a_B^{e(h)}=(\hbar\varepsilon_0/e^2m_{e(h)})$ is the Bohr radius of the electron (hole). The first of these inequalities allows one to take the kinetic energy of the hole and potential energy of the electron-hole interaction into account using perturbation theory. Here, generally speaking, it is not assumed that the kinetic energy of the hole is much greater than the potential energy. The solution yields the energy of an electron-hole pair as a function of the pair momentum. The energy correction depends on the momentum $\boldsymbol{\pi}$ and electric field $\mathbf{E}$ as

$$\Delta\varepsilon=\frac{1}{2M_*}\left(\pi+\alpha(B)\frac{[\mathbf{E}\times\mathbf{B}]}{c}\right)^2-\frac{\alpha(B)}{2}E^2. \tag{8}$$

Here the effective mass of a pair is

$$M_*=M+M_B, \tag{9}$$

where the magnetic mass

$$M_B=\frac{4}{\sqrt{2\pi}}\frac{\varepsilon_0\hbar^2}{e^2l_B} \tag{10}$$

depends only on the magnetic field.

The quantity

$$\alpha(B)=M_B\frac{c^2}{B^2} \tag{11}$$

has the meaning of the electric polarizability of a pair. An expression analogous to (8) was obtained in Ref. 17 for an electrically neutral atom in crossed fields at low magnetic

fields. In that case Eq. (8) contains the polarizability of an atom in zero magnetic field, $\alpha(0)$, instead of $\alpha(B)$, and the mass of the atom, M, instead of the effective mass M_*. The expression obtained in Ref. 17 was rediscovered 20 years later in Ref. 18.

By differentiating (8) with respect to $\boldsymbol{\pi}$ we find the velocity $\mathbf{v}$ of a pair, and differentiation of (8) with respect to $\mathbf{E}$ gives (with the opposite sign) the dipole moment $\mathbf{p}$ of a pair.

Equation (6) can also be solved for large d. We assume that d is much greater than the size of a pair in the plane of a conducting layer. (The corresponding restriction on the parameters of the system will be obtained below.) Then the potential energy in Eq. (6) can be expanded in powers of $(r/d)^2$. As a result, the potential energy is written in the form $-(e^2/\varepsilon_0 d)+\frac{1}{2}(e^2r^2/\varepsilon_0 d^3)$. After this substitution Eq. (6) can be solved exactly. We seek a wave function $\Phi_\pi(\mathbf{r})$ in the form[16,19]

$$\Phi_\pi(\mathbf{r})=\Phi(\mathbf{r}-\eta\rho_0)\exp\left(i\frac{\mathbf{r}\cdot\boldsymbol{\pi}}{2\hbar}\gamma\eta\right). \tag{12}$$

We shall start by assuming, as in Ref. 19, that there is no electric field. Then

$$\boldsymbol{\rho}_0=c\frac{(\mathbf{B}\times\pi)}{eB^2}. \tag{13}$$

The function η is chosen in such a way that the terms containing $\boldsymbol{\pi}\times\mathbf{r}$ and $\boldsymbol{\pi}\times(\partial/\partial\mathbf{R})$ in Eq. (6) vanish. As a result, we find that

$$\eta=4\frac{m}{M}\frac{1}{\beta^2-\gamma^2}, \tag{14}$$

where $\beta^2=1+(4l_B^4/a_B d^3)$ (we have corrected the numerical error in β that was made in Ref. 19), and $a_B=\varepsilon_0\hbar^2/me^2$ is the effective Bohr radius.

After substituting (12) into (6), we obtain

$$\varepsilon=\frac{|\boldsymbol{\pi}|^2}{2M}(1-\eta)-\frac{e^2}{\varepsilon_0 d}+\varepsilon_{n,s}. \tag{15}$$

Here $\varepsilon_{n,s}$ are the eigenvalues of the equation

$$\left(-\frac{h^2}{2m}\frac{\partial^2}{\partial\mathbf{r}}-i\hbar\frac{e}{c}\frac{1}{2m}\gamma(\mathbf{B}\times\mathbf{r})\cdot\frac{\partial}{\partial\mathbf{r}}+\frac{e^2}{8mc^2}B^2r^2\beta^2\right)\Phi_{n,s}(\mathbf{r})$$
$$=\varepsilon_{n,s}\Phi_{n,s}(\mathbf{r}). \tag{16}$$

It follows from (16) that the wave function $\Phi_{n,s}(\mathbf{r})$ has the form

$$\Phi_{n,s}(\mathbf{r})=\sqrt{\frac{n!\beta}{2\pi(n+|s|!)}}\exp\left(\frac{is\varphi}{l_B}\right)$$
$$\times\left(\sqrt{\frac{\beta}{2}}\frac{r}{l_B}\right)^{|s|}L_n^{|s|}\left(\frac{\beta r^2}{2l_B^2}\right)\exp\left(\frac{\beta r^2}{4l_B^2}\right). \tag{17}$$

Using Eq. (12), one can easily verify that an electron-hole pair with nonzero momentum $\boldsymbol{\pi}$ has a nonzero dipole moment $\mathbf{p}$.

Indeed, the dipole moment of a pair is

$$\mathbf{p}=-e\langle\mathbf{r}\rangle=-e\int\Phi^*(\mathbf{r}-\eta\rho_0)\mathbf{r}\Phi(\mathbf{r}-\eta\rho_0)d\mathbf{r}$$
$$=-e\int\Phi^*(\mathbf{r})(\mathbf{r}+\eta\rho_0)\Phi(\mathbf{r})d\mathbf{r}$$
$$=-e\eta\rho_0=-\eta c\frac{(\mathbf{B}\times\boldsymbol{\pi})}{B^2}. \tag{18}$$

It is useful to obtain this result in another way also. As Gor'kov and Dzyaloshinskii showed,[16] the following relation holds between the momentum $\boldsymbol{\pi}$ of a pair, its velocity $\mathbf{v}$, and its dipole moment $\mathbf{p}$:

$$\boldsymbol{\pi}=M\mathbf{v}+\frac{1}{c}\mathbf{p}\times\mathbf{B}. \tag{19}$$

But it follows from (15) that

$$\mathbf{v}=\frac{\partial\varepsilon}{\partial\boldsymbol{\pi}}=(1-\eta)\frac{\pi}{M}. \tag{20}$$

Substituting this expression for the velocity into (19), we find

$$\eta\boldsymbol{\pi}=(\mathbf{B}\times\mathbf{p})/c, \tag{21}$$

which agrees with Eq. (18). Hence we arrive at an important conclusion: for calculating the dipole moment of a pair one does not need to know its wave function. The dipole moment can be calculated if an expression for the energy is known.

Up until now we have assumed that the electric field $\mathbf{E}$ is equal to zero. It is easy to generalize the results obtained to the case of nonzero electric fields. For this it is sufficient to notice that in the presence of an electric field the terms linear in $\mathbf{r}$ in Eq. (6) are

$$\left(\frac{e}{cM}[\boldsymbol{\pi}\times\mathbf{B}]+e\mathbf{E}\right)\cdot\mathbf{r}=\frac{e}{cM}\left[\left(\boldsymbol{\pi}+\frac{cM}{B^2}\mathbf{B}\times\mathbf{E}\right)\times\mathbf{B}\right]\cdot\mathbf{r}. \tag{22}$$

Therefore in the presence of an electric field the pair momentum $\boldsymbol{\pi}$ in Eq. (6) is replaced by an effective momentum

$$\boldsymbol{\pi}_{\text{eff}}=\boldsymbol{\pi}+\frac{cM}{B^2}\mathbf{B}\times\mathbf{E}. \tag{23}$$

Then the energy of a pair is [cf. Eq. (15)]

$$\varepsilon=\frac{|\pi|^2}{2M}-\eta\frac{|\pi_{\text{eff}}|^2}{2M}-\frac{e^2}{\varepsilon_0 d}+\varepsilon_{n,s}. \tag{24}$$

We now introduce the notation

$$M_*\equiv\frac{M}{1-\eta} \tag{25}$$

and

$$\alpha(B)=(M_*-M)\frac{c^2}{B^2}. \tag{26}$$

Then it is easily verified that the first two terms in Eq. (24), i.e., that part of the energy which depends on the momentum $\boldsymbol{\pi}$ and electric field $\mathbf{E}$, coincides exactly with the energy $\Delta\varepsilon$ from (8). The new definition of the electric polarizability (26) is more general than definition (11); it goes over to (11) for $a_B^e\gg a_B^h$, $l_B\gg d$.

3. SUPERFLUIDITY OF PAIRS IN THE LOW DENSITY LIMIT

We now turn from an individual electron-hole pair to a system of pairs. In the low density limit the pairs can be treated as true bosons, and if they did not interact, then for $T=0$ Bose condensation would occur in the system, and all the pairs would condense to the state with minimum energy. In reality there is an interaction between pairs, which is short-ranged because of their electrical neutrality. In this case at low density the interaction leads to a weak "depletion" of the Bose condensate. As a result, the well-known arguments of Gross and Pitaevskii (see, e.g., Ref. 20) are applicable to this system, and one can replace the field operator of a pair by a c-number order parameter ψ. It follows from Eq. (8) that the order parameter must satisfy the nonlinear Schrödinger equation

$$i\hbar\frac{\partial\psi}{\partial t}=\frac{1}{2M_*}\left(-i\hbar\nabla+\alpha(B)\frac{[\mathbf{E}\times\mathbf{B}]}{c}\right)^2\psi-\frac{\alpha(B)}{2}E^2\psi+\gamma|\psi|^2\psi. \tag{27}$$

The last term on the right-hand side of (27) describes the interaction between pairs. An explicit expression for it will be given below.

For Eq. (27) one can easily obtain a continuity equation for the superfluid component and an expression for the superfluid current density $\mathbf{j}_s$:

$$\mathbf{j}_s=\frac{i\hbar}{2M_*}(\psi\nabla\psi^*-\psi^*\nabla\psi)+\frac{\alpha(B)}{M_*c}\mathbf{E}\times\mathbf{B}\psi^*\psi. \tag{28}$$

If the order parameter is written in the form $\psi=|\psi|e^{i\varphi(r)}$, then the superfluid velocity $\mathbf{v}_s$ will be equal to ($\mathbf{j}_s=\mathbf{v}_s\psi^*\psi$)

$$\mathbf{v}_s=\frac{1}{M_*}\left(\hbar\nabla\varphi+\alpha(B)\frac{\mathbf{E}\times\mathbf{B}}{c}\right). \tag{29}$$

It follows from this expression that crossed electric and magnetic fields induce undamped flows in an electrically neutral superfluid liquid, similarly to how a vector potential field induces supercurrents in a superconductor. The analogy with superconductors will be even more complete if it is noted that the following equation holds in superconductors (the field accelerates electrons continuously)

$$m\frac{d\mathbf{v}_s}{dt}=e\mathbf{E}=-\frac{e}{c}\frac{\partial\mathbf{A}}{\partial t}. \tag{30}$$

The total derivative is related to the partial derivative describing the variation of $\mathbf{v}_s$ at a given point in space by the relation $(d/dt)=(\partial/\partial t)+\mathbf{v}\cdot(\partial/\partial\mathbf{r})$.

In view of the fact that the current velocities $\mathbf{v}$ are small compared with the Fermi velocity, one can replace the total derivative by the partial. Integrating the resulting equation and taking the constant of integration equal to zero, we obtain the familiar result

$$\mathbf{v}_s=-\frac{e}{mc}\mathbf{A}. \tag{31}$$

In a similar way, in crossed electric and magnetic fields a superfluid liquid is continuously accelerated by the Abragam force, which in the case of a medium with magnetic permeability $\mu=1$ is equal to[21]

$$\mathbf{F}_A=\frac{\alpha(B)}{c}\frac{\partial}{\partial t}(\mathbf{E}\times\mathbf{B}), \tag{32}$$

so that

$$M_*\frac{d\mathbf{v}_s}{dt}=\frac{\alpha(B)}{c}\frac{\partial}{\partial t}(\mathbf{E}\times\mathbf{B}). \tag{33}$$

Replacing the total derivative in (33) by a partial derivative, in view of the low current velocities, and assuming that only the electric field varies with time, after integration over time, under the condition that the constant of integration is equal to zero, we obtain

$$\mathbf{v}_s=\frac{\alpha(B)}{M_*c}\mathbf{E}\times\mathbf{B}. \tag{34}$$

Expression (34) coincides with the second term in Eq. (29). Substituting into (34) the polarizability $\alpha(B)$ from (26), we obtain

$$\mathbf{v}_s=\left(1-\frac{M}{M_*}\right)c\frac{\mathbf{E}\times\mathbf{B}}{B^2}. \tag{35}$$

As we shall see below, the mass M_* increases with increasing magnetic field, so that the ratio M/M_* decreases with increasing B. Under the conditions $a_B^e, a_B^h \gg l_B$ the ratio $M/M_* \ll 1$, so that in this case

$$\mathbf{v}_s=c\frac{\mathbf{E}\times\mathbf{B}}{B^2}. \tag{36}$$

But the expression standing on the right-hand side of Eq. (36) is the velocity at which the free charge is moving in the crossed electric and magnetic fields. Since this velocity is independent of the value of the charge, both the electron and hole, and, hence, the pair as a whole, will move at this velocity. This result is completely natural, since for $a_B^e, a_B^h \gg l_B$ the Coulomb energy of a pair is small in comparison with the energy of the pair in the magnetic field and, consequently, the pair can to a first approximation be assumed free.

Let us return to the question of the dipole moment of the superfluid component. With the aid of Eqs. (19) and (29) one can without difficulty find that the dipole moment per unit area is equal to

$$\mathbf{P}=\alpha(\mathbf{B})\left(\mathbf{E}+\frac{1}{c}\mathbf{v}\times\mathbf{B}\right)|\psi|^2. \tag{37}$$

This result means that not only the electric field but also the Lorentz force polarizes the medium, acting in opposite directions on the positive and negative charges of a pair. The coefficient multiplying $|\psi|^2$ is the dipole moment of an individual pair, and $|\psi|^2$ is the number of pairs per unit area. It follows from Eq. (37) that the motion of the superfluid component will be accompanied by the appearance of a dipole moment in it. The nonuniform velocity field $\mathbf{v}_s(\mathbf{r})$ will lead to a nonuniform dipole moment, which in turn gives rise to a polarization electric charge in the system:

$$\rho_{\mathrm{pol}}=-\operatorname{div}\mathbf{P}. \tag{38}$$

If the dipole moment $\mathbf{P}$ from Eq. (37) is substituted into this expression, and it is taken into account that the superfluid

velocity $\mathbf{v}_s$ is given by expression (29), then in the absence of electric field we obtain (the field $\mathbf{B}$ is assumed uniform)

$$\rho_{\rm pol}=-\frac{B}{c}\alpha(B)\,{\rm curl}_z\mathbf{v}_s|\psi|^2$$

$$=-\frac{c}{B}(M_*-M)|\psi|^2{\rm curl}_z\mathbf{v}_s\,. \qquad (39)$$

We are interested in the charge $\rho_{\rm pol}$ associated with a vortex. If one is not interested in the structure of the vortex core, then the vortices can be considered as mathematical lines (points). Then $|\psi|^2$ can be replaced by the pair density n and, taking into account the singularity of the velocity field $\mathbf{v}_s$ on these lines, we obtain

$${\rm curl}_z\mathbf{v}_s=2\pi\frac{\hbar}{M_*}\sum_i\ \delta(\mathbf{r}-\mathbf{r}_i)n_i\,. \qquad (40)$$

Here $n_i=\pm1$, and the upper and lower signs correspond to vortices rotating counterclockwise and clockwise, respectively, and the summation is over the coordinates of the vortices (vortex cores). As a result,

$$\rho_{\rm pol}=\pm\frac{\hbar c}{B}\left(1-\frac{M}{M_*}\right)2\pi n\sum_i\ \delta(\mathbf{r}-\mathbf{r}_i)n_i\,. \qquad (41)$$

If only the lowest Landau level is filled, and the filling factor is equal to ν (we recall that the electronic and hole filling factors are equal, $\nu_e=\nu_h=\nu$), then, taking into account the relation $\nu=2\pi l_B^2 n$, we can rewrite expression (41) in the form

$$\rho_{\rm pol}=\pm\left(1-\frac{M}{M_*}\right)\nu e\sum_i\ \delta(\mathbf{r}-\mathbf{r}_i)n_i\,. \qquad (42)$$

The vortex charge is equal to the coefficient in front of the δ function. At small d (more precisely, for $a_B^e\gg a_B^h$, $l_B\gg d$), we have $M_*-M=M_B$, and we obtain[14] for the vortex charge q

$$q=\pm\frac{M_B}{M_*}\nu e. \qquad (43)$$

At large d, in accordance with (25), we have $M_*=(M/1-\eta)$, and the vortex charge $q=\pm\eta\nu e$.

With the aid of this expression it is easy to find out how the vortex charge depends on the insulator thickness d. Since the filling factor ν of the layers is independent of the thickness d, everything will be determined by the dependence on d of the coefficient η. But before we find this dependence, let us remark that expression (14) for δ is obtained on the assumption that d is substantially greater than the size of a pair in the plane of the conducting layer. From the form of the pair wave function (17) it follows that the size of a pair is of the order of $2l_B/\sqrt{\beta}$. Therefore the following inequality must hold:

$$d^2\gg 4l_B^2/\beta, \qquad (44)$$

i.e.,

$$d^4(1+4l_B^4/a_Bd^3)\gg 16l_B^4. \qquad (45)$$

It is easily verified that for $d\gg a_B$ inequality (46) holds for both $l_B\gg d$ (low magnetic fields) and $d_B\ll d$ (high fields). We shall assume further that $d\gg a_B$. In this case the theory constructed here is valid both at low and high magnetic fields.

Returning to expression (14) for η, we obtain

$$\eta=4\frac{m}{M}\frac{1}{1+\dfrac{4l_B^4}{a_Bd^3}-(m_h-m_e)^2/(m_h+m_e)^2}. \qquad (46)$$

Let us give the results separately for the cases $m_h=m_e$ and $m_e\ll m_h$. In the first case, which is realized in a two-layer system consisting of two identical electronic layers,

$$\eta=a_Bd^3/4l_B^4 \quad \text{for } l_B\gg d\gg a_B,$$

$$\eta=1-\frac{4l_B^4}{a_Bd^3} \quad \text{for } l_B\ll d. \qquad (47)$$

In the second case (a heterojunction consisting of an electronic and a hole-type layer)

$$\eta=\frac{m_e}{m_h}\frac{a_Bd^3}{l_B^4} \quad \text{for } \frac{l_B^4}{a_Bd^3}\gg\frac{m_e}{m_h},$$

$$\eta=1-\frac{m_h}{m_e}\frac{l_B^4}{a_Bd^3} \quad \text{for } \frac{l_B^4}{a_Bd^3}\ll\frac{m_e}{m_h}. \qquad (48)$$

Thus at low magnetic fields the vortex charge increases as d^3 with increasing thickness of the insulator layer. For example, for $m_h=m_e$ the vortex charge is equal to

$$q=\frac{a_Bd^3}{4l_B^4}\nu e. \qquad (49)$$

At high fields the vortex charge ceases to depend on d and becomes equal to the universal value $q=\nu e$.

The expressions found for η permit immediate determination of the pair effective mass M_*. It follows from Eqs. (25), (48), and (49) that at low magnetic fields $M_*\cong M$. At high fields

$$M_*=\frac{1}{2}\frac{a_Bd^3}{l_B^4}m_e \quad \text{for } m_h=m_e, \qquad (50)$$

and

$$M_*=\frac{a_Bd^3}{l_B^4}m_e \quad \text{for } m_e\ll m_h. \qquad (51)$$

It is seen that, unlike the vortex charge, the pair effective mass increases as d^3 at high rather than at low magnetic fields. Furthermore, the mass M_* increases with increasing magnetic field in proportion to B^2. This increasing pair mass at high magnetic fields leads to a decrease of the pair kinetic energy, which, in turn, can lead to crystallization of the pairs.

4. CRYSTALLIZATION OF PAIRS

Although the problem of stability of pairs against transition to a crystalline state cannot be solved exactly, it does admit a number of estimates that allow one to understand the situation qualitatively. Let us suppose that crystallization of the pairs has occurred, and consider the problem of the melting of the dipole crystal formed. Since this crystal is two-dimensional, in a classical treatment of the problem of melting it is natural to assume that the melting occurs by the Kosterlitz-Thouless mechanism (i.e., by dissociation of dis-

location pairs with antiparallel Burgers vectors at the melting point). The melting temperature of a two-dimensional crystal can be expressed in terms of the Lamé coefficients μ and λ of the dipole crystal:

$$T_m=\frac{a^2\mu(T_m)(\mu(T_m)+\lambda(T_m))}{4\pi(2\mu(T_m)+\lambda(T_m))}, \tag{52}$$

where a is the lattice constant of the crystal.

The Lamé coefficients can be calculated in the case of a dilute dipole crystal (i.e., for $d\ll a$). In the harmonic approximation at $T=0$ (Ref. 22)

$$\mu=\frac{A}{S_0}, \quad \lambda=9\frac{A}{S_0}. \tag{53}$$

Here S_0 is the area of the unit cell of a dipole crystal, and

$$A=\frac{3}{16}\frac{e^2d^2}{\varepsilon_0}\mathrm{Q}, \tag{54}$$

where

$$\mathrm{Q}=\sum\frac{1}{r^3(n)}\sim\frac{1}{S_0}\int\frac{2\pi rdr}{r^3}\sim\frac{2\pi}{a^3}. \tag{55}$$

It follows from Eqs. (52)–(55) that the melting temperature of a dipole crystal is equal to

$$T_m\approx\frac{1}{10}\frac{(ed)^2}{\varepsilon_0a^3}\approx\frac{1}{10}\frac{(ed)^2}{\varepsilon_0}n^{3/2}. \tag{56}$$

This temperature should be compared to the transition temperature T_c of a Bose gas of pairs to the superfluid state. For the temperature T_c we have the Kosterlitz–Thouless relation

$$T_c=\frac{\pi}{2}\frac{\hbar^2n_s(T_c)}{M_*}. \tag{57}$$

Here $n_s(T_c)$ is the density of the superfluid component of the electron-hole gas at the temperature T_c. The density n_s is related to the total pair density n by the relation $n_s=n-n_n$, where n_n is the density of the normal component. In the absence of impurities and crystal lattice defects the density of the normal component is determined by the well-known Landau expression, which in the present case of a two-dimensional Bose gas has the form

$$n_n=\int\left(-\frac{dn_p}{d\varepsilon}\right)\frac{p^2}{2M_*}\frac{d^2p}{(2\pi\hbar)^2}, \tag{58}$$

where n_p is the distribution function of the elementary excitations in the Bose gas. At low temperatures the density of elementary excitations is low, and the elementary excitations can be assumed noninteracting. Therefore in a state of thermodynamic equilibrium the function n_p is the Bose–Einstein distribution (with chemical potential equal to zero). The elementary excitation spectrum $\varepsilon(\mathbf{p})$ can be found by considering it as the dispersion relation of small oscillations of the condensate wave function $\psi(\mathbf{r},t)$.[23] As a result, we find that the spectrum has the Bogolyubov shape:

$$\varepsilon(p)=\left[\left(\frac{p^2}{2M_*}\right)^2+\frac{\gamma np^2}{M_*}\right]^{1/2}. \tag{59}$$

This dispersion relation of elementary excitations does not permit one to obtain an analytical expression for the integral in (59) and to find the normal density n_n at arbitrary values of the interaction constant γ. A calculation can be done in the important case of high magnetic fields and small thicknesses of the insulator layer, more precisely, for $a_B\gg l_B\gg d$. For this case the interaction constant is equal to[14]

$$\gamma=\left(\frac{\pi}{2}\right)^{3/2}\frac{e^2d^2}{\varepsilon_0l_B} \tag{60}$$

and, as subsequent calculations will show, the critical temperature T_c obeys the inequality $T_c\gg\gamma n$. Then, after changing from integration over p to integration over $\xi=p^2/2M_*$ in (58), it is convenient to separate the integration interval over ξ into two parts: from zero to ξ_c, and from ξ_c to λ. The energy ξ_c must satisfy the inequalities

$$T\gg\xi_c\gg\gamma n. \tag{61}$$

By virtue of inequalities (61), in the first integral we can replace $n(\varepsilon)$ by T/ε, and in the second we can replace ε by ξ. Summing the results obtained, we find that

$$n_n=\frac{M_*T}{2\pi\hbar^2}\ln T/\gamma n. \tag{62}$$

Substituting this expression into (58), we easily find the superfluid transition temperature T_c. It is necessary, however, to pay attention to the following circumstance. It turns out that the superfluid density $n_s(T_c)$ found using formula (58) is substantially lower than the total pair density n. This means that at the temperature T_c there are many elementary excitations and their interaction must not be neglected, while expression (63) was obtained on the assumption of an ideal gas of excitations. Therefore, at small d we can calculate T_c only in order of magnitude. To do this we equate the normal density n_n from (62) to the total pair density n. Expressing the density n in terms of the Landau level filling factor ν, in the case $m_h=m_e$ we obtain to logarithmic accuracy

$$T_c\approx\sqrt{\frac{\pi}{2}}\nu\frac{e^2}{\varepsilon_0l_B}\left(\ln\frac{l_B}{d}\right)^{-1}. \tag{63}$$

A comparison of expressions (56) and (63) shows that with decreasing insulator thickness d both the melting temperature T_m and the superconducting transition temperature T_c decrease. However $T_m\sim d^2$, while $T_c\sim(\ln l_B/d)^{-1}$, and therefore, it is obvious that $T_m\ll T_c$, and, moreover, $(T_m/T_c)\approx(\sqrt{\nu}/5\pi^2)(d^2/l_B^2)\ln(l_B^2/d^2)\ll1$. Thus at small d the crystallization of pairs should occur at a temperature T_m substantially lower than the superconducting transition temperature T_c. It should be noted that T_c from (63) is lower than the degeneracy temperature of the pair Bose gas $T_0\approx(\hbar^2n/M_*)\approx\nu(e^2/\varepsilon_0l_B)$ (the ratio $(T_c/T_0)\approx(\ln(l_B/d))^{-1}$. In this way the system under discussion differs from a 3D Bose gas, and the reason lies in the absence of a Bose condensate at nonzero temperatures in 2D systems.

We have considered the case of small insulator thicknesses d. We now turn to large d. The case of large d presupposes that the inequality $d^2\gg\langle r^2\rangle$ holds. When that inequality holds jointly with the condition that the pair Bose gas is dilute, $n\langle r^2\rangle\ll1$, the pairs can be considered as two-

dimensional impermeable spheres (or disks) of radius $r_0 = \sqrt{\langle r^2 \rangle}$. The interaction constant of such a 2D Bose gas was first found in Ref. 24 and is equal to

$$\gamma = \frac{4\pi\hbar^2}{M_* \ln(1/nr_0^2)}. \tag{64}$$

Although formally the constant γ can be made small by decreasing the pair density n, in real physical systems the pair interaction energy γn remains of the order of their degeneracy temperature $\hbar^2 n/2M_*$. The reason is not only that the logarithm is hard to make large enough, but also that structure defects and roughness of the conducting layers will lead to localization of the carriers as their density decreases. Thus the pair density n should be larger than a certain critical value (in the experiment 10^9 cm^{-2}). Therefore in the case of large d the superconducting transition temperature T_c is of the order of the pair degeneracy temperature $\hbar^2 n/2M_*$, and the condition for the existence of a superfluid phase is of the form

$$\frac{\hbar^2 n}{M_*} > \frac{1}{10}\frac{e^2 d^2}{\varepsilon} n^{3/2}. \tag{65}$$

At a fixed Landau level filling factor ν the pair density $n = \nu/2\pi l_B^2$. Then inequality (65) can be written in the form

$$l_B > \frac{1}{5\pi}\left(\frac{\nu}{2\pi}\right)^{1/2} \frac{e^2 M_* d^2}{\varepsilon_0 \hbar^2}. \tag{66}$$

A calculation shows that the magnetic fields at which a superfluid phase exists are low, so that the inequality $l_B^4 \gg a_B d^3$ holds. At such fields the effective mass $M_* \cong M$. As a result, in the case when $m_h = m_e$ it follows from (66) that

$$l_B \approx \frac{4}{5}\left(\frac{\nu}{2\pi}\right)^{1/2} \frac{d^2}{a_B}. \tag{67}$$

Now, by equating the two sides of the above inequality, we find a relation between the magnetic length l_B^* at the critical field B_*, i.e., the field above which the superfluid phase vanishes at a fixed thickness d. The relation obtained can also be considered as an equation for the critical thickness d_* above which the superfluid phase vanishes at a fixed magnetic field B.

5. CONCLUSION

We have investigated the properties of two-layer electron-hole systems in a magnetic field normal to the layers. We have shown that spatially separated electrons and holes form bound pairs, the Hamiltonian of which has a universal form (8) that does not depend on the distance between conducting layers. At a fixed pair bare mass $M = m_e + m_h$ this Hamiltonian contains only one parameter—the effective pair mass M_*, which is a function of the magnetic field and the distance between conducting layers. The Hamiltonian contains the pair electric polarizability α, which is expressed in terms of the pair bare mass M and the pair effective mass, M_*. A coherent state of a system of pairs in the low density limit is described by a dynamical equation of the Gross-Pitaevskii type for the order parameter. An important difference of that dynamical equation from that of Gross–Pitaevskii consists in the fact that instead of the momentum operator $(-i\hbar\nabla)$ this equation contains the operator $(-i\hbar\nabla - (\alpha(B)/c)\mathbf{E}\times\mathbf{B})$, where $\mathbf{E}$ is the local electric field, which is the sum of the external electric field and the field created by the quantum vortices. The appearance of vortices gives rise to an electric field, since, as we have shown in this paper, each vortex carries a real electric charge. The presence of charge on the vortex is due to the fact that in a magnetic field the Lorentz force leads to polarization of the medium, which has a nonzero velocity. The total charge of a vortex is proportional to the circulation of the superfluid velocity along a contour enclosing the vortex. Since the circulation is independent of the shape of the contour and is quantized, the charge of the vortex is a topological invariant and is quantized. In the general case, however, the vortex charge is not a universal quantity. In this paper we have investigated in detail how this charge depends on the magnetic field and the distance between conducting layers and have shown that the charge has a universal value only under the conditions $a_B^h, a_B^e \gg l_B \gg d$. That universal value is equal to $q = \nu e$.

We have investigated the stability of the superfluid phase of electron-hole pairs against transition to the crystalline state. As a criterion of stability we used positivity of the difference between the superfluid transition temperature T_c and the melting temperature T_m of the crystal. Here, in view of the two-dimensionality of the system, it was assumed that destruction of the superfluid and crystalline order is due to a Kosterlitz-Thouless mechanism (i.e., dissociation of vortex pairs in the superfluid phase and dissociation of dislocation pairs in the crystalline phase). We have established that at small thicknesses d of the insulator separating the conducting layers, more precisely, for $a_B \gg l_B \gg d$, the superfluid transition temperature is substantially higher than the pair crystallization temperature. This means that in the given case the superfluid phase should exist, at least at nonzero temperatures. However, it seems that quantum effects neglected in this study will prevent the crystallization of pairs even at zero temperature, and in that case the superfluid phase will persist down to $T = 0$.

With increase of d the situation changes. At a fixed pair density n there is a critical value of the thickness d_* at which the existence region of the superfluid phase vanishes. If n is expressed in terms of the Landau level filling factor ν and the magnetic length l_B ($n = \nu/2\pi l_B^2$), then the critical thickness $d_* \approx (a_B l_B)^{1/2}(2\pi/\nu)^{1/4}$. It is useful to compare this result, obtained under the assumption that $l_B \gg a_B$, with the result obtained in the case when the Bohr radius is large compared to the magnetic length. It has been shown[25,26] that for $a_B \gg l_B$ an increase of d also leads to destruction of the superfluid phase, but in that case the critical thickness of the insulator layer $d_* \approx l_B$. Thus, although quantitatively the critical thicknesses are different, the trend is qualitatively the same in both cases: increasing d leads to destruction of the superfluid phase. The vanishing of the superfluid phase at d close to but somewhat larger than the magnetic length l_B is attested by experiment.[3]

The destruction of superfluidity with increasing distance between conducting layers is completely natural from a physical point of view. However, the mechanism of this destruction is not completely clear at the present time. If one is interested in the possibility of obtaining the superfluid phase

and not in the mechanism of its destruction, then one should choose the thickness d as small as possible in comparison with the length l_B. Although the superfluid transition temperature decreases in that case, the decrease is only logarithmic [see Eq. (63)]. It must be kept in mind, however, that at small d the amplitude of the tunneling of carriers between conducting layers can increase. Tunneling transitions between layers lead to a gap spectrum of elementary excitations and to the possibility of Josephson vortices arising in the system. As a result, the superfluidity of the pairs will have a soliton character.[27]

*E-mail: shevchenko@ilt.kharkov.ua

[1] I. B. Spielman, J. P. Eisenstein, L. N. Pfeiffer, and K. W. West, Phys. Rev. Lett. **84**, 5808 (2000).
[2] M. Kellog, I. B. Spielman, J. P. Eisenstein, L. N. Pfeiffer, and K. W. West, Phys. Rev. Lett. **88**, 126804 (2002).
[3] M. Kellog, J. P. Eisenstein, L. N. Pfeiffer, and K. W. West, Phys. Rev. Lett. **93**, 036801 (2004).
[4] Yu. E. Lozovik and V. I. Yudson, Zh. Éksp. Teor. Fiz. **71**, 738 (1976) [Sov. Phys. JETP **44**, 389 (1976)].
[5] S. I. Shevchenko, Fiz. Nizk. Temp. **2**, 505 (1976) [Sov. J. Low Temp. Phys. **2**, 251 (1976)].
[6] Y. Kuramoto and C. Horie, Solid State Commun. **25**, 137 (1978).
[7] Daijiro Yoshioka and A. H. MacDonald, J. Phys. Soc. Jpn. **59**, 4211 (1990).
[8] X. G. Wen and A. Zee, Phys. Rev. Lett. **69**, 1811 (1992).
[9] K. Moon, H. Mori, K. Yang, S. M. Girvin, and A. H. MacDonald, Phys. Rev. B **51**, 5138 (1995).
[10] L. Balents and L. Radzihovsky, Phys. Rev. Lett. **86**, 1825 (2001).
[11] Ady Stern, S. M. Girvin, A. H. MacDonald, and Ning Ma, Phys. Rev. Lett. **86**, 1829 (2001).
[12] Michael M. Fogler and Fraun Wilczek, Phys. Rev. Lett. **86**, 1833 (2001).
[13] A. H. MacDonald, Physica B **298**, 129 (2001).
[14] S. I. Shevchenko, Phys. Rev. B **67**, 2145159 (2003).
[15] E. H. Rezayi and A. H. MacDonald, Phys. Rev. B **42**, 3224 (1990).
[16] L. P. Gor'kov and N. E. Dzeloshinskiĭ, Zh. Éksp. Teor. Fiz. **53**, 717 (1967) [Sov. Phys. JETP **26**, 449 (1968)].
[17] S. I. Shevchenko, JETP Lett. **28**, 103 (1978).
[18] V. Leonhardt and P. Piwnicki, Phys. Rev. Lett. **82**, 2426 (1999).
[19] Yu. E. Lozovik and A. M. Ruvinskiĭ, Zh. Éksp. Teor. Fiz. **112**, 1791 (1997) [JETP **85**, 979 (1997)].
[20] F. Dalfovo, S. Giorgini, L. P. Pitaevskii, and S. Stringari, Rev. Mod. Phys. **71**, 463 (1999).
[21] L. D. Landau and E. M. Lifshitz, *Electrodynamics of Continuous Media*, 2nd ed., rev. and enl., by E. M. Lifshitz and L. P. Pitaevskii, Pergamon Press, Oxford (1984), Nauka, Moscow (1982), Russ. p. 361; E. M. Lifshitz and L. P. Pitaevskii, Statisticheskaya fizika, ch. **2**, Nauka, Moscow (1978), s. 233.
[22] A. M. Kosevich, *Theory of the Crystal Lattice*, Wiley–VCH, Berlin–New York (1999), Vishcha Shkola, Kharkov (1988), Russ. p. 51.
[23] E. M. Lifshitz and L. P. Pitaevskiĭ, *Statistical Physics*, 3rd ed., Pergamon Press (1980), Nauka, Moscow (1978), Russ. part 2, p. 146.
[24] M. Schick, Phys. Rev. A **3**, 1067 (1971).
[25] Kyungsun Moon, Phys. Rev. Lett. **78**, 3741 (1997).
[26] Y. N. Joglekar and A. H. MacDonald, Phys. Rev. B **64**, 155315 (2001).
[27] S. I. Shevchenko, Phys. Rev. Lett. **72**, 3242 (1994).

Translated by Steve Torstveit

SUPERCONDUCTIVITY, INCLUDING HIGH TEMPERATURE SUPERCONDUCTIVITY

Critical current, pinning, and the resistive state of superconducting single-crystal niobium with various types of defect structure

V. I. Sokolenko* and Ya. D. Starodubov

National Science Center "Kharkov Institute of Physics and Technology," ul. Akademicheskaya 1, Kharkov 61108, Ukraine

(Submitted November 16, 2004; revised February 8, 2005)
Fiz. Nizk. Temp. **31**, 745–751 (July 2005)

The critical current, pinning, and resistive state of single-crystal niobium of texture orientation are studied in various structural states obtained by rolling by 42% at 20 K and subsequent polishing of the surface layers. It is found that the heterogeneous structures typical of the strained sample have a lower current-carrying capacity even after thinning to ~10% on account of the enhancement of the thermomagnetic instability in the parts with fragmented structure in the subsurface layers. For the case of a homogeneous defect structure of the mid-region of a sample with a uniformly distributed dislocation density of 1.3×10^{11} cm^{-2} in the resistive state a correlation between the component of the normal current and the critical current density is found, in accordance with the concepts of flux creep due to the scatter of the local values of J_c. © *2005 American Institute of Physics.* [DOI: 10.1063/1.2001633]

INTRODUCTION

Elemental type-II superconductors are traditionally used for experimental study of the interaction of the vortex lattice with various kinds of defects of the crystal structure created by the influence of temperature and strain. The deformation temperature and the type of loading have a substantial influence on the character of the defect structure, and that is reflected in the features of the current-voltage (I–V) characteristics, field dependence of the critical current density $J_c(b)$, and bulk pinning force $F_p(b)$ ($b=H/H_{c2}$ is the reduced magnetic field, H is the applied field, and H_{c2} is the second critical field). The results reported in the literature have been obtained mainly for materials with defect structures formed under deformation at room temperature (see, e.g., Refs. 1–3). For superconductors strained at low temperatures ($T \ll \Theta$, where Θ is the Debye temperature) there are considerably fewer data, and those pertain mainly to studies of the critical current and pinning at twin boundaries created under deformation by twisting (Nb, V),[4,5] bending (Nb),[6] and rolling by low degrees $\delta \leqslant 10\%$ (Nb).[7] With increasing degree of deformation by rolling the effects of interaction of the contact surfaces of the rollers and sample become noticeable, causing a macroscopically nonuniform flow of material, and that causes specific properties of the stress-strain state formed in the cross section of the sample. It is shown in Ref. 8 that as a result of rolling to a "moderate" degree ($\delta \sim 40-80\%$) at 20 K, single-crystal Nb is transformed to a heterogeneous superconductor in which defect structures of qualitatively different character are combined in the cross section. The layers found near the surface of the sample have a fragmented structure, while the mid-region is a region of uniformly distributed dislocations with a high density ($N_d \sim 10^{11}$ cm^{-2}). In the case of symmetric thinning of such a sample a nontrivial variation of H_{c2} and of the superconducting transition temperature T_c is observed. For the "set" of structural states thus realized in Nb it was of interest to study the critical current, pinning, resistive state, and destruction of superconductivity in the passage of a transport current over a wide range of magnetic fields. We note that the possibility of formation of qualitatively different defect structures in the cross section of a sample is due to the fact that on changing from room-temperature deformation to low-temperature deformation there is a shift of the onset of fragmentation of the material to higher degrees of deformation.[9]

SAMPLES AND TECHNIQUES

Samples of single-crystal Nb with texture orientation (001)[110] were cut from a massive billet, ground, chemically polished in a mixture of fluoric (40%) and nitric (60%) acids, and annealed at $T=1620$ K for 8 hours in an oil-free vacuum at a pressure of $P\approx1.3\times10^{-2}$ Pa; the finished samples had dimensions of $35\times2.5\times0.5$ mm. The samples were characterized by the values $T_c=9.15$ K, $H_{c2}=336$ kA/m, and resistivity $\rho_{n0}=0.937$ $\mu\Omega\cdot$cm, measured at $T=T_c+0.5$ K. The deviation of the longitudinal axis of the sample from the [110] direction and of the wide faces from the (001) plane did not exceed 2°. Deformation by rolling along the longitudinal axis to a degree $\delta=42\%$, defined as the relative change of thickness, was done in a medium of liquid hydrogen. After heating to room temperature, potential contacts were spot welded to the sample in a medium of liquid nitrogen. Successive symmetric thinning of the sample was done in a chemical polishing regime.

The superconducting transition temperature was determined by a resistive method. The sample was placed in a horizontal Dewar, with a low-gradient electrical resistance furnace in the form of a hollow cylindrical copper sleeve with a bifilarly wound Constantan wire, lying above the liq-

uid helium level in the cryostat. The temperature sensor used was a Cu/Au+0.01%Fe differential thermocouple. Its working junction was pressed tight to the mid-region of the sample, and the free junction was immersed in a medium of liquid helium. The accuracy of determination of T_c was ± 0.01 K. Measurements of T_c were done at a working current of 20 mA, corresponding to a measurement current density from $\sim 2.5\times 10^{-3}$ A/cm^2 for the deformed sample to $\sim 6\times 10^{-3}$ A/cm^2 after the sample was thinned to the greatest degree. The experiments showed that increasing the working current by a factor of 5 or reducing it by a factor of 2 did not lead to changes in the value of T_c outside the measurement error. This indicates that the field of the current did not have a noticeable influence on the accuracy of measurement of T_c.

For determination of the dependence $J_c(H)$ the current-voltage characteristics $U(J,H=\text{const})$ (U is the voltage drop, J is the current density) were measured in a medium of liquid helium in a transverse magnetic field perpendicular to the wide face of the sample. The values of J_c corresponded to the value $U=0.5\times 10^{-6}$ V/cm. The values of H_{c2} were determined by extrapolation of the steeply falling part of the $J_c(H)$ curves in linear coordinates to the abscissa.[3] For the current leads we used the massive jaws consisting of cut copper cylinders whose polished plane surfaces were tightly pressed to the sample, ensuring the absence of heat release during the establishing of the current. The current leads were located in the peripheral region of the field produced by the solenoid, while the working part of the sample with the potential contacts was in the uniform field of the central part of the solenoid. The technique used to measure T_c and J_c is described in detail elsewhere.[10]

RESULTS AND DISCUSSION

After deformation by rolling at 20 K by $\delta=42\%$ the sample was characterized by the values $T_c=9.27$ K, $H_{c2}=393$ kA/m, and $\rho_{n0}=1.515\ \mu\Omega\cdot$cm. The as-strained sample was successively thinned by 1.6, 6.9, 11.5, 15.4, 28.1, and 53.8%. Figure 1 illustrates the evolution of $J_c(b)$ in the transition from the initial heterogeneous state (after deformation by rolling) to a homogeneous structure in the form of uniformly distributed dislocations, which is dominant over the whole cross section of the sample after it is maximally thinned.[1)] The extremely weak dependence $J_c(b)$ in a wide range of fields ($0.2\leqslant b\leqslant 0.85$) is characteristic for the as-strained sample and that sample after thinning by 1.9% (the curve is not shown in the figure) and 6.9%, and with increasing $\Delta h/h_0$ there is a "subsiding" of the whole curve and first a decrease and then an increase of T_c and H_{c2} (see Table I). With further increase of $\Delta h/h_0$ a transformation of the plateau-like part occurs: the values of J_c at low fields and near H_{c2} increase substantially, with an accompanying monotonic decrease of T_c and H_{c2}. Thinning of the sample also influences the "tails" of surface superconductivity at $b>1$. It is seen that in this case the values of the critical currents are largest for the initial state (curve *1*) and decrease with increasing $\Delta h/h_0$.

TABLE I. Values of ΔT_c, δT_c, ΔH_{c2}, and $F_p^{\max}$ for different values of $\Delta h/h_0$ for a single-crystal niobium sample deformed 42% beforehand by rolling at 20 K. ΔT_c and ΔH_{c2} characterize the difference of the values of T_c and H_{c2} in the as-strained state and after thinning, and δT_c is the width of the superconducting transition.

$\Delta h/h_0$,%	ΔT_c, K	δT_c, K	ΔH_{c2}, kA/m	$F_p^{\max}$, 10^5 N/m^3
0	0	0.09	0	11.91
1.9	−0.06	0.11	−5.56	11.33
6.9	+0.13	0.11	+2.38	9.57
11.5	+0.10	0.15	−16.76	17.19
15.4	+0.03	0.15	−19.84	19.47
28.1	−0.02	0.11	−21.75	29.85
53.8	−0.05	0.065	−21.81	22.35

Figure 2 characterizes the current-carrying capacity of the sample after maximum thinning. The inset shows data from Ref. 3 for the mid-region of a niobium single crystal of similar orientation, deformed by rolling by 50% at room temperature. It is seen in the figure that for these samples the field dependence of J_c has the same shape, but after low-

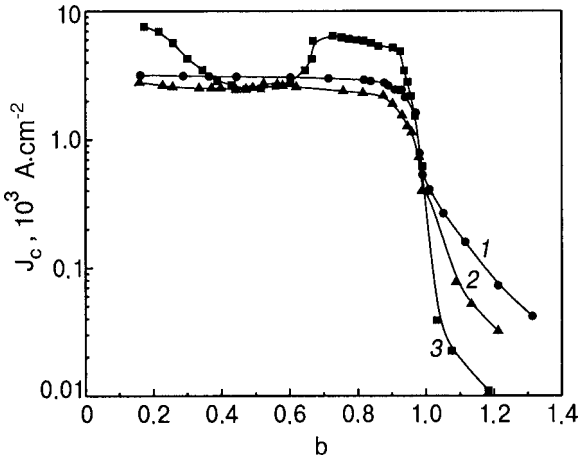

FIG. 1. Dependence of the current density J_c on the reduced magnetic field b for single-crystal niobium deformed by 42% by rolling at 20 K (*1*) and after relative reductions of the thickness of the sample by thinning by $\Delta h/h_0=6.9\%$ (*1*) and 53.8% (*3*).

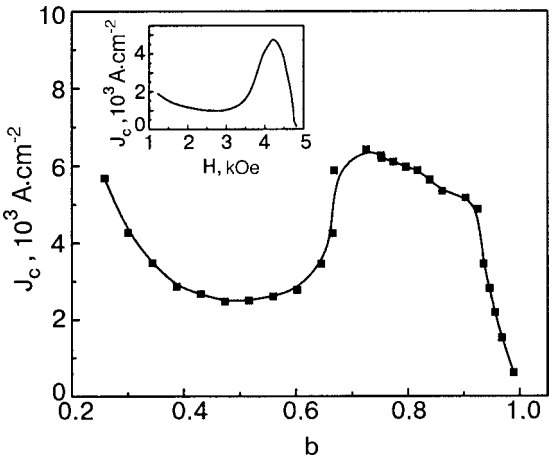

FIG. 2. Dependence of j_c on b in the central part of a sample of single-crystal niobium deformed by 42% by rolling at 20 K. The inset shows data of Ref. 3.

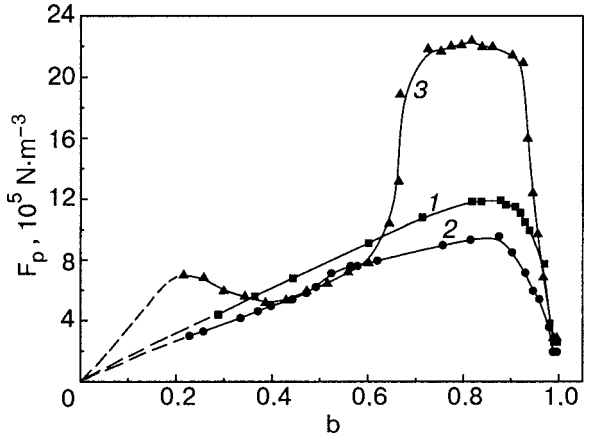

FIG. 3. Dependence of F_p on b for single-crystal niobium deformed by 42% by rolling at 20 K (*1*) and after a relative reduction of its thickness by $\Delta h/h_0 = 6.9\%$ (*2*) and 53.8% (*3*).

temperature deformation the absolute values of J_c are several times higher than the characteristic of a sample deformed at room temperature. This is a consequence of the higher defect density in the structure formed during rolling at liquid helium temperature.

A successive increase of $\Delta h/h_0$ has a substantial influence on the character of the dependence $F_p(b)$ (see Fig. 3). It is seen that after a comparatively small decrease in thickness ($\Delta h/h_0 \leqslant 6.9\%$) a monotonic increase of F_p occurs in the interval $0.2 \leqslant b \leqslant 0.86$, which gives way to a decrease for $b > 0.86$. Further increase of $\Delta h/h_0$ leads to substantial growth of the values of F_p both in the high-field region ($b \sim 0.7-0.9$) and also for $b \sim 0.2$.

It follows from Table I and the figures that for a strained sample the lowest values of $F_p^{\max}$ correspond to a structural state with maximum values of T_c and H_{c2}, which is reached after a decrease of thickness by 6.9%, while the highest values correspond to the structure of the mid-region, where T_c and H_{c2} are lower than the initial (after deformation) values.

The experimental data presented reveal the following:

—the variation of the values of the critical current and bulk pinning force with increasing $\Delta h/h_0$ is correlated with the variations of T_c and H_{c2}: with increase of the latter a decrease of J_c and F_p occurs in the region of high and low fields, and *vice versa*;

—the minimum values of $F_p^{\max}$ are realized for the heterogeneous structural state with maximum values of T_c and H_{c2};

—the pinning of the structure with predominantly uniformly distributed dislocations (the mid-region of the deformed samples) in the region of low and high fields is substantially greater than the pinning of the heterogeneous structure.

Let us consider the possible causes of the observed variation of the current-carrying capacity of niobium containing defects of the dislocation-disclination type, which are characteristic for the heterogeneous state. According to the data of Ref. 9, in the peripheral regions of single-crystal niobium of texture orientation, deformed by rolling by a moderate degree at 77 K the angles of misorientation of the fragmented structure do not exceed 10°. With decreasing deformation temperature a shift of the onset of fragmentation of the material to larger deformations occurs.[9] Thus there are no grounds for assuming that a structure with large misorientation angles is formed in the subsurface layers of the niobium single crystal deformed by rolling by an "intermediate" degree at 20 K. This, at first glance, admits a qualitative analogy of the data of Ref. 11 and the results of the present studies. In Ref. 11 the variations of the critical current in deformed and polygonized niobium are attributed to a change of the Ginzburg–Landau parameter ($\Delta\kappa$) at low-angle boundaries. In the framework of the $\Delta\kappa$ pinning mechanism $F_p \approx H_{c2}^2$ (Ref. 12). However, the results presented above indicate rather that F_p is inversely proportional to H_{c2}, and that precludes their analysis with the use of the $\Delta\kappa$ pinning model or other known models.[13] Therefore the "anomalous" behavior of J_c and F_p in the transition from the heterogeneous to the homogeneous structural state should be attributed to manifestation of a specific mechanism of destruction of superconductivity.

It has been shown previously that substantial lowering of the critical currents and pinning in zero and relatively low fields for vanadium[4] and niobium[5] deformed by twisting at 4.2 K are due to enhancement of the thermomagnetic instability (TMI) mechanism at places where the plastic deformation is localized. In the thin-walled cylindrical samples studied in Refs. 4 and 5 such places are twin boundaries and regions of rotational plasticity. In this case there is practically no gradient of the concentration of deformation defects over the cross section of the sample. In the present study the samples investigated had been deformed by rolling. By virtue of the specifics of this type of deformation, after rolling by an "intermediate" degree there are no twin boundaries in the structure of the niobium, and for macroscopically nonuniform structural states there are special elements of the defect structure in the subsurface layers in the form dislocation boundaries of misorientation, which appear at a distance of 1.5–2 μm from the surface. One can assume that for such structural states the TMI will arise with greater probability in the region with the fragmented structure. As a growing transport current is passed through the heterogeneous superconductor the density of local currents j_c^{loc} associated with the misorientation boundaries in the peripheral regions with higher local values of T_c and H_{c2} will exceed the values of the critical currents in microvolumes with lower defect density. Therefore upon local perturbations, in particular, fluctuational increases in temperature, catastrophic jumps of the flow will initiate a TMI spike in neighboring microvolumes with lower values of T_c and H_{c2}, as follows from the expression for the maximum value of the induction drop $B < B_j \sim [\mu_0 C_p (T_c - T_0)]^{1/2}$ (Ref. 4). Here μ_0 is the magnetic permeability, C_p is the heat capacity, and $T_0 = \text{const}$. On the I–V characteristics the growth of the TMI is manifested in the appearance of a segment with avalanche-like growth of the the voltage drop, while the exponential part is absent completely or extremely short. The increase of the external field leads to a decrease of the local currents, and when the "store" of enthalpy exceeds the magnetic energy density, which depends on the value of j_c^{loc}, the probability of catastrophic jumps of the flux is lessened, and the TMI mecha-

nism is "turned off."[4] Indeed, it is seen in Figs. 2 and 3 that with growth of b in the interval $0.2<b\leqslant 0.45$ a decrease of the difference of the values of J_c and F_p occurs for heterogeneous and homogeneous structural states. The substantial increase of the current-carrying capacity observed in the field region $b\sim 0.7-0.9$ for a sample with a high density of uniformly distributed dislocations is probably due to a manifestation of the peak effect. It is known[14] that the peak effect reflects the growth of the pinning due to softening of the vortex lattice as the field approaches H_{c2}. In regard to elements of the fragmented structure, the increase of j_c^{loc} due to the growth of the pinning will promote the development of the TMI and act to decrease the current-carrying capacity of the heterogeneous samples.

It is known that the magnetic field of the transport current penetrates into the bulk of a type-II superconductor in the form circular and helicoidal vortices. The influence of fluxoids of this nature on the properties of type-II superconductors has been the subject of a number of studies. In particular, in Ref. 15 the density of circular fluxoids and the value of the transport current were obtained as functions of the radius of the conductor. In Ref. 16 a model was proposed in which the destruction of superconductivity of a high-T_c superconductor with weak pinning ($J_c\leqslant 10^7$ A/m^2) is linked to the entry of vortex rings or helicoids into the sample. It can be assumed that the generation by the transport current of vortex lines of the given configuration in heterogeneous niobium samples can influence the current-carrying capacity to a certain degree. Helicoidal vortices which are pinned in subsurface layers with an elevated defect density will effectively lower the maximum value of the induction drop, and that is an additional factor enhancing the TMI.

It is known (see, e.g., Ref. 14) that an exponential character of the I–V characteristic promotes a flux creep regime. For a number of type-II superconductors in the region of weak electric fields ($U\leqslant U_f$, U_f is the electric field strength above which viscous flow of the vortex lattice occurs) the experimental data are described to good accuracy by the equation $J(U)=J_c+J_1\ln(U/U_0)$.[17] In this equation the normal current component $J_1=U\sigma_f$ (σ_f is the differential conductivity due to displacement of the normal core of the vortices) and $U_0=\mathrm{const}$. Current-voltage characteristics with segments corresponding to magnetic flux creep have been used to determine the parameters of the equation for $J(U)$. The calculations showed that the correct values of J_1 in different magnetic fields can be obtained only for homogeneous defect structures corresponding to the central part of the deformed sample. In the remaining cases the presence of pinning centers of various strength in the bulk of the material is a complicating factor. Figure 4a shows the $J_1(b)$ and $J_c(b)$ curves corresponding to the core of the strained sample. The $J_1(b)$ curve obtained includes all of the cases characteristic for superconducting materials:[17] a maximum at large values of b; a part where $J_1\cong\mathrm{const}$; a decrease of J_1 with increasing b. It follows from the figure that J_1 and J_c are correlated over a wide field interval $0.2\leqslant b\leqslant 0.86$. The quantitative relation between $J_1(b)$ and $J_c(b)$ is illustrated in Fig. 4b: with increase of b in the indicated interval a monotonic decrease of J_1/J_c occurs, from $\sim 5\times 10^{-2}$ to $\sim 5\times 10^{-3}$. For $b>0.86$ the accuracy of the calculations is substantially lower,

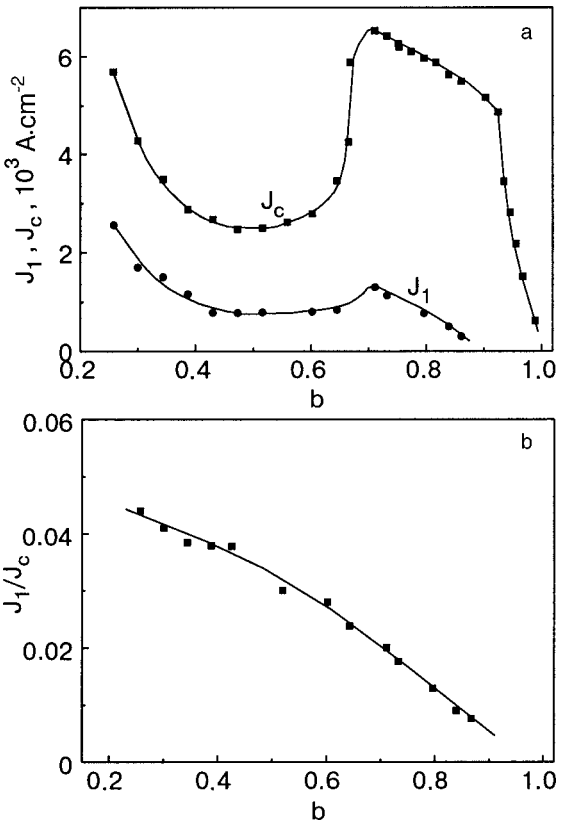

FIG. 4. Dependence of the normal current density J_1 and critical current density J_c on b for the central part of the sample (a) and the dependence of J_1/J_c on b (b).

and the corresponding data are not presented.

In the framework of the a thermally activated nature of the magnetic flux creep the nonlinearity of the I–V characteristic is due to the collapse of a part of the vortices owing to thermal fluctuations, and the values of J_1 and J_c are related by $J_1/J_c=k_BT/U_m$ (Ref. 17), where k_B is Boltzmann's constant, $U_m\sim a_0J_c\Phi_0$ is the characteristic binding energy of a vortex core to a pinning center (a_0 is the size of the pinning center, and Φ_0 is the magnetic flux quantum). If it is assumed that the size of a pinning center depends weakly on field, then the change of the value of U_m at $T=\mathrm{const}$ will be mainly determined by $J_c(b)$. In our case the dependence $J_c(b)$ is substantially nonmonotonic (see Fig. 4a), and that causes nonmonotonicity of $U_m(b)$. It follows from this that J_1/J_c should exhibit noticeable nonmonotonic behavior with variation of the field, in disagreement with experiment (see Fig. 4b). Thus, as compared to the heterogeneous structures, where the destruction of superconductivity over a wide range of fields should be linked with the thermal-fluctuational growth of the TMI for a weakly expressed precursor creep stage, the pinning on a homogeneous dislocation structure is less sensitive to thermal fluctuations.

Nonlinearity of the I–V characteristic can also be a comparison of a differences of the local values of the pinning force.[17] In such a conceptual framework the parameter J_1 determines the characteristic scatter of the values of the local critical current density, which is related to nonuniformity of the pinning force, and on a qualitative level the correlation of J_1 and J_c is natural. Nevertheless, the experimentally de-

duced lowering of the values of J_1/J_c with increasing field is not apparent. It is possible that with increasing b collective effects are manifested which narrow the scatter of the local values of the critical current density. This question requires separate theoretical studies.

CONCLUSIONS

We have investigated the I–V characteristics, the field dependence of the critical current, and the bulk pinning forces of single-crystal niobium of texture orientation in different structural states obtained as a result of rolling at 20 K and a subsequent polishing of surface layers: heterogeneous, combining a fragmented defect structure in the subsurface layers and uniformly distributed dislocations of high density $(1.3\times10^{11}\ \mathrm{cm}^{-2})$ in the central part of the sample, and homogeneous, characterized by only dislocations distributed in a uniform manner.

We have established that the change of the values of the critical current and bulk pinning force with increasing thickness of the polished layer is correlated with the changes of T_c and H_{c2}: when these parameters rise, J_c and F_p fall, and *vice versa*. The lower current-carrying capacity of the heterogeneous structures in the region of low and high fields is due to enhancement of the TMI in the parts with the fragmented defect structure.

For a homogeneous defect structure the resistive state is described well by the equation $J(U)=J_c+J_1\ln(U/U_0)$. In a wide field interval $0.2\leqslant b\leqslant 0.86$ a correlation between the normal current component J_1 and the critical current density J_c is established which corresponds qualitatively to the concepts of flux creep due to scatter of the local values of the critical current density. The observed monotonic lowering (by about a factor of 10) of the values of J_1/J_c with increasing b requires theoretical investigation.

Taken together with the previously observed manifestations of thermomagnetic instability in polycrystalline vanadium[4] and niobium[5] containing deformation twins and low-angle boundaries of misorientation, the results of the present study argue in favor of commonality of the TMI effects in heterogeneous monoatomic type-II superconductors with interfacial boundaries of deformation origin that are formed in low-temperature deformation.

The authors thank I. F. Borisova for assistance in doing the experiments.

*E-mail: vsokol@kipt.kharkov.ua

[1)] It has been shown[8] that in the mid-region of a sample deformed by rolling at 20 K in the interval of degrees of reduction 42–78%, a structure in the form of uniformly distributed dislocations with mean density $N_d=(1.3-1.4)\cdot10^{11}\ \mathrm{cm}^{-2}$ is formed. In a subsurface layer comprising 8–10% of the cross section the dislocation density is higher by a factor of 1.5–2, and at a distance of 1.5–2 μm from the surface a turbulent character of the material flow is realized in the deformation process, and a structure with a high degree of fragmentation is formed. Nontrivial behavior of T_c and H_{c2} in the course of successive thinning of the deformed sample is due to a change in the internal stress fields and in the ratio of the layers with uniformly distributed dislocations and with fragmented defect structure.

[1] H. C. Freyhardt, Philos. Mag. **23**, 345 (1971).
[2] A. M. Campbell and J. E. Evetts, *Critical Currents in Superconductors*, Taylor and Francis, London (1972), Mir, Moscow (1975).
[3] L. Ya. Vinnikov, V. I. Grigor'ev, and O. V. Zharikov, Zh. Éksp. Teor. Fiz. **71**, 252 (1976) [Sov. Phys. JETP **44**, 130 (1976)].
[4] V. I. Sokolenko and Ya. D. Starodubov, Fiz. Nizk. Temp. **18**, 1183 (1992) [Low Temp. Phys. **18**, 827 (1992)].
[5] V. K. Aksenov, V. I. Sokolenko, and Ya. D. Starodubov, Fiz. Nizk. Temp. **22**, 798 (1996) [Low Temp. Phys. **22**, 613 (1996)].
[6] V. S. Bobrov and M. A. Lebëdkin, JETP Lett. **47**, 715 (1988).
[7] V. I. Sokolenko, V. K. Aksenov, Ya. D. Starodubov, and I. F. Borisova, Czech. J. Phys. **46**, Suppl. **S2**, 879 (1996).
[8] V. K. Aksenov, I. F. Borisova, V. I. Sokolenko, and Ya. D. Starodubov, Fiz. Nizk. Temp. **19**, 1077 (1993) [Low Temp. Phys. **19**, 763 (1993)].
[9] I. A. Gindin, E. A. Levikov, L. V. Levikova, V. M. Matsevityĭ, Ya. D. Starodubov, and F. G. Bar'yakhtar, Fiz. Met. Metalloved. **30**, 426 (1970).
[10] V. I. Sokolenko and Ya. D. Starodubov, Zavodsk. Lab. **50**, 78 (1984).
[11] L. Ya. Vinnikov, V. G. Glebovskiĭ, I. V. Ermolaeva, and S. I. Moskvin, Fiz. Met. Metalloved. **54**, 268 (1982).
[12] D. Dew-Hughes and H. I. Wittkomb, Philos. Mag. **26**, 73 (1972).
[13] E. J. Kramer, "Flux pinning in high-carrying superconductors," Adv. Cryog. Eng. Mat. **28**, 307 (1982).
[14] V. V. Shmidt, *Introduction to the Physics of Superconductivity* [in Russian], Nauka, Moscow (1982).
[15] H. A. Ullmaier and R. H. Kernohan, Phys. Status Solidi **17**, K233 (1966).
[16] V. F. Khirnyĭ, V. P. Seminozhenko, and A. A. Kozlovskiĭ, Fiz. Tverd. Tela (St. Petersburg) **38**, 2951 (1996) [Phys. Solid State **38**, 1614 (1996)].
[17] A. Vl. Gurevich, R. G. Mints, and A. L. Rakhmanov, *Physics of Composite Superconductors* [in Russian], Nauka, Moscow (1976).

Translated by Steve Torstveit

Dynamic behavior of Josephson-junction qubits: crossover between Rabi oscillations and Landau–Zener transitions

S. N. Shevchenko*

B. Verkin Institute for Low Temperature Physics and Engineering of the National Academy of Sciences of Ukraine, 47 Lenin Ave., Kharkov 61103, Ukraine; Friedrich Schiller University, Institute for Solid State Physics Helmholtzweg 5, D-07743 Jena, Germany

A. S. Kiyko and A. N. Omelyanchouk

B. Verkin Institute for Low Temperature Physics and Engineering of the National Academy of Sciences of Ukraine, 47 Lenin Ave., Kharkov 61103, Ukraine

W. Krech

Friedrich Schiller University, Institute for Solid State Physics Helmholtzweg 5, D-07743 Jena, Germany

(Submitted January 6, 2005)
Fiz. Nizk. Temp. **31**, 752–760 (July 2005)

We study the dynamic behavior of a quantum two-level system with periodically varying parameters by solving numerically the master equation for the density matrix. Two limiting cases are considered: multiphoton Rabi oscillations and Landau–Zener transitions. The approach is applied to the description of the dynamics of superconducting qubits. In particular, the case of the interferometer-type charge qubit with periodically varying parameters (gate voltage or magnetic flux) is investigated. The time-averaged energy level populations are calculated as functions of the qubit's control parameters. © *2005 American Institute of Physics.*
[DOI: 10.1063/1.2001634]

1. INTRODUCTION

The quantum two-level system is a model used to describe a number of physical objects such as atoms, quantum dots, molecular magnets, etc. The system can be excited from the ground state to the upper state by changing its parameters in time (by means of external fields). If the parameters vary adiabatically slowly, the excitation mechanism is called Landau–Zener (LZ) transition;[1,2] if the amplitude of the field is small and its frequency is comparable to the level distance, Rabi oscillations occur.[3,4] Thus the occupation of the levels in a two-state system can be controlled by several parameters, e.g., the amplitude and frequency of an external field.[5]

Recently, the two-level model was used to describe Josephson-junction systems,[6] i.e., both charge qubits[7] and flux qubits.[8] The subject of the present work is the investigation of the dynamic behavior of superconducting qubits with periodically swept parameters, which is important from the point of view of state control and readout. We will relate our results to some other articles concerning the resonant excitation of a two-level system[9–13] which has been shown to be relevant for superconducting qubits, too.[14–17] In particular, we will describe the dynamic behavior of the interferometer-type charge qubit.[18–21]

To study theoretically the dynamic behavior of a Josephson qubit, we make use of the master equation for the density matrix rather than the Schrödinger equation because this allows one to take into account both relaxation and nonzero-temperature effects. (However, in this paper we will assume the zero-temperature limit, because we are interested in the influence of relaxation processes only on the qubit dynamics.)

The diagonal components of the density matrix give the probabilities of finding the system in the respective states of the basis in which the density matrix is presented. Thus, in executing the calculations we ought to deal with a particular basis. Our calculations are mostly carried out in the stationary basis $\{|-\rangle,|+\rangle\}$ of the eigenstates of the Hamiltonian $\hat{H}^{(0)}$ in the absence of time-dependent terms. We do that for two reasons. First, it is convenient to describe Rabi oscillations and multiphoton transitions. Second, in the case of the charge qubit these states $\{|-\rangle,|+\rangle\}$ are eigenstates of the current operator, which is related to the experimentally measurable values.[21] The important point is that we can get the occupation probability of any state provided we know the probabilities for the states in a particular basis. To demonstrate this, we will change over from the stationary basis to the so-called adiabatic basis (consisting of the instantaneous eigenstates of the time-dependent Hamiltonian $\hat{H}$) to describe the LZ effect. We emphasize that the results presented are valid for the description of any two-level system with periodically swept parameters, particularly, of a superconducting qubit. In a Josephson-junction qubit the gate voltage or the magnetic flux can be modulated periodically.

The paper is organized as follows. In Sec. 2 the basic equations are presented. In Sec. 3 we study multiphoton processes and LZ transitions in a two-level system with time-dependent parameters. We apply the respective results to the phase-biased charge qubit in Sec. 4.

2. THE BASIC EQUATIONS

We start from the Hamiltonian of a two-level system (see, e.g., Ref. 6)

$$\hat{H}^{(0)} = -\frac{B_x^{(0)}}{2}\hat{\sigma}_x - \frac{B_z^{(0)}}{2}\hat{\sigma}_z \tag{1}$$

in the basis of "physical" states $\{|0\rangle,|1\rangle\}$, where $\hat{\sigma}_z|0\rangle = |0\rangle$, $\hat{\sigma}_z|1\rangle = -|1\rangle$; $\hat{\sigma}_{x,y,z}$ are the Pauli matrices. The "physical" states are the eigenstates of the Hamiltonian $\hat{H}^{(0)}$ for $B_x^{(0)}/B_z^{(0)} \to 0$. In the case of a charge qubit, these states correspond to a definite number of Cooper pairs on the island. For a flux qubit, they correspond to a definite direction of the current circulating in the ring. The Hamiltonian (1) is diagonalized by means of the matrix

$$\hat{S} = \exp\left(i\frac{\lambda}{2}\hat{\sigma}_y\right) = \begin{bmatrix} \cos\lambda/2 & \sin\lambda/2 \\ -\sin\lambda/2 & \cos\lambda/2 \end{bmatrix},$$

where

$$\sin\lambda = -\frac{B_x^{(0)}}{\Delta E}, \quad \cos\lambda = \frac{B_z^{(0)}}{\Delta E}, \quad \Delta E = \sqrt{B_x^{(0)2} + B_z^{(0)2}}.$$

The eigenstates $|-\rangle$ and $|+\rangle$ of the time-independent Hamiltonian $\hat{H}^{(0)}$ are connected with the initial basis:

$$\begin{bmatrix} |-\rangle \\ |+\rangle \end{bmatrix} = \hat{S}\begin{bmatrix} |0\rangle \\ |1\rangle \end{bmatrix}.$$

Next, we introduce the time-dependent terms into the Hamiltonian (1),

$$\hat{H}^{(0)} \to \hat{H} = \hat{H}^{(0)} + \hat{H}^{(1)}(t).$$

We consider two situations,

$$(a):\ B_x = B_x^{(0)}, \quad B_z = B_z(t) = B_z^{(0)} + B_z^{(1)}(t), \tag{2}$$

$$(b):\ B_z = B_z^{(0)}, \quad B_x = B_x(t) = B_x^{(0)} + B_x^{(1)}(t), \tag{3}$$

where the time-independent/dependent terms are marked with (0)/(1) indices. Making use of the transformation $\hat{H}' = \hat{S}^{-1}\hat{H}\hat{S}$, we get the Hamiltonian $\hat{H}'$ in the energy representation $\{|-\rangle,|+\rangle\}$ corresponding to these cases:

$$\hat{H}'_a = -\frac{\Delta E}{2}\hat{\tau}_z - \frac{B_z^{(1)}(t)}{2}(\sin\lambda\,\hat{\tau}_x + \cos\lambda\,\hat{\tau}_z), \tag{4}$$

$$\hat{H}'_b = -\frac{\Delta E}{2}\hat{\tau}_z - \frac{B_x^{(1)}(t)}{2}(\cos\lambda\,\hat{\tau}_x - \sin\lambda\,\hat{\tau}_z). \tag{5}$$

For convenience, we use different notations for the Pauli matrices, $\hat{\sigma}_i$ and $\hat{\tau}_i$, which operate in the bases $\{|0\rangle,|1\rangle\}$ and $\{|-\rangle,|+\rangle\}$, respectively.

We emphasize that after the substitution

$$B_x^{(1)}(t) \to B_z^{(1)}(t) \tag{6}$$
$$B_z^{(0)} \to -B_x^{(0)}$$
$$B_x^{(0)} \to B_z^{(0)}$$

problem (b) coincides with problem (a). This transition from Eq. (5) to Eq. (4) corresponds to a $\pi/2$ rotation about the y axis.

To unify expressions (4) and (5) to get the equations for numerical calculations, we write down the Hamiltonian $\hat{H}'$ as follows:

$$\hat{H}' = \frac{A}{2}\hat{\tau}_x + \frac{C}{2}\hat{\tau}_z. \tag{7}$$

The quantum dynamics of our two-level system can be characterized within the standard density-matrix approach.[22] The time evolution of the total system composed of the two-level system and the reservoir is described by the Liouville equation. After tracing over the reservoir variables, the Liouville equation can be simplified to the so-called master equation for the reduced density matrix $\hat{\rho}$. It can be written in the form

$$\hat{\rho} = \frac{1}{2}\begin{bmatrix} 1+Z & X-iY \\ X+iY & 1-Z \end{bmatrix}$$

which ensures the condition $\mathrm{Tr}\hat{\rho} = 1$. The effect of relaxation processes in the system due to the weak coupling to the reservoir can be described phenomenologically with the dephasing rate Γ_φ and the relaxation rate Γ_{relax} (Ref. 23). Then the master equation takes the form of Bloch equations:[22]

$$\frac{dX}{dt} = -CY - \Gamma_\varphi X, \tag{8}$$

$$\frac{dY}{dt} = -AZ + CX - \Gamma_\varphi Y, \tag{9}$$

$$\frac{dZ}{dt} = AY - \Gamma_{\mathrm{relax}}(Z - Z(0)). \tag{10}$$

(Throughout the paper we set $\hbar = 1$.) From these equations we get $Z(t)$ which defines the occupation probability of the upper level $|+\rangle$, $P_+(t) = \rho_{22}(t) = \frac{1}{2}(1 - Z(t))$. We choose the initial condition to be $X(0) = Y(0) = 0$, $Z(0) = 1$, that corresponds to the system in the ground state $|-\rangle$. We have calculated the time evolution of $P_+(t)$ (which is essential, e.g., for the snapshot measurements[24]) as well as the time-averaged probability $\bar{P}_+$ (which is essential, e.g., for the impedance measurement technique[25]). We note that the asymptotic expression, $P_+(t)|_{t\to\infty}$, is periodic in time with the period $T = 2\pi/\omega$ of the time-dependent term of the Hamiltonian $\hat{H}^{(1)}(t)$ (see Sec. 12 of Ref. 5).

3. NON-STATIONARY EFFECTS IN A TWO-LEVEL SYSTEM

3.1. Rabi oscillations

Hereafter we will treat the problem (a) [see Eq. (2)], making use of the following notation:

$$\hat{H} = \Delta\hat{\sigma}_x + x(t)\hat{\sigma}_z, \quad x(t) = x_{\mathrm{off}} + x_0\sin\omega t \tag{11}$$

with

$$B_x^{(0)} = -2\Delta, \quad B_z^{(0)} = -2x_{\mathrm{off}}, \quad B_z^{(1)}(t) = -2x_0\sin\omega t. \tag{12}$$

This reformulation is convenient for comparing our results with the results of other papers.[9–12] Then the Hamiltonian (4) can be rewritten:

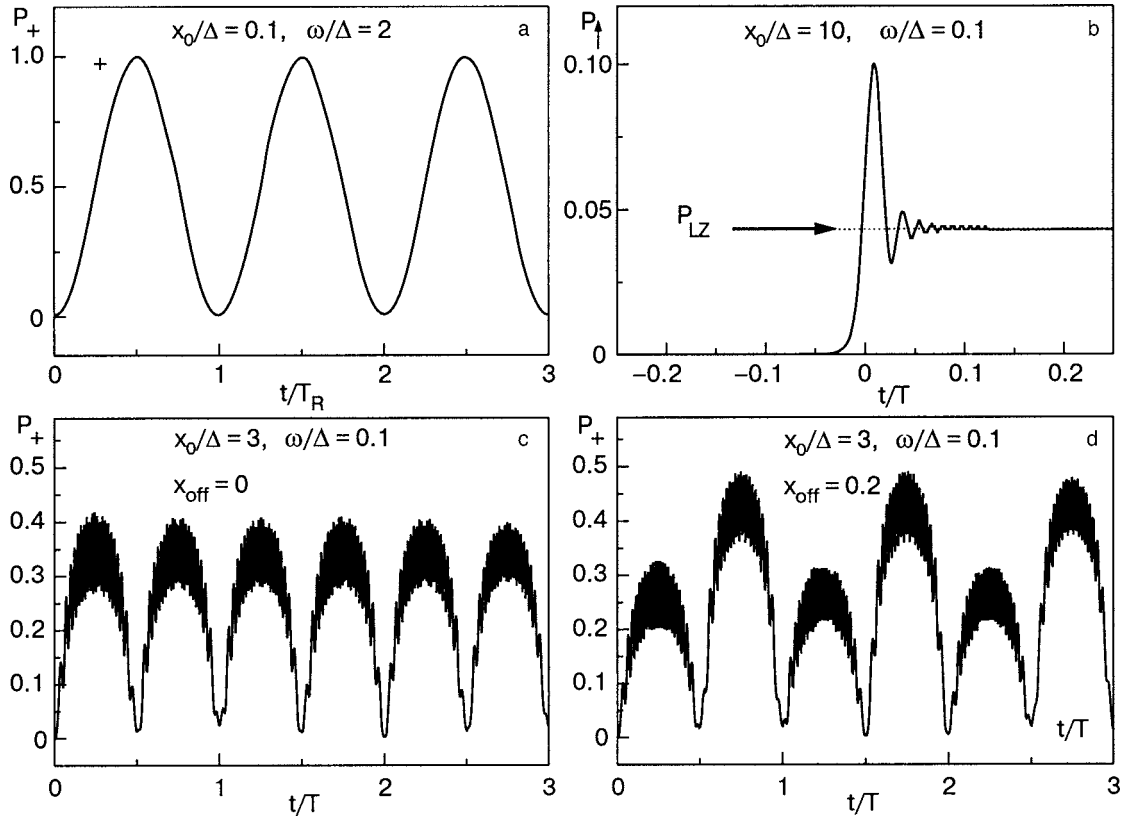

FIG. 1. Time dependence of upper-level occupation probabilities. Rabi oscillations in P_+ with the period $T_R=2\pi/x_0$ (a), LZ transition in $P_\uparrow$ (see Sec. 3.2.) (b), P_+ probability evolution in the case of periodically swept parameters at $x_{\rm off}=0$ (c) and $x_{\rm off}\neq 0$ (d). Here $\Gamma_\varphi=\Gamma_{\rm relax}=0$; $T=2\pi/\omega$.

$$\hat{H}' = -\frac{\Delta E}{2}\hat{\tau}_z + x_0 \sin\omega t\cdot\hat{V},$$

$$\hat{V}=\frac{2\Delta}{\Delta E}\hat{\tau}_x-\frac{2x_{\rm off}}{\Delta E}\hat{\tau}_z. \tag{13}$$

First consider the situation $x_{\rm off}=0$; then the difference between the stationary energy levels is $\Delta E=2\Delta$. In the case

$$\Delta\omega\equiv\omega-\Delta E\ll\Delta E \quad \text{and} \quad x_0\ll\Delta E, \tag{14}$$

one can use the so-called rotating wave approximation, and the result is[26]

$$P_+(t)=\frac{1}{2}\frac{x_0^2}{x_0^2+(\Delta\omega)^2}\left(1-\cos\sqrt{x_0^2+(\Delta\omega)^2}\,t\right). \tag{15}$$

For the average probability, it follows that

$$\bar{P}_+=\frac{1}{2}\frac{x_0^2}{x_0^2+(\Delta\omega)^2}. \tag{16}$$

This means that at $\omega=\Delta E$ there is resonance, $\bar{P}_+=\frac{1}{2}$, and $P_+(t)$ is an oscillating function with the frequency x_0. This is illustrated in Fig. 1a. The peak at $\omega=\Delta E$ on the $\bar{P}_+-\omega$ curve has a width at half maximum (i.e., at $P_+=1/4$) of approximately $2x_0$ (see the upper panels of Fig. 2).

Resonant excitations of a two-level system for $x_0/\Delta E\ll 1$ may occur not only at $\omega=\Delta E$. In the Kth order approximation, $(x_0/\Delta E)^K$, resonances exist at $\omega\simeq\Delta E/K$.[4,27] For $x_{\rm off}=0$, the resonances occur at odd K only. The dependence of P_+ on time in the vicinity of the Kth resonance is described by a relation similar to Eq. (15) (with substitutions $\Delta\omega\to\Delta\omega^K\simeq K\omega-\Delta E$ and $x_0\to x_0^K$). Hence, the width of the Kth resonance is of the order of x_0^K. At resonance, $\Delta\omega^{(K)}=0$, the energy levels $|-\rangle$ and $|+\rangle$ are equally populated, so that $\bar{P}_+(\omega=\omega^{(K)}\simeq\Delta E/K)=1/2$, which is the maximum value of $\bar{P}_+$, since population inversion is not possible in a two-level system.

When $x_{\rm off}\neq 0$, the matrix $\hat{V}$ has nonzero diagonal elements [see Eq. (13)]. The appearance of the nonzero diagonal elements does not influence Rabi resonances at odd K, but rather results in the generation of resonances at even K. This is demonstrated in Fig. 2 and discussed in Sec. 3.3.

3.2. LZ effect

The LZ effect is manifested in the nonadiabatic transition with the probability

$$P_{LZ}=\exp\left(-\frac{\pi\Delta^2}{\omega x_0}\right) \tag{17}$$

between two adiabatic energy levels during a single-sweep event.[1]

The time-dependent Hamiltonian $\hat{H}$ is diagonalized in the adiabatic basis, denoted as $\{|\downarrow\rangle,|\uparrow\rangle\}$, by the matrix $\hat{S}_1$,

$$\hat{S}_1=\begin{bmatrix}\cos\dfrac{\eta}{2} & \sin\dfrac{\eta}{2}\\ -\sin\dfrac{\eta}{2} & \cos\dfrac{\eta}{2}\end{bmatrix},$$

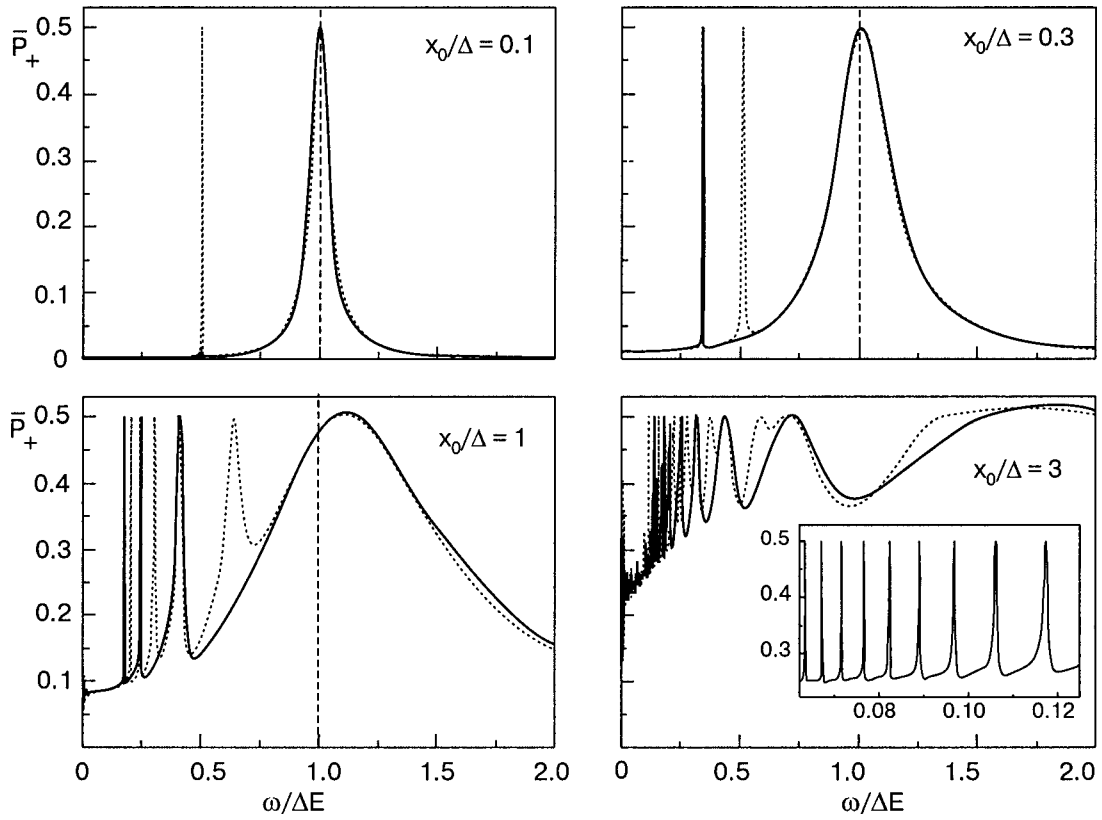

FIG. 2. Dependence of the probability $\bar{P}_+$ on the frequency ω for different x_0 at $\Gamma_\varphi = \Gamma_{\text{relax}} = 0$ and at $x_{\text{off}} = 0$ (solid line) and $x_{\text{off}} = 0.2\Delta$ (dashed line). (Only the first few resonant peaks are plotted; the others, which are very narrow, are not shown on the graphs.) Inset: enlargement of the low-frequency region.

$$\sin\eta = -\frac{B_x}{\Delta E_1} = \frac{2\Delta}{\Delta E_1},$$

$$\cos\eta = \frac{B_z}{\Delta E_1} = -\frac{2x(t)}{\Delta E_1},$$

$$\Delta E_1(t) = 2\sqrt{\Delta^2 + x(t)^2}.$$

The instantaneous eigenvalues of $\hat{H}$ are $E_{\downarrow,\uparrow} = \pm\Delta E_1(t)/2$.

We now can change over from the stationary basis to the adiabatic one,

$$\begin{bmatrix} |\downarrow\rangle \\ |\uparrow\rangle \end{bmatrix} = \hat{S}_1 \begin{bmatrix} |0\rangle \\ |1\rangle \end{bmatrix} = \hat{S}_1 \hat{S}^{-1} \begin{bmatrix} |-\rangle \\ |+\rangle \end{bmatrix} \equiv \hat{S}_2 \begin{bmatrix} |-\rangle \\ |+\rangle \end{bmatrix}.$$

Assuming $x_{\text{off}} = 0$, we obtain

$$\hat{S}_2 = \frac{1}{\sqrt{2}} \begin{bmatrix} \cos\frac{\eta}{2} + \sin\frac{\eta}{2} & -\cos\frac{\eta}{2} + \sin\frac{\eta}{2} \\ \cos\frac{\eta}{2} - \sin\frac{\eta}{2} & \cos\frac{\eta}{2} + \sin\frac{\eta}{2} \end{bmatrix}.$$

Thus, provided we calculate the density matrix in the stationary basis $\hat{\rho}$, we find it in the adiabatic basis $\hat{\rho}_{\text{adiab}}$,

$$\hat{\rho}_{\text{adiab}} = \hat{S}_2^{-1} \hat{\rho} \hat{S}_2. \tag{18}$$

The initial condition for $\hat{\rho}$ can be obtained from the initial condition for $\hat{\rho}_{\text{adiab}}$ by inverting the relation (18).

Let us now consider as an illustrative example the one-sweep process,

$$t \in \left(-\frac{T}{4}, \frac{T}{4}\right), \quad T = \frac{2\pi}{\omega},$$

$$x(t) = x_0 \sin\omega t, \quad x(t) \in (-x_0, x_0), \quad x_0 \gg \Delta \gg \omega,$$

which corresponds to the LZ model.[28] We choose the initial condition to be

$$\hat{\rho}_{\text{adiab}}\left(-\frac{T}{4}\right) = \begin{bmatrix} 1 & 0 \\ 0 & 0 \end{bmatrix},$$

which means that the system at $t = -T/4$ is in the lower adiabatic state. We look for the occupation probability $P_\uparrow = \rho^{22}_{\text{adiab}}(t)$ of the upper adiabatic level $|\uparrow\rangle$, which is equal to the LZ probability at the end of the sweep,[28] $P_\uparrow(T/4) = P_{LZ}$. Thus, for the functions X, Y, Z introduced in Sec. 2, we get the initial condition

$$X\left(-\frac{T}{4}\right) = \frac{x_0}{\sqrt{\Delta^2 + x_0^2}}, \quad Y\left(-\frac{T}{4}\right) = 0,$$

$$Z\left(-\frac{T}{4}\right) = \frac{\Delta}{\sqrt{\Delta^2 + x_0^2}}$$

and find

$$P_\uparrow(t) = \frac{1}{2} - \frac{\Delta}{2\sqrt{\Delta^2 + x(t)^2}} Z(t) + \frac{x(t)}{2\sqrt{\Delta^2 + x(t)^2}} X(t).$$

This is illustrated in Fig. 1b, which is equivalent to Fig. 3d in Ref. 10.

In the general case, $x_{\text{off}} \neq 0$, we calculate $\hat{S}_2$ and then $\hat{\rho}_{\text{adiab}}$ according to Eq. (18). Then the probability $P_\uparrow$ is given by

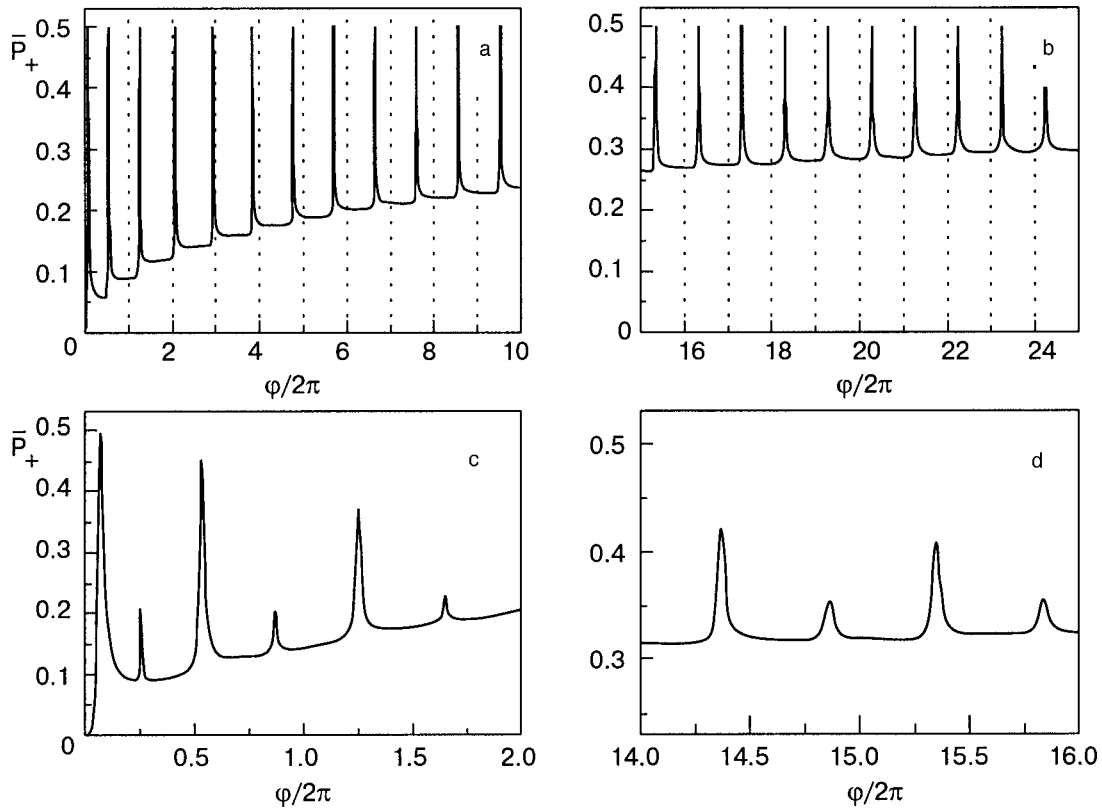

FIG. 3. Dependence of the probability $\bar{P}_+$ on $\varphi = 4x_0/\omega$ at $x_0\omega/\Delta^2 = 0.45$ (which corresponds to $P_{LZ} = 10^{-3}$); $\Gamma_\varphi = \Gamma_{\text{relax}} = 0$ and $x_{\text{off}} = 0$ for graphs (a) and (b); $\Gamma_\varphi/\Delta = \Gamma_{\text{relax}}/\Delta = 10^{-3}$ and $x_{\text{off}}/\Delta = 0.05$ for graphs (c) and (d).

$$P_\uparrow(t) = \frac{1}{2} - \frac{(\Delta^2 + x(t)x_{\text{off}})}{2\sqrt{\Delta^2 + x(t)^2}\sqrt{\Delta^2 + x_{\text{off}}^2}} Z(t) + \frac{\Delta(x(t) - x_{\text{off}})}{2\sqrt{\Delta^2 + x(t)^2}\sqrt{\Delta^2 + x_{\text{off}}^2}} X(t).$$

This should be supplemented with the corresponding initial condition.

3.3. Crossover from multiphoton Rabi resonances to LZ-interferometry: numerical results

Now making use of the numerical solution of Eqs. (8)–(10) for the Hamiltonian (13), we study the dependence of the time-averaged probability $\bar{P}_+$ on the frequency ω and amplitude x_0. For small amplitudes, $x_0 \ll \Delta E$, there are resonant peaks in the $\bar{P}_+ - \omega$ dependence at $\omega \simeq \Delta E/K$, as described in Sec. 3.1 and illustrated in Fig. 2. With increasing amplitude x_0, the resonances shift to higher frequencies. For $x_{\text{off}} = 0$, the resonances appear at "odd" frequencies ($K = 1,3,5,\ldots$) only, as was studied in Ref. 9. For $x_{\text{off}} \neq 0$ there are also resonances at "even" frequencies ($K = 2,4,\ldots$), which is demonstrated in Fig. 2. We note that Fig. 2 is plotted for the ideal case of the absence of decoherence and relaxation, $\Gamma_\varphi = \Gamma_{\text{relax}} = 0$, when the resonant value is $\bar{P}_+ = 1/2$. The effect of finite dephasing, $\Gamma_\varphi \neq 0$, and relaxation, $\Gamma_{\text{relax}} \neq 0$, is to decrease the resonant values of $\bar{P}_+$ and to widen the peaks for $\Gamma_\varphi > \Gamma_{\text{relax}}$. Thus from the comparison of the theoretically calculated resonant peaks with the experimentally observed ones, the dephasing Γ_φ and the relaxation rates Γ_{relax} can be obtained.[16]

When the system is driven slowly, $\omega \ll \Delta$, and with large amplitude, $x_0 \gg \Delta$, the LZ excitation mechanism is relevant for the description of the system dynamics. In the previous subsection we considered the LZ transition for a single-sweep event. Now we study the periodic driving of the system: interferences between multiple LZ transitions arise, leading to resonant excitations.[2,12,13] We will compare these resonances with the multiphoton Rabi ones.

First, we note that the resonance positions depend on the amplitude; this is demonstrated for $\omega \ll \Delta < x_0$ in the inset of Fig. 2. But it is more illustrative to study the resonance properties via the dependence of $\bar{P}_+$ on the ratio x_0/ω (or, more precisely, on the phase the state vector picks up per half period,[12] $\varphi = 4x_0/\omega$). It is reasonable to carry out the calculation for a fixed value of the product x_0/ω, which in turn defines the LZ probability [see Eq. (17)]. This allows us not only to compare our results with the results of Ref. 12, where the periodicity of the resonances in φ was predicted, but also to demonstrate the transition from the multiphoton Rabi resonances to the ones induced due to the interference of LZ excitations by means of the $\bar{P}_+ - \varphi$ dependence.

In Fig. 3a,b we plotted the dependence of $\bar{P}_+$ on φ for $x_{\text{off}} = 0$ and $\Gamma_\varphi = \Gamma_{\text{relax}} = 0$. The first few peaks, in the region $x_0 \lesssim \Delta$), corresponding to the multiphoton Rabi resonances, are situated at $\varphi \sim K^2$ (that follows from the resonance relation $\omega = \Delta E/K$). With increasing φ (which is proportional to x_0) we observe the overall rising of the curve in accordance with the conclusions of Ref. 9. At $\varphi \gg 1$, i.e., at $\omega \ll \Delta \ll x_0$, the resonance position is 2π-periodic, in agreement with Ref. 12. A nonzero offset $x_{\text{off}} \neq 0$ results in the appearance of ad-

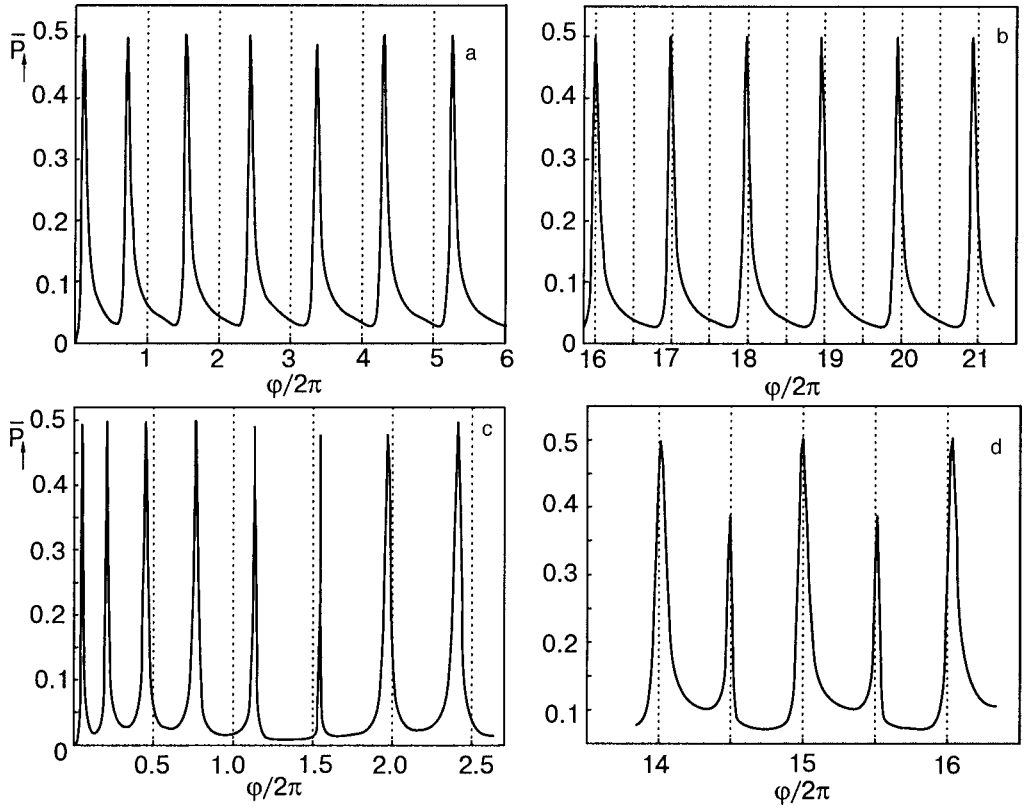

FIG. 4. Dependence of the probability $\bar{P}_\uparrow$ on the phase $\varphi = 4x_0/\omega$; $\Gamma_\varphi = \Gamma_{\text{relax}} = 0$ and $\varphi_{\text{off}} = 0$ for graphs (a) and (b), $\Gamma_\varphi = \Gamma_{\text{relax}} = 0$ and $\varphi_{\text{off}} = \pi/4$ for graph (c), $\Gamma_\varphi = 5\times10^{-4}$, $\Gamma_{\text{relax}} = 2.5\times10^{-4}$, $x_{\text{off}} = 0.35$ for graph (d).

ditional resonances between the basic ones,[12] which is demonstrated in Fig. 3c,d. Such a feature is similar to the multiphoton Rabi resonances. Nonzero decoherence decreases and widens the peaks, as we have also demonstrated in Fig. 3c,d.

In Fig. 4 we present the dependence of $\bar{P}_\uparrow$ on φ for the calculations carried out in the adiabatic basis (cf. Sec. 3.2.). In Fig. 4a,b we plotted such a dependence for different values of φ at $x_{\text{off}} = 0$ and $\Gamma_\varphi = \Gamma_{\text{relax}} = 0$. For $\varphi \gg 1$ (see Fig. 4b) the resonances are 2π-periodic, and the peaks are situated at the integer values of $\varphi/2\pi$, as predicted in Ref. 12. We also plotted the dependence of $\bar{P}_\uparrow$ on φ for nonzero offset $x_{\text{off}} \neq 0$ [see Fig. 4c,d)], namely for $\varphi_{\text{off}} = 4x_{\text{off}}/\omega = \pi/4$.

4. MULTIPHOTON EXCITATIONS IN THE INTERFEROMETER-TYPE CHARGE QUBIT

4.1. Interferometer-type charge qubit

In this Section, we consider the quantum dynamics of the interferometer-type charge qubit with periodically varying control parameters.[19–21] This qubit consists of two Josephson junctions closed by a superconducting ring. The charge *en* of the island between the junctions is controlled by the gate voltage V_g via the capacitance C_g. The junctions are characterized by Josephson energies E_{J1}, E_{J2} and phase differences δ_1, δ_2. The relevant energy values are the island's Coulomb energy, $E_C = e^2/2C_{\text{tot}}$, where C_{tot} is the total capacitance of the island, and the effective Josephson energy

$$\varepsilon_J = (E_{J1}^2 + E_{J2}^2 + 2E_{J1}E_{J2}\cos\delta)^{1/2}.$$

An important feature of the qubit is that its Josephson energy is controlled by the external magnetic flux Φ_e piercing the ring. In this paper, the ring inductance L is assumed to be small. Then the total phase difference, $\delta = \delta_1 + \delta_2$, is approximately equal to $\delta_e = 2\pi\Phi_e/\Phi_0$, and thus $\varepsilon_J = \varepsilon_J(\delta) \simeq \varepsilon_J(\delta_e)$.

Within the two-level model with the basis of "charge states" $|0\rangle$ and $|1\rangle$ corresponding to the excess number of Cooper pairs on the island, the Hamiltonian of the interferometer-type charge qubit can be written as[6]

$$\hat{H} = -\frac{1}{2}\varepsilon_J\hat{\sigma}_x - \frac{1}{2}E_{\text{ch}}\hat{\sigma}_z, \tag{19}$$

where $E_{\text{ch}} = 4E_C(1-n_g)$ and $n_g = C_gV_g/e$. Here the domination of the Coulomb energy of a Cooper pair $4E_C$ over the coupling energy ε_J is assumed, $4E_C/\varepsilon_J > 1$. The eigenstates, $\{|-\rangle, |+\rangle\}$, of this Hamiltonian are discriminated by the direction of the supercurrent in the ring.[21]

The qubit is considered to be coupled not only to the gate but also to the tank circuit that enables both phase control and readout. Thus there are two possibilities for making the Hamiltonian of the two-level system (19) time-dependent. First, the gate voltage V_g can be driven,

$$n_g = n_g^{(0)} + n_g^{(1)}\sin\omega t, \tag{20}$$

and, second, the dc and ac components of the current in the tank circuit can induce a periodically varying magnetic flux,

$$\delta = \delta_{dc} + \delta_{ac}\sin\omega t. \tag{21}$$

Here we restrict our consideration to the case of sinusoidal time dependence of the parameters.

Further we study the time-averaged occupation probability of the excited state $\bar{P}_+$. We note that because the two states $|-\rangle$ and $|+\rangle$ belong to oppositely circulating currents in the ring, they correspond to different signs of the qubit's Josephson inductance. The latter can be probed by the impedance measuring technique,[25] which makes it possible to observe the resonant behavior of $\bar{P}_+$ studied in the following subsection.

4.2. Resonant excitation of the interferometer-type charge qubit

The case of the excitation of the interferometer-type charge qubit via the gate [Eq. (20)] can easily be related to the case considered in Sec. 3; see the Hamiltonians (11) and (19) with the diagonal time-dependent parameters defined by Eq. (20). Then the ratio x_0/Δ is given by

$$\frac{x_0}{\Delta}=\frac{4E_C}{\varepsilon_J}n_g^{(1)}.$$

Thus, both mechanisms considered in Sec. 3 can be realized: multiphoton excitations ($x_0/\Delta \ll 1$) and LZ interferometry ($x_0/\Delta \gg 1$).

Let us now consider the second possibility, excitation of the qubit by a time-dependent magnetic flux. The Hamiltonian of the interferometer-type charge qubit (19) with the periodically varying phase δ [Eq. (21)] is related to the Hamiltonian of a two-level system considered in Sec. 2 [Eq. (5)] by the following relations:

$$B_x(t)\equiv\varepsilon_J,$$

$$B_x^{(0)}=B_x(0)\equiv B_x|_{\delta_{ac}=0},$$

$$B_x^{(1)}(t)=B_x(t)-B_x(0),$$

$$B_z^{(0)}=E_{\rm ch}.$$

In two limiting cases, the expressions can be simplified to result in a time-dependent term of the form

$$B_x^{(1)}(t)\propto\sin\omega t. \tag{22}$$

Namely, for

$$\delta-\pi\gg\frac{|E_{J1}-E_{J2}|}{\sqrt{E_{J1}E_{J2}}},\quad \delta_{ac}\lesssim\delta_{dc}-\pi\ll\pi \tag{23}$$

we have

$$B_x^{(0)}\simeq\sqrt{E_{J1}E_{J2}}(\delta_{dc}-\pi), \tag{24}$$

$$B_x^{(1)}(t)\simeq\sqrt{E_{J1}E_{J2}}\delta_{ac}\sin\omega t, \tag{25}$$

and for

$$\delta-\pi\ll\frac{|E_{J1}-E_{J2}|}{\sqrt{E_{J1}E_{J2}}},\quad \delta_{ac}\ll\delta_{dc}-\pi\ll\pi, \tag{26}$$

it follows that

$$B_x^{(1)}(t)\simeq|E_{J1}-E_{J2}|, \tag{27}$$

$$B_x^{(1)}(t)\simeq\frac{E_{J1}E_{J2}}{|E_{J1}-E_{J2}|}(\delta_{dc}-\pi)\delta_{ac}\sin\omega t. \tag{28}$$

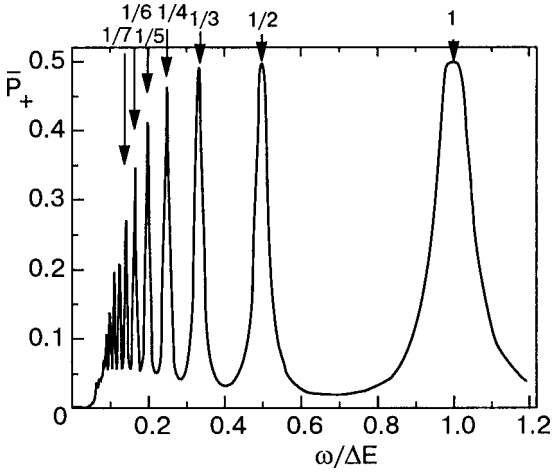

FIG. 5. Dependence of the probability $\bar{P}_+$ on the frequency ω for the phase-biased charge qubit at $n_g=0.95$, $E_{J1}/E_C=12.4$, $E_{J2}/E_C=11$, $\Gamma_{\rm relax}/E_C=10^{-4}$, $\delta_{ac}=0.2\pi$, $\delta_{dc}=\pi+0.2\pi$.

When relation (22) holds, the present problem (of the charge qubit with time-dependent magnetic control) can be related to the problem considered above in Sec. 3 by the expressions (6). Then we can estimate the ratio $x_0/\Delta E$, which characterizes the mechanism of the excitation of the qubit. For example, at $x_0/\Delta E\lesssim 1$ we expect multiphoton resonances in the qubit's response to the external alternating magnetic flux. We consider this case below in detail.

We note that the width of the resonant peaks is defined by the off-diagonal components of the Hamiltonian (13), i.e., by the product $x_0\Delta$. Then looking at Eqs. (25) and (28), we conclude that the width of the resonances is defined by the product $\delta_{ac}(1-n_g)$.

Finally, we illustrate the multiphoton resonant excitations of the interferometer-type charge qubit. Making use of the numerical solution of the master equation (Sec. 2), we find the time-averaged probability $\bar{P}_+$ plotted in Fig. 5. The position of the multiphoton resonant peaks is defined by the relation $\omega=\Delta E/K$, where $\Delta E=\Delta E(\delta_{dc})$ is supposed to be fixed. Alternatively, when the δ_{dc} component of the phase is changed and the frequency ω is fixed, a similar graph can be plotted with resonances at $\delta_{dc}=\delta_{dc}^{(K)}$ defined by the relation $\Delta E(\delta_{dc}^{(K)})=K\omega$.

5. CONCLUSIONS

We have studied the dynamic behavior of a quantum two-level system subjected to periodic sweeping of its parameters. The energy levels population was calculated by solving the master equation for the density matrix with relaxation terms. Studying the population of the excited state in both stationary and adiabatic bases, we analyzed some features of the multiphoton Rabi and LZ effects. Particularly, we have shown certain similarities of the multiphoton resonances at $x_0\ll\omega$ with the resonances at $x_0\gg\Delta\gg\omega$ due to the interference between multiple LZ transitions. Based on the solution of the master equation for the density matrix, we described in detail the dynamic behavior of the interferometer-type charge qubit subjected to periodically changing gate voltage or magnetic flux.

This work was supported in part by the program ''Nanosystems, nanomaterials, and nanotechnology'' of the National Academy of Sciences of Ukraine. S.N.S. acknowledges the support of the German Academic Exchange Service (DAAD). The authors thank V. I. Shnyrkov for fruitful discussions.

*E-mail: sshevchenko@ilt.kharkov.ua

[1] L. D. Landau, Phys. Z. Sowjetunion **2**, 46 (1932); C. Zener, Proc. R. Soc. London, Ser. A **137**, 696 (1932).
[2] V. A. Benderskii, E. V. Vetoshkin, and E. I. Kats, Zh. Éksp. Teor. Fiz. **124**, 259 (2003) [JETP **97**, 232 (2003)].
[3] I. I. Rabi, Phys. Rev. **51**, 652 (1937).
[4] N. B. Delone and V. P. Krainov, *Atoms in Strong Light Fields*, Vol. 28 of Springer Ser. Chem. Phys., Springer, Berlin-Heidelberg (1985), Atomizdat, Moscow (1978).
[5] M. Grifoni and P. Hänggi, Phys. Rep. **304**, 229 (1998).
[6] Yu. Makhlin, G. Schön, and A. Shnirman, Rev. Mod. Phys. **73**, 357 (2001).
[7] Y. Nakamura, Yu. A. Pashkin, and J. S. Tsai, Nature (London) **398**, 786 (1999).
[8] J. E. Mooij, T. P. Orlando, L. Levitov, Lin Tian, Caspar H. van der Wal, and Seth Lloyd, Science **285**, 1036 (1999).
[9] V. P. Krainov and V. P. Yakovlev, Zh. Exp. Theor. Fiz. **105**, 2204 (1980) [Sov. Phys. JETP **78**, 2204 (1980)].
[10] N. V. Vitanov, Phys. Rev. A **59**, 988 (1999).
[11] D. A. Garanin and R. Schilling, Phys. Rev. B **66**, 174438 (2002).
[12] A. V. Shytov, D. A. Ivanov, and M. V. Feigel'man, Europhys. B **36**, 263 (2004).
[13] Y. Teranishi and H. Nakamura, Phys. Rev. Lett. **81**, 2032 (1998).
[14] Y. Nakamura, Yu. A. Pashkin, and J. S. Tsai, Phys. Rev. Lett. **87**, 246601 (2001).
[15] J. Q. You and F. Nori, Phys. Rev. B **68**, 064509 (2003).
[16] S. Saito, M. Thorwart, H. Tanaka, M. Ueda, N. Nakano, K. Semba, and H. Takayanagi, Phys. Rev. Lett. **93**, 037001 (2004).
[17] D. Born, V. I. Shnyrkov, W. Krech, Th. Wagner, E. Il'ichev, M. Grajcar, U. Hübner, and H.-G. Meyer, Phys. Rev. B **70**, 180501(R) (2004).
[18] G. Falci, R. Fazio, G. M. Palma, J. Siewert, and V. Vedral, Nature (London) **407**, 355 (2000).
[19] A. B. Zorin, Physica C **368**, 284 (2002).
[20] J. R. Friedman and D. V. Averin, Phys. Rev. Lett. **88**, 050403 (2002).
[21] W. Krech, M. Grajcar, D. Born, I. Zhilyaev, Th. Wagner, E. Il'chev, and Ya. Greenberg, Phys. Lett. A **303**, 352 (2002).
[22] K. Blum, *Density Matrix Theory and Applications*, Plenum Press, New York-London (1981).
[23] The phenomenological description of the relaxation processes in terms of the rates was shown[12] to be equivalent to the microscopic description, which intrinsically includes the reservoir. Such a phenomenological approach was successfully applied to the description of the quantum dynamics of phase qubits.[16]
[24] A. Aassime, G. Johansson, G. Wendin, R. J. Schoelkopf, and D. Delsing, Phys. Rev. Lett. **86**, 3376 (2001).
[25] E. Il'ichev, N. Oukhanski, Th. Wagner, H.-G. Meyer, A. Yu. Smirnov, M. Grajcar, A. Izmalkov, D. Born, W. Krech, and A. Zagoskin, Fiz. Nizk. Temp. **30**, 823 (2004) [Low Temp. Phys. **30**, 620 (2004)].
[26] S. Flügge, *Practical Quantum Mechanics II*, Springer, Berlin-Heidelberg-New York (1971), task 180.
[27] C. Cohen-Tannoudji, J. Dupont-Roc, and G. Grynberg, *Atom-Photon Interactions*, Wiley, New York (1992).
[28] In the vicinity of the transition point $x=0$ (where the excitation happens), $x(t)$ is a linear function of t, $x(t)\simeq x_0\omega t$, which is exactly the LZ model. Deviations of the function $x(t)$ from the linear dependence far from the transition point do not matter.[11] This explains the quantitative coincidence of the results presented in this Section with the results obtained with $x(t)$ being a linear function.

This article was published in English in the original Russian journal. Reproduced here with stylistic changes by AIP.

LOW-TEMPERATURE MAGNETISM

Stabilization of the magnetic resonance position by a harmonized field

E. A. Ivanchenko*

National Research Center "Kharkov Institute of Physics and Technology," ul. Akademicheskaya 1, Kharkov 61108, Ukraine

(Submitted January 14, 2005)
Fiz. Nizk. Temp. **31**, 761–768 (July 2005)

A two-level system in a magnetic field with a periodic temporal modulation that stabilizes the position of the magnetic resonance is investigated in the density matrix formalism. An exact solution is found for the density matrix at resonance. It is shown that at resonance the probability of a spin-flip transition is independent of the form of the field, i.e., the main resonance is stable against harmonized variation of the longitudinal and transverse components of the magnetic field. The Bloch polarization vector and the geometric phase at resonance are calculated. A differential equation for the transition probability is obtained. The dependence of the time-averaged probability of a spin flip on the normalized Larmor frequency is investigated numerically for different parameters of the model. It is shown that the position of the main resonance is independent of the deformation of the field; only the width of the resonance peak changes upon deformation. The odd parametric ('multiphoton) resonance transitions are investigated. The static magnetization induced by the harmonized field is considered. This study may find application in the analysis of interference experiments, for refining the designs of magnetic spectrometers, and for controlling qubits. © *2005 American Institute of Physics.*
[DOI: 10.1063/1.2001636]

1. INTRODUCTION

The standard implementation of magnetic resonance utilizes a dc magnetic field perpendicular to a linearly polarized monochromatic ac magnetic field varying with time t. In that case a shift of the resonance frequency (the Bloch–Siegert shift[1]) occurs. The goal of this study is to find a magnetic field configuration for which the position of the principal resonance is determined solely by the Larmor frequency at arbitrary parameters of the system. This goal can be reached by a generalization of the Rabi model.[2] Rabi studied the temporal dynamics of a particle with a magnetic dipole moment and spin 1/2 in a dc magnetic field H_0 directed along the z axis and an ac magnetic field perpendicular to it, rotating uniformly with frequency $\omega/2\pi$: $H_x = h_0 \cos \omega t$, $H_y = h_0 \sin \omega t$, where H_0 and h_0 are the field amplitudes.

There are a number of ways of modulating the magnetic field in studying the resonance, depending on the purpose of the experiment (see Ref. 3 and the works cited therein). In this paper we investigate the time evolution of a particle with a magnetic dipole moment and spin 1/2 in a deformed magnetic field of the form

$$\mathbf{H}(t) = (h_0 \mathrm{cn}(\omega t,k), h_0 \mathrm{sn}(\omega t,k), H_0 \mathrm{dn}(\omega t,k)), \tag{1}$$

in which cn, sn, and dn are the Jacobi elliptic functions.[4] Such a modulation of the field, as the modulus of the elliptic functions is varied from zero to unity, describe a whole class of field forms, from trigonometric,[2]

$$(\mathrm{cn}(\omega t,0) = \cos \omega t, \mathrm{sn}(\omega t,0) = \sin \omega t, \mathrm{dn}(\omega t,0) = 1),$$

to pulsed exponential,[5]

$$\left(\mathrm{cn}(\omega t,1) = \frac{1}{\mathrm{ch}\omega t}, \mathrm{sn}(\omega t,1) = \tanh \omega t, \right.$$

$$\mathrm{dn}(\omega t,1) = \frac{1}{\cosh \omega t}.$$

The elliptic functions $\mathrm{cn}(\omega t,k)$ and $\mathrm{sn}(\omega t,k)$ have a real period $4K/\omega$, while the function $\mathrm{dn}(\omega t,k)$ has a real period half as long. Here K is the complete elliptic integral of the first kind.[4] In other words, although the field is periodic with a common real period of $4K/\omega$, one can see that the frequency of the amplitude modulation of the longitudinal field is twice that of the amplitude modulation of the transverse field. We shall call such a field "harmonized."

The Schrödinger equation for the wave function $\Psi(t)$ describing the dynamics of a spin-1/2 particle possessing a magnetic moment in a time-varying magnetic field $\mathbf{H}(t)$ has the form

$$i\hbar \partial_t \Psi(t) = \frac{g\mu_0}{2} \boldsymbol{\sigma} \cdot \mathbf{H}(t) \Psi(t), \tag{2}$$

where g is the Lande factor, μ_0 is the Bohr magneton, and the Pauli matrices are

$$\boldsymbol{\sigma} = (\sigma_x, \sigma_y, \sigma_z) = \left(\begin{pmatrix} 0 & 1 \\ 1 & 0 \end{pmatrix}, \begin{pmatrix} 0 & -i \\ i & 0 \end{pmatrix}, \begin{pmatrix} 1 & 0 \\ 0 & -1 \end{pmatrix} \right).$$

The solution of the Schrödinger equation can be represented in the form an expansion in eigenfunctions of the matrix σ_z:

$$\Psi(t) = \begin{pmatrix} 1 \\ 0 \end{pmatrix} \Psi_1(t) + \begin{pmatrix} 0 \\ 1 \end{pmatrix} \Psi_2(t). \tag{3}$$

The functions $\Psi_1(t)$ and $\Psi_2(t)$ are the probability amplitudes without and with a spin flip, respectively, and by definition obey the normalization condition

$$|\Psi_1(t)|^2+|\Psi_2(t)|^2=1 \tag{4}$$

and are assumed fixed at the initial time t.

2. GENERAL PROPERTIES OF THE MODEL

In this paper, which is a continuation of Ref. 6, we go over from a description with the aid of the wave function (3) to the density matrix formalism, with the density matrix

$$\rho=\begin{pmatrix}\Psi_1\Psi_1^* & \Psi_1\Psi_2^*\\ \Psi_2\Psi_1^* & \Psi_2\Psi_2^*\end{pmatrix}. \tag{5}$$

We introduce the dimensionless independent variable $\tau=\omega t$. Equation (2) implies the following equation for the density matrix:

$$i\partial_\tau\rho=[\hat{H},\rho]_- \tag{6}$$

with the Hermitian Hamiltonian

$$\hat{H}=\begin{pmatrix}\frac{\omega_0}{2\omega}\mathrm{dn}(\tau,k) & \frac{\omega_1}{2\omega}(\mathrm{cn}(\tau,k)-i\mathrm{sn}(\tau,k))\\ \frac{\omega_1}{2\omega}(\mathrm{cn}(\tau,k)+i\mathrm{sn}(\tau,k)) & -\frac{\omega_0}{2\omega}dn(\tau,k)\end{pmatrix}, \tag{7}$$

in which $\omega_0=g\mu_0H_0/\hbar$ is the Larmor frequency, and $\omega_1=g\mu_0h_0/\hbar$ is the amplitude of the transverse field in angular frequency units. The following properties derive from the definition of the density matrix: $\mathrm{Tr}\rho=1$, $\rho^+=\rho$, $\rho^2=\rho$. Further, as in Ref. 6, we shall assume that at the initial moment $\binom{\psi_1(0)}{\psi_2(0)}=\binom{1}{0}$, i.e.,

$$\rho(0)=\begin{pmatrix}1 & 0\\ 0 & 0\end{pmatrix}, \tag{8}$$

we make the substitution $\rho=\alpha^{-1}r\alpha$ with the matrix $\alpha=\binom{f\ \ 0}{0\ \ f^*}$, where the function f has the form

$$f=\sqrt{\mathrm{cn}\tau-i\mathrm{sn}\tau}=\sqrt{\frac{1+\mathrm{cn}\tau}{2}}-i\,\mathrm{sgn}(\mathrm{sn}\tau)\sqrt{\frac{1-\mathrm{cn}\tau}{2}}. \tag{9}$$

The equation for the transformed matrix takes the form

$$i\partial_\tau r=\frac{\omega_1}{2\omega}[\sigma_x,r]_-+\frac{\delta_r}{2\omega}\mathrm{dn}\tau[\sigma_z,r]_-, \tag{10}$$

where the detuning δ_r is equal to

$$\delta_r=\omega_0-\omega. \tag{11}$$

Since the detuning appears explicitly in the equation, the position of the principal resonance does not shift upon variations of the model parameters. At sharp resonance, when $\omega_0=\omega$, we obtain the equation

$$i\partial_\tau r^{(0)}=\frac{\omega_1}{2\omega}[\sigma_x,r^{(0)}]_-,\quad r^{(0)}(0)=\rho(0) \tag{12}$$

with the solution

$$r^{(0)}(\tau)=\exp\left(-i\frac{\omega_1}{2\omega}\tau\sigma_x\right)r^{(0)}(0)\exp\left(i\frac{\omega_1}{2\omega}\tau\sigma_x\right). \tag{13}$$

Therefore, at resonance the density matrix has the form

$$\rho^{(0)}=\begin{pmatrix}\cos^2\frac{\omega_1}{2\omega}\tau & if^2\sin\frac{\omega_1}{2\omega}\tau\cos\frac{\omega_1}{2\omega}\tau\\ -if^{*2}\sin\frac{\omega_1}{2\omega}\tau\cos\frac{\omega_1}{2\omega}\tau & \sin^2\frac{\omega_1}{2\omega}\tau\end{pmatrix} \tag{14}$$

and, hence, the transition probability

$$P_{1/2\to-1/2}(\tau,\delta_r=0)=\sin^2\frac{\omega_1}{2\omega}\tau \tag{15}$$

does not contain the modulus k, i.e., is independent of the harmonized deformation of the field.[6]

Let us investigate the solution of Eq. (10) in the form of a power series in the expansion parameter $\delta_r/2\omega$:

$$r(\tau)=r^{(0)}(\tau)+r^{(1)}(\tau)+\dots. \tag{16}$$

We substitute expansion (16) into Eq. (10) and equate terms with the same powers of $\delta_r/2\omega$. As a result, we obtain a system of equations for finding $r^{(l)}(\tau)$:

$$ir_\tau^{(0)}=\frac{\omega_1}{2\omega}[\sigma_x,r^{(0)}]_-, \tag{17}$$

$$ir_\tau^{(l)}=\frac{\omega_1}{2\omega}[\sigma_x,r^{(l)}]_-+\frac{\delta_r}{2\omega}\mathrm{dn}\tau[\sigma_z r^{(l-1)}]_-, \tag{18}$$

where $l=1,2,\dots$.

We left-multiply Eq. (18) by the matrix $\exp(i(\omega_1/2\omega)\tau\sigma_x)$ and right-multiply by the matrix $\exp(-i(\omega_1/2\omega)\tau\sigma_x)$. Now the terms $r^{(l)}$ in the series (16) are determined with the aid of the previous $r^{(l-1)}$ terms:

$$r^{(l)}=-i\exp\left(-i\frac{\omega_1}{2\omega}\tau\sigma_x\right)\times\left\{\int_0^\tau d\tau'\exp\left(i\frac{\omega_1}{2\omega}\tau'\sigma_x\right)\frac{\delta_r}{2\omega}\mathrm{dn}\tau[\sigma_z,r^{(l-1)}\times(\tau')]_-\exp\left(-i\frac{\omega_1}{2\omega}\tau'\sigma_x\right)\right\}\exp\left(i\frac{\omega_1}{2\omega}\tau\sigma_x\right). \tag{19}$$

Since the commutator $[\sigma_z,r^{(0)}(\tau')]_-=i\sin(\omega_1/\omega)\tau'\sigma_x$, the first correction

$$r^{(1)}(\tau)=\frac{\delta_r}{2\omega}\int_0^\tau d\tau'\,\mathrm{dn}\tau'\sin\frac{\omega_1}{\omega}\tau'\sigma_x \tag{20}$$

does not contribute to the transition probability. Using the Pauli matrix algebra, we obtain the density matrix including the second-order corrections:

$$\rho^{(\mathrm{II})}=\alpha^{-1}(r^{(0)}+r^{(1)}+r^{(2)})\alpha$$

$$=\begin{pmatrix} \cos^2\frac{\omega_1}{2\omega}\tau+\left(\frac{\delta_r}{2\omega}\right)^2 F_2 & if^2\sin\frac{\omega_1}{2\omega}\tau\cos\frac{\omega_1}{2\omega}\tau+\frac{\delta_r}{2\omega}f^2S-\left(i\frac{\delta_r}{2\omega}\right)^2 f^2F_1 \\ -if^{*2}\sin\frac{\omega_1}{2\omega}\tau\cos\frac{\omega_1}{2\omega}\tau+\frac{\delta_r}{2\omega}f^{*2}S+i\left(\frac{\delta_r}{2\omega}\right)^2 f^{*2}F_1 & \sin^2\frac{\omega_1}{2\omega}\tau-\left(\frac{\delta_r}{2\omega}\right)^2 F_2 \end{pmatrix}, \quad (21)$$

where

$$F_1=2\left(\Phi_1\sin\frac{\omega_1}{\omega}\tau+\Phi_2\cos\frac{\omega_1}{\omega}\tau\right),$$

$$F_2=2\left(-\Phi_1\cos\frac{\omega_1}{\omega}\tau+\Phi_2\sin\frac{\omega_1}{\omega}\tau\right),$$

$$\Phi_1=\frac{S^2}{2},\quad S=\int_0^\tau d\tau'\,\mathrm{dn}\tau'\,\sin\frac{\omega_1}{\omega}\tau',$$

$$\Phi_2=\int_0^\tau d\tau'\,\mathrm{dn}\tau'\,\cos\frac{\omega_1}{\omega}\tau' S(\tau'). \quad (22)$$

It is not hard to show that at any order in $\delta_r/2\omega$ the diagonal elements of the matrix ρ, which characterize the quantum dynamics of the probability without and with a spin flip, contain only terms of even order in $\delta_r/2\omega$, while the off-diagonal elements depend on both the even and odd powers of the expansion parameter, just as in the case of the exact density matrix in the Rabi model, ρ^R, which has long been used in the resonance spectroscopy of neutron, atomic, and molecular beams:

$$\rho^R=\begin{pmatrix} \cos^2\frac{\Omega_R}{2\omega}\tau+\frac{\delta_r^2}{\Omega_R^2}\sin^2\frac{\Omega_R}{2\omega}\tau & \left(i\frac{\omega_1}{\Omega_R}\sin\frac{\Omega_R}{\omega}\tau+\frac{\delta_r\omega_1}{2\Omega_R^2}\sin^2\frac{\Omega_R}{2\omega}\tau\right)e^{-i\tau} \\ \left(-i\frac{\omega_1}{2\Omega_R}\sin\frac{\Omega_R}{\omega}\tau+\frac{\delta_r\omega_1}{\Omega_R^2}\sin^2\frac{\Omega_R}{2\omega}\tau\right)e^{i\tau} & \frac{\omega_1^2}{\Omega_R^2}\sin^2\frac{\Omega_R}{2\omega}\tau \end{pmatrix}, \quad (23)$$

where $\Omega_R=\sqrt{\delta_r^2+\omega_1^2}$ is the Rabi frequency.

3. DIFFERENTIAL EQUATIONS FOR DETERMINING THE TRANSITION PROBABILITY

In the general case for arbitrary detuning δ_r (11) we represent the matrix r in the form of an expansion in the complete set of Pauli matrices:

$$r=\frac{1}{2}(1+\boldsymbol{\sigma}\cdot\mathbf{R}),\quad r=r^+,\quad \mathrm{Tr}\ r=1. \quad (24)$$

From the condition $\det\rho=0$ we obtain a relation between the unknown functions $(R_x,R_y,R_z)=\mathbf{R}$:

$$R_x^2+R_y^2+R_z^2=1 \quad (25)$$

for all τ. We substitute the expression for r (24) into Eq. (10). As a result we obtain a system of three first-order differential equations for the unknown real functions R_x,R_y,R_z:

$$\partial_\tau R_x=-\frac{\delta_r}{\omega}\mathrm{dn}\tau R_y, \quad (26)$$

$$\partial_\tau R_y=\frac{\delta_r}{\omega}\mathrm{dn}\tau R_x-\frac{\omega_1}{\omega}R_z, \quad (27)$$

$$\partial_\tau R_z=\frac{\omega_1}{\omega}R_y \quad (28)$$

with the initial conditions $R_x(0)=R_y(0)=0$, $R_z(0)=1$. The system of Eqs. (26)–(28) is equivalent to the vector equation $\partial_\tau\mathbf{R}=[\mathbf{f},\mathbf{R}]$, where $\mathbf{f}=((\omega_1/\omega),0,(\delta_r/\omega)\mathrm{dn}\tau)$ and is formally identical to the Frenet equations (for the first components of the moving trihedron) of a space curve on a sphere. Therefore, following Ref. 7, we introduce the complex function

$$y=\frac{R_z+iR_y}{1-R_x}.$$

The introduction of this function allows us, by making use of the conservation law (25), to reduce the system of three differential Eqs. (26)–(28) to a single complex Riccati equation:

$$\partial_\tau y=-i\frac{\omega_1}{\omega}y-i\frac{\delta_r}{2\omega}\mathrm{dn}\tau+i\frac{\delta_r}{2\omega}\mathrm{dn}\tau y^2,\quad y(0)=1. \quad (29)$$

Knowing y, we can easily find the functions R_x,R_y,R_z:

$$R_x=\frac{yy^*-1}{1+yy^*},\quad R_y=i\frac{y^*-y}{1+yy^*},\quad R_z=\frac{y+y^*}{1+yy^*}. \quad (30)$$

Now in terms of R_x,R_y,R_z the density matrix ρ takes the form

$$\rho=\frac{1}{2}\begin{pmatrix} 1+R_z & f^2(R_x-iR_y) \\ f^{*2}(R_x+iR_y) & 1-R_z \end{pmatrix}. \quad (31)$$

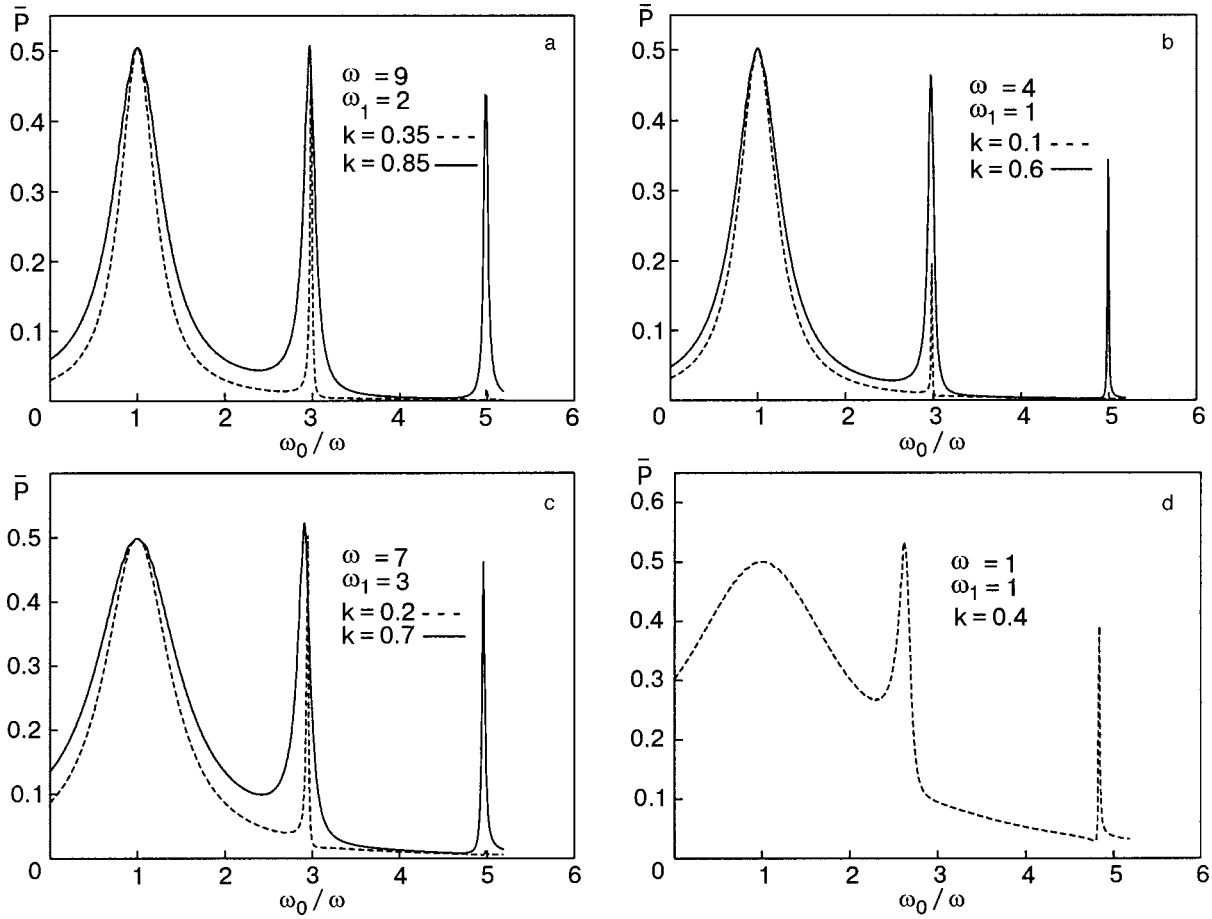

FIG. 1. Time-averaged transition probability as a function of the normalized Larmor frequency for different parameters.

The spin-flip transition probability is equal to the matrix element ρ_{22}, i.e.,

$$P_{1/2\to -1/2}(\tau,\delta_r,k)=\frac{1}{2}(1-R_z). \tag{32}$$

Using expression (32) and the system of Eqs. (26)–(28), one can easily obtain a differential equation for the transition probability, which we shall not write out here.

4. VISUALIZATION OF DYNAMICS ON THE BLOCH SPHERE. GEOMETRIC PHASE AT RESONANCE

The Bloch sphere is widely used for visualizing the dynamics of two-level systems.[8,9] The Bloch vector (polarization vector) **P** is defined for pure states as

$$\mathbf{P}=\mathrm{Tr}\ \ \rho\boldsymbol{\sigma}. \tag{33}$$

In the resonant case the matrix ρ is represented by formula (14). A simple calculation using formula (33) gives the result

$$\mathbf{P}=(\mathrm{sn}(\omega_0 t,k)\sin\omega_1 t,-\mathrm{cn}(\omega_0 t,k)\sin\omega_1 t,\cos\omega_1 t). \tag{34}$$

The polarization vector satisfies the Bloch equation

$$\partial_t\mathbf{P}=\gamma_m[\mathbf{H},\mathbf{P}],\quad \gamma_m=\frac{g\mu_0}{\hbar},\quad \mathbf{P}^2=1. \tag{35}$$

At times $\{t_n:\ \omega_1 t_n=2\pi n,\ n=1,2,\ldots\}$ the vector **P** takes on the initial value (0,0,1), i.e., the end of the vector traces out a closed trajectory on the Bloch sphere.

An Hermitian "phase" operator for a two-level systems is constructed in Ref. 9:

$$X_\Psi=\frac{1}{2}(|\Psi\rangle\langle\Psi A|+|A\Psi\rangle\langle\Psi|), \tag{36}$$

where $A=CU$, C is the operator of complex conjugation, and $U=\left(\begin{smallmatrix}0 & -1\\ 1 & 0\end{smallmatrix}\right)$. Information about the changes of the phase of motion is obtained from the three-dimensional "phase" vector

$$\mathbf{c}=\mathrm{Tr}\ \ X_\Psi\sigma, \tag{37}$$

which has the explicit form

$$\mathbf{c}=(\mathrm{cn}(\omega_0 t,k),\mathrm{sn}(\omega_0 t,k),0),\quad \mathbf{c}^2=1,\quad [\mathbf{c},\mathbf{P}]=0. \tag{38}$$

The "phase" vector **c** satisfies the vector equation

$$\partial_t\mathbf{c}=\gamma_m[\mathbf{H},\mathbf{c}],\quad \mathbf{c}(0)=(1,0,0). \tag{39}$$

Thus with the aid of this vector **c** one can determine the geometric (topological) phase, since the scalar product

$$\mathbf{c}(0)\cdot\mathbf{c}(t)=\mathrm{cn}(\omega_0 t,k) \tag{40}$$

on cyclic evolution does not coincide with the value at $t=0$. It is only in the exceptional case when $(\omega_0/\omega_1)2\pi n=4Kn_1$ $(n_1=1,2,\ldots)$ that the "phase" vector fails to give information about the phase. The third unit vector $\mathbf{a}=[\mathbf{P},\mathbf{c}]$, as is readily verified, satisfies the vector equation

$$\partial_t\mathbf{a}=\gamma_m[\mathbf{H},\mathbf{a}],\quad \mathbf{a}(0)=(0,1,0) \tag{41}$$

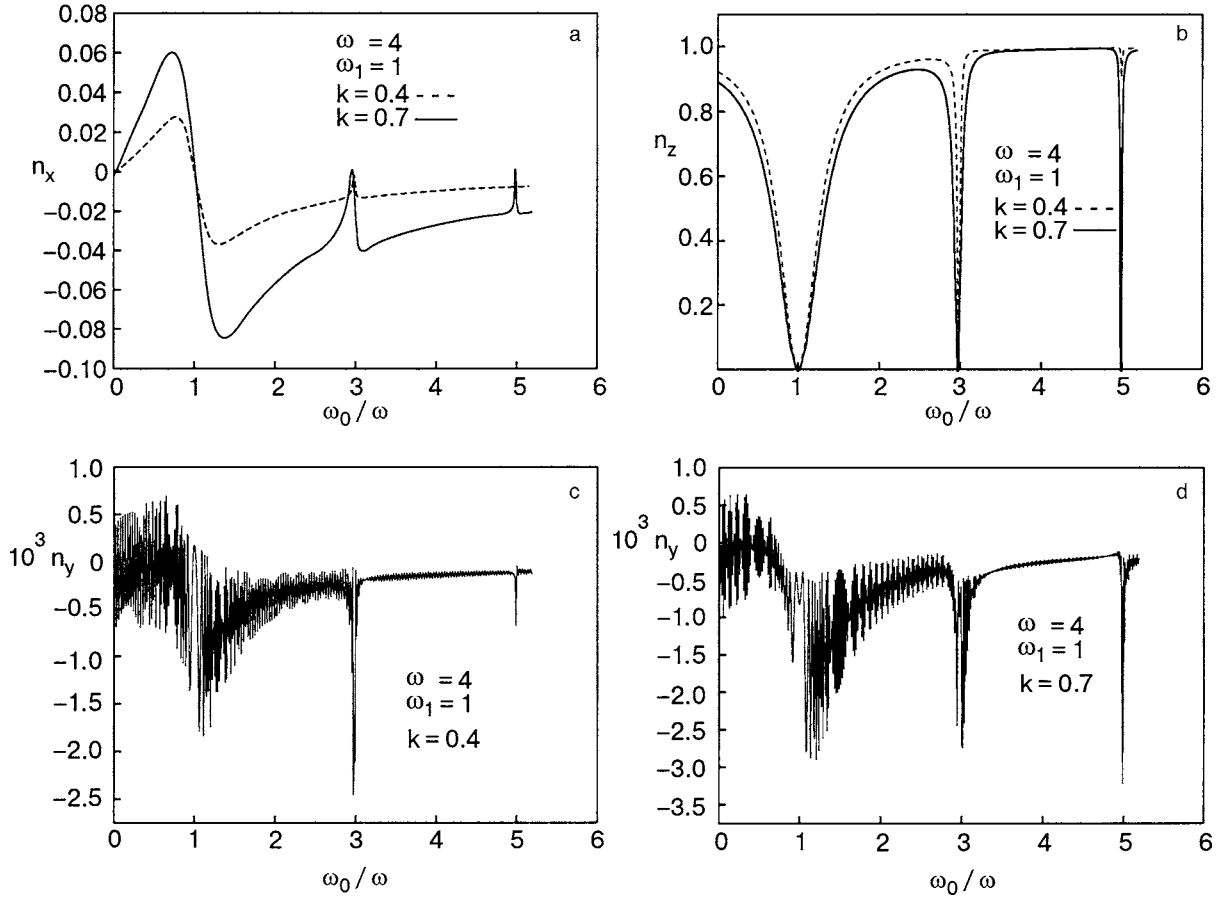

FIG. 2. The dc polarization n_x, n_y, n_z as a function of the normalized Larmor frequency.

and is equal to

$$\mathbf{a}=(-\mathrm{sn}(\omega_0 t,k)\cos\omega_1 t,\ \mathrm{cn}(\omega_0 t,k)\cos\omega_1 t,\ \sin\omega_1 t),$$
$$\mathbf{a}^2=1. \tag{42}$$

The evolution of the orthogonal positively oriented triad **P**, **c**, **a** determines the dynamics of the two-level system and admits a visual representation with the aid of the Bloch sphere.

5. NUMERICAL RESULTS

5.1. Time-averaged transition probability

The time-averaged probability of a spin-flip transition is given by the expression

$$\bar{P}=\lim_{T\to\infty}\frac{1}{T}\int_0^T d\tau\frac{1-R_z(\tau)}{2}. \tag{43}$$

The dependence of the probability (43) on the form of the field obtained by varying the modulus parameter k for different values of δ_r is found by numerical solution of system (26)–(28) or, equivalently, Eq. (29).

Figure 1 shows the dependence of the averaged probability (43) on the normalized Larmor frequency ω_0/ω and the form of the field, k, for different model parameters. It is seen that there is no shift of the position of the principal resonance. At exact resonance the probability of transition is independent of the deformation of the magnetic field. A numerical calculation confirms that the probability (43) is independent of the sign of δ_r/ω. As was shown in Ref. 6, parametric resonances (multiphoton resonances in the terminology of the Floquet formalism)[10] arise only at nonzero value of the detuning δ_r and modulus k, since the detuning and deformation enter Eq. (10) in the form of a product. When one of the parameters δ_r or k is equal to zero, parametric resonances are absent. Increasing the deformation of the field leads to broadening of the resonance peaks. The position of the resonances is determined by the given initial value of the spin (8). The first resonance corresponds to one absorbed resonance photon, and the second is determined by absorption-emission-absorption, etc. The position of the odd parametric resonances is extremely close to $\omega_0/\omega=2p+1$, where $p=1,2,\ldots$ but it has a tendency to shift appreciably with increasing ratio ω_0/ω (Fig. 1d).

5.2. Generation of the dc magnetic field

The time-averaged components of the polarization vector are determined by the formulas

$$n_x=\lim_{T\to\infty}\frac{1}{T}\int_0^T d\tau(cR_x+sR_y), \tag{44}$$

$$n_y=\lim_{T\to\infty}\frac{1}{T}\int_0^T d\tau(sR_x-cR_y), \tag{45}$$

$$n_z=\lim_{T\to\infty}\frac{1}{T}\int_0^E d\tau R_z, \tag{46}$$

where $c=\mathrm{cn}^2(\tau,k)-\mathrm{sn}^2(\tau,k)$, $s=-2\,\mathrm{sn}(\tau,k)\mathrm{cn}(\tau,k)$. As we see in Fig. 2, a dc magnetic field (at resonance in the xOy plane) is generated as a result of the harmonized magnetic field. If the modulus parameter goes to zero, then the generation of this field vanishes, as follows from formula (34). The components of the dc polarization n_x, n_y have sharp spikes in amplitude in the vicinity of the parametric resonances, but with increase of the parameter ω_0/ω their amplitude and the width of the resonance peaks decrease. It should be noted that the appearance of the zeroth harmonic is due solely to the deformation of the field without the inclusion of dissipation, whereas in Ref. 11, for a different modulation of the magnetic field, this effect vanishes in the absence of dissipation.

All of the numerical results in the solution of system (26)–(28) were obtained by the Runge–Kutta method with steps of $\tau=0.01$ and $\omega_0/\omega=0.01$. A value of 500 was chosen for the averaging interval T.

6. CONCLUSION

In this paper the behavior of a spin-1/2 particle with a magnetic dipole moment in an time-varying magnetic field $(h_0\mathrm{cn}(\omega t,k), h_0\mathrm{sn}(\omega t,k), H_0\mathrm{dn}(\omega t,k))$ was considered in the density matrix formalism. Variation of the parameter k from zero to unity generates a wide set of field-modulating functions, from trigonometric to pulsed exponential. An exact solution for the density matrix at resonance was found for any k. We showed that in the given case the probability of a spin flip is independent of k. We calculated the Bloch polarization vector and geometric phase at resonance. We obtained differential equations for the transition probability. The dependence of the time-averaged spin-flip probability on the normalized Larmor frequency was investigated numerically for different model parameters. It was shown that the position of the main resonance does not shift upon variation of the parameters, but only the width of the resonance peak changes. The position of the odd parametric (multiphoton) resonances has a tendency to shift noticeably with increasing amplitude of the transverse field at a fixed frequency. In this case the deformation of the field leads to broadening of the resonance peaks. We calculated the dc polarization induced by the harmonized field.

It is advisable to do an experimental check on the theoretical predictions as to the stability of the position of the magnetic resonance for different model parameters. Such an experiment is clearly an extension of the experimental situation in a circularly polarized field. Since the parametric resonances in a harmonized magnetic field have appreciable width, it may be preferable to investigate the magnetic resonance at parametric frequencies. The results of the present study may find application for analysis of interference experiments and for refining the design of magnetic spectrometers.

The author thanks A. G. Anders and I. A. Gromov for interest in this study and helpful comments.

*E-mail: yevgeny@kipt.kharkov.ua

[1] M. Grifoni and P. Hanggi, Phys. Rep. **304**, 229 (1998).
[2] I. I. Rabi, Phys. Rev. **51**, 652 (1937); J. Schwinger, *ibid.* **51**, 648 (1937).
[3] M. Kälin, I. Gromov, and A. Schweiger, J. Magn. Reson. (1969-1992) **160**, 166 (2003); M. Fedin, I. Gromov, and A. Schweiger, *ibid.* **171**, 80 (2004).
[4] M. Abramovitz and I. A. Stegun (eds.), *Handbook of Mathematical Functions*, Dover, New York (1968).
[5] N. Rosen and C. Zener, Phys. Rev. **40**, 502 (1932); A. Bambini and P. R. Berman, Phys. Rev. A **23**, 2496 (1981).
[6] E. A. Ivanchenko, "Magnetic resonance in an elliptic magnetic field," ArXiv: quant-ph/0404114 (2004); Physica B **358**, 308 (2005).
[7] Yu. A. Aminov, *Differential Geometry and Topology of Curves*, Gordon and Breach, Amsterdam (2000).
[8] H. Urbantke, Am. J. Phys. **59**, 503 (1990).
[9] A. Müller, Phys. Rev. A **57**, 731 (1998).
[10] I. Gromov and A. Schweiger, J. Magn. Reson. (1969-1992) **146**, 110 (2000); J. H. Shirley, Phys. Rev. B **138**, 987 (1965).
[11] S. Flach and A. A. Ovchinnikov, Physica A **292**, 268 (2001); S. Flach, A. E. Miroshnichenko, and A. A. Ovchinnikov, Phys. Rev. B **65**, 104438 (2002).

Translated by Steve Torstveit

LOW-DIMENSIONAL AND DISORDERED SYSTEMS

On the thermodynamics of quasi-two-dimensional electron gas

V. M. Gokhfeld*

A. A. Galkin Donetsk Physicotechnical Institute, ul. R. Lyuksemburg 72, Donetsk 83114, Ukraine
(Submitted September 13, 2004; revised December 21, 2004)
Fiz. Nizk. Temp. **31**, 769–773 (July 2005)

The equilibrium properties of an anisotropic electron system whose spectrum is characterized by open isoenergetic surfaces, typical of charge carriers in layered conducting crystals, are considered. The equation of state and other thermodynamic relations are obtained in explicit form; the differences from the thermodynamic properties of an ordinary electron gas are pointed out. © *2005 American Institute of Physics.* [DOI: 10.1063/1.2001638]

1. INTRODUCTION

It is known that a number of the so-called synthetic conductors are characterized by a layered crystals structure, and their electronic properties—in particular, the relatively low conductivity across the layers (the OZ axis)—are in good accord with the concept of a substantially anisotropic single-particle spectrum of the carriers.[1)] At low concentrations of the latter the situation could be described simply by the numerical difference of the corresponding effective masses; however, the situation of greatest interest, and one that is actually realized in many such substances, is the case of ''topological anisotropy,'' i.e., of Fermi surfaces open along the z direction in $\mathbf{p}$ space.

In a significant number of theoretical studies, more or less concrete models of such a spectrum have been used for studying kinetic electronic phenomena, including high-frequency ones, in layered conductors.[4–7] Of the equilibrium properties, in contrast, only the de Haas-van Alphen effect, which is observed in quantizing magnetic fields at low temperatures, has been given a detailed theoretical examination (see, e.g., Refs. 8–10). However, the thermodynamics of a layered metal merit attention even in the absence of magnetic field (or at low fields), since the effectively lowered dimensionality of the motion of the carriers should lead to unusual dependences of the thermodynamic quantities of the anisotropic electron gas on its temperature T and the particle volume density N.

2. SPECTRAL DENSITY

Separating out the dependence of the electron energy on the z projection of the quasimomentum $\mathbf{p}$, we consider a spectrum of the general form

$$\varepsilon(\mathbf{p})=\sum_{n=0}^{\infty}\varepsilon_n(\mathbf{p}_\perp)\cos\left(n\frac{a_z p_z}{\hbar}\right), \tag{1}$$

where a_z is the corresponding lattice period; in layered crystals it is, as a rule, considerably larger than the period $a_\perp$ in the plane of the layers.[2)] We assume that the in-plane motion of the carriers can be described (at least approximately) in the framework of the effective mass method, i.e., each of the harmonics ε_n is written in the form

$$\varepsilon_n(\mathbf{p}_\perp)\cong\frac{p_i p_k}{2m_{ik}^{(n)}}-C_n\equiv A_n(\varphi)p_\perp^2-C_n, \tag{2}$$

where C_n are constants; $i,k=(x,y)$; $(p_z,p_\perp,\varphi)$ are cylindrical coordinates in $\mathbf{p}$ space. Placing the origin of the coordinate system at the absolute minimum of the energy $\varepsilon(\mathbf{p})$, we assume the functions

$$A(p_z,\varphi)\equiv\sum_{n=0}^{\infty}A_n(\varphi)\cos\left(n\frac{a_z p_z}{\hbar}\right) \tag{3}$$

and

$$C(p_z)\equiv 2\sum_{n=1}^{\infty}C_n\sin^2\left(n\frac{a_z p_z}{2\hbar}\right) \tag{4}$$

to be positive definite and non-negative, respectively. Generally speaking, the spectrum can have several branches $\varepsilon_\alpha(p_\perp,p_z,\varphi)$; here, however, we restrict consideration to the comparatively simple case when the functions (3) and (4) are single-valued and bounded. Then the equation of the surface $\varepsilon(\mathbf{p})=\varepsilon$ has the form

$$p_\perp^2=\frac{\varepsilon-C(p_z)}{A(p_z,\varphi)} \tag{5}$$

and shows that under the condition

$$\varepsilon>\varepsilon_{\min}\equiv\max\{C(p_z)\} \tag{6}$$

the isoenergetic surfaces are open; they have the shape of a ''corrugated cylinder'' with an ellipsoidal base and a periodic generatrix $p_\perp(p_z,\varphi)$.

Such a spectrum will be called *quasi-two-dimensional*. In spite of the presence of three degrees of freedom of the particles, it has the exclusive property inherent to purely two-dimensional electron systems,[3)]—of constancy of the energy density of states $g(\varepsilon)$. Indeed, the momentum volume

$$\Gamma(\varepsilon)=\frac{1}{2}\int_{-\pi\hbar/a_z}^{\pi\hbar/a_z}dp_z\int_0^{2\pi}d\varphi p_\perp^2,$$

included in one period of the *open* surface (5) is linear in ε; thus, independently of the concrete form of the function $C(p_z)$, the density of states is equal to

$$g(\varepsilon)\equiv\frac{2}{(2\pi\hbar)^3}\frac{\partial\Gamma}{\partial\varepsilon}=(2\pi\hbar)^{-3}\int_{-\pi\hbar/a_z}^{\pi\hbar/a_z}\int_0^{2\pi}\frac{dp_z d\varphi}{A(p_z,\varphi)}$$

$$=\text{const}. \tag{7}$$

For example, keeping in expression (3) only the zeroth harmonic

$$A_0(\varphi)=\frac{\cos^2\varphi}{2m_1^{(0)}}+\frac{\sin^2\varphi}{2m_2^{(0)}},$$

according to formula (7) we obtain

$$g_0=\frac{\sqrt{m_1^{(0)}m_2^{(0)}}}{\pi a_z\hbar^2}\equiv\frac{m_\perp}{\pi a_z\hbar^2}, \tag{8}$$

where $m_1^{(0)}$ and $m_2^{(0)}$ are the principal values of the effective mass tensor $m_{ik}^{(0)}$ [see Eq. (2)]. Expression (8) is analogous to the density of states of a purely two-dimensional electron gas with a quadratic spectrum.[11]

A weak dependence $\varepsilon(p_z)$ is usually considered to be a characteristic of layered conductors. In other words, the nonzero harmonics C_n in them are small compared with the characteristic energies of in-plane motion,[4)] so that the condition $\varepsilon_F>\varepsilon_{\min}$ [see Eq. (6)] is easily met.

For real crystals, of course, the energy interval in which the spectrum is quasi-two-dimensional must be bounded from above as well, since expansion (2) has meaning only at radii $p_\perp$ that do not go beyond the boundaries of the Brillouin cell in the plane (p_x,p_y). However, what we have said implies that $\varepsilon_{\max}\simeq\hbar^2/m_\perp a_\perp^2\gg\varepsilon_{\min}$, i.e., the interval in question obviously exists and is rather wide. If the Fermi level ε_F falls on this interval, then for calculating the thermodynamic quantities—at least at low temperatures—it appears to be quite acceptable to extrapolate the conclusion (7) to *all* values of ε. For $T\ll\varepsilon_F$ one does not even need a marked numerical anisotropy of the spectrum (1): it is actually sufficient to assume that the Fermi surface is open and that its transverse sections are elliptical.

3. THERMODYNAMIC FUNCTIONS AND THE EQUATION OF STATE

Since, unlike the case of two-dimensional electron systems, we are talking about a massive sample with a significant volume density of carriers, the contribution of the latter to the thermodynamic properties of the sample is of interest, since it can be distinguished in experiment.

Knowing the spectral density g and using the standard methods of statistical mechanics (see, e.g., Refs. 12 and 13), one can in principle find all the thermodynamic functions of the system. In the case $g(\varepsilon)=\text{const}$ this turns out to be possible not only asymptotically (in the limits of low and high temperatures) but also exactly, i.e., for all values of the variables. The simplification is due to the fact that the condition of conservation of the number of particles here can be easily solved in respect to the chemical potential μ:[5)]

$$N\equiv\int_0^\infty\frac{d\varepsilon g(\varepsilon)}{1+\exp\dfrac{\varepsilon-\mu}{T}}=gT\ln\left(1+\exp\frac{\mu}{T}\right), \tag{9}$$

$$\mu(N,T)=T\ln\left(\exp\left(\frac{N}{gT}\right)-1\right), \tag{10}$$

where, obviously, $N/g=\varepsilon_F$. We note that for $T\to0$ the temperature correction to $\mu(0)=\varepsilon_F$ is *exponentially* small, unlike the three-dimensional (i.e., qualitatively isotropic) case, where, as is known,[12,13] $\mu(T)-\mu(0)\propto T^2$; this remark also pertains to the results in Eqs. (21) and (22).

Solution (10) should be substituted into the known expressions for the thermodynamic potentials, e.g., for the internal energy (per unit volume)

$$U\equiv\int_0^\infty\frac{d\varepsilon\varepsilon g(\varepsilon)}{1+\exp\dfrac{\varepsilon-\mu}{T}} \tag{11}$$

and the pressure

$$P\equiv T\int_0^\infty d\varepsilon g(\varepsilon)\ln\left(1+\exp\frac{\mu-\varepsilon}{T}\right). \tag{12}$$

Integrating by parts, we see that for $g(\varepsilon)=\text{const}$ these quantities coincide, unlike the case of an isotropic gas, where it is known[12] that $P=(2/3)U$ always.

Expression (12) together with (7) and (10) gives the dependence of the pressure on the density and temperature, i.e., the equation of state of a quasi-two-dimensional electron gas:

$$P(N,T)=\frac{N^2}{g}f(t);\quad t\equiv\frac{Tg}{N}=\frac{T}{\varepsilon_F};$$

$$f(t)=t^2\int_0^\infty dx\ln[1+(e^{1/t}-1)e^{-x}]. \tag{13}$$

The function $f(t)$ is shown in Fig. 1. It has the following asymptotics:

$$f(t)\approx\begin{cases}t+1/4, & t\gg1;\\ 1/2+t^2\pi^2/6, & t\ll1,\end{cases} \tag{14}$$

i.e.,

$$P=U\approx\begin{cases}NT+N^2/4g, & T\gg\varepsilon_F;\\ N^2/2g+(\pi^2/6)gT^2, & T\ll\varepsilon_F\end{cases} \tag{15}$$

for high (in comparison with $\varepsilon_F=N/g$) and low temperatures, respectively.

Using expressions (13)–(15), we obtain the following general formulas for the entropy density $S\equiv(\partial P/\partial T)_{V,\mu}$ and specific heat $C\equiv(\partial U/\partial T)_V$:

$$S=N\left[\frac{2f}{t}-\ln(e^{1/t}-1)\right]; \tag{16}$$

$$C=Nf'(t)=\frac{1}{t}[2f-(1-e^{-1/t})^{-1}] \tag{17}$$

and the asymptotics

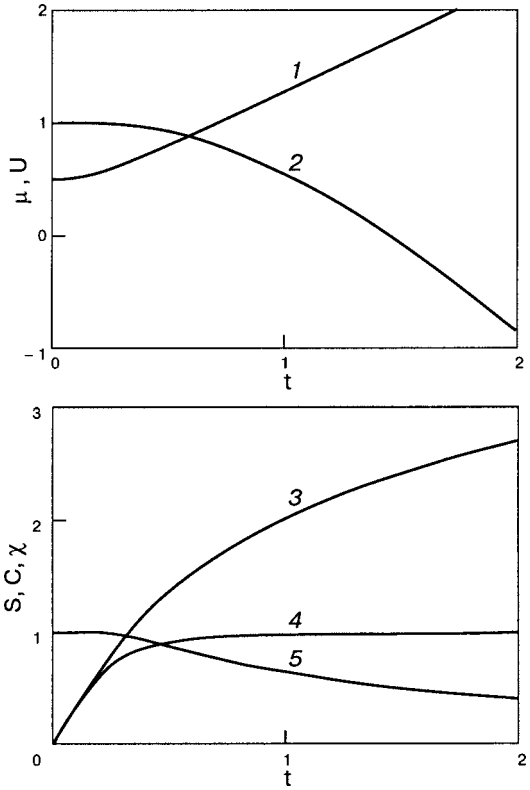

FIG. 1. Relative thermodynamic quantities of a quasi-two-dimensional electron gas as functions of the reduced temperature $t \equiv T/\varepsilon_F = gT/N$: the chemical potential $\mu(t)/\varepsilon_F$ (*1*); the internal energy $U(t)/N\varepsilon_F$ (*2*), the entropy $S(t)/N$ (*3*); the specific heat $C(t)/N$ (*4*); the paramagnetic susceptibility $\chi_{\text{para}}(t)/\chi_{\text{para}}(0)$ (*5*). N is the volume density of particles; $g = \text{const}$ is the spectral density of states.

$$S \approx \begin{cases} N(\ln(gT/N)+2), & T \gg \varepsilon_F \\ (\pi^2/3)gT, & T \ll \varepsilon_F \end{cases}; \tag{18}$$

$$C \approx \begin{cases} N, & T \gg \varepsilon_F \\ (\pi^2/3)gT, & T \ll \varepsilon_F \end{cases}. \tag{19}$$

The character of the temperature dependence of these quantities (Fig. 1) remains approximately the same as for an isotropic electron gas, for which, as we know,

$$C_{3D} \approx \begin{cases} (3/2)N, & T \gg \varepsilon_F \\ (\pi/3)^{2/3} m N^{1/3} T/\hbar^2, & T \ll \varepsilon_F \end{cases} \tag{20}$$

(see Refs. 12–14). However, the dependence on the density of particles turns out to be completely different: in the degenerate case the entropy and heat capacity of a quasi-two-dimensional system is completely independent of N. At high temperatures, on the other hand, as we see from Eq. (19), only the in-plane degrees of freedom contribute to the heat capacity (1/2 from each), just as for purely two-dimensional motion of the particles.

With a constant density of states it is also easy to calculate the other thermodynamic characteristics of a quasi-two-dimensional electron gas. For example, using formula (10), we easily obtain explicit expressions for the temperature dependence of the screening decrement of the longitudinal electric field,

$$\kappa^2 = 4\pi e^2 g(1 - e^{-1/t}); \tag{21}$$

and the electronic paramagnetic susceptibility,

$$\chi_{\text{para}}(t) \equiv 4\pi\beta^2 \left(\frac{\partial N}{\partial \mu}\right)_{T,V} = 4\pi\beta^2 g(1 - e^{-1/t}), \tag{22}$$

where $\beta = e\hbar/2mc$ is the Bohr magneton, and the reduced temperature as before is equal to $t \equiv gT/N = T/\varepsilon_F$. In the limit of low temperatures the quantities (21) and (22), like the heat capacity (19), are independent of the volume density of carriers.

The isothermal compressibility has the same temperature dependence $k_T(t)$, with $k_T(0) = gN^{-2}$, unlike the isotropic Fermi gas, for which this quantity is $\propto N^{-5/3}$.

4. DISCUSSION OF THE RESULTS

As we have said, open Fermi surfaces are typical for the electronic structure of layered conductors, so that essentially the only model representation assumed here is that the spectrum of carriers is quadratic with respect to the quasimomenta in the plane of the layers [see Eq. (2)]. In this case the concrete form of the dependence $\varepsilon(p_z)$, i.e., the shape of the corrugation of the Fermi cylinder, is unimportant: independently of it, the equilibrium properties of such a gas turn out to be very close to those of a purely two-dimensional electron system, for which the spectral density $g(\varepsilon)$ is constant, and the thermodynamic functions can be described by extremely transparent explicit formulas for arbitrary values of the temperature T and particle density N. They contain only the parameter g, so that the results (17), (21), and (22) in principle admit direct experimental verification. Of course, at densities N typical for a metal or even a semimetal only the low-temperature asymptotics of these formulas have actual significance; however, they, too, differ appreciably from those in the case of closed Fermi surfaces, where the spectral density is inevitably energy dependent.

In the case of a pronounced "layeredness," i.e., the isoenergetic surfaces remain open for energies quite close to the band edges, the proposed concept is also applicable to cases of more-complicated electron spectra with several types of carriers.

The author thanks V. G. Peschansky, V. D. Natsik, and Yu. G. Pashkevich for discussion of this study.

*E-mail: gokhfeld@teor.fti.ac.donetsk.ua

[1)] This pertains to many organic conductors, in particular, those synthesized on the basis of the planar molecule BEDT-TTF (bis-diethylene-dithiotetrathiofulvalene), the dichalcogenides of transition metals and their intercalates, graphite intercalates; etc.[1–3] High-T_c superconducting cuprates (in the normal state) can also be regarded as layered conductors.

[2)] In graphite, for example, $a_z \approx 3.35$ Å and $a_\perp \approx 1.42$ Å; in intercalates and organic layered conductors usually $a_z \gg a_\perp$ (Ref. 3).

[3)] Systems that can be regarded as such include, under certain conditions, inversion layers on the surface of semiconductors, conducting films, and planar heterostructures of microscopic thickness and also electrons on the surface of liquid helium. The two-dimensional electron spectrum of such objects is usually assumed to be quadratic (see Ref. 11 and the literature cited therein).

[4)] They also fall off rapidly with the index n. It can be assumed that the ε_n ($n = 1,2,\ldots$) are expressed in terms of the overlap integrals of the wave functions of electrons found in neighboring conducting layers, across one, two, etc., layers, respectively (see, e.g., Ref. 9).

[5)] This problem is known: it was stated in Ref. 13, for example. The subsequent results follow directly from it.

[1] J. Wosnitza, *Fermi Surfaces of Low-Dimensional Organic Metals and Superconductors*, Vol. 134 of Springer Tracts in Modern Physics, Springer (1996).
[2] J. Singleton, ''Studies of quasi-two-dimensional organic conductors based on BEDT-TTF using high magnetic fields,'' Rep. Prog. Phys. **63**, 1111 (2000).
[3] A. I. Buzdin and L. N. Bulaevskiĭ, Usp. Fiz. Nauk **144**, 415 (1984) [Sov. Phys. Usp. **27**, 830 (1984)].
[4] V. M. Gokhfel'd, M. I. Kaganov, and V. G. Peschanskii, Fiz. Nizk. Temp. **12**, 1173 (1986) [Sov. J. Low Temp. Phys. **12**, 661 (1986)].
[5] V. M. Gokhfeld and V. G. Peschansky, *Nonlocal Acoustoelectronic Effects in Metals and Layered Conductors*, Vol. 17, Part 1 of Soviet Scientific Reviews, I. M. Khalatnikov (ed.), Harwood Academic Publishers, Gmbh, Switzerland-USA (1993).
[6] V. M. Gokhfel'd, O. V. Kirichenko, and V. G. Peschanskiĭ, Zh. Éksp. Teor. Fiz. **108**, 2147 (1995) [JETP **81**, 661 (1995)].
[7] O. V. Kirichenko, Yu. A. Kolesnichenko, and V. G. Peschansky, *Electron Phenomena in Layered Conductors*, Vol. 18, Part 4 of Soviet Scientific Reviews, I. M. Khalatnikov (ed.), Harwood Academic Publishers, Gmbh, Switzerland-USA (1998).
[8] D. Shoenberg, J. Low Temp. Phys. **56**, 417 (1984).
[9] V. M. Gvozdikov, Fiz. Tverd. Tela (Leningrad) **26**, 2574 (1984) [Sov. Phys. Solid State **26**, 1560 (1984)].
[10] T. Champel and V. P. Mineev, Philos. Mag. B **81**, 55 (2001).
[11] T. Ando, A. Fowler, and F. Stern, ''Electronic properties of two-dimensional systems,'' Rev. Mod. Phys. **54**, No. 2, 437–672 (1982).
[12] R. Balescu, *Equilibrium and Nonequilibrium Statistical Mechanics*, Wiley, New York (1975), Mir, Moscow (1978).
[13] C. Kittel, *Introduction to Solid State Physics*, 5th ed., Wiley, New York (1976), Nauka, Moscow (1978).
[14] J. M. Ziman, *Principles of the Theory of Solids*, 2nd ed., Cambridge University Press, London (1972), Russ. transl. of 1st ed., Mir, Moscow (1966).

Translated by Steve Torstveit

Electromagnetic absorption of a bimetallic spherical particle

E. V. Zavitaev*

Moscow State University of Forestry, Mytishchi-5, Moscow District 141005, Russia
(Submitted November 5, 2004; revised February 8, 2005)
Fiz. Nizk. Temp. **31**, 774–783 (July 2005)

The cross section for absorption of electromagnetic radiation in a bimetallic spherical particle are calculated. The general case of arbitrary values of the ratio of the radius of the core to the radius of the particle is considered. The boundary conditions adopted are the condition of diffuse reflection of electrons from the internal and external surfaces of the metallic layer of the particle. The limiting cases are considered and the results are discussed. © *2005 American Institute of Physics.* [DOI: 10.1063/1.2001639]

1. INTRODUCTION

The electromagnetic property of small metallic particles can differ substantially from those of bulk metal samples.[1] If the linear dimension R of the metal sample is of the order of the electron mean free path Λ or smaller (this effect is most pronounced at low temperatures, when the electrons have a large mean free path) then the interaction of electrons with the boundary of the metal sample begins to have a noticeable influence on their response in an external electromagnetic field. A consequence of this is that the metal particle has special optical properties. Therefore, when the condition $R < \Lambda$ holds, one of the main optical characteristics—the absorption cross section—has a nontrivial dependence on the ratio R/Λ. At room temperature in metals with good conductivity (aluminum, copper, silver, etc.) the electron mean free path Λ typically lies in the range 10–100 nm. The size of particles investigated experimentally reaches several nanometers, i.e., the situation $R < \Lambda$ is realized.

As a formalism capable of describing the response of electrons to an external electromagnetic field with the interaction of the electrons with the boundary of the sample taken into account, one can use the standard kinetic theory of conduction electrons in a metal.[2] In that case no restrictions are imposed on the particle size relative to the mean free path.

The equations of macroscopic electrodynamics are applicable only to the case of "bulk" samples: $R \gg \Lambda$. Therefore the known Mie theory,[2] which describes the interaction of an electromagnetic wave with metallic objects in the framework of macroscopic electrodynamics is unsuitable for describing the size effect mentioned.

A theory of the interaction of electromagnetic radiation with a spherical particle was constructed in Refs. 3 and 4. Somewhat earlier[5,6] a result consistent with Ref. 3 had been obtained in the limiting case $R \ll \Lambda$ at low frequencies (the far infrared). The studies mentioned used an approach based on solution of the Boltzmann kinetic equation for the conduction electrons in a metal. An alternative approach to the problem was proposed and developed in Refs. 7 and 8.

Recently the problem of interaction of electromagnetic radiation with nonspherical particles has been attracting a heightened interest.[9] There have been several papers[10–13] devoted to the description of the interaction of electromagnetic radiation with a cylindrical particle. We can also mention studies attempting to include quantum-mechanical effects,[14,15] which are especially important at low temperatures. All of the studies mentioned have dealt with homogeneous particles, i.e., the question of the internal structure of the absorbing particles was not addressed.

Recently, however, there have been published reports of experimental research on particles of complex structure.[16,17] Those particles consisted of an insulating (or metallic) core surrounded by a metallic sheath; this naturally influences the optical properties of these particles. For particles of complex structure the electric absorption, which is dominant in the visible region of the spectrum, was considered in Refs. 16 and 17.

In the present study, which is the logical continuation of Ref. 3, the distribution functions describing the linear response of conduction electrons in an inhomogeneous spherical particle (a metallic particle with a core of another metal) to the ac magnetic field of a plane electromagnetic wave are calculated by a kinetic method. From the distribution functions found we can calculate the dependence of the absorption cross section on the radius of the particle and the frequency and also the ratio of the radius of the core to the radius of the particle. Particular attention is paid to the important case of low frequencies of the external field and low frequencies of bulk collisions of electrons inside the core and sheath.

2. MATHEMATICAL MODEL AND THE CALCULATION

We consider a spherical particle consisting of a metallic core of radius R_1 ensheathed by a layer of another metal, of radius R_2. This particle is placed in the field of a plane electromagnetic wave of frequency ω, which is bounded from above by the frequencies of the near IR range ($\omega < 2 \times 10^{15}\ \mathrm{s}^{-1}$). The linear size R_2 of the particle is small compared to the wavelength λ of the electromagnetic radiation. The nonuniformity of the external field of the wave and the skin effect are not taken into account (it is assumed that $R_2 < \delta$, where δ is the skin depth). In the frequency range under consideration the contribution of the electric dipole polarization will be small compared to the contribution of the eddy currents induced by the external magnetic field of the wave.[3] Therefore the effect of the external electric field of the wave will not be taken into account.

In addition, we have used the standard physical assumptions: the conduction electrons in the metallic sheath and metallic core of the particle are treated as a degenerate Fermi gas; their response to an external ac magnetic field is described with the aid of the Boltzmann equation in the relaxation-time approximation. For the boundary conditions it is assumed that the reflection of the relations from the surfaces of the metallic sheath and the surface of the metallic core is of a diffuse character.

The uniform magnetic field of the wave, periodic in time, $\mathbf{H}=\mathbf{H}_0\exp(-i\omega t)$, gives rise to an induced solenoidal electric field. By virtue of the symmetry of the problem, it is determined from Maxwell's induction equation and can be represented in the form

$$\text{curl}\ \ \mathbf{E}=-\left(\frac{1}{c}\right)\frac{\partial \mathbf{H}}{\partial t}$$

$$\mathbf{E}=\frac{1}{2c}\left[\mathbf{r}\times\frac{\partial \mathbf{H}}{\partial t}\right]=\frac{\omega}{2ic}[\mathbf{r}\times\mathbf{H}_0]\exp(-i\omega t), \tag{1}$$

where $\mathbf{r}$ is the radius vector (the coordination origin O is at the center of the particle), and c is the speed of light. The solenoidal induced electric field acts on the conduction electrons in the particle and causes a deviation f_1 of their distribution function f from the equilibrium Fermi distribution f_0:

$$f(\mathbf{r},\mathbf{v})=f_0(\varepsilon)+f_1(\mathbf{r},\mathbf{v}),\quad \varepsilon=\frac{m\mathbf{v}^2}{2},$$

where $\mathbf{v}$ and m are the velocity and effective mass of the electron.

This gives rise to an eddy current in the core and sheath of the particle:

$$\mathbf{j}=e\int \mathbf{v}f\frac{2d^3(mv)}{h^3}=2e\left(\frac{m}{h}\right)^3\int \mathbf{v}f_1 d^3v \tag{2}$$

(where h is Planck's constant, and e is the charge of the electron), and also to energy dissipation in the volume of the particle. The energy $\bar{Q}$ dissipated per unit time is equal to[18]

$$\bar{Q}=\int \overline{(\mathrm{Re}\,\mathbf{E})\cdot(\mathrm{Re}\,\mathbf{j})}d^3r=\frac{1}{2}\mathrm{Re}\int \mathbf{j}\cdot\mathbf{E}^* d^3r, \tag{3}$$

where the overbar denotes averaging over time, and the asterisk denotes complex conjugation.

In formula (2) the standard normalization of the distribution function f is used, wherein the electron density of states is equal to $2/h^3$. For the equilibrium function $f_0(\varepsilon)$ we henceforth use the step approximation:[19]

$$f_0(\varepsilon)=\theta(\varepsilon_F-\varepsilon)=\begin{cases}1, & 0\leqslant\varepsilon\leqslant\varepsilon_F\\ 0, & \varepsilon_F<\varepsilon\end{cases},$$

where $\varepsilon_F=mv_F^2/2$ is the Fermi energy (v_F is the Fermi velocity). It is assumed that the Fermi surface is of a spherical shape.

In this paper we have used the assumption of continuity of the electron energy spectrum (the quasiclassical approximation). This assumption is valid in the case when the characteristic linear dimensions of the conductor exceed 3–4 nm, so that the de Broglie wavelength for an electron on the Fermi surfaces in the core and sheath of the particle should be many times less than the corresponding linear dimension of the metal. Thus the radius of the core and the thickness of the sheath of the particle will be assumed greater than the given limiting value.

The problem reduces to that of finding the deviation f_2 of the electron distribution function from the equilibrium distribution f_0 arising under the influence of the induced solenoidal field (1). In the approximation linear in the external field the function f_1 satisfies the kinetic equation[2,19]

$$-i\omega f_1+\mathbf{v}\cdot\frac{\partial f_1}{\partial \mathbf{r}}+e(\mathbf{v}\cdot\mathbf{E})\frac{\partial f_0}{\partial \varepsilon}=-\frac{f_1}{\tau}, \tag{4}$$

where a steady time dependence [$f_1\sim\exp(-i\omega t)$] is assumed, and the collision integral is taken in the relaxation-time approximation:

$$\left(\frac{df_1}{dt}\right)_s=-\frac{f_1}{\tau},$$

where τ is the electron relaxation time.

Solving Eq. (4) by the method of characteristics,[20] we obtain

$$f_1=A[\exp(-\nu t')-1]/\nu,\quad t'\geqslant 0, \tag{5}$$

where

$$\nu=\frac{1}{\tau}-i\omega,$$

$$A=e(\mathbf{v}\cdot\mathbf{E})\frac{\partial f_0}{\partial \varepsilon}=\frac{e\omega}{2ic}\left(\frac{\partial f_0}{\partial \varepsilon}\right)[\mathbf{v}\times\mathbf{r}]\cdot\mathbf{H}_0\exp(-i\omega t). \tag{6}$$

Here ν and A are constants along the trajectory (i.e., they are characteristics).

We shall assume that the electrons do not penetrate from one metal to the other (i.e., the core and sheath are separated by a thin insulating layer) and the electrons have different Fermi velocities (v_F and u_F) in the sheath and core of the particle. In addition, in the general case the sheath and core of the particle are assigned different relaxation times (τ_1 and τ_2) and, hence, different complex electron scattering frequencies (ν_1 and ν_2).

For the function f_1 to be uniquely determined one must specify boundary conditions for it at the spherical surfaces of the metallic sheath and metallic core of the particle. We take these boundary conditions to be diffuse reflection of electrons from these surfaces.[2] Since the electrons found in the core of the particle can reflect off the core boundary (R_1) and electrons found in the sheath can reflect off the inner (R_1) and outer (R_2) boundaries of the metallic layer, it is necessary to specify three boundary conditions:

$$f_{11}(\mathbf{r},\mathbf{v})=0\quad \text{for}\ \begin{cases}|\mathbf{r}|=R_1\\ \mathbf{rv}<0\end{cases}, \tag{7}$$

$$f_{12}(\mathbf{r},\mathbf{v})=0\quad \text{for}\ \begin{cases}|\mathbf{r}|=R_1\\ \mathbf{rv}>0\end{cases}, \tag{8}$$

$$f_{13}(\mathbf{r},\mathbf{v})=0\quad \text{for}\ \begin{cases}|\mathbf{r}|=R_2\\ \mathbf{rv}<0\end{cases}. \tag{9}$$

For reflection of electrons found in the core from the core boundary (R_1) the parameter t' in expression (5) is defined as

$$t_1=\{\mathbf{r}\cdot\mathbf{v}+[(\mathbf{r}\cdot\mathbf{v})^2+(R_1^2-r^2)v^2]^{1/2}\}/v^2. \tag{10}$$

For reflection of an electron off the inner boundary (R_1) of the metallic sheath the parameter t' in expression (5) is defined as

$$t_2=\{\mathbf{r}\cdot\mathbf{v}-[(\mathbf{r}\cdot\mathbf{v})^2+(R_1^2-r^2)v^2]^{1/2}\}/v^2, \tag{11}$$

and for reflection of an electron off the outer boundary (R_2) of the metallic sheath it is defined as

$$t_3=\{\mathbf{r}\cdot\mathbf{v}+[(\mathbf{r}\cdot\mathbf{v})^2+(R_2^2-r^2)v^2]^{1/2}\}/v^2. \tag{12}$$

This is clear from the following geometric arguments. Starting from the obvious vector relation $\mathbf{r}=\mathbf{r}_0+\mathbf{v}t'$ (where $\mathbf{r}_0$ is the radius vector of the electron at the time of its reflection off either of the surfaces inside the particle), squaring both sides of this relation, and solving the resulting equation for the parameter t', we can obtain expression (10), (11), or (12).

Therefore, Eq. (4) has three different solutions, depending on the place where the conduction electron is reflected inside the particle.

Relations (5), (6), and (10)–(12) completely determine the solutions f_{11}, f_{12}, and f_{13} of Eq. (4) with boundary conditions (7)–(9); this allows us to calculate the current (2) and dissipated power (3).

For evaluating the integrals (2) and (3) it is convenient to use spherical coordinates in both real space (r, θ, ρ; the Z axis is the polar axis and the vector $\mathbf{H}_0$ is parallel to the Z axis) and in velocity space (v, α, β; the v_r axis is the polar axis). In spherical coordinates the field (1) has only a φ component:

$$\mathbf{E}=E_\varphi\mathbf{e}_\varphi;\quad E_\varphi=\frac{i\omega}{2c}rH_0\sin\theta\exp(-i\omega t). \tag{13}$$

Accordingly, the currents (2) in the core and in the sheath of the particle also have only a φ component (the current streamlines are closed circles centered on the Z axis in planes perpendicular to the Z axis):

$$j_{\varphi 1}=\frac{3n_1e^2}{4\pi u_F^3}\frac{E_\varphi}{v_1}\int v_\varphi^2\delta(\varepsilon-\varepsilon_F)[1-\exp(-v_1t')]d^3v, \tag{14}$$

$$j_{\varphi 2}=\frac{3n_2e^2}{4\pi u_F^3}\frac{E_\varphi}{v_2}\int v_\varphi^2\delta(\varepsilon-\varepsilon_F)[1-\exp(-v_2t')]d^3v. \tag{15}$$

Here we have taken into account that the densities of conduction electrons in the constituent metals of the particle are determined as

$$n_1=2\left(\frac{m}{h}\right)^3\int f_0d^3v=2\left(\frac{m}{h}\right)^3\frac{4}{3}\pi u_F^3,$$

$$n_2=2\left(\frac{m}{h}\right)^3\int f_0d^3v=2\left(\frac{m}{h}\right)^3\frac{4}{3}\pi v_F^3.$$

In the integration of expressions (14) and (15) it should be kept in mind that the place where the electrons are reflected inside the particle is determined by the polar angle α in velocity space.

For electrons inside the core, $\alpha=0-\pi$. The function f_1 in this case is understood to be $f_{11}(\mathbf{r}\cdot\mathbf{v})$ $(t'=t_1)$.

For electrons inside the metal sheath of the particle one can distinguish three regions:

1. If the inequality $\alpha_0\leqslant\alpha\leqslant\pi-\alpha_0$ holds, where the angle α_0 is determined by the expression

$$\alpha_0=\arccos\left(\frac{\sqrt{r^2-R_1^2}}{r}\right), \tag{16}$$

then the trajectory of the electron does not intersect with the core, and it suffers reflection from the outer boundary of the metallic layer of the particle. In this case the function f_1 is understood to be $f_{13}(\mathbf{r},\mathbf{v})$ $(t'=t_3)$.

2. If $\pi-\alpha_0<\alpha\leqslant\pi$, then the electrons are moving toward the core of the particle, and the function f_1 is again understood to be $f_{13}(\mathbf{r},\mathbf{v})$ $(t'=t_3)$.

3. Finally, if $0<\alpha\leqslant\alpha_0$, then the electrons are moving away from the core of the particle, and the function f_1 means $f_{12}(\mathbf{r},\mathbf{v})$ $(t'=t_2)$.

It is easy to see that the integrals for the first two cases can be combined.

The cross section σ for absorption of electromagnetic radiation is found by dividing the mean dissipated power $\bar{Q}$ [see Eq. (3)] by the mean energy flux density in the wave, $cH_0^2/8\pi$:

$$\sigma=\frac{1}{2}\frac{8\pi}{cH_0^2}\mathrm{Re}\left\{\int j_\varphi E_\varphi^*d^3r\right\},$$

or, taking Eqs. (14) and (15) into account,

$$\begin{aligned}\sigma=\frac{1}{2}\frac{8\pi}{cH_0^2}\mathrm{Re}\Bigg\{&\int\frac{3n_1e^2E_\varphi}{4\pi u_F^3\nu_1}\Bigg[\int v_\varphi^2\delta(\varepsilon-\varepsilon_F)\\&\times[1-\exp(-\nu_1t')]d^3v\Bigg]E_\varphi^*d^3r\\&+\int\frac{3n_2e^2E_\varphi}{4\pi v_F^3\nu_2}\Bigg[\int v_\varphi^2\delta(\varepsilon-\varepsilon_F)\\&\times[1-\exp(-\nu_2t')]d^3v\Bigg]E_\varphi^*d^3r\Bigg\}.\end{aligned}$$

Further, using Eq. (13), we get

$$\begin{aligned}\sigma=\frac{1}{2}\frac{8\pi}{cH_0^2}\mathrm{Re}\Bigg\{&\frac{3n_1e^2}{4\pi u_F^3\nu_1}\int\frac{i\omega}{2c}rH_0\sin\theta\exp(-i\omega t)\\&\times\Bigg[\int v_\varphi^2\delta(\varepsilon-\varepsilon_F)[1-\exp(-\nu_1t')]d^3v\Bigg]\\&\times\frac{(-i\omega)}{2c}rH_0\sin\theta\exp(i\omega t)d^3r\\&+\frac{3n_2e^2}{4\pi v_F^3\nu_2}\int\frac{i\omega}{2c}rH_0\sin\theta\exp(-i\omega t)\\&\times\Bigg[\int v_\varphi^2\delta(\varepsilon-\varepsilon_F)[1-\exp(-\nu_2t')]d^3v\Bigg]\\&\times\frac{(-i\omega)}{2c}rH_0\sin\theta\exp(i\omega t)d^3r\Bigg\}.\end{aligned}$$

After straightforward manipulations we obtain

$$\sigma=\mathrm{Re}\left\{\frac{3n_1e^2\omega^2}{4mc^3u_F^4\nu_1}\int\left[\int v_\varphi^2\delta(v-u_F)\times[1-\exp(-\nu_1t')]d^3v\right]r^2\sin^2\theta d^3r+\frac{3n_2e^2\omega^2}{4mc^3v_F^4\nu_2}\int\left[\int v_\varphi^2\delta(v-v_F)\times[1-\exp(-\nu_2t')]d^3v\right]r^2\sin^2\theta d^3r\right\}.$$

Taking into account that $v_\varphi=v\sin\alpha\cos\beta$, and putting the limits of integration on the internal integrals of the sum, we arrive at the expression

$$\sigma=\mathrm{Re}\left\{\frac{3n_1e^2\omega^2}{4mc^3u_F^4\nu_1}\int\left[\int_0^{u_F}\int_0^{\pi}\int_0^{2\pi}v^4\sin^3\alpha\cos^2\beta\delta(v-u_F)[1-\exp(-\nu_1t')]dvd\alpha d\beta\right]r^2\sin^2\theta d^3r+\frac{3n_2e^2\omega^2}{4mc^3v_F^4\nu_2}\int\left[\int_0^{v_F}\int_0^{\pi}\int_0^{2\pi}v^4\sin^3\alpha\cos^2\beta\delta(v-v_F)[1-\exp(-\nu_2t')]dvd\alpha d\beta\right]r^2\sin^2\theta d^3r\right\}.$$

Integrating over the variables v and β and putting the limits of integration on the internal integrals of the sum, we have

$$\sigma=\mathrm{Re}\left\{\frac{3n_1e^2\omega^2}{4mc^3u_F^4\nu_1}u_F^4\pi\int_0^{R_1}\int_0^{\pi}\int_0^{2\pi}\left[\int_0^{\pi}[1-\exp(-\nu_1t')]\times\sin^3\alpha d\alpha\right]r^4\sin^3\theta drd\theta d\varphi+\frac{3n_2e^2\omega^2}{4mc^3v_F^4\nu_2}v_F^4\pi\times\int_{R_1}^{R_2}\int_0^{\pi}\int_0^{2\pi}\left[\int_0^{\pi}[1-\exp(-\nu_2t')]\sin^3\alpha d\alpha\right]\times r^4\sin^3\theta drd\theta d\varphi\right\}.$$

The integrals over the variables θ and φ are elementary, and therefore

$$\sigma=\mathrm{Re}\left\{\frac{3n_1e^2\omega^2}{4mc^3u_F^4\nu_1}v_F^4\pi\frac{4}{3}2\pi\int_0^{R_1}r^4dr\int_0^{\pi}[1-\exp(-\nu_1t')]\times\sin^3\alpha d\alpha+\frac{3n_2e^2\omega^2}{4mc^3v_F^4\nu_2}v_F^4\pi\frac{4}{3}2\pi\int_{R_1}^{R_2}r^4dr\times\int_0^{\pi}[1-\exp(-\nu_2t')]\sin^3\alpha d\alpha\right\}.$$

Finally, we obtain

$$\sigma=\mathrm{Re}\left\{\frac{2\pi^2n_1e^2\omega^2}{mc^3\nu_1}\int_0^{R_1}r^4dr\int_0^{\pi}[1-\exp(-\nu_1t')]\times\sin^3\alpha d\alpha+\frac{2\pi^2n_2e^2\omega^2}{mc^3\nu_2}\int_{R_1}^{R_2}r^4dr\times\int_0^{\pi}[1-\exp(-\nu_2t')]\sin^3\alpha d\alpha\right\}. \tag{17}$$

For further calculations and analysis of the results we write the compound expression (17) determining the absorption cross section in the convenient form

$$\sigma=\sigma_1+\sigma_2+\sigma_3, \tag{18}$$

where

$$\sigma_1=\mathrm{Re}\left\{\frac{2\pi^2n_1e^2\omega^2}{mc^3\nu_1}\int_0^{R_1}r^4dr\times\int_0^{\pi}[1-\exp(-\nu_1t_1)]\sin^3\alpha d\alpha\right\}, \tag{19}$$

$$\sigma_2=\mathrm{Re}\left\{\frac{2\pi^2n_2e^2\omega^2}{mc^3\nu_2}\int_{R_1}^{R_2}r^4dr\times\int_0^{\alpha_0}[1-\exp(-\nu_2t_2)]\sin^3\alpha d\alpha\right\}, \tag{20}$$

$$\sigma_3=\mathrm{Re}\left\{\frac{2\pi^2n_2e^2\omega^2}{mc^3\nu_2}\int_{R_1}^{R_2}r^4dr\times\int_{\alpha_0}^{\pi}[1-\exp(-\nu_2t_3)]\sin^3\alpha d\alpha\right\}. \tag{21}$$

We introduce the new variables

$$\xi=\frac{r}{R_2},\quad z=\nu_2\frac{R_2}{v_F}=\left(\frac{1}{\tau_2}-i\omega\right)\frac{R_2}{v_F}=x-iy,$$

$$K=\frac{R_1}{R_2},\quad \gamma=\frac{u_F}{v_F},\quad \delta=\frac{\tau_1}{\tau_2}$$

and transform formulas (10)–(12) and (16) to

$$t_1=\frac{R_2}{u_F}\mu,\quad \mu=\xi\cos\alpha+\sqrt{K^2-\xi^2\sin^2\alpha},$$

$$t_2=\frac{R_2}{v_F}\psi,\quad \psi=\xi\cos\alpha-\sqrt{K^2-\xi^2\sin^2\alpha},$$

$$t_3=\frac{R_2}{v_F}\eta,\quad \eta=\xi\cos\alpha+\sqrt{1-\xi^2\sin^2\alpha},$$

$$\alpha_0=\arccos\left(\sqrt{1-\frac{K^2}{\xi^2}}\right).$$

Here we have taken into account that $\mathbf{r}\cdot\mathbf{v}=ru_F\cos\alpha$ or $\mathbf{r}\cdot\mathbf{v}=rv_F\cos\alpha$ (all the electrons on the Fermi surface inside the metallic core of the particle move with velocity u_F, and all the electrons on the Fermi surface inside the metallic sheath of the particle move with velocity equal to v_F).

Expressing the characteristics of the metallic core of the particle (ν_1 and n_1) in terms of the characteristics of the metallic sheath of the particle ($\nu_2=\nu$, $n_2=n$, $\tau_2=\tau$), we have

$$\nu_1=\nu+\frac{1-\delta}{\delta\tau}=\left(\frac{x}{\delta}-iy\right)\frac{v_F}{R_2}=z'\frac{v_F}{R_2},\quad n_1=n\gamma^3.$$

Then formulas (19)–(21) take the following form:

$$\sigma_1=\mathrm{Re}\left\{\frac{2\pi^2ne^2v_FR_2^4}{mc^3}\frac{\gamma^3\delta y^2}{x-iy\delta}\int_0^K\xi^4d\xi\times\int_0^\pi[1-\exp(-z'\mu/\gamma)]\sin^3\alpha d\alpha\right\},$$

$$\sigma_2=\mathrm{Re}\left\{\frac{2\pi^2ne^2v_FR_2^4}{mc^3}\frac{y^2}{z}\int_K^1\xi^4d\xi\times\int_0^{a_0}[1-\exp(-z\psi)]\sin^3\alpha d\alpha\right\},$$

$$\sigma_3=\mathrm{Re}\left\{\frac{2\pi^2ne^2v_FR_2^4}{mc^3}\frac{y^2}{z}\int_K^1\xi^4d\xi\times\int_{\alpha_0}^\pi[1-\exp(-z\eta)]\sin^3\alpha d\alpha\right\}.$$

We write the absorption cross section (18) in the form

$$\sigma=\sigma_0(F_1+F_2+F_3),$$

where

$$\sigma_0=\frac{2\pi^2ne^2v_FR_2^4}{mc^3},\tag{22}$$

$$F_1=\mathrm{Re}\left\{\frac{\gamma^3\delta y^2}{x-iy\delta}\int_0^K\xi^4d\xi\int_0^\pi[1-\exp(-z'\mu/\gamma)]\sin^3\alpha d\alpha\right\},\tag{23}$$

$$F_2=\mathrm{Re}\left\{\frac{y^2}{z}\int_K^1\xi^4d\xi\int_0^{\alpha_0}[1-\exp(-z\psi)]\sin^3\alpha d\alpha\right\},\tag{24}$$

$$F_3=\mathrm{Re}\left\{\frac{y^2}{z}\int_K^1\xi^4d\xi\int_{\alpha_0}^\pi[1-\exp(-z\eta)]\sin^3\alpha d\alpha\right\}.\tag{25}$$

Formulas (23)–(25) can be used to calculate the dimensionless absorption cross section of an inhomogeneous spherical particle:

$$F(x,y,K,\gamma,\delta)=F_1(x,y,K,\gamma,\delta)+F_2(x,y,K,\gamma,\delta)+F_3(x,y,K,\gamma,\delta)\tag{26}$$

and the absorption cross section of electromagnetic radiation

$$\sigma=\sigma_0F(x,y,K,\gamma,\delta).\tag{27}$$

When $K=0$ or 1 (since the particle is homogeneous, then $\gamma=1$ and $\delta=1$), it follows from (26) that

$$F(x,y)=\mathrm{Re}\left\{y^2\int_0^1\xi^4d\xi\int_0^\pi\frac{1-\exp(-z\eta)}{z}\sin^3\alpha d\alpha\right\}.$$

This expression coincides with the result obtained in Ref. 3 for a homogeneous spherical metallic particle.

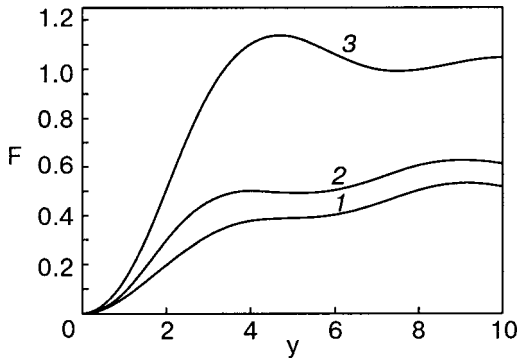

FIG. 1. Dependence of the dimensionless absorption cross section F on the dimensionless frequency y for $\gamma=0.5$ (*1*), 1 (*2*), 1.5 (*3*) ($x=0$, $K=0.8$).

The case of a compound particle made of one substance ($\gamma=1,\delta=1$) (the sheath and core of the particle are separated by an infinitely thin insulating layer) can be considered separately. In such a case the additional scattering of electrons on the surface separating the core and sheath leads to a difference in the physical properties of such a particle from those of a homogeneous spherical metallic particle.

The results of a numerical calculation of $F(x,y,K,\gamma,\delta)$ are presented in Figs. 1–4 (to simplify the analysis of the results, all of the figures are drawn under the assumption that $\tau_1=\tau_2$).

3. ABSORPTION IN THE LOW-FREQUENCY AND HIGH-FREQUENCY REGIMES

Let us discuss in detail the case when the frequency ω of the external field and the electron collision frequency in the volume of the metal ($1/\tau$) is low compared to the electron collision frequency with the surfaces of the metallic sheath of the particle. In other words, we consider the case $|z|\ll1$.

In this case the exponents appearing in expressions (23)–(25) can be expanded according to the well-known Taylor formula, keeping the first two terms of the expansion. As a result, we obtain

$$F_1=y^2\gamma^2\int_0^K\xi^4d\xi\int_0^\pi(\xi\cos\alpha+\sqrt{K^2-\xi^2\sin^2\alpha})\sin^3\alpha d\alpha,\tag{28}$$

$$F_2=y^2\int_K^1\xi^4d\xi\int_0^{\alpha_0}(\xi\cos\alpha-\sqrt{K^2-\xi^2\sin^2\alpha})\sin^3\alpha d\alpha,\tag{29}$$

$$F_3=y^2\int_K^1\xi^4d\xi\int_{\alpha_0}^\pi(\xi\cos\alpha+\sqrt{1-\xi^2\sin^2\alpha})\sin^3\alpha d\alpha.\tag{30}$$

Expressions (28)–(30) admit analytical calculation. Let us give the final result:

$$F_1=y^2\gamma^2\frac{1}{6}K^6,$$

$$F_2 = y^2\left[-\frac{1}{16}K+\frac{1}{24}K^3+\frac{1}{8}K^4-\frac{1}{16}K^5-\frac{1}{24}K^6 + \frac{1}{32}(1-K^2-K^4+K^6)\ln\frac{1+K}{1-K}\right],$$

$$F_3 = y^2\left[\frac{1}{6}-\frac{1}{16}K+\frac{1}{24}K^3-\frac{3}{8}K^4-\frac{1}{16}K^5+\frac{7}{24}K^6 + \frac{1}{32}(1-K^2-K^4+K^6)\ln\frac{1+K}{1-K}\right].$$

Then we obtain the following result for the absorption cross section:

$$\sigma = \sigma_0 y^2\left[\frac{1}{6}-\frac{1}{8}K+\frac{1}{12}K^3-\frac{1}{4}K^4-\frac{1}{8}K^5+\frac{1}{4}K^6 + \frac{\gamma^2}{6}K^6+\frac{1}{16}(1-K^2-K^4+K^6)\ln\frac{1+K}{1-K}\right]. \quad (31)$$

We consider the possible limiting cases.

1. In the case of a metallic particle without a core ($K=0$ or 1) (since the particle is homogeneous, $\gamma=1$ and $\delta=1$) it follows from (31) with (22) that

$$\sigma = \frac{\pi^2 n e^2 v_F R_2^4}{3mc^3}y^2,$$

which agrees with the result obtained in Refs. 3, 5, and 6.

If the particle has a metallic core with a radius much less than the radius of particle, i.e., when $K \ll 1$, then one can find the correction to the absorption by expanding formula (31) in a series:

$$\sigma \approx \sigma_0 y^2 \frac{1}{6}\left(1-\frac{3}{2}K^4-\frac{8}{5}K^5+\gamma^2K^6\right).$$

2. In the case of a thin metallic sheath, when $K\to 1$, for finding the correction to the absorption according to formula (31) it is necessary to do another series expansion in the small parameter $(1-K)$. In this case the absorption cross section is determined as

$$\sigma \approx \sigma_0 y^2\left\{\frac{5}{4}\left[1-\frac{2}{5}\ln\frac{1-K}{2}\right](1-K)^2+\frac{1}{6}\gamma^2(6K-5)\right\}.$$

In the case when $|z| \gg 1$, expression (26) has an asymptotic expansion. Neglecting the terms with the exponentials in view of their rapid decay and doing some algebraic manipulations, we arrive at the following expression for the dimensionless absorption cross section $F(z)$:

$$F(z) = \mathrm{Re}\left\{\frac{\gamma^3\delta y^2}{x-iy\delta}\int_0^K \xi^4 d\xi \int_0^\pi \sin^3\alpha d\alpha + \frac{y^2}{z}\int_K^1 \xi^4 d\xi \int_0^\pi \sin^3\alpha d\alpha\right\}.$$

This expression is easily integrated:

$$F(z) = \mathrm{Re}\left\{\frac{\gamma^3\delta y^2}{x-iy\delta}\frac{4}{15}K^5+\frac{y^2}{x-iy}\frac{4}{15}(1-K^5)\right\}.$$

As a result of these manipulations, we arrive at the following expression for the absorption cross section (27):

$$\sigma(z) = \sigma_0\,\mathrm{Re}\left\{\frac{\gamma^3\delta y^2}{x-iy\delta}\frac{4}{15}K^5+\frac{y^2}{x-iy}\frac{4}{15}(1-K^5)\right\} = \sigma_0\frac{4}{15}\left\{K^5\frac{\gamma^3\delta x y^2}{x^2+y^2\delta^2}+(1-K^5)\frac{xy^2}{x^2+y^2}\right\}. \quad (32)$$

In the case of a metallic particle without a core ($K=0$) this expression corresponds to the classical result (the Drude formula):[3]

$$\sigma(z) = \sigma_0\frac{4}{15}\frac{xy^2}{x^2+y^2}.$$

In the case of a thin metal sheath, when $K\to 1$, for finding the corrections to the absorption according to formula (32) it is convenient to make the substitution $K=1-\varepsilon$, where ε is a small quantity ($\varepsilon\to 0$) and to use the formulas of the approximate calculation.

Indeed, since $1-K^5 = 1-(1-\varepsilon)^5 \approx 1-(1-5\varepsilon) = 5\varepsilon = 5(1-K)$, while $K^5 = (1-\varepsilon)^5 \approx 1-5\varepsilon = 1-5(1-K) = 5K-4$, the absorption cross section in this case is given by the formula

$$\sigma \approx \sigma_0\frac{4}{3}\left[\frac{\gamma^3\delta x y^2}{x^2+y^2\delta^2}\left(K-\frac{4}{5}\right)+\frac{xy^2}{x^2+y^2}(1-K)\right].$$

4. ANALYSIS OF THE RESULTS

The dimensionless absorption cross section F depends in a complex way on a combination of four dimensionless quantities: x, y, K, γ (the behavior of F is not influenced strongly by the quantity $\delta = \tau_1/\tau_2$). The presence of a core has an appreciable influence on the character of the frequency dependence of the dimensionless absorption cross section, because this leads to a change of the amplitude and period of the oscillations (we note that the classical theory is fundamentally incapable of reproducing these oscillations). This is due to the fact that besides reflection of electrons off the inner surface of the particle, additional scattering of the electrons on the core and inside the core also appears.

Figure 1 shows the dependence of the dimensionless absorption cross section F on the dimensionless frequency y of the external field. This figure is drawn for the case of fixed values of the dimensionless inverse mean free path x and of the ratio K of the core radius to the particle radius, and so the ratio of the Fermi velocities in the core and sheath is different for each curve in the figure. It follows from an analysis of the trend of the curves that the a feature of the dimensionless absorption cross section is a phase shift for curves constructed at different values of γ. At all frequencies the absorption cross section increases with increasing parameter γ. With increasing radius of the particle (increasing x) the oscillations of the absorption cross section become less pronounced, as is explained by the influence of bulk collisions of electrons in the core and in the sheath of the particle.

Figure 2 shows plots of the dependence of the dimensionless absorption cross section F on the dimensionless electron mean free path x. If the ratio K of the core to the particle radius and the dimensionless frequency y of the external field are constant, then at all values of x the dimen-

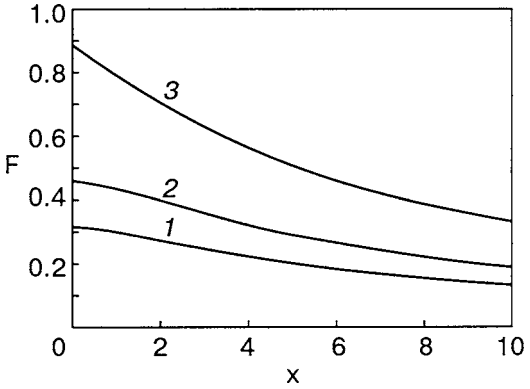

FIG. 2. Dependence of the dimensionless absorption cross section F on the dimensionless inverse mean free path x of the electrons for $\gamma=0.5$ (*1*), 1 (*2*), 1.5 (*3*) ($y=3$, $K=0.8$).

sionless absorption cross section F decreases with decreasing ratio γ of Fermi velocities in the core and sheath of the particle.

For analysis of the dependence of the dimensionless absorption cross section F on the ratio K of the core radius to particle radius we use Fig. 3, which shows the dimensionless absorption cross section of a bimetal particle at fixed values of the other parameters (x, y, and γ). In the case of particles having an outer sheath of a pure metal (the electrons in such metals have a long mean free path) or for very small particles, when the condition $x \ll 1$ holds, in the entire interval of K values the absorption cross section is larger for particles having dominant values of the ratio γ of the Fermi frequencies in the core and sheath.

Figure 4 reflects the dependence of the dimensionless absorption cross section F on the ratio γ of the Fermi velocities in the core and sheath of the particle. The figure is drawn for the case of different ratios K of the core radius to the particle radius (it is assumed that the sheath of the particle is made of a pure metal and the particle is found in an external

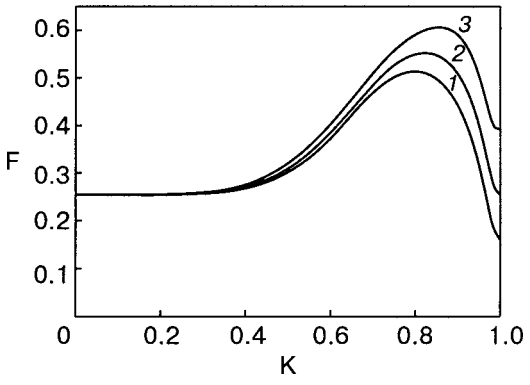

FIG. 3. Dependence of the dimensionless absorption cross section F on the ratio K of the radius of the core to the radius of the particle for $\gamma=0.9$ (*1*), 1 (*2*), 1.1 (*3*) ($x=0$, $y=7$).

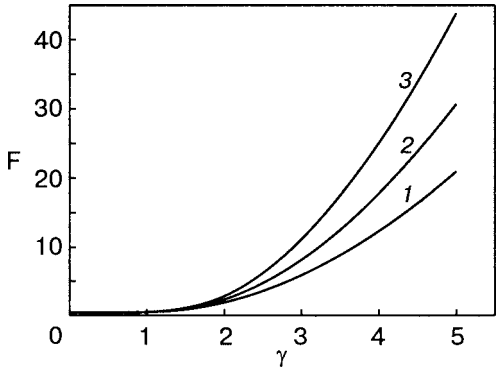

FIG. 4. Dependence of the dimensionless absorption cross section F on the ratio γ of Fermi velocities in the core and sheath of the particle for $K=0.7$ (*1*), 0.75 (*2*), 0.8 (*3*), ($x=0$, $y=7$).

electromagnetic field of a fixed frequency). For each value of γ the dimensionless absorption cross section is larger for particles having sheaths with a volume greater than that of the inner core.

*E-mail: zav.mgul@rambler.ru

[1] Yu. I. Petrov, *Physics of Small Particles* [in Russian], Nauka, Moscow (1984).
[2] J. M. Ziman, *Electrons and Phonons*, Clarendon Press, Oxford (1960), Inostr. Lit., Moscow (1962).
[3] A. G. Lesskis, V. E. Pasternak, and A. A. Yushkanov, Zh. Éksp. Teor. Fiz. **83**, 310 (1982) [Sov. Phys. JETP **56**, 170 (1982)].
[4] A. G. Lesskis, A. A. Yushkanov, and Yu. I. Yalamov, Poverkhnost', No. 11, 115 (1987).
[5] H. J. Trodahl, Phys. Rev. B **19**, 1316 (1979).
[6] H. J. Trodahl, J. Phys. C: Solid State Phys. **15**, 7245 (1982).
[7] E. A. Bondar', Opt. Spektrosk. **75**, 837 (1993) [Opt. Spectrosc. **75**, 496 (1993)].
[8] E. A. Bondar', Opt. Spektrosk. **80**, 89 (1996) [Opt. Spectrosc. **80**, 78 (1996)].
[9] P. M. Tomchuk and B. P. Tomchuk, Zh. Éksp. Teor. Fiz. **112**, 661 (1997) [JETP **85**, 360 (1997)].
[10] É. V. Zavitaev, A. A. Yushkanov, and Yu. I. Yalamov, Zh. Tekh. Fiz. **71**(11), 114 (2001) [Tech. Phys. **46**, 1460 (2001)].
[11] É. V. Zavitaev, A. A. Yushkanov, and Yu. I. Yalamov, Opt. Spektrosk. **92**, 851 (2002) [Opt. Spectrosc. **92**, 784 (2002)].
[12] É. V. Zavitaev, A. A. Yushkanov, and Yu. I. Yalamov, Zh. Tekh. Fiz. **73**, 16 (2003) [Tech. Phys. **48**, 290 (2003)].
[13] É. V. Zavitaev, A. A. Yushkanov, and Yu. I. Yalamov, Zh. Éksp. Teor. Fiz. **124**, 1112 (2003) [JETP **97**, 996 (2003)].
[14] R. J. Kubo, Phys. Soc. Jpn. **17**, 975 (1962).
[15] E. A. Manykin, P. P. Poluéktov, and Yu. G. Rubezhnyĭ, Zh. Éksp. Teor. Fiz. **70**, 2117 (1976) [Sov. Phys. JETP **43**, 1105 (1976)].
[16] R. D. Averitt, S. L. Westcott, and N. J. J. Halas, J. Opt. Soc. Am. B **16**, 1824 (1999).
[17] A. Henglein, J. Phys. Chem. B **104**, 2201 (2000).
[18] L. D. Landau and E. M. Lifshitz, *Electrodynamics of Continuous Media*, 2nd ed., rev. and enl., by E. M. Lifshitz and L. P. Pitaevskii, Pergamon Press, Oxford (1984), Nauka, Moscow (1982).
[19] W. A. Harrison, *Solid State Theory*, McGraw-Hill, New York (1970), Mir, Moscow (1972).
[20] R. Courant, "Partielle Differentialgleichungen," unpublished lecture notes, Göttingen (1932), Mir, Moscow (1964).

Translated by Steve Torstveit

One-dimensional electron lattice system with a long-range interelectron repulsion on a disordered host lattice

A. A. Slutskin* and H. A. Kovtun†

B. Verkin Institute for Low Temperature Physics and Engineering of the National Academy of Sciences of Ukraine, 47 Lenin Ave., Kharkov 61103, Ukraine

(Received November 29, 2004)
Fiz. Nizk. Temp. **31**, 784–795 (July 2005)

We study what happens to a generalized Wigner crystal, GWC (a regular structure formed by narrow-band electrons on a one-dimensional periodic host lattice), when the host lattice suffers a random distortion that *does not break* its long-range order. We show that an arbitrarily weak distortion of this kind gives rise to soliton-like GWC defects (discrete solitons, DS) in the ground state, and thereby converts the ordered GWC into a new *disordered* macroscopic state—lattice Wigner glass (LWG). The ground-state DS concentration is found to be proportional to λ^4 (λ is the typical host-lattice strain). We show that the low-temperature LWG thermodynamics and kinetics are fully described in DS terms. A new phenomenon of a super-slow logarithmic relaxation in the LWG is revealed. Its time turns out to be tens orders of magnitude greater than the microscopic ones. Analytical dependences of LWG thermodynamic quantities on temperature and λ are obtained for an arbitrary relationship between the relevant Coulomb energies and the electron bandwidth. © *2005 American Institute of Physics.* [DOI: 10.1063/1.2001641]

1. INTRODUCTION

In the last two decades layered and low-dimensional conductors have been a focus of attention. In such systems the charge carriers are commonly well separated from the dopants, so that a mutual Coulomb repulsion of the charge carriers turns out to be an essential factor. Among these conductors, of especial interest are lattice (narrow-band) systems wherein hopping (tunneling) of electrons/holes between host-lattice sites is suppressed by their mutual repulsion, and, as a consequence of this, the whole charge carrier ensemble is self-localized. The criterion for such a Coulomb self-localization (CSL) is the inequality

$$t < u_c \sim (a_0/r_{ee})^2 \varepsilon_{ee},$$

where t is the bandwidth, u_c is the typical change of the Coulomb energy of a charge carrier as it hops between neighboring host-lattice sites, a_0 is the host-lattice spacing, r_{ee} is the mean separation between charge carriers, and ε_{ee} is the mean energy of the Coulomb repulsion per charge carrier. There exists a wide class of CSL conductors. Different semiconductor heterostructures[1,2] and organic quasi-one-dimensional conductors[3] fall into this class. The latest achievements of nanotechnology permit the creation of CSL conductors of a new type: arrays of quantum dots exchanging electrons/holes (see, for example, Ref. 4 and references therein), electrons on the helium surface,[5] and nets and chains of metal nano-grains linked by organic-molecule wires as (weak) tunnel junctions.[6] There are also good reasons to think that the CSL criterion is fulfilled in layered metaloxides of a type of high-temperature superconductors, provided the dopant concentration is not too low.

Impetus to theoretical research on CSL conductors was given by Hubbard,[3] who considered the ground state of an electron ensemble on a one-dimensional (1D) *periodic* host lattice in the limit $t/u_c \to 0$. Hubbard suggested that in the thermodynamic limit (the numbers of electrons N and host-lattice sites N_s tend to ∞) the ground-state electron structure at a given chemical potential μ is a periodic ''generalized Wigner crystal'' (GWC) with a rational electron density (filling factor) $n_e = P/Q$ (P,Q are arbitrary coprime integers), with spacing Qa_0 and P electrons per unit cell, which does not depend on the pair potential of the interelectron repulsion $v(x)$ (x is the interelectron distance), provided $v(x)$ meets some simple, physically reasonable conditions (Sec. 2). Hubbard also postulated a universal algorithm to find GWCs. This hypothesis was justified in Refs. 7 and 8, where Hubbard's algorithm was put into a compact form. In recent years Hubbard's results were augmented to the low-temperature thermodynamics of 1D GWCs[9] and the ground state of two-dimensional (2D) CSL conductors on an arbitrary ideal host lattice.[10] The regular 2D CSL conductor was found to be characterized by an effective lowering of dimension, which lies in the fact that even in the case of an isotropic pair potential of electron-electron repulsion the structure elements forming the 2D ground-state structure are electron stripes arranged by Hubbard's algorithm.[10]

The above studies, having revealed a number of unusual features of GWC and its 2D modification, have prompted consideration of the influence of host-lattice disorder on low-temperature properties of CSL conductors. This is of importance not only because there are a number of disordered CSL conductors (e.g., MOSFETs, some nanostructures), but also in respect to the known fact (Larkin,[11] Imri and Ma[12]) that an arbitrarily weak static random peturbation imposed on a *continuous* Wigner crystal (i.e., a crystal formed by electrons that are free to move) breaks (for dimension $d \leqslant 3$) the ground-state crystalline long-range order, producing slowly varying random distortions that become increasingly smooth

as the perturbation goes to zero. Such a structure has been named "Wigner glass." Unlike the continuous case, the electron displacements in CSL conductors cannot be less than the host-lattice spacing a_0, so that the Larkin–Imri–Ma argument is inapplicable to clarify whether lattice electron structures are unstable with respect to weak random perturbations, and what is the mechanism of the possible instability. As far as we know, there is no answer to this question at present.

We are going to fill this gap, considering the low-temperature properties of disordered 1D and 2D CSL conductors in a series of publications. This paper is the first of the series. Here we study the ground state, elementary excitations, their lifetimes, and the low-temperature thermodynamics of a 1D CSL conductor (the temperature $T \ll u_c$) in the limit of strong CSL ($t \ll u_c$) with the assumption that random host-lattice distortions *do not break* the long-range order of the arrangement of host-lattice sites. For definiteness, the charge carriers are further considered to be electrons.

Specifically, we consider the host lattice to be a chain of sites $i=1,\ldots,N_s$ with coordinates

$$X_i = i + \lambda \xi_i , \tag{1}$$

where $\lambda \xi_i$ is a random deviation of the ith site from its ideal position $X_i^0 = i$ ($a_0 = 1$); ξ_i as a function of i takes random values on the interval $[-1,1]$; the disorder parameter λ is assumed to be $< 1/2$ to provide the *periodic* correlation in the host lattice. At first glance such a disorder cannot break the GWC long-range order. However, this seemingly evident statement turns out to be untrue: we show here that for any finite $\lambda \ll 1$ the ground-state electron configuration contains soliton-like GWC defects, *discrete solitons* (DSs), each changing the length of the system (at a given N) by $+1$ (the defect of rarefaction) or -1 (the defect of compression). Being randomly arranged, they do break the GWC long-range order. This is a novel phenomenon rooted in the *discreteness* of the system. The key point is that the discrete solitons differ from common point defects in that a transfer of a discrete soliton over $\mathcal{L}$ unit cells of a GWC leaves behind a "trace"—a cluster of electrons shifted by one host-lattice site from their ground-state positions, the number of the electrons being $\mathcal{L}$. Owing to the host-lattice disorder the Coulomb energy of the trace is a sum of $\mathcal{L}$ random alternating-sign quantities $\propto \lambda^2$, which grows in modulus as $\sqrt{\mathcal{L}}$, attaining values $\sim u_c$ for sufficiently big $\mathcal{L}$. It is this fact that accounts for discrete solitons coming into existence in the ground state. Since the random 1D lattice electron structure just described is bound to be converted into a GWC as $\lambda \to 0$, it can be conceived of, by anology with the (continual) Wigner glass, as a "lattice Wigner glass" (LWG). It is the discrete-soliton transfer that underlies the distinctive features of both LWG thermodynamics and kinetics. Therefore, the macroscopic behavior of LWG is expected to differ essentially from that of the continual Wigner glass. This is dramatically manifested in relaxation of high-energy LWG excitations: our analysis shows that their lifetimes are anomalously great, the concentration of the excitations decreasing with time in a logarithmic fashion. Broadly speaking, the relaxation is by annihilation of DSs of the compression and rarefaction type. This requires the DSs to overcome (by tunneling or in a thermal way) "giant" random Coulomb barriers of many-electron origin. The phenomenon is somewhat reminiscent of the mechanism of the nonergodic behavior of spin glass.[13,14]

The layout of the material in our paper is as follows. In the next Section the Hamiltonian of the system under consideration is described. In Sec. 3 we show that for an arbitrary small λ the GWC long-range order is unstable with respect to formation of GWC defects (DSs) at zero temperature, and find the ground-state dependence of the GWC defects concentration on λ and μ in the limit $t=0$. The LWG low-temperature thermodynamics ($T \ll u_c$) is considered in Sec. 4, where the dependence of thermodynamic quantities on T is found in terms of low-lying LWG excitations. The anomalously slow relaxation in LWG is discussed in Sec. 5. In the last Section we discuss experimental possibilities for studying LWG.

2. HAMILTONIAN

At a given μ the general Hamiltonian $\mathcal{H}$ of an electron system on an 1D host lattice is of the form

$$\mathcal{H} = t\sum_i (c_i^+ c_{i-1} + \text{h.c.}) + \frac{1}{2}\sum_{i \neq i'} v(X_i - X_{i'}) n_i n_{i'} - \mu \sum_i n_i . \tag{2}$$

Here the index i enumerates host-lattice sites, c_i^+ and c_i are operators of creation and annihilation of an electron at the ith site, respectively; n_i is the operator of the electron density at the ith site, which takes only values 0 and 1, since n_e is assumed to be not too close to 1/2; for this reason the electron spin indices are dropped; summation is over all host-lattice sites; the pair potential of an electron-electron repulsion $v(x) = v(-x) > 0$. The dependence of the site coordinate X_i on i is given by Eq. (1).

To find the ground-state structure in the $t \ll u_c$ limit under consideration, one can put $t=0$, the Hamiltonian Eq. (2) reducing to

$$\mathcal{H} = \mathcal{H}\{i(m)\} = \frac{1}{2}\sum_{m \neq m'} v(x_m - x_{m'}) - \mu N, \tag{3}$$

where the index $m=1,\ldots,N$ enumerates the electrons, $x_m = X_{i(m)}$ is the coordinate of the mth electron, and $i(m)$ is the number of the site at which the mth electron is localized. The reduced Hamiltonian Eq. (3) is a functional of electron configurations $\{i(m)\} = i(1),\ldots,i(N)$. It differs from that considered by Hubbard[3] only in that X_i contains the random addition $\lambda \xi_i$. To proceed with our studies it is of benefit to formulate briefly, following Refs. 3, 7, 8, the main properties of the ground state at $\lambda = 0$.

Below we consider the pair potential $v(x) > 0$ to be an everywhere convex function of x that goes to zero with increase of x faster than x^{-1}; its dependence on x is otherwise arbitrary. In such a case the ground-state space structure of the 1D electron gas on the ideal host lattice $X_i^0 = i$ is given by the above-mentioned universal Hubbard algorithm that is expressed by the simple formula

$$i(m)=i_H(m,n_e)\equiv[m/n_e+\varphi], \tag{4}$$

where [...] is the integer part of a number, and φ is an arbitrary phase that reflects the arbitrariness of the choice of the first electron site coordinate $i(1)$. As was mentioned in the Introduction, only rational $n_e=P/Q$ survive at zero temperature and a given μ, the function $i_H(m,P/Q)$ determining the GWC. The ground-state dependence of n_e on μ is a devil's staircase: for each pair P,Q there is an interval $\mu_-(P,Q)\leqslant\mu\leqslant\mu_+(P,Q)$ within the limits of which $n_e(\mu)$ remains equal to P/Q. The left and right endpoints of the devil's-staircase interval are a decrease and an increase in the Coulomb energy of the system as N changes by -1 and $+1$, respectively. The length of the interval $\Delta\mu=\mu_+-\mu_-$ depends only on Q:

$$\Delta\mu=Qu_Q,$$

$$u_Q=\sum_{k=1}^{\infty} k[v(Qk+1)-2v(Qk)+v(Qk-1)]. \tag{5}$$

As is seen from this expression, $u_Q\sim u_c$, and hence, $\Delta\mu$ vanishes rapidly together with u_c as Q tends to ∞.

3. THE GROUND STATE OF LWG

3.1. GWC instability

In this Section we deal with the Hamiltonian of Eq. (3). First we consider devil's-staircase intervals with $n_e=1/Q$. Generalization to an arbitrary $n_e=P/Q$ is performed without difficulty (Sec. 5). In the case of $P=1$ the Hubbard algorithm Eq. (4) gives the simple periodic dependence $i_H(m,1/Q)=i_m^\nu\equiv Qm+\nu$ with $\nu=0,\ldots,Q-1$. (We will call this the "ν-configuration.") If the ground-state electron arrangement $i_g(m)$ were the same as in the GWC (i.e., $i_g(m)=i_m^\nu$), despite the random small displacements $\lambda\xi_i$ ($\lambda\ll1$), a weak disorder of the form Eq. (1) would affect only the energy of the ν-configuration E_{GWC}. The latter is independent of ν to an accuracy of fluctuation corrections $\propto\sqrt{N}$

$$E_{\mathrm{GWC}}=N\epsilon+\mathcal{O}(\sqrt{N}),$$

$$\epsilon=\epsilon_0+\epsilon_\lambda,\quad \epsilon_\lambda=\lambda^2\langle\xi^2\rangle\sum_{k=1}^{\infty} v''(kQ). \tag{6}$$

Here ϵ is the mean energy per electron, ϵ_0 is that for the ideal host lattice, ϵ_λ is the addition to ϵ_0 produced by a weak host-lattice disorder, $\langle...\rangle$ is the average on the ξ distribution, and $v''(x)=d^2v/dx^2$.

Let us show that the periodic (in site coordinates) ν-configuration is unstable under conditions of a weak disorder. To reveal this, let us find out what happens to the energy Eq. (3) if some ν-configuration cluster formed by electrons with numbers $m_1,\ldots,m_2$ is shifted as a whole by ±1: $i_m^\nu\to i_m^{\nu\pm1}$, $m_1\leqslant m\leqslant m_2$.

The energy of the cluster $E(m_1,m_2,\nu)$ is the sum

$$E(m_1,m_2,\nu)=\epsilon_b+E_i(m_1,m_2,\nu) \tag{7}$$

whose first term is the cluster boundary energy, i.e., the energy of the interaction of the cluster with its surroundings. The second term is the internal cluster energy:

$$E_i(m_1,m_2,\nu)=(m_2-m_1)\epsilon+\tilde{E}(m_1,m_2,\nu); \tag{8}$$

$\tilde{E}(m_1,m_2,\nu)$ is its fluctuating part. Expanding energy Eq. (3) in powers of λ, we obtain

$$\tilde{E}(m_1,m_2;\nu)=\sum_{m=m_1}^{m_2}(\epsilon_m^\nu-\epsilon),$$

$$\epsilon_m^\nu=\frac{\lambda^2}{2}\sum_{m'=-\infty}^{\infty} v''(Q(m-m'))[\xi(i_m^\nu)-\xi(i_{m'}^\nu)]^2+\mathcal{O}(\lambda^3). \tag{9}$$

The shift of the cluster, on the one hand, creates two defects at the ends of the cluster, which are pairs of electrons separated by distances $Q+1$ (rarefaction defect, "$-$dimer") and $Q-1$ (compression defect, "$+$dimer"). Using expression (5), one can show that in the case of $\pm$dimers well-separated dimer formation *increases* the cluster boundary energy by

$$\delta\epsilon_b=\Delta\mu/Q+\tilde{\epsilon}_-+(m,\nu)\tilde{\epsilon}_++(m,\nu), \tag{10}$$

where $\Delta\mu/Q$ is the total energy of dimer formation at $\lambda=0$; $\tilde{\epsilon}_\pm(m,\nu)$ is a small ($\sim\lambda u_c$) random addition produced by the host-lattice disorder. On the other hand, the shift changes $\tilde{E}(m_1,m_2;\nu)$ by

$$\Delta_{\nu,\nu'}=\Delta_{\nu,\nu'}(m_1,m_2)=\sum_{m=m_1}^{m_2}(\epsilon_m^{\nu'}-\epsilon_m^\nu),\quad \nu'=\nu\pm1. \tag{11}$$

This energy change, being a sum of random quantities $\epsilon_m^{\nu'}-\epsilon_m^\nu$ with zero average, fluctuates in m_1, m_2, taking both positive and negative values. Its modulus $|\Delta_{\nu,\nu'}|\sim\lambda^2u_c(m_2-m_1)^{1/2}$ therewith grows as m_2-m_1 increases. Therefore, despite the smallness of λ there are many sufficiently long clusters for which $\Delta_{\nu,\nu'}+\delta\epsilon_b<0$, and hence, their shifts *decrease* the energy of the system. What this means is that the GWC is *unstable* relative to dimer formation for an arbitrarily small λ.

3.2. The space structure of the LWG ground state

As follows from the general theory of GWCs[3,7,8] (see also Ref. 9), in the case under consideration ($P=1$) the $\pm$dimers are the GWC defects with the least energies of formation at a given pressure. This fact together with the above reasoning suggests that for any finite $\lambda\ll1$ the ground-state configuration $i_g(m)$ consists of long periodic electron clusters, segments of ν-configurations, alternating with $\pm$dimers. One should thus seek $i_g(m)$ among functions $i(m)$ of the form

$$i(m)=Qm+\nu^\alpha,\quad m_1^\alpha\leqslant m\leqslant m_2^\alpha,$$

$$m_1^\alpha=m_2^{\alpha-1}+1,\quad \nu^\alpha=\nu^{\alpha-1}-\sigma_\alpha, \tag{12}$$

where index α enumerates periodic clusters of the configuration $i(m)$, $\sigma_\alpha=-1$ or 1 depending on whether the $(\alpha-1)$-th and α-th clusters are joined by a $-$ or $+$dimer, respectively. The coordinates m_{1g}^α, m_{2g}^α of the end electrons of ground-state clusters are obviously random, and, hence, there is no long-range interelectron correlation in the ground state. This is just the LWG mentioned in the Introduction, the $\pm$dimers being the discrete solitons. The LWG correlation

radius $L_g \sim 1/(n_-^g + n_+^g)$ (in units of $r_{ee}=Q$), where $n_\pm^g = \mathcal{N}_\pm^g/N$ is the ground-state concentration of $\pm$dimers, and $\mathcal{N}_\pm^g$ is their number in the ground state.

The next step is to find $n_\pm^g$. To this end one should consider the general expression for the energy E of the configuration (12). It is appropriate to compare E with E_{GWC} [Eq. (6)], mapping the configuration on a set of ν-configurations. In so doing the α-th cluster is considered as the cluster of the $\bar{\nu}^\alpha$-configuration ($\bar{\nu}^\alpha = \nu^\alpha - Q[\nu^\alpha/Q]$ is the reduced phase less than Q) with the end electrons $\bar{m}_{1,2}^\alpha = m_{1,2}^\alpha + [\nu^\alpha/Q]$. The mapping gives

$$E = E_{\mathrm{GWC}} + E_{\mathrm{dim}} + \tilde{E}, \tag{13}$$

where E_{dim} is the total energy of dimer formation, and $\tilde{E}$ is the fluctuating part of the energy.

To the zero approximation in λ

$$E_{\mathrm{dim}} = (n_- u_- + n_+ u_+)N \tag{14}$$

($n_\pm = \mathcal{N}_\pm/N$ is the $\pm$dimer concentration for a given configuration (12), $\mathcal{N}_\pm$ is the number of $\pm$dimers), and

$$u_\pm(\mu) = \frac{u_Q}{2}(1 \mp z) > 0,$$

$$z = 2(\mu - \bar{\mu})/\Delta\mu, \bar{\mu} = \frac{\mu_- + \mu_+}{2} \tag{15}$$

are the $\pm$dimer formation energies at a given μ; the variable z takes values on the interval $[-1,1]$ as μ is varied from μ_- to μ_+; u_Q has been defined in Eq. (5). Writing Eqs. (14), (15), we allow for the fact that a small variation $\pm\delta n_e$ of n_e about $n_e = 1/Q$ gives rise to $Q\delta n_e$ $\pm$dimers [this follows immediately from Eq. (4)], i.e.,

$$N = N_0 + Q(\mathcal{N}_+ - \mathcal{N}_-); \tag{16}$$

$N_0 = N_s/Q$ is the ground-state number of electrons at $\lambda = 0$.

The energy $\tilde{E}$, unlike the two previous terms in Eq. (13), depends upon the dimer coordinates m_1^α essentially:

$$\tilde{E} = \sum_\alpha \tilde{E}(\bar{m}_1^\alpha, \bar{m}_2^\alpha; \bar{\nu}^\alpha). \tag{17}$$

As follows from Eq. (9), the quantities $\tilde{E}(\bar{m}_1^\alpha, \bar{m}_2^\alpha; \bar{\nu}^\alpha)$ are sums of $l_\alpha = m_2^\alpha - m_1^\alpha \sim (n_- + n_+)^{-1/2}$ random terms with zero average and moduli $\sim \lambda^2 u_c$. Since the $\tilde{E}(\bar{m}_1^\alpha, \bar{m}_2^\alpha; \bar{\nu}^\alpha)$ fluctuate randomly, it is easy to conclude that in the limit $n_\pm \ll 1$ the cluster endpoints m_1^α, m_2^α can be chosen in such a way that terms of the sum (17) are all negative, and hence, at a given $n_\pm$ the minimum $\tilde{E}_{\mathrm{min}}$ of $\tilde{E}$ with respect to dimer arrangement is bound to be <0.

Random sequences $\epsilon_1^\nu, \epsilon_2^\nu, \ldots, \epsilon_N^\nu$ ($\nu = 0, \ldots, Q-1$), whose terms are involved in expression (9), are all statistically equivalent. Therefore, $\tilde{E}_{\mathrm{min}}$ does not depend on the sequence $\{\sigma_\alpha\} = \sigma_1, \sigma_2, \ldots$, being a function of the dimer density $n_- + n_+$ and system parameters only. Taking this into account together with the fact that $|\tilde{E}(\bar{m}_1^\alpha, \bar{m}_2^\alpha; \bar{\nu}^\alpha)| \sim \lambda^2 u_c l_\alpha^{1/2}$, one can write $\tilde{E}_{\mathrm{min}}$ as

$$\tilde{E}_{\mathrm{min}} = -u_\xi \lambda^2 (n_- + n_+)^{1/2} N, \tag{18}$$

where, as will be shown below, the energy factor $u_\xi \sim u_c$ is uniquely determined by Q, $v(x)$, and the moments of the distribution of the random quantity ξ_i [see Eq. (1)].

The ground-state concentrations of $\pm$dimers, $n_\pm^g$, are those which minimize the sum $\tilde{E}_{\mathrm{min}} + E_{\mathrm{dim}}$. Using Eqs. (14), (15), and (18), we find that for any $\lambda \neq 0$

$$n_-^g(z) = \begin{cases} \dfrac{u_\xi^2}{u_Q^2} \dfrac{\lambda^4}{(1+z)^2}, & -1 < z < 0 \\ 0, & 0 < z < 1 \end{cases};$$

$$n_+^g(z) = \begin{cases} 0, & -1 < z < 0 \\ \dfrac{u_\xi^2}{u_Q^2} \dfrac{\lambda^4}{(1-z)^2}, & 0 < z < 1. \end{cases} \tag{19}$$

It remains to find the explicit form of u_ξ. This requires rather sophisticated calculations. Here we only outline them. Since u_ξ does not depend on $\{\sigma_\alpha\}$, it is convenient to choose the sequence $\{\sigma_\alpha\}$ with alternating σ_α signs, considering the minimum of $\tilde{E} + u\mathcal{N}$ instead that of $\tilde{E}$; here u is a given arbitrary positive parameter, and $\mathcal{N} = \mathcal{N}_- = \mathcal{N}_+$ is the variable that is to be found as the result of the minimization. This value, $\mathcal{N} = \bar{\mathcal{N}}$, can be calculated in terms of a random walk of the sum $\Delta_{0,1}(1,m)$ (see expression (11)) as a function of m. In so doing, one should take into account that the $\tilde{E} + u\mathcal{N}$ minimum is realized if dimers of a given sign are all positioned at the points m_α ($\alpha = 1,2,\ldots,\bar{\mathcal{N}}$) such that $\Delta_{0,1}(1,m) - \Delta_{0,1}(1,m_\alpha)$ *first* attains u value at some points $m = m_\alpha^r > m_\alpha$ (a random walk toward the right) and $m = m_\alpha^l < m_\alpha$ (a random walk toward the left) without taking zero value on the intervals $[m_\alpha, m_\alpha^r]$ and $[m_\alpha^l, m_\alpha]$. The total number $\bar{\mathcal{N}}$ of points m_α is found on the basis of the probability theory methods[15] that are used in consideration of the so-called first passage and renewal problems. The factor u_ξ is obtained in view of the fact that the minimum of $\tilde{E} + u\mathcal{N}$ is also $\min_{\mathcal{N}}(-u_\xi \mathcal{N}^{1/2} + u\mathcal{N})$. The net result of the calculation is the following:

$$u_\xi = (D/2\pi^2)^{1/2}; \tag{20}$$

$D \sim u_c^2$ is the diffusion coefficient for the random walk of $\Delta_{\nu,\nu'}/\lambda^2$, which is given by the formula

$$D = v_1^2(\langle\xi^4\rangle - \langle\xi^2\rangle^2) + v_2(\langle\xi^4\rangle + 3\langle\xi^2\rangle^2);$$

$$v_1 = \sum_{\substack{k=-\infty \\ k\neq 0}}^{\infty} v''(Qk), \quad v_2 = \sum_{\substack{k=-\infty \\ k\neq 0}}^{\infty} (v''(Qk))^2. \tag{21}$$

The existence of dimers in the ground state not only renders a long-range order impossible, but also accounts for the difference between the ground-state electron density of LWG $n_e(\mu,\lambda)$ and that of GWC $n_e(\mu,0)$. According to Eq. (16) we have $n_e(\mu,\lambda) - n_e(\mu,0) = \pm n_\pm^g/Q$. As is seen from Eq. (19), dimers of one sign are fully replaced by those of the opposite sign as μ passes through the point $\bar{\mu}$, both $n_+^g(\bar{\mu}+0)$ and $n_-^g(\bar{\mu}-0)$ being equal to $\bar{n}_g = (u_\xi/u_q)^2\lambda^4$. This results in a jump of the electron density by $2Q^{-1}\bar{n}_g$ at $\mu = \bar{\mu}$, i.e., in a *first-order transition* in μ.

Another remarkable point is that $n_\pm^g$ grows significantly as μ approaches the endpoints $\mu_\pm$. Close to them a mutual

repulsion of dimers (which is negligibly small for $|\mu-\mu_{\pm}| \sim \Delta\mu$) should be taken into account. That problem is beyond the scope of this paper.

From the above expressions for u_{ξ} and u_Q it follows that the factor u_{ξ}^2/u_Q^2 appearing in Eq. (19) is ~ 1 both for $Q \sim 1$ and $Q \gg 1$, i.e., $n_{\pm}^g \sim \lambda^4$ for $|1 \pm z| \sim 1$. According to Eq. (19) the LWG correlation radius $L_g \sim 1/n_{\pm}^g \propto 1/\lambda^4$ remains $\gg 1$ even if λ is not too small. This suggests that the description of LWG in terms of dimers works up to $\lambda = 1/2$.

4. LOW-LYING ELEMENTARY EXCITATIONS AND THE LOW-TEMPERATURE THERMODYNAMICS OF LWG

4.1. The low-lying excitation spectrum

The low-lying LWG excitations are those whose energies are much less than the typical increase (u_c) in the energy of the system as an interior electron of a regular claster is shifted by one site or more. They are produced by ground-state dimer displacements, and hence, they are of a many-electron nature. To find the low-lying excitation spectrum let us consider the state $|s\rangle$ created by displacement of the $\pm$dimer adjacent, for definiteness, to the left end of the α-th cluster from its ground-state position, say, to the right by $s = 1,2,\ldots$ steps. This occurs as s electrons $m_{1g}^{\alpha},\ldots,m_{1g}^{\alpha}+s-1$ are shifted to the left ($-$dimer) or to the right ($+$dimer) neighboring sites all together. The Coulomb energy of this electron "trace" is the sum

$$u_{\alpha}^{\pm}(s) = \varepsilon_{\alpha}^{\pm}(s) + \tilde{\varepsilon}_{\alpha}^{\pm}(s), \tag{22}$$

where

$$\varepsilon_{\alpha}^{\pm}(s) = \Delta_{\bar{\nu}_{\alpha}\pm 1,\bar{\nu}_{\alpha}}(\bar{m}_{1g}^{\alpha}, \bar{m}_{1g}^{\alpha}+s), \tag{23}$$

$\Delta_{\nu,\nu'}$ is defined by Eq. (11);

$$\tilde{\varepsilon}_{\alpha}^{\pm}(s) = \tilde{\epsilon}_{\pm}(\bar{m}_{1g}^{\alpha}+s, \nu_{\alpha}) - \tilde{\epsilon}_{\pm}(\bar{m}_{1g}^{\alpha}, \nu_{\alpha}), \tag{24}$$

$\tilde{\epsilon}_{\pm}(m,\nu)$ is the quantity appearing in Eq. (10); $u(0) = 0$. From this point on, we do not show dependence on α or the sign of the dimer, provided that no misunderstanding will result. The explicit form of $\tilde{\varepsilon}(s)$ is of no importance for further consideration; what matters is only the fact that $\tilde{\varepsilon}(s)$ takes random values within some interval $[-\Delta_{\lambda}/2, \Delta_{\lambda}/2]$ whose width $\Delta_{\lambda} \sim \lambda u_c$. The quantity $\varepsilon(s)$ can be considered as the "coordinate" of a "particle" that executes a random walk with the typical step $\delta\varepsilon \sim \lambda^2 u_c \ll \Delta_{\lambda}$ as the "time" s increases. With an increase in s the energy $\varepsilon(s)$ grows as $\lambda^2 u_c \sqrt{s}$, so that it becomes more than Δ_{λ} for $s \sim s_{\lambda} \equiv \lambda^{-2}$ ($s_{\lambda} \ll L_g$). Since $\varepsilon(s)$ randomly undergoes "returns" into the interval $[-\Delta_{\lambda}/2, \Delta_{\lambda}/2]$, there are inevitably such s at which $u(s) \lesssim t$. Therefore, the low-lying excitations should be considered with regard to the electron hopping, despite the inequality $t \ll u_c$.

At $t \neq 0$ the dimer, owing to the smallness of t/u_c, can be considered as a quasiparticle whose Hamiltonian $\mathcal{H}_{\rm dim}$ acts in the subspace of states $|s\rangle$ (s space). As follows from the general expression (2), it is of the form

$$\mathcal{H}_{\rm dim} = t\sum_s \left(|s-1\rangle\langle s| + |s+1\rangle\langle s|\right) + \sum_s u(s)|s\rangle\langle s|, \tag{25}$$

where the first term is the kinetic-energy operator, $u(s)$ plays the role of an effective potential, and the summation is over the whole s space. The state vectors of the low-lying excitations and their energies are eigenvectors $|\Psi\rangle$ of $\mathcal{H}_{\rm dim}$ and its eigenvalues $\varepsilon_{\rm exc}$, respectively. Due to the randomness of the "potential" $u(s)$ the dimer is Anderson localized in the s space, so that the eigenvectors

$$|\Psi\rangle \equiv |\Psi_l\rangle = \sum_s \psi_l(s)|s\rangle$$

can be classified in the coordinates $l = 0, \pm 1, \ldots$ of points (localization centers) about which the stationary wave functions $\psi_l(s)$ are centered. Since $|u(s+1) - u(s)| \sim \Delta_{\lambda}$, the Anderson parameter governing the $|\Psi_l\rangle$ structure is $\gamma = \Delta_{\lambda}/t \sim \lambda u_c/t$. It can be both less than or more than 1, despite the smallness of t/u_c. If $\gamma \gg 1$, the kinetic energy operator is a weak perturbartion. In such a case

$$\psi_l(s) = \delta_{sl} + \mathcal{O}(1/\gamma), \quad \varepsilon_{\rm exc}(l) = u(l) + \mathcal{O}(1/\gamma),$$

and the localization radius r is thus equal to 1. For $\gamma \ll 1$ the 1D Anderson localization under a weak random potential takes place. In this limit

$$r \sim \gamma^{-2} \sim (t/u_c)^2 \lambda^{-2}. \tag{26}$$

For the following consideration of the thermodynamics it is necessary to know the typical separation $\varepsilon_{\rm min}$ between the least of $\varepsilon_{\rm exc}$ and the ground-state energy.

If $\gamma \gg 1$, $\varepsilon_{\rm min}$ is determined, as is seen from Eqs. (22)–(24), by the number of "returns" R of the random sum $\varepsilon(s)$ to the above-mentioned domain $|\varepsilon(s)| \lesssim \Delta_{\lambda}$. Since $\varepsilon(s)$ values fall into this domain randomly, we have $\varepsilon_{\rm min} \sim \Delta_{\lambda}/R$. By definition

$$R = \int_{-\Delta_{\lambda}/2}^{\Delta_{\lambda}/2} d\varepsilon \sum_{s=0}^{L_g} \mathcal{P}(s,\varepsilon),$$

where $\mathcal{P}(s,\varepsilon)d\varepsilon$ is the probability that $\varepsilon(s)$ will fall into the interval $[\varepsilon, \varepsilon + d\varepsilon]$ after s steps; for $s \gg 1$ it satisfies the diffusion equation

$$\partial\mathcal{P}/\partial s = \mathcal{D}\partial^2\mathcal{P}/\partial\varepsilon^2 \tag{27}$$

with the diffusion coefficient $\mathcal{D} = \lambda^2 D \sim (\delta\varepsilon)^2$ (D is given by expression (21)). Solving Eq. (27) subject to the boundary condition $\mathcal{P}(s, -\Delta_{\lambda}/2) = 0$ (this is necessary since $\varepsilon_{\rm exc}(l) \approx u(l)$ is positive) and substituting the solution into the expression for R, we find

$$\varepsilon_{\rm min} \sim \lambda^3 u_c \ll \delta\varepsilon. \tag{28}$$

It should be added that the main contribution to R is given by $s \sim s_{\lambda}$. Therefore, the localization center of the eigenvector with the excitation energy $\varepsilon_{\rm min}$ is generally $\sim s_{\lambda}$ distant from the ground-state position of the dimer.

For $\gamma \ll 1$ the localization radius according to Eq. (26) is $\ll s_{\lambda}$, the eigenenergies $\varepsilon_{\rm exc}(l)$ randomly filling a band of width $\sim t$ as l varies within a domain of a length $\sim s_{\lambda}$. Therefore, in this limit

$$\varepsilon_{\rm min} \sim t/s_{\lambda} \sim \lambda^2 t. \tag{29}$$

4.2. The LWG thermodynamics

According to the above consideration, in the limiting case $T \ll u_c$ the LWG is in essence an ensemble of independent Anderson localized dimers. The dependence of their number on T can be ignored with accuracy to exponentially small (in T/u_c) corrections. The thermodynamic potential $\Omega = \Omega(\mu, T)$ of such a system is expressed in terms of a distribution of excitation energies $\varepsilon^{\alpha}_{\mathrm{exc}}(l)$ over the dimer ensemble:

$$\Omega = \Omega_g - \mathcal{N}^g T \int' \ln\left(1 + \sum_{k=1} \exp\left(-\frac{\varepsilon_k}{T}\right)\right) \times W(\varepsilon_1, \varepsilon_2, \ldots) d\varepsilon_1 d\varepsilon_2 \ldots, \tag{30}$$

where Ω_g is the ground-state value of Ω; $W(\varepsilon_1, \varepsilon_2, \ldots)$ is the probability density that the least excitation energy of the system is ε_1, the next one is ε_2, etc.; the symbol prime means that the integration is performed over the region $\varepsilon_1 < \varepsilon_2 < \ldots$ from $\varepsilon_k = 0$ $(k = 1,2,\ldots)$ to the upper bound of the dimer energy spectrum (it is $\sim u_c$). The upper bound of the summation over k is $\sim L_g$. We do not show it as it is immaterial to an accuracy of an exponentially small term $\propto \exp(-u_c/T)$.

As was proved by Molchanov,[16] there is no mutual repulsion of neighboring energy levels in 1D Anderson localized systems, unlike Wigner–Dyson statistical ensembles.[17] This holds for the energy spectrum considered, since $L_g \gg r$. In such a case the eigenenergies are arranged quite randomly, similar to particle coordinates in an 1D ideal gas, and W is completely determined by the density of states (per dimer), $g(\varepsilon)$, with a given energy ε:

$$W(\varepsilon_1, \varepsilon_2, \ldots) = \prod_{k=1} w(\varepsilon_k, \varepsilon_{k+1}), \tag{31}$$

where the two-level correlation function $w(\varepsilon, \varepsilon')$ obeys the Poisson law

$$w(\varepsilon', \varepsilon) = g(\varepsilon) \exp\left(-\int_{\varepsilon'}^{\varepsilon} g(\varepsilon'') d\varepsilon''\right). \tag{32}$$

The density of states $g(\varepsilon)$ increases monotonically with growth in ε from

$$g(0) \sim 1/\varepsilon_{\min} \sim 1/\lambda^2(\lambda u_c + t) \tag{33}$$

to values $\sim 1/\lambda^4 u_c$. The most important dimensionless parameter governing the temperature dependence of Ω is thus $Tg(0)$. In the limit $Tg(0) \ll 1$ the thermodynamic potential can be expanded in powers of $Tg(0)$. To find the nth term of this series, all exponents $\exp(-\varepsilon_k/T)$ with $k > n$ appearing in expression (30) should be discarded. So doing, we find that to the first nonvanishing approximation Ω is of the form

$$\Omega = \Omega_g - \frac{\pi^2}{12} \mathcal{N}^g g(0) T^2. \tag{34}$$

Consequently, both the entropy S and the heat capacity C per site tend to zero as T with $T \to 0$. In view of Eqs. (19), (33), and (34) we obtain

$$S, C = \frac{\pi^2}{6} n^g g(0) T \sim \lambda^2 (\lambda u_c + t)^{-1} T,$$

i.e., the proportionality coefficient is linear or quadratic in λ depending on whether $\gamma \gg 1$ or $\gamma \ll 1$.

In the opposit limit $Tg(0) \gg 1$, the excitation spectrum can be considered as a continuous one. This gives

$$\Omega = \Omega_g - \mathcal{N}^g T \ln\left(\int_0^{\infty} \exp(-\varepsilon/T) g(\varepsilon) d\varepsilon\right). \tag{35}$$

We have expanded the integration to infinity as the integrand is reduced rapidly for $\varepsilon \gg T$. Expression (35) shows that in the case $Tg(0) \gg 1$, C depends slightly on T, being $\sim n^g$.

5. SUPER-SLOW RELAXATION IN LWG

Below we consider low-temperature $(T \ll u_c)$ relaxation of strongly nonequilibrium LWG states formed by excitations with energies $\sim u_c$. The simplest excitation of this type arises if an interior electron of some regular ground-state cluster is shifted by one site from its ground-state position. Such an excitation can be considered as a pair of bound "odd" (as compared to the ground state) $+$dimer and $-$dimer. The electron shifted reverts to its ground-state site, emitting phonons with energies $\sim u_c$. Obviously, this takes a microscopic time of the order of the reciprocal Debye frequency. The situation is drastically changed if some external perturbation, for example, light excitation, disrupts the pair, separating the "odd" $\pm$dimers to a sufficiently large distance (within the limits of the cluster). A dimer cannot disappear by itself, since this would cause, by virtue of dimer's topological nature, a simultaneous shift of a macroscopic number of electrons.

Therefore, the "odd" dimers can only disappear by their mutual annihilation. We will show below that under slight-disorder conditions this process takes an anomalously long time.[1)]

5.1. The Hamiltonian and eigenvectors of a separate pair of "odd" dimers

To the main approximation in t/u_c the state space of the pair is a set of state vectors

$$|\mathbf{s}\rangle = \hat{D}_-(s_-)\hat{D}_+(s_+ + 1)|\Phi_g\rangle,$$

where $|\Phi_g\rangle$ is the ground-state eigenvector, s_-, s_+ are arbitrary integers meeting the condition $\bar{m}^{\alpha}_{1g} \leqslant s_-, s_+ \leqslant \bar{m}^{\alpha}_{2g}$ (here the reduced coordinates of the regular-cluster end electrons defined in Sec. 3 are used; we denote them $\bar{m}_{1,2}$ from this point on); $\hat{D}_-(s)$ and $\hat{D}_+(s) = \hat{D}_-^{-1}(s)$ are the operators that shift all electrons with numbers $\geqslant s$ one site leftwards and rightwards, respectively. The integers $s_{\pm}$ play the role of the coordinates of the "odd" $\pm$dimer. The Hamiltonian of the pair $\mathcal{H}_{\mathrm{pair}}$ can be written as

$$\mathcal{H}_{\mathrm{pair}} = t \sum_{\langle \mathbf{s}'\mathbf{s} \rangle} |\mathbf{s}'\rangle\langle\mathbf{s}| + \sum_{\mathbf{s}} u(\mathbf{s})|\mathbf{s}\rangle\langle\mathbf{s}| + \Delta\mu/Q; \tag{36}$$

the first term is the operator of the kinetic energy of the pair; the symbol $\langle \mathbf{s}'\mathbf{s} \rangle$ means summation over all nearest neighbors of $\mathbf{s}$; the "potential" energy of the pair

$$u(\mathbf{s}) = u^{\sigma}_-(s_-) + u^{\sigma}_+(s_+), \quad \sigma = \mathrm{sgn}(s_+ - s_-),$$
$$u^{\sigma}_{\pm}(s_{\pm}) = \pm\sigma\Delta_{\bar{\nu}, \bar{\nu}-\sigma}(\bar{m}_1, s_{\pm}) + \tilde{\boldsymbol{\epsilon}}_{\pm}(s_{\pm}), \tag{37}$$

where $\Delta_{\nu,\nu'}$ is the sum of random quantities defined by Eq. (11); $\tilde{\epsilon}_{\pm}(s)=\tilde{\epsilon}_{\pm}(s,\bar{\nu})$ [see Eq. (10)] oscillates randomly with the amplitude λu_c. The third term in Eq. (36) is the energy of pair formation at $\lambda=0$.

The structure of Hamiltonian (36) is akin to that of the one-dimer Hamiltonian (25). It immediately follows that the $+$dimer and $-$dimer of a pair are both Anderson localized in the **s** representation, the localization radius r being $\sim 1+(t/\lambda u_c)^2$. Classifying the pair's eigenvectors $|\Phi\rangle$ by the coordinates l_-, l_+ of the $\pm$dimer localization centers, we can write $|\Phi\rangle$ as

$$|\Phi\rangle=|\Phi_{\mathbf{l}}\rangle=\sum_{\mathbf{s}}\psi_{\mathbf{l}}(\mathbf{s})|\mathbf{s}\rangle. \tag{38}$$

Here $\mathbf{l}=\{l_-,l_+\}$, the summation is over all **s**, and $\psi_{\mathbf{l}}(\mathbf{s})$ is the pair's wave function, which is localized in the **s**-space region $|\mathbf{l}-\mathbf{s}|\lesssim r$. In the general case that the pair's length $l_p=|l_--l_+|\gg r$ one can replace σ in Eq. (37) with $\mathrm{sgn}(l_+-l_-)$. This allows $\psi_{\mathbf{l}}(\mathbf{s})$ to be factorized:

$$\psi_{\mathbf{l}}(\mathbf{s})=\varphi_{l_-}(s_-)\varphi_{l_+}(s_+), \tag{39}$$

the $\pm$dimer wave function $\varphi_{l_\pm}(s_\pm)$ satisfying the Schrödinger equation

$$t(\varphi_{l_\pm}(s_\pm+1)+\varphi_{l_\pm}(s_\pm-1))+u^{\sigma}_{\pm}(s_\pm)\varphi_{l_\pm}(s_\pm)=E_{\pm}(l_\pm)\varphi_{l_\pm}(s_\pm). \tag{40}$$

The eigenenergy $E_p(\mathbf{l})$ of the Hamiltonian (36) is related to the eigenvalues $E_\pm(l_\pm)$ by the formula

$$E_p(\mathbf{l})=E_-(l_-)+E_+(l_+)+\Delta\mu/Q>0. \tag{41}$$

If $\gamma\gg 1$ $(r=1)$, we have $E_-(l_-)+E_+(l_+)\approx\Delta_{\bar{\nu},\bar{\nu}-1}(l_-,l_+)$ or $\Delta_{\bar{\nu},\bar{\nu}+1}(l_+,l_-)$, depending on whether $l_-<l_+$ or $l_->l_+$. For $\gamma\lesssim 1$ $[r=(t/u_c)^2]$ the sum $E_-(l_-)+E_+(l_+)$ represents the behavior of $\Delta_{\bar{\nu},\bar{\nu}\mp 1}(l_\mp,l_\pm)$ in outline. Therefore, $E_p(\mathbf{l})$ as a function of l_p undergoes, together with $\Delta_{\nu,\nu\pm1}$, random alternating-sign fluctuations whose amplitude grows as $\lambda^2 u_c l_p^{1/2}$ with increasing l_p. The minimal energy $\bar{E}_p$ of the energy spectrum of the pair is generally $\sim u_c$, the pair's length in the state $|\Phi_{\mathbf{l}}\rangle$ with $E_p(\mathbf{l})=\bar{E}_p$ being $\sim L_g$.

5.2. Transition frequencies

At $T=0$ the annihilation of the pair is by phonon emission. First one should consider the frequency $\nu(\mathbf{l})$ of the direct quantum transition $|\Phi_{\mathbf{l}}\rangle\to|\Phi_g\rangle$ for an arbitrary $|\Phi_{\mathbf{l}}\rangle$. According to Fermi's golden rule, we have

$$\nu(\mathbf{l})\propto\overline{|A(\mathbf{l})|^2}, \tag{42}$$

where

$$A(\mathbf{l})=\langle\Phi_{\mathbf{l}}|H_{e-\mathrm{ph}}|\Phi_g\rangle \tag{43}$$

is the amplitude of the transition $|\Phi_{\mathbf{l}}\rangle\to|\Phi_g\rangle$, $H_{e-\mathrm{ph}}$ is the Hamiltonian of the electron-phonon interaction, and the line over $|A|^2$ symbolizes averaging over all finite phonon states with energy $E_p(\mathbf{l})$.

Since the electron-phonon interaction is of a local character, only $\psi_{\mathbf{l}}(\mathbf{s})$ with $|s_--s_+|\sim 1$ or $s_-=s_+$ contribute to expression (43). To estimate $\nu(\mathbf{l})$ it is sufficient to consider $\psi_{\mathbf{l}}(s,s)$, using the factorized expression (39). Since the typical l_p is L_g, it is necessary to clarify the asymptotic behavior of $\varphi_{l_\pm}$ for $|l_\pm-s_\pm|\sim L_g$. In so doing one should take into consideration that the difference $u^{\sigma}_{\pm}(s_\pm)-u^{\sigma}_{\pm}(l_\pm)$, being a random sum of $|l_\pm-s_\pm|$ terms, undergoes fluctuations with the typical amplitude $\Delta u\sim\lambda^2 u_c|l_\pm-s_\pm|^{1/2}$. It is these effective-potential fluctuations rather than the dimer Anderson localization that govern the decreasing of $\varphi_{l_\pm}(s)$ when Δu exceeds $\Delta^*_\lambda\sim\lambda u_c+t$. The latter is the typical spread of eigenenergies of a reduced Schrödinger equation which would come from Eq. (40) with the randomly oscillating bounded function $\tilde{\epsilon}_{\pm}(s_\pm)$ [see Eqs. (10) and (37)] in place of $u^{\sigma}_{\pm}(s_\pm)$. This takes place for $|l_\pm-s_\pm|\gtrsim s^*_\lambda=(\Delta^*_\lambda/\lambda^2 u_c)^2$ $(s^*_\lambda\ll L_g)$. In such a case $\varphi_{l_\pm}(s)$ is nonzero owing to dimer tunneling through the fluctuation barrier. On the basis of the Schrödinger equation (40), we find that in the above forbidden region

$$\varphi_{l_\pm}(s)=B\left(\frac{t}{|l_\pm-s_\pm|^{1/2}}\right)^{b|l_\pm-s_\pm|}, \tag{44}$$

where the factor

$$B=\exp\left(-b_1\frac{s^*_\lambda}{r}\ln\frac{\Delta^*_\lambda}{t}\right),$$

results from the fall-off of the dimer wave function (over a distance $\sim s^*_\lambda$) due to the Anderson localization; b, b_1 are some constants ~ 1. Here we omit a pre-exponential factor ~ 1. Substitution of expression (40) in Eqs. (39) and (42) gives

$$\nu(\mathbf{l})=\nu_0 l_p B^4\exp(-\theta l_p),\quad \theta=4b\ln\frac{\lambda^2 l_p^{1/2}}{t}. \tag{45}$$

The pre-exponential factor $\nu_0\lesssim\omega_D$ is expressed in terms of electron-phonon interaction characteristics; ω_D is the Debye frequency. The expression holds for $l_p\gtrsim s^*_\lambda$. The exponential decline of $\nu(\mathbf{l})$ with increasing l_p is in essence of a many-electron origin. It becomes clear if one recalls that in the state $|\Phi_{\mathbf{l}}\rangle$ there are $\sim l_p\gg 1$ electrons shifted about their groundstate positions. The annihilation of a pair's dimers occurs if all electrons shifted revert to the ground-state sites *simultaneously*. Naturally, this results in small $\nu(\mathbf{l})$ values.

The foregoing argument can be easily extended to find the frequencies $\nu(\mathbf{l},\mathbf{l}')$ of quantum transitions $|\Phi_{\mathbf{l}}\rangle\to|\Phi_{\mathbf{l}'}\rangle$, which occur with emission of phonons with energies $E_p(\mathbf{l})-E_p(\mathbf{l}')$. The expression for $\nu(\mathbf{l},\mathbf{l}')$ is of the form

$$\nu(\mathbf{l},\mathbf{l}')=\nu_0 d_\pm B^4\exp(-\theta_\pm d_\pm),\quad \theta_\pm=4b\ln\frac{\lambda^2 d_\pm^{1/2}}{t}, \tag{46}$$

where $d_\pm=|l_\pm-l'_\pm|$. It is implied that only one difference, d_- or d_+, is nonzero. Otherwise, the transition frequencies are exponentially small as compared with those given by Eq. (46).

5.3. Relaxation of a separate pair of "odd" dimers

To find the time τ_p of the annihilation of a pair, one should keep track of how a pair's density matrix $\hat{\rho}=\rho(\mathbf{l},\tau)\delta_{\mathbf{l},\mathbf{l}'}$ varies with time τ. The quantities $\rho(\mathbf{l},\tau)$ that are the probabilities of finding the pair in the states $|\Phi_{\mathbf{l}}\rangle$ at an instant of time τ satisfy a Pauli-like kinetic equation

$$\frac{\partial\rho(\mathbf{l},\tau)}{\partial\tau}=\sum_{\mathbf{l}'}{}^{>}\nu(\mathbf{l},\mathbf{l}')\rho(\mathbf{l}')-(\nu^{<}(\mathbf{l})+\nu(\mathbf{l})\rho(\mathbf{l},\tau), \quad (47)$$

where

$$\nu^{<}(\mathbf{l})=\sum_{\mathbf{l}'}{}^{<}\nu(\mathbf{l},\mathbf{l}'). \quad (48)$$

Here the symbols $>$ and $<$ mean that the summation extends only to $\mathbf{l}'$ for which $E_p(\mathbf{l}')-E_p(\mathbf{l})>0$ and <0, respectively. If $l_p, d_\pm \sim r$, the transition frequencies $\nu(\mathbf{l}), \nu(\mathbf{l},\mathbf{l}') \sim \nu_0$; for $l_p, d_\pm \gg r$ they are determined by Eqs. (45) and (46).

The annihilation of a pair is governed by two equations. One is for the probability of existence of the pair at an instant τ,

$$P(\tau)=\sum_{\mathbf{l}}\rho(\mathbf{l},\tau)$$

(the summation is over all $\mathbf{l}$). The other is for the energy-average value

$$\eta(\tau)=\sum_{\mathbf{l}}\tilde{E}_p(\mathbf{l})\rho(\mathbf{l},\tau),$$

where $\tilde{E}_p(\mathbf{l})$ is the eigenenergy measured from the minimal energy $\bar{E}_p$. Both equations follow immediately from Eq. (47):

$$dP/d\tau=-\sum_{\mathbf{l}}\nu(\mathbf{l})\rho(\mathbf{l},\tau); \quad (49)$$

$$\frac{d\eta(\tau)}{d\tau}=-\sum_{\mathbf{l},\mathbf{l}'}{}^{<}(E_p(\mathbf{l})-E_p(\mathbf{l}'))\nu(\mathbf{l},\mathbf{l}')\rho(\mathbf{l},\tau)$$

$$-\sum_{\mathbf{l}}\nu(\mathbf{l})\tilde{E}_p(\mathbf{l})\rho(\mathbf{l},\tau)<0. \quad (50)$$

These equations show that the zero-temperature lifetime τ_p of a pair is conditioned on which of two processes is the faster: the fall in $\eta(\tau)$ caused by $|\Phi_\mathbf{l}\rangle\to|\Phi_{\mathbf{l}'}\rangle$ transitions, or the decreasing of $\eta(\tau)$ together with $P(\tau)$ as a result of direct transitions $|\Phi_\mathbf{l}\rangle\to|\Phi_g\rangle$. In the first case the annihilation occurs in two stages: in the first stage $P(\tau)$ remains close to unity, while $\eta(\tau)$ approaches a vicinity of zero; in the next stage $P(\tau)$ vanishes, $\rho(\mathbf{l},\tau)$ being nonzero only at such $\mathbf{l}$ for which $\tilde{E}_p(\mathbf{l})\approx 0$. For this scenario τ_p does not depend on the initial state $\rho(\mathbf{l},0)=\delta_{\mathbf{l}_0\mathbf{l}}$. In the second case a pronounced dependence of τ_p on the initial $\mathbf{l}=\mathbf{l}_0$ should be expected.

It is shown in the Appendix that

$$\tau_p=1/\min_{\mathbf{l}}(\nu^{<}(\mathbf{l})+\nu(\mathbf{l})) \quad (51)$$

(the minimum in $\mathbf{l}$ is implied), i.e., τ_p does not depend on $\mathbf{l}_0$, and hence, the first of the above-mentioned scenarios takes place. In such a case the $\tilde{E}_p(\mathbf{l})$ value at the minimum point $\mathbf{l}=\mathbf{l}^{\min}$ of the function $\nu^{<}(\mathbf{l})+\nu(\mathbf{l})$ is bound to be among a few eigenenergies closest to zero. This can be justified on the following grounds. As follows from item 5.1, $\tilde{E}_p(\mathbf{l})$ as a function of $\mathbf{l}$ executes a random walk with a diffusion coefficient of the order of $\mathcal{D}$ appearing in Eq. (27). Simple estimates based on this fact show that the number $N_\mathbf{l}$ of eigenenergies between a given $\tilde{E}_p(\mathbf{l})$ and zero is $\sim\tilde{E}_p(\mathbf{l})\sqrt{L_g/\mathcal{D}}\sim\tilde{E}_p(\mathbf{l})/\lambda^4 u_c$. Since, on the one hand, the mean separation of points $\mathbf{l}'$ at which $E_p(\mathbf{l}')<E_p(\mathbf{l})$ is $\sim L_g/N_\mathbf{l}$, and, on the other hand, $\nu(\mathbf{l},\mathbf{l}')$ falls exponentially as $d_\pm$ increases, we see [in view of the definition (48)] that the smaller is $N_\mathbf{l}$ the less is $\nu^{<}(\mathbf{l})+\nu(\mathbf{l})$, i.e., at the minimum point $\mathbf{l}^{\min}$ we really have $N_{\mathbf{l}^{\min}}\sim 1$. Hence $|l_+^{\min}-l_-^{\min}|\sim L_g$. Taking into account this fact together with Eqs. (45) and (46), we thus arrive at the conclusion that

$$|\ln\nu_0\tau_p|\sim\ln(u_c/t)\lambda^{-4}. \quad (52)$$

This τ_p value is anomalously great: it is more than ω_D^{-1} by tens of orders of magnitude even if λ is not too small ($\lambda=1/3-1/4$).

At finite temperatures activation transitions caused by phonon absorbtion can provide annihilation of dimers by bringing them to distances $\sim r$, whatever the initial l_p may be. If the pair's length $l_p\gg s_\lambda^*$, drawing dimers into proximity requires them to overcome a fluctuation energy barrier $\sim\lambda^2 u_c l_p^{1/2}$. Within an exponential factor the activation transition frequency is

$$\nu_{\text{act}}=-\exp(-\lambda^2 u_c l_p^{1/2}/T). \quad (53)$$

In the temperature region $T\ll\Delta_\lambda^*$ the pre-exponential factor omitted is determined by the Mott's variable-range-hopping[18] over distances $\lesssim s_\lambda^*$. For the typical $l_p\sim L_g$ we obtain for the activation time of the dimer annihilation $\tau_{\text{act}}=1/\nu_{\text{act}}$

$$\tau_{\text{act}}\propto\exp(u_c/T).$$

The time τ_{act} becomes less than the tunnel relaxation time Eq. (52) when $\lambda<(T/u_c)^{1/4}$. At helium temperatures and in the most realistic case $u_c\sim 10^2-10^3$ K this gives $\lambda<1/5$. However, τ_{act} remains anomalously great.

5.4. Relaxation of an ensemble of odd-dimer pairs

Experimentally, it is possible to create (e.g., by optical excitation) a set of $\pm$dimer pairs whose density is $\gg n_g^{\pm}$ but $\ll n_e$. It should be elucidated how the density of pairs $n(\tau)$ or, quite the same, the concentration of alternating "odd" + and $-$dimers reduces with time τ. The decrease in $n(\tau)$ is expected to be so slow (this is verified below) that the ensemble of pairs has time to come to the partial equilibrium corresponding to the current value of $n(\tau)$. (In such a case the energy of the state at an instant τ is approximately equal to the energy Eq. (18) at $n_\pm=n(\tau)$.) This allows a "reduction of the description," so that we may restrict ourselves to consideration of the differential equation

$$dn/d\tau=-\omega(n)n, \quad (54)$$

wherein the transition frequency $\omega(n)$ comes from expression (45) (the dimer tunneling prevails) or from Eq. (53) (the activation prevails) by substitution of $L(\tau)=1/n(\tau)$ for l_p. Correspondingly, there are two different asymptotic dependences of n on τ. If the activation can be neglected, we have

$$n=\frac{b\ln\ln\nu_0\tau}{\ln\nu_0\tau}. \quad (55)$$

In the case that the activation is paramount, Eq. (54) gives

$$n=(\lambda^2 u_c/T)^2 \ln^{-2} \nu_0 \tau. \quad (56)$$

Expressions (55) and (56) have been written to the main logarithmic approximation. They hold for $L(\tau) \gg s_\lambda^*$, $L(\tau) \lesssim L_g$. The logarithmic decreasing of $n(\tau)$ with time is a salient feature of LWG.

The super-slow relaxation in LWG and its logarithmic time-dependence recall to some extent those in spin glass,[13] which features a nonergodic behavior and an infinite spectrum of relaxation times caused by a macroscopic multivalley degeneracy of the ground state. As is known, a spin-glass valley is a state whose energy is close to the ground-state one, but its space structure differs from that of the ground state macroscopically. Transition from the valley to the ground state takes place only if a macroscopically great number of spin flips occur simultaneously. In the LWG the analogs of the spin-glass valleys are the above-mentioned electron subclusters containing a great (but by no means macroscopic) numbers of electrons. This gives grounds to consider the "spin-glass" LWG features as a quasi-nonergodic behavior.

The above consideration is extended to the case of an arbitrary rational $n_e=P/Q$ with $P\neq 1$ (see Secs. 1 and 2) almost without modifications. The only difference is that in the general case the discrete solitons (GWC defects of compression and rarefaction) arising in the system with a change of the electron number are not simple $\pm$dimers but more-complicated structures.[10] However, this is immaterial since only the formation energy of the GWC defect $\pm(\mu_\pm - \mu)/Q$ $[\mu_\pm=\mu_\pm(P/Q)]$ is relevant.

The long-range order in GWC is also broken if the system is exposed to an external weak random potential. The above line of argument can be extended to this situation without change. Bearing this in mind, it is easy to find that the ground-state dimer concentration depends on the potential amplitude quadratically.

6. CONCLUSION

Our results show that the low-temperature thermodynamics and kinetics of LWG are fully described in terms of GWC point defects of a many-electron origin (discrete solitons). It is the soliton nature of these defects (for definiteness, we will consider them to be dimers) that imparts to the LWG its distinctive features differing qualitatively from those of the known Wigner glass: the spontaneous dimer formation in the ground state caused by an arbitrarily weak disorder of the host lattice, first-order phase transitions in μ at zero temperature, and the almost nonergodic macroscopic behavior. These facts raise questions inviting further investigation. Below we outline some of them.

First of all, the transport and high-frequency properties of LWG should be clarified, taking into account that each $\pm$dimer carries the fractional charge $e^*=\pm e/Q$ (e is the free electron charge). Conduction in LWG is by dimer transfer over distances $\sim L_g=1/n_\pm^g(\mu)$. This requires the dimers to overcome a fluctuation barrier of the order of the energy of dimer formation $u_\pm(\mu)$ [see Eq. (15)], so that the LWG static conductivity σ_{LWG} is expected to be proportional to

$$\exp\left(-L_g(\mu)\ln\frac{u_\pm(\mu)}{t}\right) \text{ or to } \exp\left(-\frac{u_\pm(\mu)}{T}\right),$$

depending on which of the two mechanisms prevails: dimer tunneling through the barrier or the activation transitions. Since $L_g(\mu)$ and $u_\pm$ fall when μ approaches the endpoints $\mu_\pm$ of the devil's-staircase intervals [see Eqs. (15) and (19)], σ_{LWG} is bound to show pronounced splashes in vicinities of $\mu_\pm$. These giant oscillations of σ_{LWG} as a function of μ are not only of interest by themselves, but also can be an effective experimental instrument for investigating the super-slow (logarithmic) relaxation of a strongly nonequilibrium LWG state. At a fixed μ a proper way to observe the relaxation is to keep track of photoabsorbtion of low-intensity light.[2)]

Since the fluctuation energy barriers responsible for LWG resistance cover long intervals of the order of $L_g \sim 1/\lambda^4$, a noticeable deviation from Ohm's law is expected to arise even for low strengths $\mathcal{E}$ of the applied electric field. Namely, this takes place if $e^*\mathcal{E}L_g$ becomes comparable with the typical barrier height $u_\pm$. The electric intensities that meet this condition, $\mathcal{E}\sim\lambda^4 u_\pm^3/e$, decline rapidly as λ decreases. They are especially low in vicinities of the endpoints of the devil's-staircase intervals. It is remarkable that this nonlinear effect can be pronounced even though the LWG conductance is low.

Results obtained in Sec. 3 (see also the note at the end of Sec. 5) show that the length of space correlation in LWG L_gQ is inversely proportional to the square of the typical energy of a random static perturbation, i.e., it behaves in the same way as the correlation length in continuous Wigner glass,[12] wherein the inverse quadratic dependence takes place for any dimension $d\leqslant 3$. This raises the very interesting question of whether such an accordance between discrete (lattice) electron systems and continuous ones remains for $d>1$, and moreover, whether discrete electron systems with $d>1$ are unstable with respect to an arbitrarily weak random external perturbation. Our preliminary studies leads us to the conclusion that, owing to the phenomenon of the effective lowering of dimension mentioned in Sec. 1, the 2D modification of GWC is *stable* in this sense: at a given μ a random distortion of the host lattice breaks the long-range order of this system only if the disorder parameter exceeds some critical value, which vanishes at the endpoints of the devil's-staircase intervals. This suggests that macroscopic behavior of a 2D electron lattice system on a weakly disordered host lattice has nothing in common with that of 2D Wigner glass.

We are going to carry out detailed studies of the above problems in the immediate future.

The authors are grateful to V.D. Natsik and L.A. Pastur for fruitful discussions.

APPENDIX

To find the general expression for the relaxation time τ_p of a pair of dimers, it is convenient to enumerate the eigenenergies $E(\mathbf{l})$ in increasing order: $E_i=E(\mathbf{l}_i)<E_{i+1}$, $i=1,2,\ldots$; energy E_1 is the least of $E(\mathbf{l})$. In these terms the kinetic Eq. (47) takes the form

$$d\rho(\tau)/d\tau=\hat{\nu}\rho(\tau), \quad (A1)$$

where $\boldsymbol{\rho}=(\rho_1,\rho_2,\ldots)$, $\rho_i(\tau)\equiv\rho(\mathbf{l}_i,\tau)$,

$$\hat{\nu}\rho(\tau)=\sum_{k\geqslant i}\nu_{ik}\rho_k(\tau), \quad (A2)$$

and ν_{ik} is a triangular matrix:

$$\nu_{ik}=\begin{cases} \nu(\mathbf{l}_i,\mathbf{l}_k), k>i; & \nu_{ik}=0,\ k<i; \\ -\nu(\mathbf{l}_i)-\sum_{i'=1}^{i}\nu_{i'i}, & k=i. \end{cases} \tag{A3}$$

The general solution of Eq. (A1) can be expressed in terms of eigenvectors $\mathbf{f}_j$ and $\mathbf{f}'_j$ $(j=1,2,\ldots)$ of the operator $\hat{\nu}$ and the conjugate operator $\hat{\nu}'$ $(\nu'_{ik}=\nu_{ki})$, respectively. They satisfy the equations

$$\hat{\nu}\mathbf{f}_j=\Lambda_j\mathbf{f}_j, \quad \hat{\nu}'\mathbf{f}'_j=\Lambda_j\mathbf{f}'_j, \tag{A4}$$

where

$$\Lambda_j=\nu_{jj}=-\nu(\mathbf{l}_j)-\sum_{i=1}^{j}\nu_{ij}<0 \tag{A5}$$

are the eigenvalues of the operators $\hat{\nu}$ and $\hat{\nu}'$.

Taking into account that $\langle\mathbf{f}'_j|\mathbf{f}_{j'}\rangle=\delta_{jj'}$ ($\langle\mathbf{a}|\mathbf{b}\rangle$ means the scalar product $\Sigma_i a_i b_i$ here and below), from Eqs. (A1) and (A4) we obtain

$$\rho(\tau)=\sum_j \langle\mathbf{f}'_j|\rho_0\rangle\exp(\Lambda_j\tau)\mathbf{f}_j, \tag{A6}$$

where $\boldsymbol{\rho}_0=\boldsymbol{\rho}(0)$.

Since the Λ_j are all negative, this expression tends asymptotically to

$$\rho(\tau)=\langle\mathbf{f}'_{j*}|\rho_0\rangle\exp(\Lambda_{j*}\tau)\mathbf{f}_{j*} \tag{A7}$$

as $\tau\to\infty$. Here j^* is the number of the eigenvalue with the least modulus. [As follows from the reasoning after formula (51), $j^*\sim 1$. Hence, $\tau_p=1/|\Lambda_{j*}|$. This coincides with expression (51)].

As to the prefactor $\langle\mathbf{f}'_{j*}|\boldsymbol{\rho}_0\rangle$, it is easy to show (in view of the triangular form of the matrix ν_{ik}) that it is ~ 1 for all $\boldsymbol{\rho}_0$ of the form $\rho_{0i}=\delta_{ii_0}$, except $i_0<j^*$. In the latter (very special) case the relaxation time is less than $1/|\Lambda_{j*}|$, but its logarithm is of the same order of magnitude.

*E-mail: slutskin@theor.kharkov.ua
†E-mail: kovtun@theor.kharkov.ua

[1)] A pair of separated "odd" dimers can also be thought of as an excitation arising as some subcluster of a regular cluster is shifted as a whole by one site. As will be clear from the following, the lifetime of an excitation produced by a shift of the subcluster by more than one site exceeds the lifetime of a pair of dimers.

[2)] Matrix elements of photoinduced one-step dimer transitions are not small.

[1] B. I. Shklovskii and A. L. Efros, *Electronic Properties of Doped Semiconductors*, Springer, Berlin (1984).
[2] M. S. Bello, E. I. Levin, B. I. Shklovskii, and A. L. Efros, Zh. Éksp. Teor. Fiz. JETP **80**, 1596 (1981) [JETP **53**, 822 (1981)].
[3] J. Hubbard, Phys. Rev. B **17**, 494 (1978).
[4] C. J. Adkins, A. I. Yakimov, A. V. Dvurechenskii, V. V. Kirienko, Yu. I. Yakovlev, and A. I. Nikiforov, Phys. Rev. B **61**, 10868 (2000).
[5] E. Y. Andrei (ed.), *2D Electron Systems on Helium and Other Substrates*, Kluwer, New York (1997), and references therein.
[6] H. Nejoh and M. Aono, Appl. Phys. Lett. **64**, 2803 (1994); R. G. Osifchin, W. J. Mahoney, J. D. Bielefeld, R. P. Andres, J. I. Henderson, and C. P. Kubiak, Superlattices Microstruct. **18**, 283 (1995).
[7] P. Bak and R. Bruinsma, Phys. Rev. Lett. **49**, 249 (1982).
[8] Ya. G. Sinai and S. E. Burkov, Usp. Mat. Nauk **38**, 205 (1983).
[9] V. V. Slavin and A. A. Slutskin, Phys. Rev. B **54**, 8095 (1996).
[10] A. A. Slutskin, V. V. Slavin, and H. A. Kovtun, Phys. Rev. B **61**, 14184 (2000).
[11] A. I. Larkin, Sov. Phys. JETP **31**, 784 (1970).
[12] Y. Imri and S.-K. Ma, Phys. Rev. Lett. **35**, 1399 (1975).
[13] M. Mezard, G. Parisi, and M. Verasoro, *Spin Glass Theory and Beyond*, World Scientific, Singapore-New Jersey-Hong Kong (1987).
[14] S. L. Ginzburg, *Irreversible Phenomema of Spin Glasses*, Nauka, Main Editorial Board for Phys. and Math. Literature, Moscow (1989).
[15] W. Feller, *An Introduction to Probability Theory and its Applications*, Volume I, Wiley, New York; Chapman and Hall, London (1958).
[16] S. Molchanov, Comm. Math. Phys. **78**, 429 (1981).
[17] K. Efetov, *Supersymmetry in Disorder and Chaos*, Cambridge University Press (1999).
[18] N. F. Mott and E. A. Davis, *Electron Processes in Non-Crystalline Materials*, Clarendon Press, Oxford (1979).
[19] M. Pepper, J. Phys. C **12**, L617 (1979).

LATTICE DYNAMICS

Incommensurate structures on the surface of an elastic half space

A. S. Kovalev* and E. S. Sokolova

B. Verkin Institute for Low Temperature Physics and Engineering, National Academy of Sciences of Ukraine, pr. Lenina 47, Kharkov 61103, Ukraine

(Submitted February 12, 2005)
Fiz. Nizk. Temp. **31**, 796–806 (July 2005)

A static incommensurate structure on the surface of an elastic half space covered by a monolayer of another substance with different stiffness and a different equilibrium interatomic spacing is considered, and a system of one-dimensional nonlinear integro-differential equations describing such a structure is derived. In the case of an absolutely rigid monolayer (the opposite case from that usually considered in the Frenkel–Kontorova model: the limit of a soft monolayer on an absolutely rigid substrate) some new classes of periodic solutions of the Peierls equation for incommensurate surface structures are found which differ substantially from those known previously. An approximate description of the structure of nonuniform surface states is obtained for a stiff monolayer with a low compliance on a soft half space and for a soft monolayer on a stiff half space with a low compliance, i.e., the approximate dependence of the period of these structures on the incommensurability parameter (the difference of the lattice periods of the half space and monolayer) and their stiffnesses is found. The results obtained permit a qualitative description of the transformation of incommensurate surface structures in the whole range of the aforementioned parameters. © *2005 American Institute of Physics.*
[DOI: 10.1063/1.2001642]

There has been a shift of focus in the physics of nonlinear phenomena to the topic of nonlinear excitations (and, in particular, solitons) in real physical systems with (for example) the finite size of the sample and the low dimensionality and discreteness of the system taken into account. Taking these circumstances and also nonlinear effects into account is essential for studying the surface of a crystal covered with a thin film of another substance. The presence of the surface and film leads to the existence of a great diversity of surface waves, which, when nonlinearity is taken into account, are ''upgraded'' into nonlinear shear and Rayleigh waves and also into the corresponding localized surface waves—dynamical solitons.[1,2] On the other hand, the nonlinearity of the interaction of a film coating with the substrate (half space) leads to the possibility of existence of localized excitations of another type—topological solitons or ''surface dislocations.'' If the equilibrium interatomic distances between atoms of the substrate and atoms of the film (adatom layer) are different, then the existence of a periodic structure of surface dislocations, corresponding to the minimum energy of the system, is possible. Since the period of such a structure is, generally speaking, incommensurate with the substrate period, these structures are called *incommensurate surface structures*.[3] A well-known example of an incommensurate surface structure is the structure of Ga atoms on the surface of silicon.[4] Moreover, an incommensurate surface structure can form on both an ideal (without the film coating) surface of a crystal, e.g., gold, when the charge state of the surface atoms differs from that for atoms in the bulk.[5] Usually incommensurate surface structures are investigated theoretically in the simplest case of an absolutely rigid substrate, where it is described in the framework of the Frenkel-Kontorova (FK) model, i.e., the sine-Gordon equation,[6] and the corresponding analytical solution for it is well known.[7] Taking the compliance of the elastic half space into account leads to a substantial complication of the problem, and it is therefore usually treated in the limit when the stiffness of the substrate is much greater than that of the film or of the surface layer of atoms.[8–11] Obviously this is not always valid. Therefore, in the present paper the problem is formulated in the general case of an arbitrary relationship between the stiffnesses of the elastic half space and the monolayer film on its surface, and it is solved exactly in the limit opposite to that considered previously, i.e., when the stiffness of the monolayer film is much greater than that of the substrate half space.

1. STATEMENT OF THE MODEL

Because of the complexity of the problem, we start by restricting discussion to the simplest ''scalar model,'' in which the displacement of atoms of both the substrate and the adatom layer is allowed in only one direction in the plane of the surface (for definiteness, in the direction of the X axis), along which the incommensurate structure will arise. The Z axis is chosen in the direction perpendicular to the surface, and the elastic half space corresponds to the region $z>0$ (see Fig. 1).

Furthermore, as usual,[8–11] both the interaction of the surface atoms with each other and the interaction of the atoms of the half space are taken into account in the harmonic

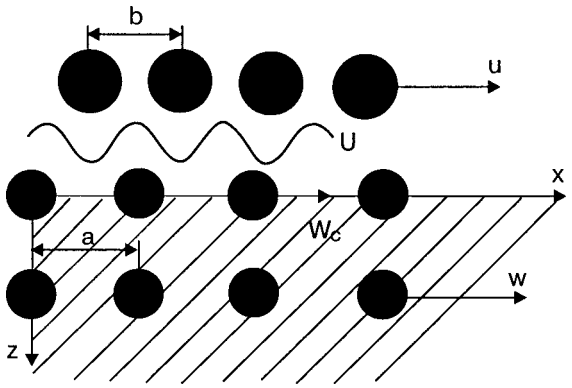

FIG. 1. Geometry of the problem.

approximation, while the interaction between atoms of the monolayer and substrate is assumed to be substantially nonlinear. The key point is that the equilibrium interatomic distance a in the material of the half space in the absence of the film is assumed to be unequal to the equilibrium distance b in the monolayer without the substrate. We introduce the coordinates of the atoms of the half space X_{nm} and atoms of the monolayer $\tilde{X}_s$ in such a way that in the ground state in the absence of interaction between the monolayer and substrate $X_{nm}^{(0)}=(an,am)$ and $\tilde{X}_s^{(0)}=bs$, respectively. (The indices n and m enumerate the atoms along the X and Z axes).

In this case the energy of the deformed monolayer and deformed half space have the form

$$E_s=\sum_s \frac{\alpha}{2}(\tilde{X}_s-\tilde{X}_{s-1}-b)^2, \tag{1}$$

$$E_b=\sum_{nm} \frac{\beta}{2}[(X_{nm}-X_{n-1,m}-a)^2+(X_{nm}-X_{n,m-1})^2], \tag{2}$$

where α and β are the corresponding elastic constants (the elastic half space is assumed isotropic). It is more complicated to write the interaction energy of a deformed monolayer with a deformed substrate (see, e.g., Ref. 12). In the case of an absolutely rigid monolayer it is easy to show that under reasonable assumptions about the character of the pair interaction of a surface atom of the substrate with all of the atoms of the monolayer, this energy in the leading approximation will have the form

$$E_{\text{int}}=U\left[1-\cos\frac{2\pi}{b}(X_{n0}-\tilde{X}_0^{(0)})\right]. \tag{3}$$

In the case of a compressible monolayer expression (3) is "upgraded" to take into account the local deformation of the monolayer at the point at which the surface atom of the elastic half space is located—the period b is renormalized (in the limit of an absolutely rigid half space it is replaced by a).

Below we shall use the long-wavelength approximation, assuming the coupling of the monolayer with the half space is weak: $U\ll\alpha b^2,\beta a^2$. It is convenient to chose a coordinate system tied to the undeformed lattice of the half space: $an\to x$, $am\to z$, and to introduce the displacements in this coordinate system. Here $X_{nm}=(an+w_{nm},am)\to(an+w(x,z),am)$ and $\tilde{X}_s=as+u_s\to bs+u(x)+x(a-b)/a$. The parameter $\xi=(a-b)/a$ that arises here, characterizing the difference of the interatomic spacings in the monolayer and substrate, will be called the incommensurability parameter (IP).

In the long-wavelength approximation expression (2) for the elastic energy of the half space is transformed in a natural way:

$$E_b=\frac{1}{a^2}\int_{-\infty}^{+\infty}dx\int_0^{+\infty}dz\,\frac{\beta a^2}{2}[\nabla w(x,z)]^2. \tag{4}$$

The expression (1) for the elastic energy of the monolayer in the long-wavelength approximation is transformed in the chosen coordinate system as

$$E_s=\frac{1}{a}\int_{-\infty}^{+\infty}dx\,\frac{\alpha a^2}{2}(u_x^2+2u_x\xi). \tag{5}$$

In this expression a subscript denotes spatial differentiation with respect to the coordinate x. Finally, expression (3) is transformed as

$$E_{\text{int}}=\frac{1}{a}\int_{-\infty}^{+\infty}dx\,U\left\{1-\cos\frac{2\pi}{b}(w_0-u)\right\}, \tag{6}$$

where w_0 represents the displacements of the surface atoms of the half space (as we have said, in the case of a rigid substrate the substrate period a must be taken as the period). In expression (6) only the mean displacement of the monolayer relative to the half space is taken into account. Taking the deformation of the monolayer into account leads to a replacement of the lattice constant b of the monolayer by the quantity $b(1+u_x(x))$. However, assuming all the deformations are small, we shall henceforth neglect these small corrections. If we introduce the displacements of the atoms of the monolayer from the equilibrium positions in the absence of interaction with the substrate $v(x)=u(x)+\xi x$ ($\tilde{X}_s=as+u_s=bs+v_s=bs+as(a-b)/a+u_s$), then we can write the elastic energy of the system in the following form:

$$E=\frac{1}{a}\int_{-\infty}^{+\infty}dx\left\{\frac{\alpha a^2}{2}v_x^2+U\left[1-\cos\frac{2\pi}{b}(w_0-v+\xi x)\right]+\frac{1}{a}\int_0^{+\infty}dz\,\frac{\beta a^2}{2}(\nabla w)^2\right\}. \tag{7}$$

(A comparison of these formulas with the corresponding formulas in Refs. 4 and 11 shows that in the latter the expression written for the energy was not completely correct).

The total energy includes an additional kinetic energy, but below we shall consider only static configurations.

2. EQUATIONS DESCRIBING STATIC INCOMMENSURATE STRUCTURES

Expression (7) for the total energy also implies equations for the deformations in the monolayer and half space:

$$\sin\frac{2\pi}{b}(w_0-v+\xi x)=-\frac{\alpha a^2 b}{2\pi U}v_{xx}, \tag{8}$$

$$\Delta_2 w=0. \tag{9}$$

The latter equation should be supplemented the boundary condition

$$w_z|_{z=0} = -\frac{2\pi U}{\beta b a}\sin(w_0 - v + \xi x). \tag{10}$$

Laplace's Eq. (9) is easily solved in a half space with a plane boundary,[13] and the relation between the different components of the deformations at the boundary

$$w_z|_{z=0} = H w_x|_{z=0}, \tag{11}$$

where the Hilbert transform H is defined as

$$Hf(x) = \frac{1}{\pi}\int_{-\infty}^{+\infty}\frac{dp}{p-x}f(p).$$

Thus the final closed system of two-dimensional equations is

$$\sin\frac{2\pi}{b}(w_0 - v + \xi x) = -\frac{\alpha a^2 b}{2\pi U}v_{xx}, \tag{12}$$

$$\sin\frac{2\pi}{b}(w_0 - v + \xi x) = -\frac{\beta b a}{2\pi U}H w_{0x}. \tag{13}$$

We recall that in the case of a rigid substrate b is replaced by a in the last two formulas. System (12), (13) is a system of nonlinear (but one-dimensional!) integro-differential equations, and its solution is a complicated mathematical problem. Therefore we should focus on illustrative cases in which it is possible to obtain asymptotic expressions for the solutions of the system (12), (13) that correspond to incommensurate structures.

3. SOFT MONOLAYER ON THE SURFACE OF A RIGID HALF SPACE

Let us start by discussing the case of a soft monolayer on the surface of a rigid half space, which in the limit of an absolutely rigid substrate goes over to the FK model. It is convenient to introduce the relative displacements of the atoms of the monolayer and substrate

$$\psi = \frac{2\pi}{a}(w_0 - v + \xi x) = \frac{2\pi}{a}(w_0 - u) \tag{14}$$

and to rewrite system (12), (13) in the form

$$\sin\psi = \frac{\alpha}{U}\left(\frac{a^2}{2\pi}\right)^2\frac{1}{a}u_{xx}, \tag{15}$$

$$\psi_x = \frac{2\pi}{a}\left(a\frac{\alpha}{\beta}Hu_{xx} - u_x\right), \tag{16}$$

$$w_{0_x} = a\frac{\alpha}{\beta}Hu_{xx}. \tag{17}$$

In the case of a rigid half space the displacements of the surface atoms of the half space are substantially smaller than the displacements of the atoms of the monolayer in the incommensurate structure, i.e., $w_0 \ll u \approx -a\psi/2\pi$. Here Eq. (15) reduces to the following:

$$\sin\psi = \frac{\alpha}{U}\left(\frac{a^2}{2\pi}\right)^2\psi_{xx} + \frac{\alpha^2}{U\beta}a\left(\frac{a^2}{2\pi}\right)^2 H\psi_{xxx}. \tag{18}$$

Since in the incommensurate structure $\sin\psi \sim \psi \sim 1$, it follows from (18) that

$$a\frac{\partial}{\partial x} \sim \frac{2\pi}{a}\sqrt{\frac{U}{\alpha}} \ll 1.$$

(The last strong inequality is necessary to permit making the long-wavelength approximation, within which all of our discussion above is valid.) Then it follows from relation (17) that $w_0 \sim a\alpha u_x/\beta$ (it must be taken into account that the Hilbert transformation does not lead to a change of the spatial scale). Consequently, the condition $w_0 \ll -a\psi/2\pi$ reduces to the following inequality:

$$\frac{\sqrt{U\alpha}}{\beta}\frac{2\pi}{a} = \varepsilon \ll 1. \tag{19}$$

In the limit considered, ε plays the role of a small parameter serving as a measure of the degree to which the case of a compliant but stiff substrate differs from the case of an absolutely rigid half space.

1. In the case of an absolutely rigid substrate ($\beta = \infty$ or $\varepsilon = 0$) the problem of the incommensurate structure reduces to the FK model. If we introduce the dimensionless coordinate

$$\kappa = x\sqrt{\frac{U}{\alpha}}\left(\frac{2\pi}{a^2}\right), \tag{20}$$

then Eq. (18) reduces to the static reduction of the sine-Gordon equation:

$$\sin\psi = \psi_{\kappa\kappa}. \tag{21}$$

The solution of Eq. (21) for an incommensurate structure is well known (see Ref. 7):

$$\psi_0 = \pi + 2\,\mathrm{am}\left(\frac{\kappa}{k}, k\right), \tag{22}$$

where $\mathrm{am}(z,k)$ is a Jacobi elliptic function and k is the modulus of the elliptic function. Solution (22) describes a periodic chain of "2π-kinks" (surface dislocations) with a distance between them of $L_0 = 2kK(k)\sqrt{\alpha/U}(a^2/2\pi)$, where $K(k)$ is the complete elliptic integral of the first kind, and its modulus k depends on the incommensurability parameter ξ. Such a solution corresponds to a nonzero mean deformation in the monolayer at a finite (for one period of the incommensurate structure) energy of the system. Then the relative displacements ψ correspond to the displacements in the monolayer, and the total energy of the system consists only of the energy of the monolayer and the energy of its coupling with the substrate. This energy becomes smaller than the energy of the undeformed monolayer (with $\psi = 0$), $E_* = (\alpha/2)a\xi_*^2 L_0$, which is the energy with respect to which the energy of the deformed adatom layer is usually measured [in our notation $\xi = \xi_* = (4/\pi a)\sqrt{U/\alpha}$; see Ref. 14]. At the critical point the period of the incommensurate structure $L_0 = \infty$.

2. In the case of a compliant but stiff substrate the situation changes: the equation and solution must be written to higher accuracy. We shall take into account the main corrections of order ε to the equations and solutions. On the right-hand side of Eq. (18) it is necessary to take the small second term into account and, in terms of the dimensionless coordinate κ it takes the form $\psi_{\kappa\kappa} + \varepsilon H\psi_{\kappa\kappa\kappa}$.

The solution of Eq. (18) must also be written to higher accuracy; it can be represented in the form

$$\psi = \psi_0 - \varepsilon H \psi_{0_\kappa}. \tag{23}$$

For finding the total energy of the incommensurate structure using expression (23) for ψ, one must calculate the displacements u in the monolayer and w in the substrate. In the limit under consideration $w_0 \ll u$ for the displacements of the atoms of the monolayer we have $u \approx -b\psi_0/2\pi$ (or $v \approx \xi x - b\psi_0/2\pi$). As one can show, the corrections to the displacements of the atoms of the monolayer are small, of order ε^2. It is more complicated to find the displacements in the compliant substrate. From Eq. (17), which can be rewritten approximately (to order ε^2) in the form $w_{0_\kappa} = \varepsilon H u_{\kappa\kappa} = -\varepsilon a \psi_{0_{\kappa\kappa}}/2\pi$, it follows that

$$w_0 = -\varepsilon \frac{a}{2\pi} H \psi_{0_\kappa} + C\kappa, \tag{24}$$

where C is a constant of integration, which, as follows from the condition that the energy of the half space be finite over the length of the period of the incommensurate structure L_0, is equal to zero. Unfortunately, an expression for w_0 in explicit form cannot be found, but one can represent it in the form of the following series:

$$w_0 = -\varepsilon \frac{2a}{kK(k)} \sum_{s=1}^{\infty} \frac{q^s}{1+q^{2s}} \sin\left(\frac{\pi\kappa}{kK(k)} s\right) = \sum_{s=1}^{\infty} C_s(k) \sin\left(\frac{2\pi s}{L_0} x\right), \tag{25}$$

where $q = \exp(-\pi K'(k)/K(k))$ is the Jacobi parameter, and $K'(k) = K(\sqrt{1-k^2})$.

The solution for the displacements in the whole volume of the substrate half space in this case has the form

$$w(x,z) = \sum_{s=1}^{\infty} C_s(k) \exp\left(-\frac{2\pi s}{L_0} z\right) \sin\left(\frac{2\pi s}{L_0} s\right). \tag{26}$$

Substituting expression (26) into formula (4) for the energy of the half space, we obtain the energy of the half space per period of the incommensurate structure:

$$E_b^{(L_0)} = \frac{\pi\beta}{2} \sum_{s=1}^{\infty} s C_s^2(k),$$

or

$$E_b^{(L_0)} = \varepsilon^2 \beta \frac{\pi a^2}{2k^2K^2(k)} \sum_{s=1}^{\infty} \frac{s}{\cosh^2 \mu(k) s}, \quad \mu(k) = \pi \frac{K'(k)}{K(k)}. \tag{27}$$

As will be shown below, in the limit of high stiffness of the substrate ($\beta \gg \alpha$), near the critical value of the IP the period of the structure takes large values ($L_0 \gg a$) and the modulus k is close to 1. Then, as is seen from Eq. (27), $\mu(k) \ll 1$, and the sum over s in formula (27) can be replaced by an integral. As a result, we obtain the following dependence of the energy of the half space (per period of the incommensurate structure) on the modulus of the elliptic function and, hence, on the period of the structure:

$$E_b^{(L_0)} = \varepsilon^2 \beta \frac{\pi a^2}{2k^2K^2(k)} \int_1^{\infty} \frac{s\,ds}{\cosh^2 \mu(k) s} = \varepsilon^2 \beta \frac{\pi a^2}{2k^2K^2(k)} \times \frac{1}{\mu^2(k)} [\ln 2 - \mu(k) \tanh \mu(k) + \ln \cosh \mu(k)]. \tag{28}$$

The energy of the deformed monolayer and of its interaction with the substrate is easily found: using expression (23) for ψ and the coupling $u \approx -b\psi/2\pi$, we obtain the relation $\cos\psi = \cos\psi_0 + \varepsilon \sin\psi_0 H\psi_{0_\kappa}$, and, after substituting the corresponding expressions into formulas (5) and (6), we find

$$E_{\text{int}}^{(L_0)} = \varepsilon\beta a^2 \frac{1}{\pi^2} (E(k)k - \pi(1+k^2)K^2(k)) - \varepsilon^2 \beta a^2 4\pi \frac{1}{k^2K^2(k)} \sum_{s=1}^{\infty} \frac{q^{2s}}{(1+q^{2s})^2}, \tag{29}$$

$$E_s^{(L_0)} = \varepsilon\beta a^2 \frac{1}{\pi^2} \frac{E(k)}{k} - \alpha a^2 \xi + \frac{\alpha}{2} a \xi^2 L_0. \tag{30}$$

In formula (30) we have omitted small terms of order $\varepsilon^2 \alpha a^2$, which for a high substrate stiffness ($\beta \gg \alpha$) are substantially smaller than the small corrections ($\sim \varepsilon^2 \beta a^2$) in formulas (28) and (29). As was pointed out above, for a high substrate stiffness the sum over s in formula (29) can be replaced by an integral, and as a result one can obtain the following dependence of the energy $E_{\text{in}}^{(L_0)}$ on the modulus of the elliptic function:

$$E_{\text{int}}^{(L_0)} = \varepsilon\beta a^2 \frac{1}{\pi^2} [E(k)k - \pi(1+k^2)K^2(k)] - \varepsilon^2 \beta \frac{4\pi a^2}{k^2K^2(k)} \int_1^{\infty} \frac{q^{2s}}{(1+q^{2s})^2} ds = \varepsilon\beta a^2 \frac{1}{\pi^2} [E(k)k - \pi(1+k^2)K^2(k)] - \varepsilon^2 \beta a^2 \frac{1-\tanh\mu}{k^2K(k)K'(k)}. \tag{31}$$

The final expression for the total energy density in the incommensurate state can be rewritten in the form

$$E_{\text{tot}}^{(L_0)} \frac{a}{L_0} = U\left\{\left[2\left(\frac{2E(k)}{k^2K(k)} - \frac{1-k^2}{k}\right) - \sqrt{\frac{\alpha}{U}}\pi \frac{(a-b)}{kK(k)}\right] - \varepsilon\left[2\pi^2 \frac{1-\tanh\mu}{k^3K^2(k)K'(k)} - \pi \frac{(\ln 2 - \mu\tanh\mu + \ln\cosh\mu)}{k^3K(k)K'^2(k)}\right]\right\} + \frac{\alpha}{2} a^2 \xi^2. \tag{32}$$

The term in the first square brackets and the last term of this expression coincide with the known result for the energy of an incommensurate structure in the FK model (absolutely rigid substrate). The term in the second set of square brackets

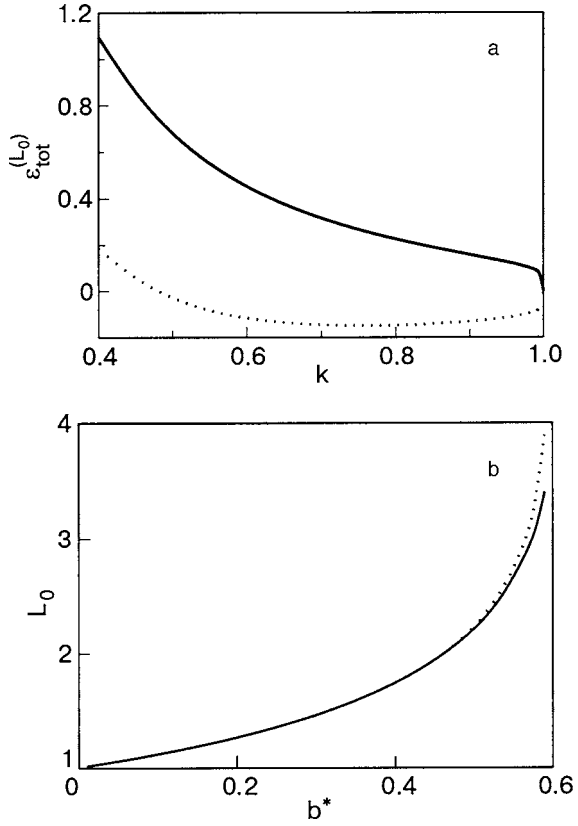

FIG. 2. Dependence of the energy density in the incommensurate structure, $\varepsilon_{\rm tot}^{(L_0)}=E_{\rm tot}^{(L_0)}/L_0$ on the modulus of the elliptic amplitude for the case $\alpha=1$, $\beta=50$, $U=0.1$, $a=1$. The energy density is measured from the energy density of the undeformed monolayer, E_*/L_0; $b=0.3<b_*$ (dotted curve), $b=0.9>b_*$ (solid curve) (a). Dependence of the period of the incommensurate structure on the incommensurability parameter for an absolutely rigid and a compliant substrate; $\beta=50$ (dotted curve), $\beta=\infty$ (solid curve) (b).

$(\sim\varepsilon)$ is due to the compliance of the substrate. It is seen that in the limit $\beta\to\infty$ (absolutely rigid substrate) the result goes over to the expression known previously.[14]

However, for any finite value of β in a narrow region of values of the icommensurability parameter near its critical value the correction to the energy due to the compliance of the substrate is no longer small, and the treatment of the problem in the framework of perturbation theory loses meaning. Thus we are unable to find the renormalized critical value of the IP. Outside that narrow region of the parameter ξ, however, the corrections to the energy are small, and one can find the modification of the incommensurate structure due to the compliance of the half space.

The dependence of the total energy density $\varepsilon_{\rm tot}^{(L_0)}$ on the parameter k at values of the IP greater than or smaller than the critical value is shown in Fig. 2a by the lower and upper curves, respectively. The minimum of the lower curve corresponds to the value of k_* that determines the period of the incommensurate structure, $L_0=2k_*K(k_*)\sqrt{\alpha/U}(a^2/2\pi)$. When the IP approaches the critical value this minimum is shifted to larger values of k, and the period of the incommensurate structure increases. However, as was pointed out above, in a narrow region near ξ_* the perturbation theory used is inapplicable, and therefore the matter of whether an incommensurate structure arises at the critical point, with an infinite or finite period, remains an open question.

The dependence of the period of the incommensurate structure on the IP for an absolutely rigid and a compliant half space is shown in Fig. 2b. It is seen that taking the compliance of the substrate into account leads to an increase in the period of the incommensurate structure. For the values of the model parameters α, β, U, and a used in the figure a critical value of the IP equal to $\xi_*\approx 0.4$ is found numerically.

4. RIGID MONOLAYER ON THE SURFACE OF A SOFT HALF SPACE

In the case of a rigid monolayer on the surface of a soft half space the initial system of Eqs. (12) and (13) is conveniently rewritten in the form

$$\sin\psi=\frac{\beta}{U}\left(\frac{ab}{2\pi}\right)Hw_{0x}, \tag{33}$$

$$\psi_x=\frac{2\pi}{b}\left(w_{0x}+\frac{1}{a}\frac{\beta}{\alpha}Hw_0-d+\xi\right), \tag{34}$$

$$u_x=-\frac{1}{a}\frac{\beta}{\alpha}Hw_0+d-\xi. \tag{35}$$

Equation (35) and the integration constant d, which will be determined below, arise after a single integration of Eq. (17).

In the case of a rigid monolayer the displacements of the surface atoms of the half space are substantially larger than the displacements of the atoms of the monolayer in the incommensurate structure, i.e., $v\ll w_0\approx b\psi_0/2\pi-\xi x$. Then Eq. (33) can be reduced approximately to the following equation containing only the function ψ:

$$\sin\psi=\frac{1}{a}\frac{\beta}{U}\left(\frac{ab}{2\pi}\right)^2H\psi_x+\delta\left\{\psi-2\pi\xi\frac{x}{b}\right\}, \tag{36}$$

where $\delta=(\beta^2/\alpha U)(b^2/(2\pi)^2)$.

Since $\sin\psi\sim\psi\sim 1$, it follows from (36) that

$$a\frac{\partial}{\partial x}\sim\frac{(2\pi)^2}{ab^2}\frac{U}{\beta}\ll 1.$$

(The last strong inequality is necessary to permit making the long-wavelength approximation, within which all of our discussion is valid.) Then it follows from relation (17) that $w_0\sim a\alpha u_x/\beta$ (it must be taken into consideration that the Hilbert transformation does not lead to a change of the spatial scale). Consequently, the condition $v\ll w_0$ reduces to the following inequality:

$$\delta\ll 1. \tag{37}$$

In the limit under consideration (the stiffness of the monolayer is much greater than the stiffness of the substrate half space) the parameter δ plays the role of a small parameter, a measure of the degree to which the case of a compliant but stiff monolayer differs from the case of an absolutely rigid film. It is seen that the first corrections in the small parameter δ are taken into account in Eq. (36) (the second term on the right-hand side).

1. In the case of an absolutely rigid monolayer ($\alpha=\infty$, $\delta=0$) Eq. (36) reduces to a well-known equation that arises in the Peierls model for a dislocation in a two-dimensional elastic system:

$$\sin\psi = H\psi_{\tilde{\kappa}}, \quad \tilde{\kappa} = x\frac{U}{\beta}\frac{1}{a}\left(\frac{2\pi}{b}\right)^2 = \frac{x}{\lambda}, \tag{38}$$

where $\lambda = (\beta/U)a(b/2\pi)^2$ is the characteristic width of a surface dislocation. The exact solutions of the Peierls equation for an isolated dislocation and for a pair of dislocations of different sign are well known:[15,16]

$$\psi_1 = 2\arctan\tilde{\kappa} - \pi, \quad \psi_2 \approx 2\arctan\left[\frac{2l}{\tilde{\kappa}^2 - l^2}\right] + \frac{1}{l}, \tag{39}$$

where l is the distance between dislocations in the limit of low shear stress (in the limit of large size of the dislocation pair).

We have found two new classes of exact periodic solutions of the Peierls equation, which have the forms

$$\psi_0 = 2\arctan\left[\frac{1}{f}\tan(g\tilde{\kappa})\right] - \pi,$$

$$\text{where } g = \frac{f}{1-f^2}, \quad 0 < f < 1; \tag{40}$$

$$\psi_0' = \pi - 2\arctan[f\sin(\tilde{g}\tilde{\kappa})], \quad \text{where } \tilde{g} = \frac{f}{(1+f^2)^{1/2}}. \tag{41}$$

Solution (40) describes an incommensurate structure, i.e., a periodic chain of "2π-kinks" (dislocations on the surface of a half space against the background of a "compensating" average deformation) with a distance between them $L_0 = \pi/g$ and is a generalization of the Peierls solution for a dislocation in a two-dimensional crystal to the case of a periodic chain of bulk dislocations. Solution (40) is parametrized by the value of f (or by the period L_0), which is determined by the IP ξ. Solution (41) describes a periodic system of dislocations of different sign with a distance between them of $2\pi/\tilde{g}$ and in a certain sense generalizes the Nabarro solution. This solution is apparently unstable in the case of the incommensurate structures under consideration and will not be discussed further.

In the case when an incommensurate structure described by solution (40) arises, the displacements on the surface of the substrate are equal to

$$w_0 = \frac{b}{2\pi}\psi_0 - \xi x = \sum_{k=1}^{\infty} b_k \sin[(2\pi/\lambda L_0)x] - b/2, \tag{42}$$

where

$$b_k = \left(-\frac{b}{\pi} + L_0\lambda\frac{a-b}{b}\frac{1}{\pi}\right)\frac{(-1)^k}{k} + \frac{\tilde{q}^k}{k}\frac{b}{\pi}, \quad \tilde{q} = \frac{1-f}{1+f}. \tag{43}$$

The term $-\xi x$ in Eq. (42) corresponds to a "compensating" deformation, in the presence of which the energy of the system (per period of the incommensurate structure) remains finite. Expression (42) is the boundary condition for the two-dimensional Eq. (9) describing the displacement in the substrate. At the indicated displacements on the surface of the half space the displacements in the volume are written in the form

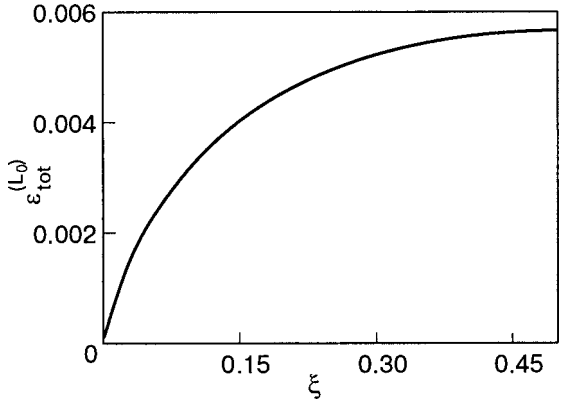

FIG. 3. Dependence of the energy density of the system in the incommensurate structure on the incommensurability parameter for the case $a=1$, $\alpha=\infty$, $\beta=0.1$, $U=0.01$.

$$w = \sum_{k=1}^{\infty} b_k \exp[(-2\pi/L_0\lambda)kz]\sin[(2\pi/L_0\lambda)x] - b/2. \tag{44}$$

In this case the total energy of the substrate per period of the incommensurate structure is equal to

$$E_b = \frac{\beta}{2}\pi\sum_{k=1}^{\infty} b_k^2 k = \frac{\beta}{2}\frac{b^2}{\pi}\ln\left[\frac{(1+f)^2}{4f}\right]. \tag{45}$$

This energy is finite only under the condition of zero average deformation (this corresponds to periodicity of the function w_0). This condition determines a unique value of the parameter $f = f_0$ and, consequently, the dependence of the period of the incommensurate structure L_0 on the IP ξ:

$$f_0 = \sqrt{(L_0/2\pi)^2 + 1} - L_0/2\pi,$$

$$L_0 = \frac{1}{\xi(1-\xi)}\frac{U}{\beta}\frac{(2\pi)^2}{a^2} = \frac{L_0^*}{1-\xi}, \tag{46}$$

where L_0^* is the asymptotic value of the period of the incommensurate structure for $\xi \to 0$.

The energy of interaction of the monolayer with the substrate is determined solely by the function ψ and is equal to

$$E_{\text{int}} = \frac{U}{a}\frac{2f_0}{f_0+1}L_0\lambda. \tag{47}$$

The expression for the total energy of the system (per period of the incommensurate structure) is

$$E_{\text{tot}}^{(L)} = U\frac{\lambda}{a}\left\{\frac{2f_0}{f_0+1} + \frac{2f_0}{1-f_0^2}\ln\left[\frac{(1+f_0)^2}{4f_0}\right]\right\}L_0. \tag{48}$$

The dependence of the energy density on the IP is given by formula (48). In the limit of small ξ its asymptotic expression is of the form

$$\frac{E_{\text{tot}}^{(L)}}{L} = \varepsilon_{\text{tot}}^{(0)} = \beta\frac{a^2}{2\pi}\frac{1}{L_0^*}\left[1 + \ln\left(\frac{L_0^*}{4\pi}\right)\right].$$

The corresponding energy density (per unit length) as a function of the IP is shown in Fig. 3.

This dependence found has meaning at not too large values of the IP ξ, for which the long-wavelength approximation holds. In the uniform state, in which the elastic half space is

not deformed, a surface structure arises which is due to the out-of-register positions of the atoms of the monolayer and substrate and which has the period b/ξ. The energy per unit length of the "uniform state" is equal to U/a and does not depend on the IP. In the particular case of the parameter values chosen in Fig. 3 this energy is equal to $U/a=0.01$ and exceeds the energy of the incommensurate structure.

The dependence of the period of the incommensurate structure on the IP is given by formula (46) and for small values of ξ has the asymptotic form

$$L_0 \approx L_0^* = \frac{1}{\xi}\frac{U}{\beta}\left(\frac{2\pi}{a}\right)^2 \sim \frac{1}{\xi}.$$

Thus the qualitative difference of the limiting case under consideration from the case of an absolutely rigid substrate consists in the absence of a nonzero critical value of the IP: an incommensurate structure with an infinite period L_0 and with zero energy arises for $\xi=0$.

2. In the case of a stiff (weakly compliant but not absolutely rigid) monolayer the situation changes: in Eq. (36) it is necessary to keep the second term on the right-hand side ($\sim\delta$), and the solution of that equation should be written to higher accuracy. Let us take the main (of the order of δ) corrections to the solution into account. In terms of the dimensionless coordinate $\tilde{\kappa}$ the right-hand side of the equation takes the form $H\psi_{\tilde{\kappa}}+\delta(\psi-2\pi\xi\lambda\tilde{\kappa}/b)$. The solution of Eq. (36) should also be written to higher accuracy and can be put in the form

$$\psi=\psi_0+\delta\frac{2\pi}{b}H\left[\int d\tilde{\kappa}\left(\frac{b}{2\pi}\psi_0-\xi\lambda\tilde{\kappa}\right)\right], \tag{49}$$

where ψ_0 is the solution (40) of Eq. (39) in the limit of an absolutely rigid monolayer; the function $\psi(x)$ can be represented in the form a sum of a purely periodic function and a linearly increasing part, equal to $\bar{\psi}=2\pi x/L$. The relation between the period L of the function ψ and the period L_0 of the function ψ_0 will be given below. To find the total energy of the incommensurate structure one must calculate the displacements v in the monolayer and w in the substrate using expression (49) for ψ. In the limit under consideration the displacements in the monolayer are small: $v \ll w_0$, and for the displacements on the surface of the substrate formula (34), with solution (49) substituted into it, gives $w_0=b\psi_0/2\pi+(d-\xi)x-b/2$ [in terms of the constant d, which is determined from the condition that the average deformation in the substrate is equal to zero and in the limit of an absolutely rigid monolayer is equal to zero, Eqs. (34), (35)]. It is a more complicated problem to find the displacements in the monolayer. From Eq. (35), which can be rewritten approximately in the form $v_{\tilde{\kappa}}=-\delta H w_0+d\lambda$, it follows that

$$v=-\delta H\int d\tilde{\kappa}[(b/2\pi)\psi_0+(d-\xi)\lambda\tilde{\kappa}-b/2]+d\lambda\tilde{\kappa}.$$

Taking into account that the average deformation on the substrate surface is equal to zero (the displacements w_0 are strictly periodic), which is dictated by the requirement that the energy of the system in a given configuration be finite, one can, by averaging Eq. (34), determine the value of the constant d: $d=\xi-b/L\lambda$ [in the limit of an absolutely rigid film we have $d=0$, and we arrive at the dependence $L=b/(\xi\lambda)$ found above]. The final expressions for the displacements in the substrate and in the monolayer have the form

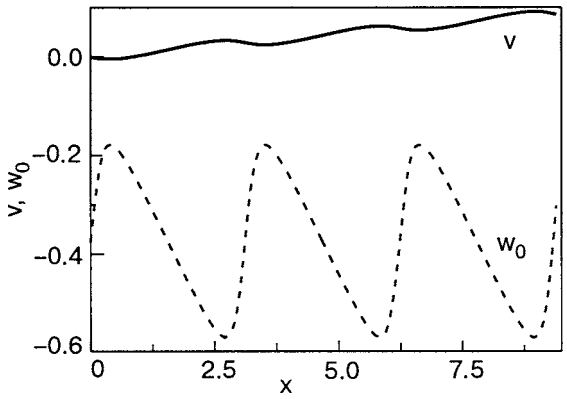

FIG. 4. Displacements in the monolayer and on the surface of the substrate for the case $a=1$, $b=0.6$, $\alpha=1$, $U=0.01$, $\beta=0.1$.

$$w=\sum_{k=1}^{\infty}\frac{b}{\pi}\frac{\tilde{q}^k}{k}\sin\left(k\frac{2\pi}{L\lambda}x\right)\exp\left(-k\frac{2\pi}{L\lambda}z\right)-b/2,$$

$$v=-\frac{1-f^2}{f}\frac{b}{2\pi}\delta\sum_{k=1}^{\infty}\frac{\tilde{q}^k}{k^2}\sin\left(k\frac{2\pi}{L\lambda}x\right)+(\xi-b/L\lambda)x, \tag{50}$$

where $\tilde{q}$ is a function, defined above, of the parameter f, which is a function of the period of the incommensurate structure. Profiles of the displacements on the surface of the substrate and in the monolayer are presented in Fig. 4.

For the displacements in the substrate and monolayer found above, the corresponding energies per period of the incommensurate structure have the form

$$E_b=\frac{\beta}{2}\pi\sum_{k=1}^{\infty}\left(\frac{b}{\pi}\frac{\tilde{q}^k}{k}\right)^2 k=\frac{\beta}{2}\frac{b^2}{\pi}\ln\left[\frac{(1+f)^2}{4f}\right], \tag{51}$$

$$E_s=\delta\frac{L\lambda}{a}U\mathrm{Li}_2(\tilde{q}^2)L\lambda+\frac{\alpha}{2}ad^2L\lambda, \tag{52}$$

where $\mathrm{Li}_2(q)$ is the polylogarithm of degree two. For finding the energy of interaction of the substrate with the monolayer we use expression (49) for the relation between the functions ψ and ψ_0:

$$\cos\psi=\cos\psi_0-\sin\psi_0\,\delta\frac{2\pi}{b}H\left[\int dx\left(\frac{b}{2\pi}\psi_0-\xi x\right)\right],$$

from which we get

$$E_{\mathrm{int}}=\frac{U}{a}\frac{2f}{f+1}L\lambda-\delta\frac{2L\lambda}{a}U\mathrm{Li}_2(\tilde{q}^2)L\lambda. \tag{53}$$

The complete expression for the energy of the system in the incommensurate state (per period of the incommensurate structure) has the form

$$E_{\mathrm{tot}}^{(L)}=\frac{2U}{a}\left\{\frac{f}{f+1}+\frac{f}{1-f^2}\ln\left[\frac{(1+f)^2}{4f}\right]-\frac{\delta}{2}\mathrm{Li}_2(\tilde{q}^2)+\frac{\alpha}{2}\frac{a^2}{2U}\left(\xi-\frac{b}{L\lambda}\right)^2\right\}L\lambda. \tag{54}$$

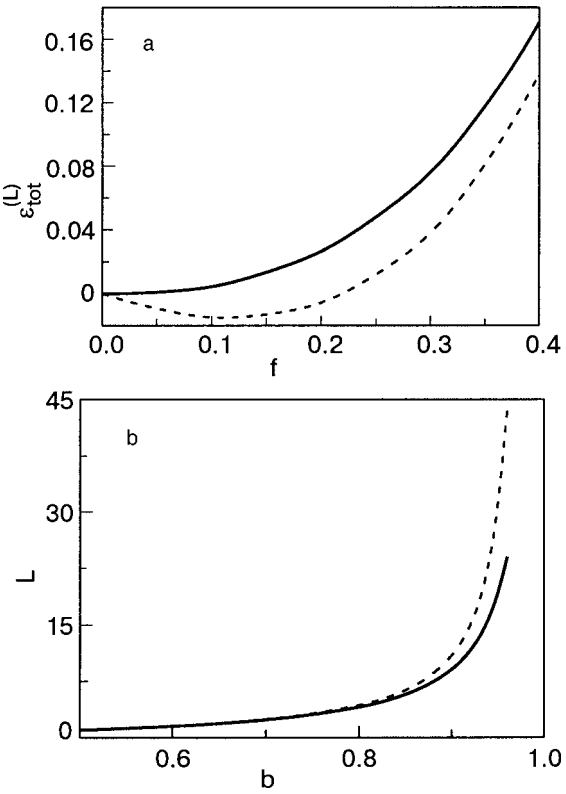

FIG. 5. Energy density of the system as a function of the parameter f (the period of the incommensurate structure) in the incommensurate state for the parameter values $\alpha=1$, $\beta=0.1$, $U=0.01$, $a=1$, $b=0.80<b_*$ (dashed curve), $b=0.99>b_*$ (solid curve) (a). The period of the incommensurate structure as a function of the interatomic spacing b in the case of an absolutely rigid and a compliant monolayer for the parameters values $\beta=0.1$, $U=0.01$, $a=1$; $\alpha=\infty$ (solid curve), $\alpha=30$ (dashed curve) (b).

In the limit of an absolutely rigid monolayer ($\alpha\to\infty\Rightarrow f\to f_0$, $L\to L_0$) this expression goes over to the previously obtained formula (48).

It can be shown that for any finite value of the parameter α in a narrow region of values of the IP near its critical value the correction to the energy due to the compliance of the monolayer is not small, and a perturbation theory treatment of the problem loses meaning. Thus in the framework of this theory one cannot find the critical value of the IP. However, outside that narrow region of the parameter ξ the corrections to the energy are small, and one can find the modification to the incommensurate structure due to the compliance of the film coating.

The corresponding energy density is shown in Fig. 5a for two values of the IP: larger than and smaller than the critical value. At a value $\xi<\xi_*$ the minimum of the function $\varepsilon_{\rm tot}^{(L)}(f)$ at the point f_* determines the period of the structure that arises: $L\sim(1-f_*^2)/f_*$. For the parameters used in Fig. 5a, the critical value of the IP is close to $\xi_*\approx 0.03$.

The condition that the corrections to the energy due to the compliance of the monolayer be small determines the interval of admissible values of the IP ξ; in that interval the following inequality is satisfied:

$$\frac{\delta}{2}\frac{1-f_0^2}{f_0}\ln\frac{(1+f_0)^2}{4f_0}=\tilde{\mu}\ll 1,$$

$$\xi\to 0\Rightarrow\tilde{\mu}\sim\delta\frac{L_0^*}{2\pi}\ln\left[\frac{L_0^*}{4\pi}\right],$$

and then the following analytical expression is valid:

$$L=L_0(1+\tilde{\mu}),\quad f=f_0\left(1-\frac{\tilde{\mu}}{\sqrt{1+(a^2(1-\xi)\xi\beta/U)^2}}\right). \tag{55}$$

It is seen from formula (55) that taking the compliance of the elastic monolayer into account causes an increase in the period of the incommensurate structure that arises ($L>L_0$), which is demonstrated in Fig. 5b. Finally, the dependence of the energy density of the incommensurate structure on the parameter f in Fig. 5a (actually, the dependence on the IP) can be written approximately in the following analytical form:

$$E_{\rm tot}^{(L)}=U\frac{\lambda}{a}\left\{\frac{2f_0}{1+f_0}+\frac{2f_0}{1-f_0^2}\ln\frac{(1+f_0)^2}{4f_0}-\delta\left[\mathrm{Li}_2\left(\frac{1-f_0}{1+f_0}\right)^2+\frac{1}{2}\ln^2\frac{(1+f_0)^2}{4f_0}\right]\right\}L_0. \tag{56}$$

In the limit of an absolutely rigid monolayer ($\delta=0$) this expression goes over to formula (48). In the case of small values of the IP the asymptotic dependence of the energy density on the IP, determined by formula (56), has the form

$$\varepsilon_{\rm tot}=\varepsilon_{\rm tot}^{(0)}-\delta\frac{\beta a^2}{24}\left[1+\frac{3}{\pi^2}\ln^2\left(\frac{L_0^*}{4\pi}\right)\right].$$

5. CONCLUSION

In this paper we have considered the possible incommensurate structures arising near the surface of an elastic half space covered by a monolayer of a substance with a different interatomic spacing from the bulk, over a wide range of values of the stiffness of the half space and of the monolayer coating and of the difference of the interatomic spacings.

1. In the framework of a simple scalar model we derived a system of effective one-dimensional nonlinear integro-differential equations for the static incommensurate surface structures which in the limits of absolutely rigid substrate and absolutely rigid monolayer describes the well-known Frenkel–Kontorova and Peierls models.

2. In the limit of an absolutely rigid monolayer (the Peierls model) we found new classes of exact solutions of the Peierls equation for an incommensurate structure. These solutions describe a periodic system of surface dislocations with a ''compensating'' average deformation of opposite sign (with zero average deformation of the half space).

3. With a weak compliance of the monolayer taken into account in the framework of perturbation theory in a small parameter (the ratio of the stiffness of the substrate to the stiffness of the monolayer) we found the corrections to the structure of the inhomogeneous surface state. In addition to the periodic surface structure of the substrate (with zero average deformation) there appears a small deformation of the monolayer with a nonzero average.

4. In the opposite case of a stiff (but having a finite compliance) half space with a soft monoatomic coating we

found approximate solutions that in the limit of an absolutely rigid half space go over to the previously known results. When a weak compliance of the half space is taken into account, the periodic system of dislocations in the monolayer is accompanied by a weak (with zero average) deformation of the half space.

Thus in a whole range of values of the ratio β/α of the stiffnesses of the half space and monolayer and of the incommensurability parameter ξ (the difference of their interatomic spacings) in different cases we have found exact, quantitative, and qualitative expressions for the form of the incommensurate surface structures, i.e., the dependence of the period of these structures on the indicated parameters: $L = L(\alpha/\beta, \xi)$.

*E-mail: kovalev@ilt.kharkov.ua

[1] A. S. Kovalev, E. S. Syrkin, and G. A. Maugin, Fiz. Nizk. Temp. **28**, 635 (2002) [Low Temp. Phys. **28**, 452 (2002)].
[2] A. S. Kovalev, E. S. Sokolova, A. P. Mayer, and G. A. Maugin, Fiz. Nizk. Temp. **29**, 530 (2003) [Low Temp. Phys. **29**, 394 (2003)].
[3] I. F. Lyuksyutov, A. G. Naumovets, and V. L. Pokrovskiĭ, *Two-Dimensional Crystals* [in Russian], Naukova Dumka, Kiev (1988).
[4] S. C. Erwin, A. A. Baski, L. J. Whitman, and R. E. Rudd, Phys. Rev. Lett. **83**, 1818 (1999).
[5] U. Harten, A. M. Lahee, J. P. Toennies, and Ch. Woll, Phys. Rev. Lett. **54**, 2619 (1985).
[6] O. M. Braun and Y. S. Kivshar, *The Frenkel-Kontorova Model. Concepts, Methods, and Applications*, Springer, Berlin (2003).
[7] I. O. Kulik and I. K. Yanson, *Josephson Effect in Superconducting Tunnel Structures* [in Russian], Nauka, Moscow (1970).
[8] F. C. Frank and J. H. Van der Merwe, Proc. R. Soc. London **198**, 205 (1949).
[9] M. B. Gordon and J. Villain, J. Phys. C **12**, L151 (1979).
[10] I. F. Lyuksyutov, Zh. Éksp. Teor. Fiz. **82**, 1267 (1982) [Sov. Phys. JETP **55**, 737 (1982)].
[11] A. L. Talapov, Zh. Éksp. Teor. Fiz. **83**, 442 (1982) [JETP **56**, 241 (1982)].
[12] V. D. Natsik and E. I. Nazarenko, Fiz. Nizk. Temp. **26**, 283 (2000) [Low Temp. Phys. **26**, 210 (2000)].
[13] M. D. Greenberg, *Application of Green's Functions in Science and Engineering*, Prentice-Hall, Englewood Cliffs, New Jersey (1971).
[14] A. S. Kovalev and I. V. Gerasimchuk, Zh. Éksp. Teor. Fiz. **122**, 1116 (2002) [JETP **95**, 965 (2002)].
[15] A. M. Kosevich, *Theory of the Crystal Lattice (Physical Mechanics of Crystals)* [in Russian], Vishcha Shkola, Kharkov (1988).
[16] F. R. Nabarro, Proc. Phys. Soc. Jpn. **59**, 256 (1947).

Translated by Steve Torstveit

Spectrum of nonlinear excitations of modulated nanoclusters

M. M. Bogdan* and A. S. Kovalev

B. Verkin Institute for Low Temperature Physics and Engineering, National Academy of Sciences of Ukraine, pr. Lenina 47, Kharkov 61103, Ukraine

E. Malyuta

Electrophysical Scientific and Technical Center of the National Academy of Sciences of Ukraine, ul. Chaĭkovskogo 28, Kharkov 61002, Ukraine

(Submitted February 1, 2005)
Fiz. Nizk. Temp. **31**, 807–814 (July 2005)

The nonlinear dynamics of a chain of four coupled anharmonic oscillators with alternating frequency parameters is investigated. This system is treated as an elementary fragment of a discrete modulated nonlinear medium, in particular, a medium of magnetic and elastic nanoclusters and coupled optical waveguides. The stationary monochromatic oscillations of the system are investigated analytically and numerically, and a complete classification of them is carried out. The bifurcation diagram for such a system is obtained: the spectral dependences of the oscillation frequencies on the integral of the number of states are found. A detailed investigation of the bifurcation process for the appearance of an excitation which is an analog of the gap soliton in a finite-size modulated medium is carried out. [DOI: 10.1063/1.2001645]

1. INTRODUCTION

Recently a great deal of attention in condensed matter physics is being devoted to the study of nonlinear self-localized excitations. Their fundamental role in the description of nonlinear phenomena follows directly from the results of the mathematical theory of solitons. This theory treats solitons and breathers as a qualitatively new basis of fundamental nonlinear excitations.[1,2]

However, in real microscopic media, when such physical factors as the discreteness and finite size of the system and dispersion and dissipation are taken into account, the properties of such nonlinear excitations can be altered significantly. This has been confirmed by the results of intensive numerical investigations of the nonlinear dynamics of discrete systems with a complex internal structure.[3–5]

The difficulties of the analytical description of the properties of nonlinear excitations in essentially discrete systems are due to the fact that the number of integrable models in this case is extremely small. It is well known that in the approximation of weak nonlinearity the problem of nonlinear localization for a wide range of applications can be discussed in the framework of the nonintegrable discrete nonlinear Schrödinger equation (DNSE).[4,6] Such an equation arises, e.g., in the description of nonlinear properties of a superlattice—in models of photonic and phononic crystals.[7,8] It is straightforward to show that solitons of the breather type in systems with distributed parameters have analogs in the DNSE system with two degrees of freedom. Thus the physical cause of the localization of excitations in nonlinear systems, i.e., the existence of solitons, can be understood from consideration of an extremely simple model of two coupled anharmonic oscillators.[9,10] For interpretation of more-complex objects and phenomena of nonlinear dynamics one must consider finite-size dynamical systems with a large number of degrees of freedom.[2,11]

Such a situation arises in systems with a complex internal structure, in particular, in finite-size modulated media. Examples of such systems are diatomic atom clusters on the surface of a crystal[12] and alternating superstructures—fragments of complex superlattices of photonic and phononic crystals. Such two-dimensional models arise in nonlinear optics, where they correspond to finite sets of nonlinear waveguides with alternating values of the frequency parameters.[8] Among electronic systems examples of one-dimensional objects with alternating charge structure that admit the existence of solitons and quantum breathers are MX chains.[13]

In low-temperature physics magnetic molecular nanoclusters are examples of finite-size modulated systems.[14–16] The total number of spins in such systems is small. A typical example of a magnetic molecule closed into a ring is the compound Mn_6R_6 (Ref. 16), in which the magnetic ions Mn with spin 5/2 alternate with ions of the radicals R having spin 1/2. Transitions in a magnetic field between states of the magnetic molecule with different values of the total spin are essentially quantum phenomena. However, the basic properties of the linear oscillation spectra of magnetic molecules and their weakly nonlinear oscillations about the ground state can be treated in the framework of the classical finite-size modulated DNSE model with a subsequent quasiclassical quantization of the spectrum of those oscillations.

A feature of the spectrum of linear excitations of a modulated system is the presence of a frequency gap in which linear oscillations are forbidden. In a nonlinear modulated medium the existence of so-called gap solitons, with frequencies lying in the gap of the spectrum of linear waves, is possible. The existence of gap (Bragg) solitons was first

predicted theoretically in Refs. 17 and 18 in a study of the propagation of nonlinear waves in optical media with a modulated index of refraction. The simplest crystal structure that admits the existence of gap solitons is a diatomic chain with alternating masses of the atoms.[19–21] Since in the case of modulated nonlinear structures there are practically no integrable models, the first order of business is to study the simplest finite-size fragments of these systems which reflect the basic properties of modulated media, their qualitative analysis, and the numerical simulation of their dynamics.

In the present article, for the purpose of understanding the nature of the gap solitons and the causes of their formation and transformation with changing frequency we study the dynamics of a fragment of an anharmonic diatomic chain of four particles in the framework of the DNSE model. In such a system it is quite simple to investigate the monochromatic oscillations corresponding to stationary states of the nonlinear system and to carry out a complete classification of them, in particular, to find analogs of the gap and ''out-of-gap'' solitons. We obtain the quasi-classical spectra of nonlinear single-frequency oscillations, and we investigate in detail the bifurcation mechanism of formation of the analog of a gap soliton and the features of its transformation to an analog of the out-of-gap soliton at the lower boundary of the gap of linear excitations.

2. FORMULATION OF THE MODEL

We consider a system of four coupled anharmonic oscillations with alternating frequency parameters. For simplicity we assume cyclic boundary conditions, i.e., we close the chain into a ring. The Hamiltonian of such an extremely simple modulated system can be written in the form:

$$\mathcal{H}=\sum_{i=1}^{4}\left\{\tilde{\omega}_0^{(i)}|\psi_i|^2-\frac{1}{2}|\psi_i|^4+\varepsilon|\psi_i-\psi_{i-1}|^2\right\}, \tag{1}$$

where $\psi_0=\psi_4$ and $\tilde{\omega}_0^{(1)}=\tilde{\omega}_0^{(3)}$, $\tilde{\omega}_0^{(2)}=\tilde{\omega}_0^{(4)}$. Such a system describes, for example, an ''elementary'' fragment of a magnetic molecule of four spins with easy-axis anisotropy. Here the complex functions ψ_i are related to the components of the spin as follows: $\psi_i=S_i^x+iS_i^y$. The parameters $\tilde{\omega}_0^{(1,2)}$ correspond to the eigenfrequencies of the linear oscillations of two sorts of oscillators, and the constant ε characterizes the interaction of the particles with each other.

The dynamical equations corresponding to Hamiltonian (1) for these oscillations have the form

$$i\psi_i-\omega_0^{(i)}\psi_i+|\psi_i|^2\psi_i+\varepsilon(\psi_{i+1}+\psi_{i-1})=0, \tag{2}$$

where we have introduced the notation $\omega_0^{(i)}=\tilde{\omega}_0^{(i)}+2\varepsilon$.

We note that Eq. (2) has an additional integral of motion besides an the total energy E of the system, viz., the number of quasiclassical states:

$$N=\sum_{i=1}^{4}|\psi_i|^2. \tag{3}$$

This quantity corresponds to an adiabatic invariant of the system and in the case of quasi-classical quantization it determines the number of quantum states with energies less than E.

The system of Eq. (2) has monochromatic solutions of the form

$$\psi_i=\varphi_i\exp(-i\omega t), \quad i=1,2,3,4, \tag{4}$$

which describe nonlinear stationary oscillations characterized by a single parameter—the frequency ω. We consider only real amplitudes φ_i. After substitution of expression (4) into system (2) we obtain a system of nonlinear algebraic equations

$$(\omega-\omega_0^{(i)})\varphi_i+\varphi_i^3+\varepsilon(\varphi_{i+1}+\varphi_{i-1})=0. \tag{5}$$

The difference of the frequencies of the oscillations is characterized by the parameter $\gamma=\omega_0^{(2)}/\omega_0^{(1)}$. Below we shall denote $\omega_0^{(1)}$ as ω_0 and $\omega_0^{(2)}=\gamma\omega_0$, and without loss of generality we can set the parameter ε equal to unity. For definiteness we shall assume $\gamma\geqslant 1$. The limit $\gamma\to 1$ corresponds to a uniform chain. For the case of a uniform chain ($\gamma=1$) the corresponding problem of monochromatic oscillations was formulated and solved completely in Ref. 5.

In the linear limit the spectrum of eigenfrequencies of the system consists of four values corresponding to in-phase oscillations with frequency $\omega_1=\Omega_+-\sqrt{\Omega_-^2+4}$, where $\Omega_\pm=\omega_0(1\pm\gamma)/2$, antiphase oscillations with frequency $\omega_4=\Omega_++\sqrt{\Omega_-^2+4}$, and two antiphase oscillations in each of the ''sublattices,'' with frequencies $\omega_2=\omega_0^{(1)}$ and $\omega_3=\omega_0^{(2)}$. These oscillations correspond to the standard notation ($\uparrow\uparrow\uparrow\uparrow$), ($\uparrow\downarrow\uparrow\downarrow$), ($\uparrow 0\downarrow 0$), and ($0\uparrow 0\downarrow$). The length and direction of the arrows characterize the relative amplitude and phase of the oscillations of the particle. The zeros correspond to nonmoving particles.

With increasing number of particles in the chain the number of frequencies in the spectrum will grow, and the new frequencies will occupy the frequency intervals (ω_1,ω_2) and (ω_3,ω_4). Here two zones of the spectrum are formed, with a gap between frequencies ω_2 and ω_3. Thus the values of the frequencies ω_2 and ω_3 play the role of the boundaries of a gap in the spectrum of linear excitations.

In the nonlinear case the frequencies of monochromatic oscillations depend on the amplitude and, hence, on the energy of the system and the number-of-states integral N: $\omega_i=\omega_i(N)$. For nonlinear oscillations it would be natural to use as the spectral characteristic the dependence of the total energy on the integral N: $E=E(N)$, which is in fact the quasi-classical spectrum of the system. It is not hard to show that for single-frequency solutions the important relation $\omega=dE/dN$ is satisfied. Therefore, in this paper we consider the spectral density $\omega=\omega(N)$ for a given oscillation, which also uniquely determines the dependence $E=E(N)$, as the basic characteristic of the nonlinear oscillations.

3. ANALYTICAL RESULTS

The initial system of nonlinear Eq. (2) cannot be integrated completely, since for the given problem the criterion of integrability is not met (the number of independent integrals is only equal to half of the total number of equations). Nevertheless, the system of algebraic Eq. (5) admits a substantial reduction to the two-particle problem. As a result, certain solutions, in particular the principal nonlinear oscillations corresponding to the boundaries of the ''nonlinear'' gap can be found exactly.

Indeed, by adding and subtracting equations of the system (5) in pairs for the 1st and 3rd and 2nd and 4th particles,

changing to the new variables $\varphi_1-\varphi_3=u$, $\varphi_1+\varphi_3=\nu$, $\varphi_2-\varphi_4=x$, and $\varphi_2+\varphi_4=z$, and introducing the notation $A=\omega_0-\omega$ and $B=\gamma\omega_0-\omega$, we obtain a system of nonlinear algebraic equations for the differences and sums of the amplitudes of the oscillations of the oscillators:

$$u[4A-(3\nu^2+u^2)]=0,$$

$$x[4B-(3z^2+x^2)]=0,$$

$$\nu[4A-(3u^2+\nu^2)]-8z=0,$$

$$z(4B-(3x^2+z^2))-8\nu=0. \tag{6}$$

The system of Eqs. (6) clearly decomposes into four independent systems of equations:

Case (I): $u=0$, $x=0$,

$$\nu(4A-\nu^2)-8z=0, \quad z(4B-z^2)-8\nu=0. \tag{7}$$

Case (II): $u=0$, $x^2=4B-3z^2$,

$$\nu(4A-\nu^2)-8z=0, \quad z(z^2-B)-\nu=0. \tag{8}$$

Case (III): $x=0$, $u^2=4A-3\nu^2$,

$$z(4B-z^2)-8\nu=0, \quad \nu(\nu^2-A)-z=0. \tag{9}$$

Case (IV): $u^2=4A-3\nu^2$, $x^2=4B-3z^2$,

$$z(z^2-B)-\nu=0, \quad \nu(\nu^2-A)-z=0. \tag{10}$$

Thus the initial problem for four particles actually reduces to four independent problems for two coupled nonlinear oscillators, and the whole frequency spectrum for the amplitudes of nonlinear monochromatic oscillations of the system (5) is composed of four sets of spectral curves $\omega_i=\omega_i(N)$, corresponding to the cases (I)–(IV). We note that the system of equations for the amplitudes ν and z in the general case can have up to 9 real solutions (one trivial solution $\nu=z=0$ and four pairs of solutions differing only in sign). This permits the assertion that in the stated problem for a given type of monochromatic oscillations there are 19 nontrivial spectral curves $\omega_i(N)$.

The principal nonlinear oscillations of the system are in-phase and antiphase oscillations and also oscillations corresponding to the boundaries of the "nonlinear" gap of the spectrum. For the in-phase and antiphase nonlinear oscillations $\varphi_1=\varphi_3$ and $\varphi_2=\varphi_4$, and the problem of finding the corresponding solutions therefore requires consideration of case (I).

Using the connection between the amplitudes of the oscillations and the integral $N\equiv n/2=(\nu^2+z^2)/2$, one can obtain expressions for ν^2 and z^2:

$$\nu^2=\frac{n(\beta-n)}{\alpha+\beta-2n}, \quad z^2=\frac{n(\alpha-n)}{\alpha+\beta-2n},$$

where $\alpha=4A$, $\beta=4B$. Substituting the expressions obtained into the equation $(A-\nu^2)(B-z^2)=64$, which follows from system (7), we arrive at a fourth-order equation for n:

$$n^4-3Cn^3+Dn^2-Fn+G=0. \tag{11}$$

Here we have introduced the notation $C=\alpha+\beta$, $D=\alpha\beta+3C^2-256$, $F=C(2\alpha\beta+C^2-256)$, $G=C^2(\alpha\beta-64)$.

The roots of Eq. (11) are the functions $n(\omega)$, which can be inverted to give the functions $\omega_i(N)$ and, most importantly, the spectral curves corresponding to the in-phase and antiphase oscillations of the particles.

Case (II) contains the exact solution $\nu=z=0$ corresponding to the upper boundary of the "nonlinear" gap $(0\uparrow 0\downarrow)$, which in terms of the amplitudes of the oscillations of the oscillators has the form $(0,\sqrt{B},0,-\sqrt{B})$. The spectral dependence for this boundary of the gap is easily found in explicit form: $\omega_3(N)=\gamma\omega_0-N/2$.

The exact solution corresponding to the lower boundary of the gap $(\uparrow 0\downarrow 0)$ is contained in case (III) and has the form $(\sqrt{A},0,-\sqrt{A},0)$. This corresponds to the spectral dependence $\omega_2(N)=\omega_0-N/2$.

In case (IV) there is yet another exact solution, corresponding to an oscillation of the type $(\uparrow\uparrow\downarrow\downarrow)$. The amplitudes of the oscillations of the particles for this solution are equal to $(\sqrt{A},\sqrt{B},-\sqrt{A},-\sqrt{B})$. The spectral density corresponding to this solution is also obtained in explicit form: $\omega_b(N)=\omega_0(1+\gamma)/2-N/4$. It is split off in the manner of a bifurcation from the upper boundary of the gap at a frequency $\omega_*=\omega_0$.

Moreover, it can be shown that all of the points of the bifurcations from the branches of the boundary of the "nonlinear" gap can be found exactly. For this we write solutions close to the solution $(0,\sqrt{B},0,-\sqrt{B})$ in the following form: $\varphi_1=\psi_1$, $\varphi_2=\sqrt{B}+\psi_2$, $\varphi_3=\psi_3$, $\varphi_4=-\sqrt{B}+\psi_4$, where $\psi_i<1$. Substituting the expressions for the functions φ_1, φ_2, φ_3, and φ_4 into the initial system of Eq. (5), we obtain the following linearized system for the small corrections ψ_i:

$$(\omega-\omega_0)\psi_1+(\psi_2+\psi_4)=0,$$

$$2(\gamma\omega_0-\omega)\psi_2+(\psi_1+\psi_3)=0,$$

$$(\omega-\omega_0)\psi_3+(\psi_2+\psi_4)=0,$$

$$2(\gamma\omega_0-\omega)\psi_4+(\psi_1+\psi_3)=0. \tag{12}$$

Equating the determinant of the matrix of coefficients of the system (12) to zero, we arrive at an equation for the bifurcation frequencies:

$$(\gamma\omega_0-\omega)(\omega_0-\omega)[(\omega-\omega_0)(\gamma\omega_0-\omega)-2]=0. \tag{13}$$

The solution $\omega=\gamma\omega_0$ is trivial. The solution with $\omega_*=\omega_0$, as we have said, corresponds to the splitting off of the exact solution $(\sqrt{A},\sqrt{B},-\sqrt{A},-\sqrt{B})$. Finally, the two roots

$$\omega_{1,2}=\frac{1}{2}(\omega_0(1+\gamma)\pm\sqrt{\omega_0^2(1-\gamma)^2-8}) \tag{14}$$

arise only above a certain critical value $\gamma_c=1+2\sqrt{2}/\omega_0$. As an analysis shows, the spectral curves $\omega_i(N)$ corresponding to these two bifurcation solutions behave in an extremely nontrivial way with increasing N. One of these curves goes into the region of the nonlinear gap, while the other splits off as an ordinary bifurcation but then, with increasing N, both functions lie outside the gap and terminate at their intersection point at a certain value N_c. When the parameter γ reaches a threshold value γ_* this point becomes a quadracritical point (at which four solutions come together), and from that point on there exist two infinite intersecting lines of the analog of the gap soliton and an ordinary primary

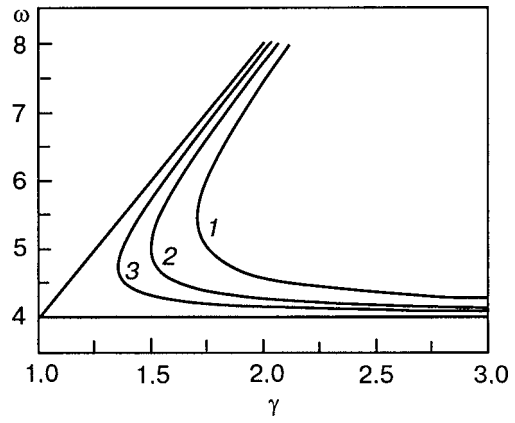

FIG. 1. Dependence of the bifurcation frequencies (upper branches of the hyperbolas) on the parameter γ for analogs of gap solitons in systems of coupled anharmonic oscillators of two sorts: for 4 particles—curve *1*; for 8 particles—curve *2*; for 12 particles—curve *3*.

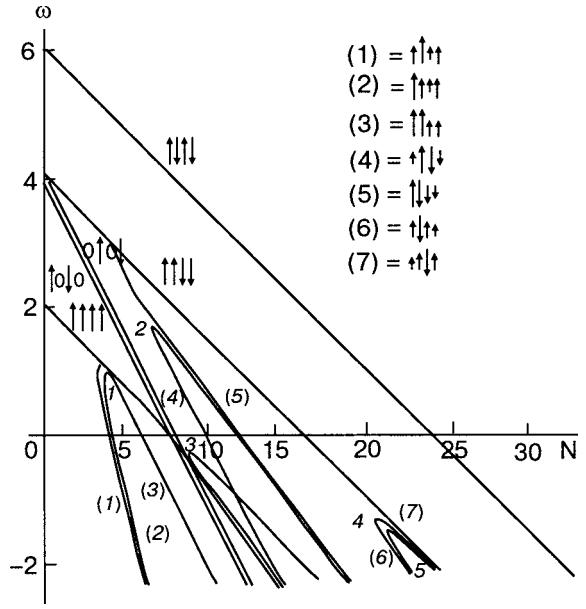

FIG. 2. Bifurcation diagram of single-frequency solutions for systems of four coupled anharmonic oscillators for $\gamma = 1.025$.

bifurcation dependence split off from the upper boundary of the gap.

Thus, starting at the value $\gamma_* = 1.750$ the upper boundary of hyperbola *1* in Fig. 1 corresponds to bifurcation points of the analog of the gap soliton, the spectral dependence of which with increasing γ occupies a larger and larger place in the gap region. It is interesting to note that all of the points of bifurcation from the upper boundary of the "nonlinear" gap for systems of 8, 12, 16 and any other multiple of four are found in explicit form. Figure 1 also gives the curves of the bifurcation frequencies for analogs of the gap solitons for the cases of 8 and 12 particles. It is seen that the critical and threshold values γ_c and γ_* fall off rather rapidly with increasing number of particles, and for an infinite system they go to zero.

In conclusion we note that since equations of the fourth order in ω are obtained for the bifurcation frequencies in the case of four particles, the spectral curves of the nonlinear oscillations can exhibit not more than four bifurcation points. One is readily convinced that bifurcations are absent on the lines of antiphase oscillations and on the lower boundary of the gap.

4. RESULTS OF A NUMERICAL CALCULATION

Since the system of nonlinear algebraic Eq. (5) obtained above cannot be completely solved analytically, numerical methods were used. The calculation was done using the Maple 8 software package. For a specified value of the parameter $\omega_0 = 4$, all of the real solutions of the system of Eqs. (7)–(10) were found and, hence, the solutions of system (5) for a fixed value of the parameter γ and arbitrary ω. As a result, for the given value of ω we obtained a set of solutions $\varphi_i^{(j)}$, where the index i enumerates particles and j enumerates solutions. For each jth solution of the system (5) at a specified value of the frequency the value of the number of states of the system (3), which is an integral of the motion, was calculated. Thus, the spectral characteristics of the system were obtained: the dependences of the oscillation frequencies ω on the integral N.

Numerical integration of the equations was done for a wide range of values of the parameter γ. The main results are shown in Figs. 2, 3, and 4 for $\gamma = 1.025$, $\gamma = 1.76$, and $\gamma = 20$.

The features of the bifurcation pattern for the functions $\omega = \omega(N)$ in the case of a small difference of the eigenfrequencies of the particles (for $\gamma = 1.025$) are presented in Fig. 2.

First of all we see that in the modulated chain the spectrum of linear excitations has a gap. The presence of particles of two different eigenfrequencies leads to lifting of the degeneracy for oscillations of the form ($\uparrow 0 \downarrow 0$). For γ close to unity the gap is narrow, but it widens rather rapidly with increasing γ. As we mentioned in the previous Section, the solution $(\sqrt{A}, \sqrt{B}, -\sqrt{A}, -\sqrt{B})$ splits off from the upper boundary of the gap at small N at a frequency equal to ω_0. Another solution splits off from the solution formed for $N \approx 4$. Now, however, unlike the case of the uniform chain, a subsequent bifurcation does not arise on the line of the new solution, and a lifting of the degeneracy occurs with the appearance of solutions (4) and (5), which form the "parabola" *2*. As will be seen later on, the position of this "parabola" varies rapidly with increasing γ.

In the case of a uniform chain a twofold degenerate dependence for oscillations with strong localization at one particle splits off in a bifurcation manner from the dependence for in-phase oscillations at a finite value of N. In the case of different particles this bifurcation splits and the degeneracy is lifted with the formation of solutions (1) and (2) (this is analogous to the lifting of the degeneracy in a system of two oscillators with different masses). Now a line *3*, which corresponds to an analog of the localized solution centered between particles in the uniform chain, splits off from line *2*. Yet another bifurcation point is found on the line of the in-phase oscillations at ω close to zero. Upon a small increase of the parameter γ a coalescence of this primary bifurcation and branch *2* occurs at a point $\gamma_* = 1.05$, with the formation

of "parabola" *1*. After the joining of the branches, "parabola" *1* begins to shift into the region of the nonlinear gap.

To describe the order of the positions of the spectral curves in the vicinity of $N=10$, $\omega\approx -1$, let us fix the value of the frequency and follow the appearance of the curves as N increases. The line of in-phase oscillations passes most closely to solution (3), and then come the lower and upper boundaries of the "nonlinear" gap. The left branch of the "parabola" *3* situated to the right of the line of the upper boundary of the gap and is inclined at the same angle to the N axis. Farther to the right, the primary bifurcation from the line of in-phase oscillations occurs, and next to it is a bifurcation formed on the left branch of "parabola" *3*.

Finally, we address the appearance of "parabolas" *4* and *5* as a result of the lifting of the degeneracy in the modulated chain. It is "parabola" *4* that with growth of the parameter γ takes part in the formation of the analog of the gap soliton.

As in an infinite modulated medium, an analog of the gap soliton in a chain with a small number of particles should correspond to a solution whose frequency lies in the region of the "nonlinear" gap. Such a solution actually arises with growth of the parameter γ, and this occurs in a threshold manner after the parameter γ reaches a critical value $\gamma_c=1.707$. We note that with increasing γ the relative size of the gap increases, and the main bifurcations on the line of in-phase oscillations and the upper boundary of the gap shift to smaller N. At the same time, the bifurcation "parabolas" *1* and *2* shift to the region of negative frequencies, penetrating into the gap region, and the sharp apex of "parabola" *4* approaches the upper boundary of the gap as the critical value γ_c is approached. The bifurcation diagram of above-threshold values of the parameter γ and in the immediate vicinity of γ_c is presented in Fig. 3 for $\gamma=1.76$. The inset shows the point of creation of the analog of the gap soliton. After the parameter γ reaches the critical value $\gamma_c=1.707$, two bifurcation points appear on the line of the upper boundary. The subsequent evolution of the solutions created at these bifurcation points occurs very specifically and in complete agreement with the description of this process in the previous Section for γ just less than the threshold value $\gamma_*=1.750$, having the form shown in the inset of Fig. 3. At a value $\gamma=1.76$ we see in Fig. 3 that instead of the sharpended "parabola" *4* there already exists a branch corresponding to the gap solution S and a branch of the ordinary primary bifurcation II. The first splits off and passes into the gap, then leaves the gap and crosses the horizontal axis at $N\approx 18.7$. The second dependence splits off upward from the boundary of the gap and behaves as a typical primary bifurcation. We note that if we follow the change of γ, moving from the region of large values to the region of small values of this parameter, then the vanishing of the branch of gap solitons occurs at the moment when its bifurcation point approaches the point of the primary bifurcation and it culminates in the formation of a "parabola," which then moves out into the region of negative values.

Finally, we note that "parabolas" *3* and *5* no longer show up on the bifurcation diagram, since they move ever deeper into the region of negative frequencies.

With increasing γ the gap increases strongly, and the bifurcation point of the gap solution approaches the weakly

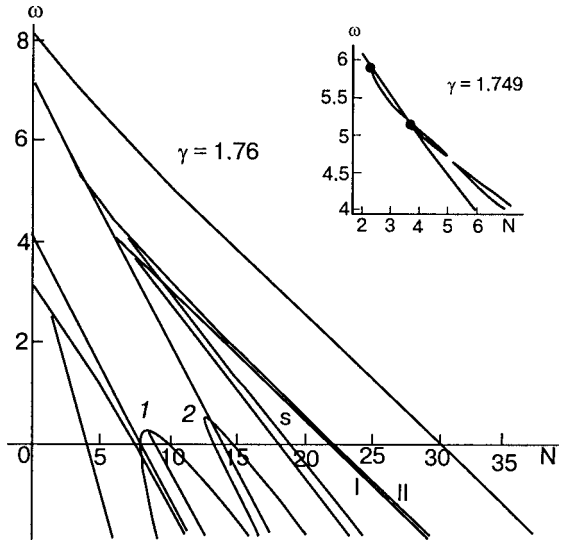

FIG. 3. Bifurcation diagram of single-frequency solutions for $\gamma=1.76$ (the inset shows the moment of creation of the analog of the gap soliton at a value just below the critical, $\gamma=1.749<\gamma_c=1.750$).

nonlinear limit and corresponds to a frequency close to $\gamma\omega_0$. In this limit at small values of N there are two qualitatively very similar bifurcation patterns at low and high frequencies. This actually corresponds to the case of oscillations of atoms with substantially different masses, i.e., there are two almost independently oscillating systems of nonlinear oscillators with renormalized effective couplings. Both on the line of the upper boundary of the gap and on the line of the in-phase oscillations there are bifurcations of creation of quasi-soliton states by the scenario described by Ovchinnikov.[9] But the main effect, which becomes obvious in the limit of large γ, is the transformation of the analog of the gap soliton into an out-of-gap soliton. It occurs at a frequency close to the lower edge of the spectrum of linear oscillations, as can be seen on the bifurcation diagram in Fig. 4. The only lines that remain on it are those that fall into the region of the "nonlinear" gap and the curve for the oscillation $(\sqrt{A},\sqrt{B},-\sqrt{A},-\sqrt{B})$. The line of the analog of the gap soliton is split off from the

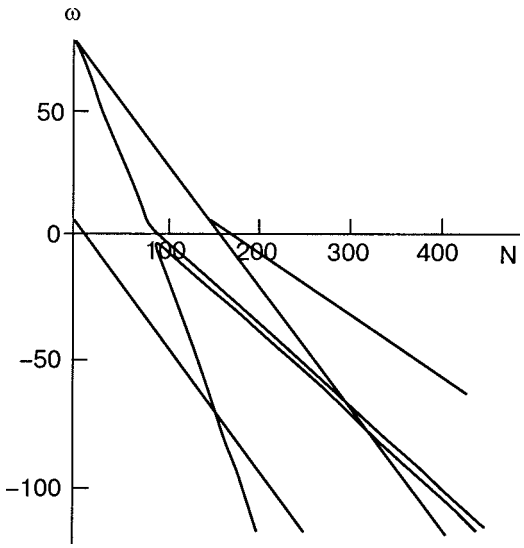

FIG. 4. Bifurcation diagram of single-frequency solutions at $\gamma=20$. The solution corresponding to the gap soliton is transformed into an out-of-gap soliton near the lower edge of the spectrum of linear waves.

upper boundary of the gap, reaches the frequency ω_0, and is continuously transformed into the line of the out-of-gap soliton. We recall that in an infinite system the out-of-gap soliton corresponds to localized oscillations of the atoms of one sort and nonlocalized oscillations of the atoms of the other sort. Anomalous changes of the relationships of the amplitudes are also traced in the finite-size system investigated here.

It should be stressed that in the case $\gamma \gg 1$ many of the characteristic features of the spectral curves of the system studied—simple and double primary bifurcations, secondary bifurcations, branching points, etc.—repeat the most essential elements of the dynamics of an anharmonic chain with a large number of degrees of freedom.[20] The appearance of a gap soliton and its transformation into an out-of-gap soliton in the investigated fragment of a modulated medium and in a system of large size occur according to an identical scenario. The presence of a larger number of degrees of freedom leads to filling of the regions below and above the ''nonlinear'' gap by frequency dependences, while the bifurcation pattern in the gap remains qualitatively the same.

From the standpoint of application of the results to magnetic molecules and systems of nonlinear optical waveguides with a small number of elements we note that the solutions found for four oscillators not only demonstrate the basic regularities of the formation of quasi-soliton states but are also part of the solutions for systems consisting of 8, 12, 16, etc., oscillators. It seems to us that it should be possible to excite quasi-soliton states (including gap solitons) by resonance methods in magnetic and elastic nanoclusters and optical waveguides. It should be kept in mind that the in-phase oscillations corresponding to quasi-soliton states and which are the discrete analogs of breathers in a finite-size system have the lowest energy for a fixed number of states. Indeed, the quasi-classical spectra of all the oscillations found are easily reproduced from the calculated dependences $\omega_i = \omega_i(N)$. Mainly these are originally quadratically growing functions that reach a maximum at points where the frequency goes to zero, after which they fall off with increasing amplitudes of the oscillations (with increasing integral N). However, it should be noted that, unlike the infinite and continuous systems of the nonlinear Schrödinger equation, the question of stability of the quasi-soliton states of the discrete nonlinear Schrödinger equation cannot be solved solely on the basis of an analysis of quasi-classical spectra, and it requires a special investigation.[22]

CONCLUSIONS

In summary, in a modulated finite-size nonlinear system the spectrum of single-frequency stationary states includes principal nonlinear oscillations and oscillations split off from the principal oscillations as a result of primary and secondary bifurcations, and also oscillations arising in pairs at finite values of the excitation energy (or integral N). The main results of our study of the stationary nonlinear oscillations of such a system can be summarized in the following statements.

1. We have obtained the complete bifurcation diagram of monochromatic solutions in a system of four oscillators and have carried out a general classification of their spectral curves $\omega_i = \omega_i(N)$ for an arbitrary relationship of the frequency characteristics of two sorts of oscillators.

2. We have described effects due to the modulated character of the system: the formation of a gap, the appearance of bifurcations and splitting (doubling) bifurcation curves, the formation of autonomous pairs of solutions which correspond to ''parabolic'' spectral curves, and also other features characteristic for systems with defects.

3. We have investigated in detail the process of formation of the solution that is the analog of the gap soliton in a distributed modulated medium. We have found the critical value γ_c (the critical ratio of eigenfrequencies of the oscillators) above which the gap solutions of the soliton type exist.

4. We have shown that at large gap sizes the existence region of such a solution is large; it arises in a bifurcation manner, similarly to the quasi-soliton state split off from the branch of uniform oscillations. At a value of the frequency close to the lower edge of the gap of linear oscillations, an analog of the gap soliton is transformed to an out-of-gap soliton. It is assumed that the quasi-soliton states, including the gap solitons, can be excited by resonance methods in magnetic and elastic nanoclusters and systems of optical waveguides.

This study was supported in part by the NATO Collaborative Linkage Program (Grant No. PSTCLG.980068).

*E-mail: bogdan@ilt.kharkov.ua

[1] S. Novikov, S. V. Manakov, L. P. Pitaevskii, and V. E. Zakharov, *Theory of Solitons: The Inverse Scattering Method*, Consultants Bureau, New York (1984), Nauka, Moscow (1980).
[2] A. M. Kosevich and A. S. Kovalev, *Introduction to Nonlinear Physical Mechanics*, Naukova Dumka, Kiev (1989).
[3] N. Flytzanis, St. Pnevmatikos, and M. Peyrard, J. Phys. A **22**, 783 (1989).
[4] D. B. Duncan, J. C. Eilbeck, H. Feddersen, and J. A. D. Wattis, Physica D **68**, 1 (1993).
[5] M. Peyrard, Physica D **123**, 403 (1998).
[6] J. C. Eilbeck, P. S. Lomdahl, and A. C. Scott, Physica D **16**, 318 (1985).
[7] A. M. Kosevich and M. A. Mamalui, Zh. Éksp. Teor. Fiz. **122**, 897 (2002) [JETP **95**, 777 (2002)].
[8] Yu. S. Kivshar and G. P. Agrawal, *Optical Solitons. From Fibers to Photonic Crystals*, Academic Press, Elsevier Science, San Diego (2003).
[9] A. A. Ovchinnikov, Zh. Éksp. Teor. Fiz. **57**, 263 (1969) [JETP **30**, 147 (1970)].
[10] S. M. Jensen, IEEE J. Quantum Electron. **QE-18**, 1580 (1982).
[11] A. S. Kovalev and M. M. Bogdan, Fizika Mnogochastichnykh Sistem **13**, 20 (1988).
[12] A. Franchini, V. Bortolani, and R. F. Wallis, Phys. Rev. B **53**, 5420 (1996-I).
[13] N. Kuroda, Y. Wakabayashi, M. Nishida, N. Wakabayashi, M. Yamashita, and N. Matsustita, Phys. Rev. Lett. **79**, 2510 (1997).
[14] W. Wernsdorfer and R. Sessoli, Science **284**, 133 (1999).
[15] A. K. Zvezdin, V. V. Kostyuchenko, V. V. Platonov, V. I. Plis, A. I. Popov, V. D. Selemir, and O. M. Tatsenko, Usp. Fiz. Nauk **45**, 9 (2002).
[16] V. V. Kostyuchenko, I. M. Markevtsev, A. V. Philippov, V. V. Platonov, V. D. Selemir, O. M. Tatsenko, A. K. Zvezdin, and A. Caneschi, Phys. Rev. B **67**, 184412 (2003).
[17] W. Chen and D. L. Mills, Phys. Rev. Lett. **58**, 160 (1987).
[18] D. Mills and J. Trullinger, Phys. Rev. B **36**, 947 (1987).
[19] St. Pnevmatikos, N. Flytzanis, and M. Remoissenet, Phys. Rev. B **33**, 2308 (1986).
[20] S. A. Kiselev, S. R. Bickham, and A. J. Sievers, Phys. Rev. B **50**, 947 (1994).
[21] A. S. Kovalev, O. V. Usatenko, and A. V. Gorbach, Phys. Rev. E **60**, 2309 (1999).
[22] A. V. Gorbach and M. Johansson, Eur. Phys. J. D **29**, 73 (2004).

Translated by Steve Torstveit

SHORT NOTES

On the sequence of quantum (meta)magnetic transitions in Ising antiferromagnets with single-ion anisotropy

V. M. Kalita

Institute of Physics of the National Academy of Sciences of Ukraine, pr. Nauki 46, Kiev 03028, Ukraine

V. M. Loktev*

N. N. Bogolyubov Institute of Theoretical Physics, ul. Metrologicheskaya 14-b, Kiev 03143, Ukraine

(Submitted March 14, 2005)
Fiz. Nizk. Temp. **31**, 815–819 (July 2005)

A simple interpretation is proposed for the series of magnetization jumps observed in two-sublattice Ising antiferromagnets with single-ion anisotropy of the easy-plane type in a longitudinal external field. © *2005 American Institute of Physics.* [DOI: 10.1063/1.2001647]

In recent years a large number of experimental and theoretical papers have appeared in which the low-temperature properties, phase diagrams, heat capacity, and magnetic susceptibility of nickel-containing antiferromagnetic systems (nickelates)[1–11] are actively discussed. The compounds studied include $Ni(C_2H_8N_2)_2NO_2(ClO_4)$ (Ref. 12), $Ni(C_2H_8N_2)_2Ni(CN)_4$ (Ref. 13), $Ni(C_{11}H_{10}N_2O)_2Ni(CN)_4$ (Ref. 13), $Ni(C_{10}H_8N_2)_2Ni(CN_4)H_2O$ (Ref. 14), and other 1D compounds (Ref. 15). A feature of these compounds observed experimentally (see, e.g., Refs. 9 and 10) is a jumplike dependence of the magnetization on the external magnetic field.

Such behavior of the magnetization is now considered to be due to the low dimensionality of the magnetic properties of these compounds, which is reflected in the peculiar character of their spectrum. It is known that this spectrum, even in isotropic (Heisenberg) chains with integer spin S, has a gap (the so-called Holstein gap)[16] which alters the low-temperature behavior of the thermodynamic characteristics of 1D magnetic objects. Because of the well-developed fluctuations, their description requires more-exact methods than the phenomenological (quasiclassical) approach that is widely used in the theory of magnetism or the dimension-sensitive random phase approximation.[17] Therefore, the theoretical papers employ such methods as the transfer matrix,[8] Monte Carlo,[18] and renormalization group[19] methods, numerical methods,[20] the integrable SU(3) model (for $S=1$),[21] and others.

The most interesting feature of the magnetization of the (strictly speaking, quasi-)1D compounds mentioned above is, as we have said, its steplike character and, accordingly, the presence of a pronounced plateau on the field curves of the magnetization, which demonstrate a close to zero value of the static magnetic susceptibility. Such behavior has long been known for ferromagnets with a large contribution from the spin-orbit motion or, equivalently, a high (stronger than the exchange) single-ion anisotropy[22] (see also the review[23]). In the compounds listed above, however, the single-ion anisotropy, though large, does not exceed the exchange interaction constant. And, if the exchange were of the Heisenberg type, then it would be hard to believe that the behavior of these antiferromagnetic systems in an external magnetic field would be conventional—the collapse of the magnetic moments of the sublattices at a finite value of the susceptibility.[23,24]

The goal of this Brief Communication is to study the spectral dependences of a simple model from which it follows that the field behavior of the magnetization (and, hence, of the susceptibility) observed in the substances listed[1–11] is not due to their low dimensionality but to the Ising character of the spin-spin exchange interaction. In particular, we shall show that the process of magnetization of a two-sublattice Ising antiferromagnet with single-ion anisotropy occurs in the form of a sequence of quantum metamagnetic phase transitions, as a result of which the two-sublattice antiferromagnetic system is converted to a ferromagnetic system. Here the problem in the self-consistent field approximation is solved trivially as in the case of ferrosystems[22] and no restriction $S=1$ is required (although such a situation is realized in the nickelates).

We write the Hamiltonian of the model spin antiferromagnetic Ising system in the form

$$\hat{H}=\frac{1}{2}\sum_{\mathbf{n}_\alpha\mathbf{m}_\beta} I_{\mathbf{n}_\alpha\mathbf{m}_\beta} S^Z_{\mathbf{n}_\alpha} S^Z_{\mathbf{m}_\beta} + D\sum_{\mathbf{n}_\alpha} (S^Z_{\mathbf{n}_\alpha})^2 - h\sum_{\mathbf{n}_\alpha} S^Z_{\mathbf{n}_\alpha}, \quad (1)$$

where $I_{\mathbf{n}_\alpha\mathbf{m}_\beta}$ are the constants of the exchange interaction between ions whose positions are specified by the vectors $\mathbf{n}_\alpha$ and $\mathbf{m}_\beta$, and the indices $\alpha,\beta=1,2$ enumerate the magnetic sublattices, $S^Z_{\mathbf{n}_\alpha}$ are spin projection operators, D is the single-ion anisotropy parameter, and $h=\mu_B g H$ is the magnetic field written in energy units (μ_B is the Bohr magneton and g is the g factor).

In the general case operator (1) would be supplemented by single-ion anisotropy terms of higher order and also by "transverse" exchange of the type $I^{\perp}_{\mathbf{n}_\alpha\mathbf{m}_\beta}(S^X_{\mathbf{n}_\alpha}S^X_{\mathbf{m}_\beta}+S^Y_{\mathbf{n}_\alpha}S^Y_{\mathbf{m}_\beta})$, which we shall ignore in this paper. Taking the anisotropic terms into account in the case of Ising exchange does not

present any particular difficulty. As to the transverse projections of the spin operators, with increasing $I^{\perp}_{\mathbf{n}_\alpha \mathbf{m}_\beta}$ a change of the ground state can occur, and the problem becomes difficult to study.

Below we shall restrict consideration in (1) to the exchange interactions of nearest neighbors only, and we shall denote the intersublattice exchange ($\alpha \neq \beta$) by I and the intrasublattice exchange by J; according to the idea of the model the first should be antiferromagnetic, $I>0$, while the constants D and J can in principle be positive or negative. If they have the positive sign (in other words, are antiferromagnetic) the value of the intrasublattice exchange should be much less than I in order for the ground state of the model to be consistent with its two-sublattice nature. Moreover, for such a sign of J the influence of magnetic field can lead to additional "generation" of sublattices[25] (see also Ref. 26), and this possibility will also be ignored below.

In the self-consistent field approximation used (and also under the assumption that the magnetic state of the system is uniform) the energy of system (1) per magnetic cell (for simplicity we consider only the case $T=0$) is

$$E_j = -IS(S-j) + (D+J)[S^2 + (S-j)^2] - hj, \qquad (2)$$

where we have taken into account that the value of the spin of the magnetic sublattice directed along the field (for definiteness we call this the first sublattice) is equal to S. It does not vary but remains constant, while the spin of the other (second) sublattice, initially directed counter to the field, can in the ground (lowest) state be equal to $-(S-j)$; here j, as is easily seen, takes on values from 0 (the ground state for $h=0$) to $2S$ at high fields. In Eq. (2) it is assumed that the parameters I and J include the number of nearest neighbors creating the exchange field.

With increasing field the energy of the ground state of the first sublattice remains unchanged, while the levels of the second begin to cross, so that the ground state successively becomes the state with projection $-(S-j)$. Using Eq. (2) it is easy to write the difference of the values of the energies of two states when the values of the spin of the second sublattice differ by unity:

$$E_j - E_{j-1} = 2IS - (D+J)(2S-2j+1) - h. \qquad (3)$$

We note that for $J<0$, $D<0$ the contribution of the second term in Eq. (3) is positive and decreasing with increase of j. This means that for such signs of the constants the system upon the introduction of h undergoes only one transition, when the spin of the second sublattice, equal to S and directed counter to the field, makes a jumplike transition to a state in which it has the same spin value S in the direction along the field. In other words, in an Ising system with an easy-axis character of the single-ion anisotropy and a ferromagnetic sign of J there can be only one metamagnetic transition. Its features were analyzed in Ref. 27.

For $J>0$ and $D>0$ the contribution of the same term in (3) is already negative, and it increases with increasing j. Consequently, in such an antiferromagnetic system one has a succession of ground states crossing into place, or a sequence of quantum phase transitions, as a consequence of which the spin projection of the second sublattice undergoes jumps, each time changing by unity.

In the framework of the assumptions made in writing the Hamiltonian (1), we find the critical fields $h^{(j)}_{\mathrm{cr}}$ of these magnetization jumps for the case of a relatively small single-ion anisotropy [more precisely, for $D<IS/(2S-1)-J$]. Expressions for the $h^{(j)}_{\mathrm{cr}}$ are determined from the obvious equality $E_j = E_{j-1}$, the use of which gives

$$h^{(j)}_{\mathrm{cr}} = IS - (D+J)(2S-2j+1), \quad j \neq 0. \qquad (4)$$

It follows directly from (4) that for fields $h^{(j)}_{\mathrm{cr}} < h < h^{(j+1)}_{\mathrm{cr}}$, as for $h < h^{(1)}_{\mathrm{cr}}$, the value of the magnetization of the Ising antiferromagnetic will be constant, and for $T=0$ it is equal to j. In other words, the field curves of the magnetization $m(h)$ have a plateau. The difference between the fields of two successive metamagnetic phase transitions depends on neither I nor j:

$$\Delta h = h^{(j+1)}_{\mathrm{cr}} - h^{(j)}_{\mathrm{cr}} = 2(D+J). \qquad (5)$$

At the same time, the value of $h^{(1)}_{\mathrm{cr}}$ depends on I: $h^{(1)}_{\mathrm{cr}} = IS - (D+J)(2S-1)$. Interestingly, for $J=D=0$ the model becomes degenerate, for at all possible values of j the critical fields are equal: $h^{(j)}_{\mathrm{cr}} = IS$, and, as we see, does not depend on j.

We emphasize that for the above-described sequence of quantum metamagnetic phase transitions from the initial (antiferromagnetic) phase to the final (ferromagnetic) phase, the ions before and after the transition are found in the same single-ion state, which, regardless of the influence of the crystalline field, is determined by the exchange interaction. However, in the process of transition the ions of the 2nd sublattice change their single-ion state (passing through a state with zero spin projection on the axis of quantization), and that is the main cause of the sequence of metamagnetic phase transitions, for which the difference (5) is independent of I.

As an illustration let us consider the simplest case of a two-sublattice Ising antiferromagnet with single-ion anisotropy. In this case $S=1$, and from (2) it is easy to write the energy of the three possible states

$$E_0 = -I + 2(D+J); \quad E_1(h) = (D+J) - h; \quad E_2(h) = I + 2(D+J) - 2h. \qquad (6)$$

Figure 1a shows plots of the variation of the energy (6) with h for $J=D=0$. It is seen that $E_1(h)$ and $E_2(h)$ cross the value E_0 at a single point, which corresponds to the aforementioned degeneracy of the model and, accordingly, to the only possible metamagnetic transition.

Figure 1b shows the same $E_1(h)$ and $E_2(h)$ curves at negative values of J and D, or $J+D<0$. Here the straight line $E_2(h)$ crosses with the energy E_0 before the lines $E_1(h)$ does, i.e., for such signs and values of the parameters only one metamagnetic transition is possible, and two plateaus are observed on the $m(h)$ curve. The fields at which $E_1(h)$ and $E_2(h)$ cross E_0 are: $h_1 = I - D - J$, $h_2 = I$, and, naturally, $h_1 > h_2$.

The case when $J>0$ and $D>0$, or $J+D>0$, is shown in Fig. 1c. Now the energy $E_1(h)$ first crosses the straight line E_0, preceding the corresponding crossing for the $E_2(h)$ curve. In other words, at these values of the parameters we

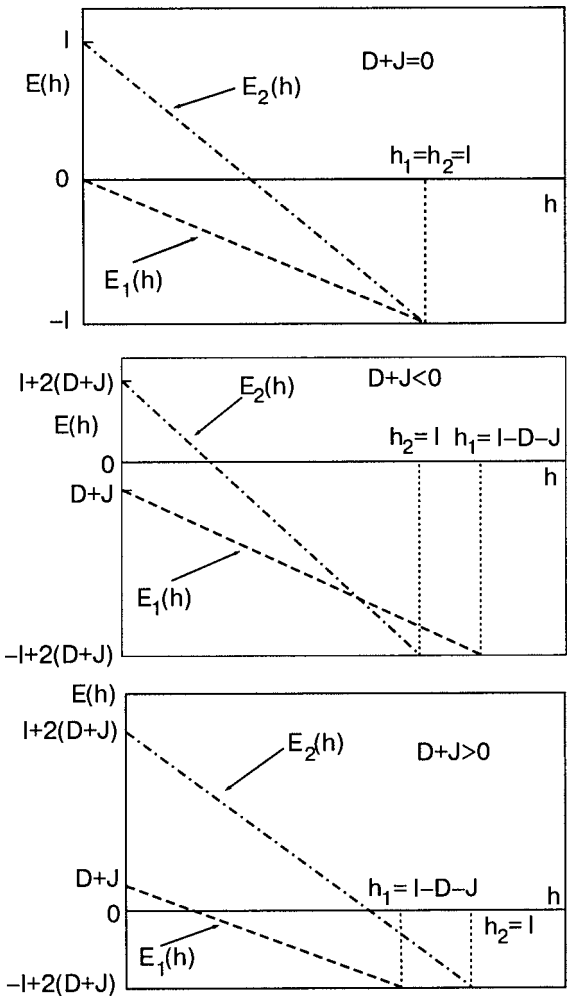

FIG. 1. Field dependence of the energies $E_1(h)$ (dashed line) and $E_2(h)$ (dotted-and-dashed line) according to expressions (6) for $D+J=0$ (a), $D+J<0$ (b), and $D+J>0$ (c). The solid line corresponds to the ground state energy E_0 in the absence of field.

have $h_1<h_2$, and two metamagnetic transitions will occur in the system, and, accordingly, three plateaus will form on the $m(h)$ curve.

As a result, the behavior of an Ising antiferromagnet with $S=1$ obtained at $T=0$ corresponds completely to that observed in low-temperature experiments.[1–11] The approximation used thus shows that Δh [see Eq. (5)] is independent of the space dimension of the system, being completely determined by the value of the single-ion anisotropy (this last is also evident from the experiment), where for all temperatures in the region $T<D(<I)$ one has to good accuracy $\Delta h \approx 2D$. Raising the temperature to values $T\sim D$ and then up to $T\sim I$ will undoubtedly lead to a smoothing of the jumps, but in the high-temperature region the metamagnetic transition in the model studied should maintain its jumplike character. Here it must be kept in mind that in the case of finite temperatures the self-consistent problem of determining the energy spectrum and the mean magnetization will include all the one-ion levels, leading to a transcendental system of equations. That case requires separate consideration.

In conclusion, it should be noted that at large values of D $[D>IS/(2S-1)-J]$ the "equidistant" character of the critical fields (5) found above no longer obtains. In particular, for $D\gg I,J$ the ground state of the magnet changes. For example, for $S=1$ the ground state of the ions become the state with spin projection equal to zero. If so, the crystal is a Van Vleck paramagnet, though one with an antiferromagnetic exchange between ions. The influence of the magnetic field then leads to the inducing of a magnetically ordered state in such a crystal,[22,23] which for $T=0$ occurs in two jumps. This also takes place for half-integer spins and, for example, for $S=3/2$ at large D the projections of the spins of the two sublattices in the ground state are equal to $\pm 1/2$. The turning on of the field first leads to a jump (by unity) in the projection of the spin of the second sublattice, while the projection of the spin of the first sublattice remains unchanged. Here the single-ion spin states are also unchanged, and for that reason this transition is considered metamagnetic. Then, with increasing field, two more jumps will happen, for which the projections of the spins of the two sublattices will progressively increase, and they will make a transition to another (higher-lying) single-ion state. However these will not be metamagnetic phase transitions but field-induced magnetization occurring upon a change of the single-ion states. Therefore, depending on the relative values of the constants D and I, one should distinguish the sequence of quantum metamagnetic transitions from the other quantum transitions that are also induced by the magnetic field but which are related to the change of the single-ion states.

We are grateful to S. M. Ryabchenko for calling our attention to Ref. 8, in which the problem of the appearance of a plateau on the field dependence of the magnetization of nickelates is discussed on the basis of a numerical calculation, and also to the referee for constructive comments.

*E-mail: vloktev@bitp.kiev.ua

[1] K. Hida, J. Phys. Soc. Jpn. **63**, 2359 (1994).
[2] M. Oshikawa, M. Yamanaka, and I. Affleck, Phys. Rev. Lett. **78**, 1984 (1997).
[3] T. Sakai and M. Takahashi, Phys. Rev. B **57**, R3201 (1998).
[4] T. Tonegawa, T. Nishida, and M. Kaburagi, Physica B **246**, 368 (1998).
[5] D. C. Cabra and M. D. Grynberg, Phys. Rev. B **59**, 119 (1999).
[6] T. Yamamoto, M. Asano, and C. Ishii, J. Phys. Soc. Jpn. **69**, 3965 (2000).
[7] V. R. Ohanyan and N. S. Ananikian, Phys. Lett. A **307**, 76 (2003).
[8] E. Aydiner and C. Akyuz, E-print Archive: preprint cond-mat/0501111 (2005).
[9] W. Shiramura, K. Takatsu, B. Kurniawan, H. Tanaka, H. Uekusa, Y. Ohashi, K. Takisawa, H. Mitamura, and T. Goto, J. Phys. Soc. Jpn. **67**, 1548 (1998).
[10] Y. Narumi, M. Hagiwara, R. Sato, K. Kindo, H. Nakano, and M. Takahashi, Physica B **246**, 509 (1998).
[11] T. Goto, M. I. Bartashevich, Y. Hosokoshi, K. Kato, and K. Inoue, Physica B **294**, 43 (2001).
[12] J. P. Renard, M. Verdaguer, L. P. Regnault, W. A. C. Erkelenes, J. R. Mignod, and W. G. Stirling, Europhys. Lett. **3**, 945 (1987).
[13] M. Orendáč, A. Orendáčová, J. Černák, A. Feher, P. J. C. Signore, M. W. Meisel, S. Merah, and M. Verdagner, Phys. Rev. B **52**, 3435 (1995).
[14] A. Feher, M. Orendáč, A. Orendáčová, and E. Gizmar, Low Temp. Phys. **28**, 551 (2002).
[15] M. Orendáč, E. Gizmar, A. Orendáčová, J. Černák, A. Feher, M. W. Meisel, K. A. Abboud, S. Zvyagin, M. Sieling, T. Reith, and B. Luthi, Phys. Rev. B **61**, 3223 (2000).
[16] F. D. M. Haldane, Phys. Rev. Lett. **50**, 1153 (1983).
[17] Yu. A. Izyumov and Yu. M. Skryabin, *Statistical Mechanics of Magnetically Ordered Systems* [in Russian], Nauka, Moscow (1987).
[18] S. Yamamoto and S. Miyashita, Phys. Rev. B **48**, 9528 (1993).

[19] S. R. White and D. A. Huse, Phys. Rev. B **48**, 3844 (1993).
[20] L. S. Campana, A. Caramico D'Auria, F. Esposito, U. Esposito, and G. Kamieniarz, Phys. Rev. B **45**, 5035 (1992).
[21] M. T. Batchelor, X. W. Guan, and N. Oelkers, Phys. Rev. B **70**, 184408 (1993).
[22] E. V. Rozenfel'd, JETP Lett. **24**, 60 (1976).
[23] V. M. Loktev and V. S. Ostrovskii, Fiz. Nizk. Temp. **20**, 983 (1994) [Low Temp. Phys. **20**, 775 (1994)].
[24] V. M. Kalita and V. M. Loktev, Zh. Éksp. Teor. Fiz. **125**, 1149 (2004) [JETP **98**, 1006 (2004)].
[25] A. I. Bugriĭ and V. M. Loktev, Fiz. Nizk. Temp. **13**, 407 (1987) [Sov. J. Low Temp. Phys. **13**, 232 (1987)].
[26] V. V. Eremenko and V. A. Sirenko, *Magnetic and Magnetoelastic Properties of Antiferromagnets and Superconductors* [in Russian], Naukova Dumka, Kiev (2004).
[27] V. G. Bar'yakhtar, I. M. Vitebskiĭ, and D. A. Yablonskiĭ, Fiz. Tverd. Tela (Leningrad) **19**, 2135 (1977) [Sov. Phys. Solid State **19**, 2135 (1977)].

Translated by Steve Torstveit

LETTER TO THE EDITOR

Observation of mechanoelectric effect in He II

A. S. Rybalko* and S. P. Rubets

B. Verkin Institute for Low Temperature Physics and Engineering, National Academy of Sciences of Ukraine, pr. Lenina 47, Kharkov 61103, Ukraine

(Submitted April 11, 2005; revised April 26, 2005)
Fiz. Nizk. Temp. **31**, 820–825 (July 2005)

An experimental study of the electrical response in ^{4}He in the temperature interval $1.5-T_\lambda$ is investigated experimentally by the torsion generator technique. It is shown that the motion of the normal component of He II, entrained by the wall of the torsion oscillator, causes dynamic polarization of the liquid. It is established that the induction potential is proportional to the square of the linear velocity of the oscillator wall. © *2005 American Institute of Physics.* [DOI: 10.1063/1.2001649]

INTRODUCTION

The possible link between the macroscopic superfluid motion and the electrical properties of the liquid is one of the little-studied problems of the physics of superfluid helium.

Recently it was established experimentally for the first time that the relative motion of the superfluid and normal components of He II in a wave of second sound is accompanied by the appearance of an electric induction (electric displacement).[1] In essence what was observed is a charge wave process that takes place together with the well-known wave process of the second sound. This suggests that the presence of a heat flux in helium will somehow lead to a redistribution of the charged constituents of the helium atoms. It became clear that in the wave process of second sound not only the superfluid and normal components (their centers of inertia) engage in periodic countermotion but so do the centers of charge. It was also shown in Ref. 1 that such an effect is not observed in the propagation of first sound.

A characteristic feature of second sound is that the wave process is accompanied by oscillations of the temperature, which complicates the interpretation of experimental data.[1]

In this paper, which is a continuation and extension of Ref. 1, we use the torsion oscillator method,[2] which is based on the fact that in the motion of a solid object in He II at a subcritical velocity, only the normal component is entrained into motion. Thus one can create relative motion of the superfluid and normal components without changing the temperature nor the normal and superfluid densities ρ_n and ρ_s and avoid the problems inherent to the thermal method of exciting motion.

EXPERIMENTAL APPARATUS AND THE MEASUREMENT TECHNIQUE

The measurement unit was a torsion oscillator developed by the Reppy group[2] for use with superfluid helium. This technique has aquitted itself well in studies of phase transitions in adsorbed helium films.

A diagram of the measurement unit is shown in Fig. 1. Chamber *1* was a brass cylinder with a height and a diameter of 10 mm. The inner walls of the chamber were polished to a mirror shine to diminish the surface losses. The chamber was suspended by a capillary *2* of length 12 mm, with outer and inner diameters of 0.8 and 0.5 mm, prepared from the needle of a medical syringe. An electrode *3* was passed through the bottom of the chamber; this electrode doubled as a lever for exciting torsional forces and a sensor for measuring the amplitude of the torsional displacements.

The essence of the technique can be summarized as follows. Chamber *1*, suspended on the elastic capillary, was set in torsional motion by an alternating force arising between capacitor plates (electrodes *3* and *4*) as a result of the application of a train of pulses of known amplitude. The resonance frequency ω_{res} was determined by the torsional modulus G of the capillary and the moment of inertia I of the chamber $[\omega_{\text{res}}=(G/I)^{0.5}]$ and equalled 136 Hz at helium temperatures. The electrode *4* was rigidly fixed, and the torsion resonator can be "driven" to displacements small compared to the distance between electrodes *3* and *4*. The amplitude of the small displacements (vibrations of the oscillator) was determined with the aid of a capacitive probe formed by electrodes *3*, *5*, and a 200 V battery. The motion of the electrode *3* alters the capacitance of the probe, and a potential proportional to the displacement of the oscillator, appears on electrode *5*. When the chamber is filled with helium, e.g., by depositing a film on its inner surface, the moment of inertia of the chamber changes. Below the λ transition the superfluid component is not entrained by the oscillating wall of the chamber, and that leads to an additional variation of the moment of inertia. All of this can be observed from measurement of the resonance frequency.

An important characteristic of the torsion oscillator is its Q, which in the unfilled chamber is determined by the internal friction in the elastic suspension (capillary). In the filled chamber there is a also a contribution to the Q from processes occurring in the condensed helium.

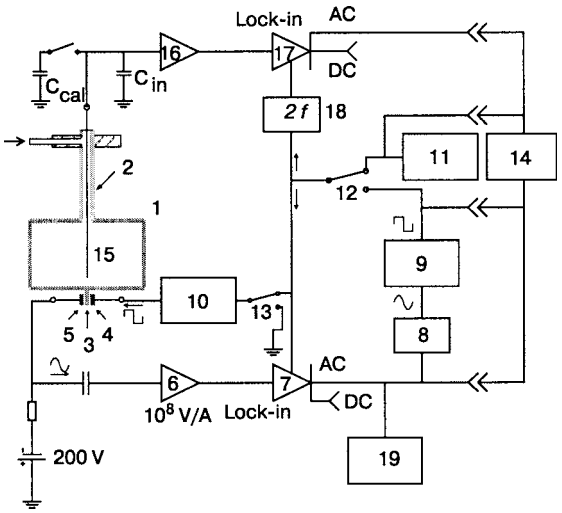

FIG. 1. Block diagram of the apparatus for measuring the dynamic polarization of He II: *1*—chamber of the torsion oscillator, *2*—rigid suspension of the oscillator and the filling capillary, *3*—drive electrode-lever. Circuit A: *4*—supply electrode, *5*—electrode for measuring the amplitude of the displacement of the chamber, *6*—preamplifier, *7*—lock-in amplifier, 8—phase shifter, 9—zero-cross detector, *10*—attenuator, *11*—generator, *12, 13*—switches, *14*—oscilloscope. Circuit B: *15*—electrode for registering the electric induction (electric displacement), *16*—preamplifier, *17*—lock-in amplifier, *18*—frequency doubler, *19*—frequency meter, C_{cal}—calibrated capacitance intended for determination of the input capacitance C_{in}.

The electrical circuit consists of measurement channels A and B.

Channel A is intended for the creation and registration of the mechanical torsional oscillations and is a closed circuit consisting of a preamplifier *6*, a lock-in amplifier *7*, a phase shifter *8*, a zero-cross detector *9*, and an attenuator *10*, all connected in series. The Reppy mechanical torsion resonator is connected into a feedback circuit. In the closed electronic/mechanical circuit formed, a self-excited oscillatory process arises. The main advantage of this ring scheme is that it permits measurement of both the frequency and amplitude of the oscillations automatically, since it requires no additional adjustment for the influence of the processes occurring in the helium on the system parameters.

In such a scheme several regimes of operation of the torsion resonator can be realized: 1) a regime of forced oscillations from the external oscillator *11* (switch *12* is in the upper position); 2) an autogenerator regime (switch *12* is in the lower position); 3) a free damping regime (switch *13* is in the lower position); 4) a regime of stopping of the vibrating oscillator. For regime 4 it was sufficient to change the phase of the supply voltage by 180° and at a certain instant to disconnect the supply (switch *13* was placed at the lower position at the time when the amplitude of the displacements had fallen to the level of noise). The shape of the signals, their phase, and the stopping time of the oscillator to come completely to rest were monitored by the oscilloscope *14*.

In channel B we upgraded the Reppy resonator: an additional electrode *15* for measuring the electric induction (electric displacement) was passed along the center of the chamber via the filling capillary; this electrode, together with the inner walls of chamber *1*, formed a capacitor for the measurement of the electric induction. An electrode of diameter 0.2 mm was mounted above the base of the suspension without touching the walls of the capillary, and therefore it was not set in motion when the oscillator ran. Channel B was intended for measurement of the electrical response to the relative motion of the components of He II imparted by the oscillating wall of the chamber. Channel B consisted of a preamplifier *16* and a lock-in amplifier *17*. The use of the lock-in amplifier, the double shielding of the input leads, and automatic supply of the preamplifer made it possible to achieve a voltage sensitivity as good as 3×10^{-9} V in a 1 Hz band or a sensitivity to the electric charge as good as 10^{-19} C. In such a case one can measure not only the dc and ac components of the signals of both circuits but also observe their phases and the phase difference.

Thus in the experiment a periodic force of excitation of oscillations of the oscillator (electrode *4*) was imposed and the amplitude A of the mechanical torsion oscillations of the chamber (electrode *5*) and the electric induction (electrode *15*) were measured. Knowing the amplitude of the oscillations of the wall of the chamber and the resonance frequency, we could calculate the velocity of the chamber wall $V=L\omega_{res}$ and the acceleration $a=M\omega_{res}^2$. (L and M are constants to be determined in the experiment.)

EXPERIMENTAL RESULTS AND DISCUSSION

The experiments were conducted in the following manner. After the chamber was cooled to a temperature below 4.2 K the temperature dependence of the resonance frequency and amplitude of the oscillations of the chamber were measured (first for the empty chamber and then for the helium-filled chamber). Typical values of the linear velocity V of the side wall of chamber *1* were 10–700 μm/s. The Q of the oscillator was determined in two ways: from the amplitude of its oscillations under conditions of a constant driving force (regimes 1 and 2); from the damping time of the oscillations of the torsion resonator after the feedback was disconnected (regime 3). Below 2.6 K the Q of the unfilled chamber was over 10^7.

The operation of the torsion generator was checked in experiments with unsaturated and saturated helium films and also with bulk liquid helium. In the experiment a periodic force was imposed, causing oscillations of the torsion generator, and the values of its resonance frequency and oscillation amplitude were registered. The temperature was varied in a stepwise manner with temperature stabilization, and in the course of time it was expected that equilibrium would be established. Since there was no porous material in the metal chamber *1*, in contrast to Ref. 2, for example, and the surface area was small, thermal equilibrium was established rapidly. Here it turned out that the shift of the frequency of the torsion generator in the presence of the saturated film was practically independent of temperature in the temperature interval 1.4–1.8 K. When the temperature approached T_λ the shift of the frequency decreased smoothly, and in the He II region it again was independent of temperature. This is direct evidence of a decrease of the contribution of helium to the moment of inertia of the oscillator below the temperature of the superfluid transition. At the λ point a kink was observed in the frequency dependence. For the saturated film the value of T_λ turned out to be equal to 2.18 K, as in the case of bulk helium. For the unsaturated films we could observe a slight

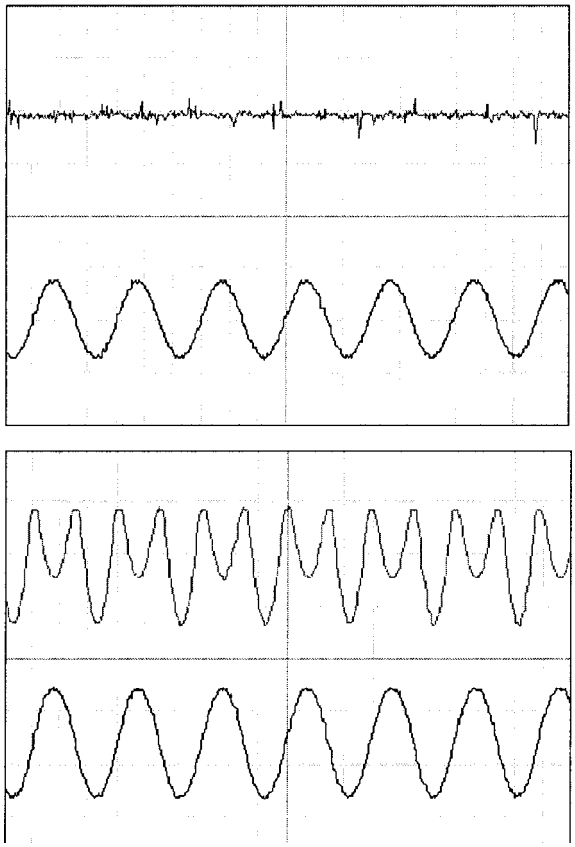

FIG. 2. Traces of the signal shape on the oscilloscope screen at temperatures of 2.3 and 2.0 K versus time: the upper curves are the amplitudes of the induction on electrode *15*; the lower curves are the amplitudes of the oscillations of the oscillator (electrode *5*).

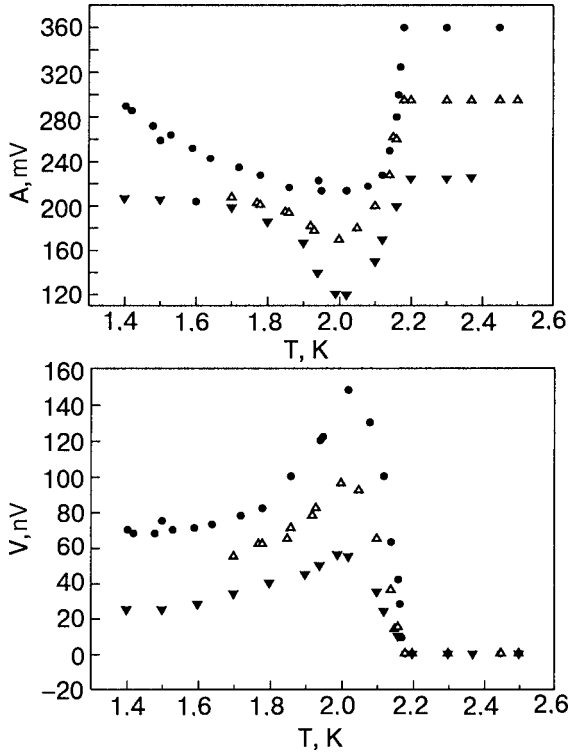

FIG. 3. Temperature dependence of the amplitude of the oscillations of the torsion oscillator (a) and of the electric induction (electric displacement) for three values of the pulses train on electrode *4* (b).

shift of T_λ to lower temperatures. The real sensitivity of the apparatus was sufficient to permit reliable observation of the change of the moment of inertia of a helium film 25 Å thick and with a total area of $\sim 5\ \mathrm{cm}^2$.

Typical time traces from a cathode-ray oscilloscope, describing the oscillations of the cylindrical wall of the chamber *1* and the electric induction on electrode *15*, are presented in Fig. 2 for two temperature regions above and below T_λ. The analogous temperature data are presented in Fig. 3: Fig. 3a shows the temperature dependence of the amplitude of the oscillations of the torsion generator for three constant but different values of the driving force (channel A), and Fig. 3b shows the temperature dependence of the electric induction arising below T_λ (channel B).

It is seen that the amplitude of the oscillations of the torsion resonator behave somewhat differently from the frequency. The amplitude of the oscillations of the oscillator or the angle of rotation and, hence, its velocity vary strongly below T_λ. At the λ point the signal suffers a kink, decreases, and then, after passing through a minimum at 1.9–2 K again rises to the level that it had below 2.2 K. This attests to the appearance of an additional channel of dissipation of mechanical energy below T_λ. It was established by special tests that the additional channel of dissipation is not due to an increase of or oscillations of the temperature to an accuracy of 1.7×10^{-6} K.

Thus the λ transition was fixed from the kink on the frequency and amplitude dependences, and the $\omega_{\mathrm{res}}(T)$ and $A(T)$ curves obtained are qualitatively the same as in Ref. 2, where the measurements were made in a torsion oscillator filled with a porous materials whose surface was coated by a helium film.

The most important result of the experiment was that below T_λ in the presence of the helium film or of the bulk liquid in the vessel an induced potential with one-sided modulation at double the frequency appears on electrode *15* (see Fig. 2a). For the saturated and unsaturated films the signal was observed in the entire interval of currents of the side wall of the cylinder, all the way up to 700 μm/s. Analogous behavior was observed for bulk helium, but only at frequencies of the cylinder wall of chamber *1* less than 30 μm/s. At higher amplitudes of oscillations (velocities) the induction signal was absent on account of the low values of the critical velocities of vortex formation in bulk helium. A film of superfluid helium has the advantage over bulk helium that the critical velocity of the motion in it is much higher than the frequencies realized in the present experiments. Above T_λ the induction signal was not observed to an accuracy of 3×10^{-9} V (see Fig. 2a, $T=2.3$ K). It is seen in Fig. 3a,b that the behavior of the induction in He II and the amplitudes of the oscillations of the oscillator and, hence, the dissipation, in the torsion resonator are correlated with each other. Furthermore, experiments with the unsaturated films showed that the amplitude of the signal induced on the electrode is proportional to the thickness of the film. This indicates the bulk character of the electrical phenomena.

Thus in the excitation of oscillations of the normal component relative to the superfluid component, as in the case of a second-sound wave,[1] an electric induction, or, in other words, a dynamic polarization, arises in He II. The dynamic

polarization of He II leads to the appearance of charge on the capacitor plates which is registered in the experiments. We stress that the amplitude of the induction is maximum at points where the angular part of the acceleration of the torsion resonator is maximum. This follows from the phase shift between the signals of the two channels observed on the oscilloscope. In the second-sound resonator the induction signal is also maximum at the time of the maximum relative acceleration of the components.[1]

Let us point out several important differences between our experiments and those done in Ref. 1.

1. In our experiments the temperature and density of the components ρ_s and ρ_n remained constant, whereas in the case of second sound they varied.

2. In the torsion experiments the relative velocity vectors $\mathbf{V}=(\mathbf{V}_n-\mathbf{V}_s)$ and the electric polarization are perpendicular, while in the second-sound resonator they are parallel to each other.

3. In the second-sound resonator the normal and superfluid components of the helium periodically change their direction of motion, and accordingly the sign of the polarization changes. In the torsion experiments the angular and radial parts of the acceleration over a single period of the motion in the clockwise and counterclockwise directions turn out to be in the same direction. In this case the induced electric signal, which is alternating in time, does not charge polarity. This accounts for the doubling of the frequency of the induction signal.

The one-sided modulation of the induction signal increases as the temperature is lowered from the λ point to $\sim$1.9 K, where the signal is maximum (see Fig. 2a). We attribute this to the spontaneous appearance in the apparatus of circular circulating flows in the apparatus. In this case the value of the relative velocity $\mathbf{V}=\mathbf{V}_n-\mathbf{V}_s$ varies in magnitude during the motion of the resonator in the clockwise and counterclockwise directions. Apparently the forced oscillations of the chamber cause precession of the z component of the angular momentum of the circulating superfluid flow, and with it the dynamic polarization vector (the z axis coincides with the axis of the capillary).

The dependence of the electric induction on the velocity of oscillation of the oscillator is shown in Fig. 4. It is seen that the induced potential is proportional to the square of the linear velocity of the wall of the chamber *1*, i.e., to its centripetal acceleration. This attests to the direct relation of the acceleration (inertial force) and electric response of He II, or, in other words, one can say that a mechanoelectric effect is observed in the system.

An unexpected result was the difference of the values of the Q of the oscillator in He II as measured by different methods. When measured by the forced oscillation method (regimes 1, 2) it turned out to be lower than for $T>T_\lambda$, attesting to the appearance of additional losses in the region $T<T_\lambda$. If the feedback of the generator is disconnected and one measures the Q from the free stopping time, then it turns out to be higher (regime 3, the stopping took several minutes longer). This may indicate that precession of the angular momentum of the superfluid flow at the doubled frequency is damped, since part of the energy and momentum is expended on maintaining the oscillations of the oscillator, i.e., a parametric amplification of the oscillations of the oscillator occurs. Above the λ point both methods give identical values of the Q. Control experiments with an empty chamber *1* at a temperature of 1.4 K also gave identical values of the Q.

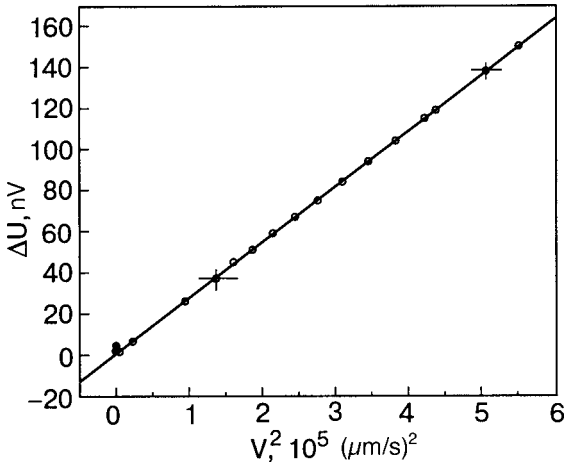

FIG. 4. Dependence of the induced potential on electrode *15* on the square of the velocity of the side wall of the chamber. The unfilled symbols are for a helium film, and the filled symbols are for bulk helium.

Evidence in favor of this assertion comes from the following experiment. As is known, one of the necessary conditions for the normal operation of the torsion generator is that not only the frequency but also the phase relations between the motion of the electrode *3* of the oscillator and the periodic force proportional to the square of the driving voltage must be obeyed. In the course of the experiments, after the stationary values of the measured quantities has been established, an artificial braking of the oscillator to a complete standstill occurred (regime 4). It turned out that after the chamber had stopped, the signal of the electric induction dried down to the noise level in several minutes, i.e., the normal component was stopped together with the wall, the temperature was constant to an accuracy of 10^{-5} K, and the oscillations of the electric induction continued for some time more. This indicates the existence of precession of the circulating current and the noninvolvement of thermal effects.

Thus in this study we have observed for the first time a dynamic polarization of liquid helium in the absence of external electric field. As we know, the polarization of a dielectric in the absence of external electric field attests to charge ordering in it, since it is characterized by the appearance of a spontaneous electric moment, the formation of a domain. A measure of the order is the value of the ordered dipole moments of the particles per unit volume. At present the only thing known about the ordering in liquid helium is that it is characterized by the appearance of a spontaneous angular momentum below T_λ. From the results of the present study we can state with a high probability that below T_λ He II is characterized by two interrelated phenomena: dynamic polarization and a circulating flow. By analogy with dielectrics, in which a spontaneous moment is observed, in He II the dynamic polarization can be taken as a sign of ordering. And the forces leading to ordering in He II may be electric forces that compensate their inertial forces. In the presence of these two forces of different nature, He II becomes similar to a centrosymmetric domain. In experiments with the use of me-

chanical oscillations of an oscillator this domain was driven to precession and its evolution observed. This point of view is supported by experiments with bulk helium. As was shown for the bulk liquid, if the velocity of the side wall of the oscillator is above the critical ($V > V_c = \hbar/mR$), the induction signal is absent, attesting to the vanishing of the ordering described above. Here m is the mass of the helium atom, R is the radius of the chamber, and $\hbar$ is Planck's constant.

We stress that the result obtained cannot be considered definitive proof but, in any case, is an indication that the coupling of the angular and electric moments is completely natural, although unexpected.

CONCLUSION

In this paper we have shown that the periodic motion of the normal component entrained by the oscillations of the wall is also accompanied by the appearance of an electric charge on the capacitor plates, as in the case of second sound.[1] The influence of the thickness of the superfluid film on the value of the induction indicates a direct dependence of the electrical effect on the volume of liquid. The relation established, $\Delta U \propto (V_s - V_n)^2$, attests to a connection between the forces of electrical origin and the inertial forces in liquid helium below T_λ, i.e., we are talking about the first observation of mechanoelectric effects in liquid helium.

The observation of this effect permits its use as a novel and effective means of registering second sound and as a contactless method of measuring the velocity of the superfluid component.

We are grateful to V. N. Grigoriev, A. M. Kosevich, E. Ya. Rudavskii, S.S. Sokolov, and S.I. Shevchenko for discussion and helpful advice. We would also like to take this occasion to thank A. F. Andreev and the participants in his seminar at the Kapitza Institute for Physical Problems, Russian Academy of Sciences, Moscow.

NOTE ADDED IN PROOF

After submission of the manuscript for publication a theoretical paper (cited as Ref. 3) devoted to polarization effects in He II appeared.

*E-mail: rybalko@ilt.kharkov.ua

[1] A. S. Rybalko, Fiz. Nizk. Temp. **30**, 1321 (2004) [Low Temp. Phys. **30**, 994 (2004)].
[2] J. E. Berthold, D. J. Bisho, and J. D. Reppy, Phys. Rev. Lett. **39**, 348 (1977).
[3] L. A. Melnikovsky, http://www.arXiv.org: cond-mat/0505102 v1 4 May (2005).

Translated by Steve Torstveit

Shubnikov–de Haas oscillations, peaks, and different temperature regimes of the diagonal conductivity in the integer quantum Hall conductor

V. M. Gvozdikov

Kharkov National University, 61077, Kharkov, Ukraine; Max-Planck-Institut für Physik Komplexer Systeme, Nöthnitzer Strasse 38, D-01187 Dresden, Germany

(Submitted April 27, 2005)
Fiz. Nizk. Temp. **31**, 826–831 (July 2005)

A theory for the Shubnikov–de Haas oscillations in the diagonal conductivity σ_{xx} of a 2D conductor is developed for the case when electron states within the broadened Landau levels are localized except for a narrow stripe in the center. The standard Shubnikov–de Haas oscillations take place only in the low-field region, which at higher magnetic fields crosses over into peaks. In the limit $\Omega\tau \gg 1$ peaks in the σ_{xx} became sharp and between them $\sigma_{xx} \to 0$ (Ω is the cyclotron frequency, τ is the electron scattering time). The conductivity peaks display different temperature behavior with the decrease of temperature T: a thermal activation regime, $\sigma_{xx} \propto \exp(-\Delta/T)$, which holds at higher temperatures, crosses over into the variable-range-hopping regime at lower temperatures with $\sigma_{xx} \propto 1/T \exp(-\sqrt{T_0/T})$ (the prefactor $1/T$ is absent in the conductance). © *2005 American Institute of Physics.* [DOI: 10.1063/1.2001651]

In spite of more than two decades of intensive experimental research and great theoretical effort, the quantum magnetic oscillations of the conductivity in 2D conductors still have some open questions. Even in the most studied case of the integer quantum Hall effect (IQHE)[1] a complete picture is missing, in particular, concerning different regimes in temperature and magnetic field dependencies of the Hall, σ_{xy}, and longitudinal, σ_{xx}, conductivities. Although the origin of the quantized plateaus in the σ_{xy} is well understood,[2] the transitional regions between them, where localization and scaling[3] play an important role, needs a deeper insight. The scaling properties of the diagonal conductivity σ_{xx} in the variable-range hopping (VRH) regime of the IQHE were recently established experimentally at low temperatures down to 60 mK.[4] To explain this universal scaling behavior as well as transitions between different regimes in the IQHE is a theoretical challenge. At the moment there is no coherent analytic description of the quantum magnetic oscillations of the diagonal conductivity σ_{xx} which takes into account the localization effects at different temperature regimes in the IQHE. In particular, it is not clear so far why quantum oscillations in σ_{xx} do survive in spite of the fact that most states within the broadened Landau levels (LL) are localized (i); why $\sigma_{xx} \to 0$ between the peaks in the limit $\Omega\tau \gg 1$, if at low fields it displays a standard Shubnikov–de Haas (SdH) oscillations (ii); why, with decrease of temperature T, the peaks in σ_{xx} display first a thermal activation behavior $\sigma_{xx} \propto \exp(-\Delta/T)$, which then crosses over into the VRH regime at low temperatures with $\sigma_{xx} \propto 1/T \exp(-\sqrt{T_0/T})$ (iii); why the prefactor $1/T$ is absent in the conductance (iv).

It is a well-established fact that localization in the IQHE picture plays a crucial role. On the other hand, nonzero conductivity is impossible without the extended states. It is believed that extended states lie within a narrow stripe at the center of the broadened LL and all the other states are localized.[5] One can not give a simple physical picture for these localized states in general. At high fields the presence of the localized states in the 2D conductor means that Landau orbits drift along the closed equipotential contours of the impurity potential.

At places where contours come close together electrons can tunnel from one contour to another, thereby providing a conductivity mechanism through the extended states. The diagonal conductivity σ_{xx} and the Hall conductivity σ_{xy} are closely related in the IQHE. The peaks in the σ_{xx} are exactly at the same fields where σ_{xy} transits from one plateau to another. An ideal picture of the IQHE at $T=0$ assumes that $\sigma_{xx}=0$ within the plateaus while the $\sigma_{xy}=ne^2/h$ is quantized (n is an integer). In real experiments $T \neq 0$ and $\sigma_{xx} \neq 0$. In the low-field region σ_{xx} displays the SdH oscillations, and the plateaus in σ_{xy} are unresolved.

In this Letter we develop a theory for the magnetic quantum oscillations of the σ_{xx} in 2D conductors with localization which explains properties (i)–(iv). The conductivity mechanism in this theory is due to the electron hopping between Landau orbits within the conducting plane. A similar mechanism for the conductivity due to the electron tunneling between Landau orbits from the neighboring layers was considered in Ref. 6 for the case of incoherent electron hopping across the layers in an organic conductor. This hopping mechanism remains in effect if the Landau orbits lie within the same conducting plane or belong to the different tunnel-coupled 2D conductors. The latter is important in view of recent observation of typical IQHE behavior in the tunneling conductance of a two coupled Hall bars reported in Ref. 7. The tunneling conductance in this experiment displays the same scaling features as those usually observed in the bulk Hall sample and, therefore, can not be explained by the tunneling between the two counterpropagating edge states. On the other hand, electron tunneling between Landau orbits from different Hall bars and within the same sample contribute equally to the total conductance. In view of that one can anticipate the standard IQHE behavior in the tunneling conductance observed in experiment.[7]

According to Ref. 6 the tunneling SdH conductivity can be written as a sum of the Boltzmann (σ_B) and quantum (σ_Q) terms: $\sigma_{xx}=\sigma_B+\sigma_Q$, where

$$\sigma_B=\sigma_0\int d\varepsilon\,\frac{dE}{\pi}g(\varepsilon)v_x^2(\varepsilon)\left(-\frac{\partial f}{\partial E}\right)\tau S[\lambda,\delta(E,\varepsilon)], \quad (1)$$

$$\sigma_Q=\sigma_0\int d\varepsilon\,\frac{dE}{\pi}g(\varepsilon)v_x^2(\varepsilon)\left(\frac{\partial f}{\partial E}\right)\frac{2\pi}{\Omega}\frac{\partial}{\partial\lambda}S[\lambda,\delta(E,\varepsilon)]. \quad (2)$$

Here $\lambda(E)=2\pi/\Omega\tau$, $\delta(E,\varepsilon)=2\pi(E+\varepsilon)/\hbar\Omega$, $\sigma_0=e^2N_L/\hbar\Omega$, $N_L=\Phi/S\Phi_0$ is the electron density at the LL, Φ is the flux through a sample, $\Phi_0=\hbar c/2\pi e$, and

$$S(\lambda,\delta)=\sum_{p=-\infty}^{\infty}(-1)^p e^{-|p|\lambda}\cos p\delta=\frac{\sinh\lambda}{\cosh\lambda+\cos\delta}. \quad (3)$$

The variable ε describes the LLs broadening by impurities with the density of states (DOS) $g(\varepsilon)$:

$$E_n(\varepsilon)=\hbar\Omega(n+1/2)+\varepsilon. \quad (4)$$

The electron velocity v_x is related to the tunneling matrix elements by[6]

$$v_x(\varepsilon)=\frac{|t_{\varepsilon,\varepsilon}|R}{\hbar\sqrt{2}}, \quad (5)$$

where R and $\hbar\sqrt{2}/|t_{\varepsilon,\varepsilon}|$ are respectively the distance and the time of tunneling. A strong point of the above equations is that we can learn much about $\sigma_{xx}(B,T)$ without resorting to specific models for the localization (B is the magnetic field). In any such model $g(\varepsilon)$ has a narrow band of delocalized states where $v_x(\varepsilon)\neq 0$. It is generally accepted[5] that only one state, precisely at the LL ($\varepsilon=0$), is delocalized. For the localized states $v_x(\varepsilon)=0$. Thus, only one level, $\varepsilon=0$, or a narrow stripe of delocalized states, contribute in Eqs. (1), (2).

The scattering time τ in general is a model-dependent function of the energy which is inversely proportional to the scattering probability for the conducting (delocalized) electrons. The latter belong to a narrow stripe in $g(\varepsilon)$, while the rest of the electrons are localized and produce a reservoir of states stabilizing oscillations in τ. Thus, we can put $\tau=\text{const}$ in Eqs. (1), (2), which yield:

$$\sigma_{xx}=\sigma_\tau\int\frac{dE}{\pi}\left(-\frac{\partial f}{\partial E}\right)[G_B(\lambda,E)+G_Q(\lambda,E)], \quad (6)$$

$$G_B(\lambda,E)=S[\lambda,\Delta(E)], \quad (7)$$

$$G_Q(\lambda,E)=-\lambda\frac{\partial}{\partial\lambda}S[\lambda,\Delta(E)]=-\lambda\frac{1+\cosh\lambda\cos\Delta}{(\cosh\lambda+\cos\Delta)^2}, \quad (8)$$

where $\Delta(E)=2\pi E/\hbar\Omega$ and

$$\sigma_\tau=\frac{e^2N_L\tau\langle v_x^2\rangle}{\hbar\Omega}. \quad (9)$$

The average of the velocity squared is given by

$$\langle v_x^2\rangle=\frac{R^2}{2\hbar^2}\int_{\varepsilon_{\min}}^{\varepsilon_{\max}}d\varepsilon g(\varepsilon)|t_{\varepsilon,\varepsilon}|^2. \quad (10)$$

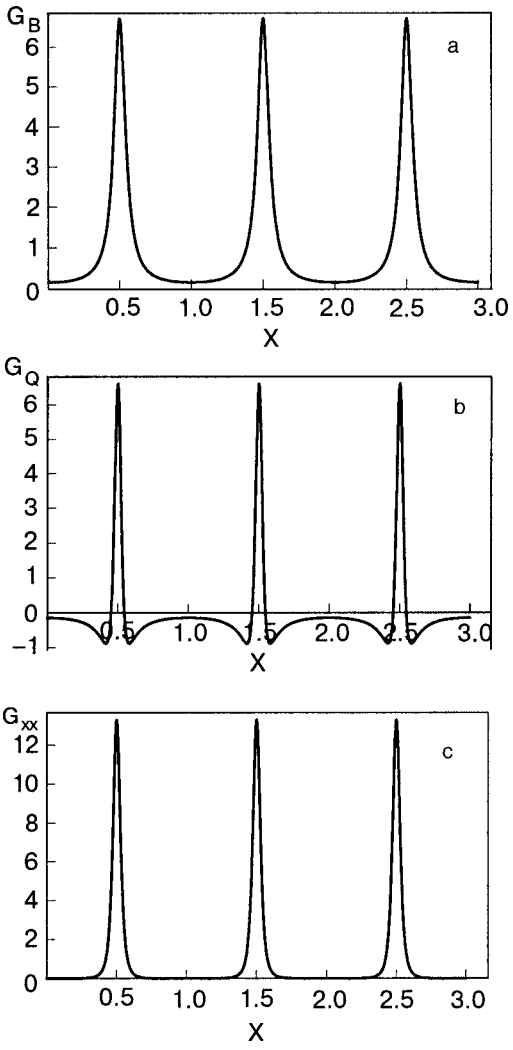

FIG. 1. The Boltzmann $G_B=S(\lambda,2\pi X)$ (a) and the quantum $G_Q=-\lambda\partial S(\lambda,2\pi X)/\partial\lambda$ (b) contributions to the conductivity σ_{xx} in Eq. (6), and their sum $G_{xx}=G_B+G_Q$ (c). $X=E/\hbar\Omega$, $\lambda=0.3$.

The integral in (10) is taken within the narrow stripe of delocalized states. The functions $G_B(\lambda,E)$ and $G_Q(\lambda,E)$ are sharply peaked at $E=E_n$ and between the LLs they nearly compensate each other, as shown in Fig. 1. This demonstrates clearly that the Boltzmann term alone, $G_B(\lambda,E)$, is insufficient for the correct description, and only by taking account of the quantum term, $G_Q(\lambda,E)$, can one explain why σ_{xx} tends to zero between the peaks in the IQHE. The width of peaks in Fig. 1 on the energy scale is of the order of $\hbar/\tau$. If $T\gg\hbar/\tau$, then the peaked function $-\partial f/\partial E$ is broader than the $G_{xx}(\lambda,E)=G_B(\lambda,E)+G_Q(\lambda,E)$, and we can approximate $G_{xx}(\lambda,E)$ in Eq. (6) by

$$G_{xx}(\lambda,E)\approx\frac{2}{\pi}\sum_{n=-\infty}^{\infty}\frac{\eta}{(n+1/2-E/\hbar\Omega)^2+\eta^2}, \quad (11)$$

where $\eta=\lambda/2\pi$. For $\eta\ll 1$ Eq. (11) can be easily proved analytically with the help of the identity[2]

$$\frac{1}{\pi}\sum_{p=-\infty}^{\infty}\frac{\eta}{(n+a)^2+\eta^2}=\frac{\sinh 2\pi\eta}{\cosh 2\pi\eta-\cos 2\pi a}. \quad (12)$$

Thus, for high temperatures, $T\gg\hbar/\tau$, we have

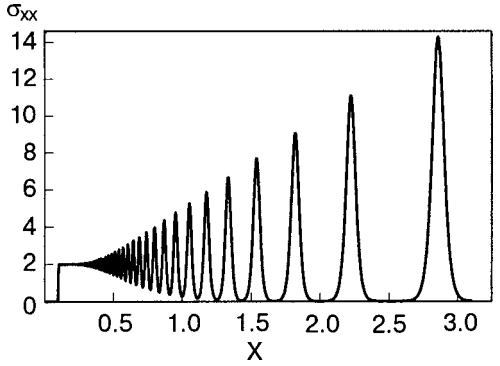

FIG. 2. The conductivity σ_{xx} [see Eq. (13)] in units of σ_τ as a function of $X=\hbar\Omega$. Conventional energy units in which $T=0.2$ and $E_F=10$ are adopted.

$$\sigma_{xx}(B)\approx\sigma_\tau\frac{\hbar\Omega}{4\pi T}\sum_n \cosh^{-2}\left(\frac{E_n-\mu}{T}\right). \tag{13}$$

This sharply-peaked function of $\hbar\Omega$ is shown in Fig. 2. The same function describes the quantum magnetic oscillations of the ultrasound absorption in metals.[8] The temperature dependence of the peaks in $\sigma_{xx}(B)$ for different temperatures is plotted in Fig. 3.

Under the condition $\hbar\Omega/T\gg 1$, the conductivity σ_{xx} at the maxima (i.e., when $E_n=\mu$) is given by $\sigma_{xx}=\sigma_\tau\hbar\Omega/4\pi T$. At the minima (i.e., when the chemical potential μ falls between the LL) the conductivity σ_{xx} is exponentially small:

$$\sigma_{xx}=\sigma_\tau\frac{\hbar\Omega}{4\pi T}\exp\left(-\frac{\hbar\Omega-E_0}{T}\right)$$

(E_0 is a position of μ between the LL). Such an activation dependence is well established for $\sigma_{xx}(T)$ in the IQHE regime.[5] At lower temperatures, $T\ll\hbar/\tau$, one can approximate $-\partial f/\partial E$ by $\delta(E-\mu)$, to obtain

$$\sigma_{xx}\approx\sigma_\tau(G_B[\lambda,\Delta(\mu)]+G_Q[\lambda,\Delta(\mu)]). \tag{14}$$

The conductivity σ_{xx} in (14) is a sharply peaked function of $\Delta(\mu)=2\pi\mu/\hbar\Omega$, as shown in Fig. 1. The Boltzmann and the quantum terms in Eq. (14) nearly compensate each other between the peaks, which in the limit $\eta\to 0$ become the narrow Lorentzians of Eq. (11). The temperature dependence of σ_{xx} at $T\ll\hbar/\tau$ in Eq. (14) comes only from the part due to the VRH mechanism, σ_τ. The VRH concept in the IQHE problem is now well established.[4,9] It was introduced in Ref. 10 and well describes the scaling properties of the peaks in the σ_{xx} within the plateau-to-plateau transition region. The diagonal and the Hall conductivities in this region are related by the "semicircle" law.[11] In samples with mobilities $\sim 10^6$ cm^2/(V·s) at a few tens of mK the best experimental fit yields:[4]

$$\sigma_\tau=\frac{A}{T}\exp(-\sqrt{T_0/T}). \tag{15}$$

The above equation describes the well-known Mott hopping conductivity[12] in which the square root $\sqrt{T_0/T}$ in the exponent means that the system is one-dimensional. For two and three dimensions there should be $(T_0/T)^\alpha$ with $\alpha=1/3$ and 1/4, respectively. Since the system in question is two-dimensional, the authors of the Ref. 10 derived Eq. (15) with $\alpha=1/2$, assuming a strong Coulomb interaction between electrons. In that case the temperature $T_0=Ce^2/(4\pi\epsilon\xi)$ is proportional to the Coulomb energy at the localization length $\xi(\nu)$, ϵ is the dielectric constant, and $C\sim 1$. Numerous experiments and calculations testify in favor of a universal (i.e., independent of the Landau-level index) critical behavior of the localization length $\xi(\nu)\propto|\nu-\nu_c|^{-\gamma}$ near the LLs.[2,3,5] Here $\nu=N\Phi_0/B$ is the filling factor, ν_c is the critical filling factor, and $\gamma\approx 2.35$ is a universal critical exponent. The diverging of $\xi(\nu)$ at ν_c means that this is a critical point for the transition from the dielectric to the conducting state.

The explanation of the $\alpha=1/2$ in Eq. (15) by the Coulomb interaction is inconsistent, at least for the case of IQHE, which is known to be a free-electron phenomenon. The coherence length as well is calculated for free electrons without the Coulomb interaction. Also, this approach meets with some difficulties in the experimental interpretations, like, for example, a divergence of the dielectric constant at the critical point.[13]

On the other hand, in our approach Eq. (15) directly follows from (9) and (10). In the spirit of the VRH concept, we can estimate $|t_{\varepsilon,\varepsilon}|^2$ as a quantity proportional to the electron hopping probability between the two 1D closed equipotential contours at which the Landau orbits are localized. If R is a hopping distance, then

$$|t_{\varepsilon,\varepsilon}|^2\propto\exp\left[-\left(\frac{1}{RN(0)T}+\frac{2R}{\xi}\right)\right]. \tag{16}$$

In this equation we take into account the thermal activation that assists the tunneling if the initial and final levels are separated in energy by a stripe of the order of $1/RN(0)$. Here $N(0)$ is some one-dimensional DOS at closed equipotential contours averaged over a random potential and taken near the Fermi level. The optimal hopping distance is $R=\sqrt{\xi/2N(0)T}$, and Eqs. (10), (16) yield $\langle v_x^2\rangle\propto 1/T\exp(-\sqrt{T_0/T})$. Therefore, in view of Eq. (9) and the fact that $T_0=8/N(0)\xi$, we arrive at the VRH conductivity (15). In fact, the quantity T_0 is a fitting parameter which can be found only from experiment. The quantity $N(0)$ determines the average energy separation (or the gap) between the initial an final states in the electron hopping. In the case when the Coulomb repulsion between electrons plays a dominant role this gap can can be estimated as $Ce^2/(4\pi\varepsilon R)$, which yields $T_0=Ce^2/(4\pi\varepsilon\xi)$, as in Ref. 10. By taking an effective DOS in the form $1/N_{\text{eff}}=1/N(0)$

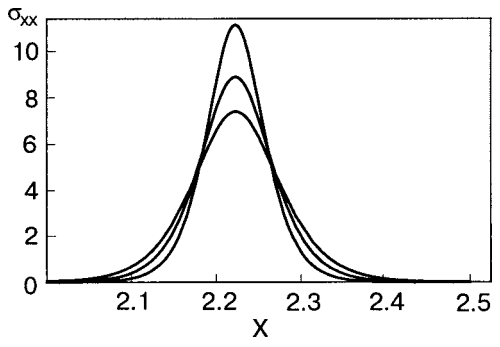

FIG. 3. The same as in Fig. 2 for three different temperatures, $T=0.2$, 0.25, and 0.3 (from top to bottom).

$+Ce^2/(4\pi\epsilon)$ one can qualitatively take account of the Coulomb effect in the Mott hopping mechanism. We see that the resulting VRH conductivity is the same as without the Coulomb interaction, with the only difference being that $N(0) \rightarrow N_{\text{eff}}$ in the DOS, which is unimportant since the DOS is a fitting parameter. In the IQHE regime the Coulomb interaction does not play a significant role and can be discarded without causing any change in the shape of the hopping conductivity given by Eq. (15).

The VRH concept based on this equation was originally applied to the problem of the conductivity peak broadening $\Delta\nu$ in Ref. 10. It was shown that the temperature, current, and frequency dependences of $\Delta\nu$ can be well described within this paradigm. Here we derived a prefactor A/T which has also been observed in $\sigma_{xx}(T)$.[4,9] However, it should be noted that the prefactor A/T is absent in the experiments in which a conductance was measured.[14,15] The difference is because the conductivity in Eqs. (1), (2) is proportional to $v_x^2 \propto R^2 \propto 1/T$. The conductance $\sigma_{xx}^c(T) \propto (e^2/\hbar)|t_{\varepsilon,\varepsilon}|^2$ and has no factor $R^2 \propto 1/T$. Therefore, at the same conditions as in Eq. (14) the conductance is

$$\sigma_{xx}^c \approx \sigma_\tau^c (G_B[\lambda, \Delta(\mu)] + G_Q[\lambda, \Delta(\mu)]), \tag{17}$$

$$\sigma_\tau^c = A_c \exp(-\sqrt{T_0/T}). \tag{18}$$

Since $T_0 \propto 1/\xi \propto |\nu - \nu_c|^\gamma$, the function $\sigma_\tau^c(\nu)$ has a fixed maximum value $\sigma_\tau^c = A_c$ at $\nu = \nu_c$ for different temperatures. This remarkable property of the conductance is firmly established in the VRH regime at low temperatures.[11,14,15]

So far we have assumed that the chemical potential is constant. In 2D conductors $\mu(B)$ is an oscillating function[14] satisfying the equation:[6]

$$\mu = E_F \pm \frac{\hbar\Omega}{\pi} \arctan\left[\frac{\sin(2\pi\mu/\hbar\Omega)}{e^\nu + \cos(2\pi\mu/\hbar\Omega)}\right]. \tag{19}$$

The sign $(-)$ here stands for the direct and $(+)$ for the inverse sawtooth. The amplitude of these oscillations is of the order of $\hbar\Omega$, which is small compared to the Fermi energy E_F. It was shown in Ref. 6 that in a quasi-2D layered conductor the peaks in the magnetic conductivity across the layers are split in the case when $\mu(B)$ is an inverse sawtooth function. The very same effect holds for σ_{xx}, as is shown in Fig. 4, which displays $\sigma_{xx}(B)$ according to Eq. (14) with $\mu(B)$ given by Eq. (19). We also take account of the spin-splitting which is easy to incorporate by the substitution $\mu \rightarrow \mu \pm \mu_e B$ into the right-hand side of Eq. (19) and average it over two spin configurations (μ_e is the magnetic moment of the electron). The spin-splitting parameter $s = 2\pi\mu_e B/\hbar\Omega$ can be rewritten in terms of the g factor and ratio of the effective mass to the electron mass, $s = \pi g m^*/m$. In GaAs $g \approx 0.44$ and $m^*/m \approx 0.068$, which yield $s \approx 0.093$. This value gives a pronounced splitting in the peaks in Fig. 4a, but it is much less noticeable in Fig. 4b for $\mu(B)$. The shape of peaks in the absence of splitting ($s = 0$) is shown in Fig. 4c. The origin of correlations between the shapes of the functions $\sigma_{xx}(B)$ and $\mu(B)$ is the same as in layered conductors.[6]

In conclusion, we suggested a model of the hopping conductivity which describes different regimes in the diagonal conductivity σ_{xx}, stated above in (i)–(iv). It explains why the square-root exponent (corresponding to a 1D system) appears in the VRH conductivity σ_{xx} of a 2D system. The tunneling-conductance oscillations in two coupled Hall bars observed in Ref. 7 display a standard IQHE behavior, which cannot be understood as a tunneling between two counter-propagating edge states. The puzzle resolves naturally in our model. A Hall line tunnel junction couples Landau orbits across the junction, but this does not change the hopping mechanism of the model, which remains basically the same as in the bulk of the sample. It is also worthy of note that the peak-split shape in Fig. 4a is typical for IQHE conductors with high electron mobility. The quantum term (2) in the σ_{xx} plays an important role in our theory. This term is of the same origin as that in the conductivity across the layers in organic conductors.[6,17,18] The principal new point of the model is that Eqs. (1) and (2) incorporate localization into the description. The approach is open for more-specific models of localization, such as models for the levitation of extended states.[19] This effect would be considered within the above model elsewhere.

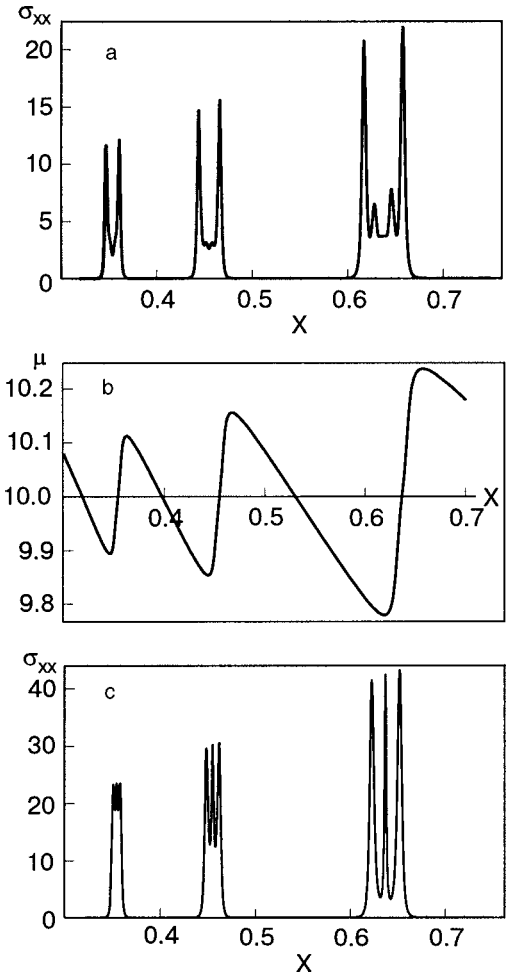

FIG. 4. The conductivity $\sigma_{xx}(X)$ given by Eq. (14) (a) in which the chemical potential $\mu(X)$ oscillates as in panel (b) [a direct sawtooth, see Eq. (17) and text]. The choice of units is the same as in Fig. 2. The spin-splitting parameter $s = 0.093$, $E_F = 10$, $\nu = 0.06$, and $X = \hbar\Omega$. In panel (c) $s = 0$.

The work was supported by INTAS, project INTAS-01-0791. The author is deeply grateful to P. Fulde, J. Wosnitza, M. Kartsovnik, W. Biberacher, I. Ya. Polishchuk, I. V. Krive, A. M. Kosevich, A. A. Slutskin, and participants of the the-

oretical seminar at FTINT in Kharkov for discussions and to S. Flach for the hospitality at MPIPKS in Dresden.

[1] K. von Klitzing, G. Dorda, and M. Pepper, Phys. Rev. Lett. **45**, 494 (1980).
[2] R. B. Laughlin, Phys. Rev. B **23**, 5632 (1981); *The Quantum Hall Effect*, R. E. Prange and S. M. Girvin (eds.), Springer (1987).
[3] B. Huckestein, Rev. Mod. Phys. **67**, 357 (1995).
[4] F. Hohls, U. Zeitler, and R. J. Haug, Phys. Rev. Lett. **88**, 036802 (2002).
[5] D. Yashioka, *The Quantum Hall Effect*, Springer (2000).
[6] V. M. Gvozdikov, Phys. Rev. B **70**, 085113 (2004).
[7] I. Yang, W. Kang, K. W. Baldwin, L. N. Pfeiffer, and K. W. West, Phys. Rev. Lett. **92**, 056802 (2004).
[8] A. A. Abrikosov, *Fundamentals of Theory of Metals*, North-Holland, Amsterdam (1988).
[9] A. Briggs, Y. Guldner, J. P. Vieren, M. Voos, J. P. Hirtz, and M. Razeghi, Phys. Rev. B **27**, 6549 (1983).
[10] D. G. Polyakov and B. I. Shklovskii, Phys. Rev. B **48**, 11167 (1993); Phys. Rev. Lett. **70**, 3796 (1993).
[11] D. Shahar, D. C. Tsui, M. Shayegan, E. Shimshoni, and S. L. Sondhi, Phys. Rev. Lett. **79**, 479 (1997).
[12] N. F. Mott, J. Non-Cryst. Solids, **1**, 1 (1968); N. F. Mott and E. A. Davis, Electronic Processes in Non-Crystalline Materials, Clarendon, Oxford (1979).
[13] M. Furlan, Phys. Rev. B **57**, 14818 (1998).
[14] B. P. Dolan, Phys. Rev. B **62**, 10287 (2000).
[15] J. Oswald, G. Span, and F. Kuchar, Phys. Rev. B **58**, 15401 (1998).
[16] T. Maniv and I. D. Vagner, Phys. Rev. B **38**, 6301 (1988); P. D. Grigoriev, JETP **92**, 1090 (2001); T. Champel, Phys. Rev. B **64**, 054407 (2001); V. M. Gvozdikov, A. G. M. Jansen, D. A. Pesin, I. D. Vagner, and P. Wyder, Phys. Rev. B **68**, 155107 (2003).
[17] P. D. Grigoriev, Phys. Rev. B **67**, 144401 (2003).
[18] T. Champel and V. P. Mineev, Phys. Rev. B **66**, 195111 (2002).
[19] D. E. Khmelnitskii, Phys. Lett. A **106**, 182 (1984); R. B. Laughlin, Phys. Rev. Lett. **52**, 2304 (1984), F. D. M. Haldane and K. Yang, Phys. Rev. Lett. **78**, 298 (1997).

This article was published in English in the original Russian journal. Reproduced here with stylistic changes by AIP.